

**PROBABILISTIC DECENTRALIZED ACTIVE
VIBRATION CONTROL:
STABILITY, PERFORMANCE, AND ROBUSTNESS**

by

Christopher John D'Angelo

B.S. Mechanical Engineering, Rensselaer Polytechnic Institute, 2009

Submitted to the Graduate Faculty of
the Swanson School of Engineering in partial fulfillment
of the requirements for the degree of

Doctor of Philosophy

University of Pittsburgh

2019

UNIVERSITY OF PITTSBURGH

SWANSON SCHOOL OF ENGINEERING

This dissertation was presented

by

Christopher John D'Angelo

It was defended on

December 12, 2018

and approved by

William W. Clark, Ph.D., Professor

Department of Mechanical Engineering and Materials Science

John C. Collinger, Ph.D., Principal Engineer

Naval Nuclear Laboratory

Zhi-Hong Mao, Ph.D., Professor

Department of Electrical and Computer Engineering

Professor, Department of Bioengineering

Jeffery S. Viperman, Ph.D., Professor and Vice Chair

Department of Mechanical Engineering and Materials Science

Professor, Department of Bioengineering

Dissertation Director: Daniel G. Cole, Ph.D., Associate Professor

Department of Mechanical Engineering and Materials Science

Copyright © by Christopher John D'Angelo
2019

PROBABILISTIC DECENTRALIZED ACTIVE VIBRATION CONTROL: STABILITY, PERFORMANCE, AND ROBUSTNESS

Christopher John D'Angelo, PhD

University of Pittsburgh, 2019

This research develops probabilistic decentralized active vibration control design and synthesis techniques for uncertain complex structures. The uncertainty and complexity of the structures studied in this thesis are concentrated at the point where two portions of a structure adjoin — the structural interconnection. This uncertainty is characterized using random variables. The controller design and synthesis approaches that are developed in this research lead to decentralized controller architectures while accounting for random uncertainty at structural interconnections. Ancillary to probabilistic robust controller design and synthesis is the development of analysis tools that enable the designer to evaluate the robust stability and robust performance of the synthesized controllers, given that the plant uncertainty is random.

The control approaches developed in this thesis fall into two distinct categories:

1. Full state feedback control design and synthesis for a lightly damped, lumped parameter model with random interconnection uncertainty.
2. Dynamic output feedback control design and synthesis for a lightly damped, high dimensional beam model derived using finite element theory with random interconnection element uncertainty.

For both the full state and dynamic output feedback control approaches that are developed in this research, the dynamic systems are modeled as generalized plants for control design and synthesis. Control laws that are decentralized, attenuate the disturbance input

to performance output channels in a system infinity-norm sense, and that are robust against random interconnection uncertainty are then designed and synthesized. The models used in this research represent random, lightly damped structures. Control design philosophies and approaches are catered to, and exploit, properties specific to lightly damped structures.

TABLE OF CONTENTS

PREFACE	xxiii
1.0 INTRODUCTION	1
1.1 RESEARCH OBJECTIVES	2
1.2 RESEARCH APPROACH	3
1.3 CONTRIBUTIONS	7
1.4 THESIS OVERVIEW	8
2.0 STATE OF THE ART AND CURRENT PRACTICE	10
2.1 A REVIEW OF DECENTRALIZED STRUCTURAL VIBRATION CONTROL	10
2.2 A REVIEW OF SOME LIMITATIONS IN DECENTRALIZED CONTROL .	13
2.3 PROBABILISTIC ROBUST CONTROL: EVOLUTION OF THE FIELD AND SOME LIMITATIONS	16
2.3.1 Stochastic Robustness and Evolutionary Algorithms in Probabilistic Ro- bust Control	17
2.3.2 Statistical Learning Theory and Control	24

2.3.3 Some Results from Probabilistic Robust Structural Control	29
3.0 PRELIMINARIES	31
3.1 SCALAR, VECTOR, AND MATRIX NOMENCLATURE	31
3.1.1 Positive and Negative (Semi)Definiteness	32
3.2 SYSTEM REPRESENTATIONS	33
3.2.1 The Linear Fractional Transformation (LFT)	33
3.2.2 State-Space Realizations of LFTs	34
3.3 SIGNAL AND SYSTEM NORMS	35
3.3.1 Norms for signals	35
3.3.2 Norms for systems	36
3.4 VECTOR NORMS AND BALLS	37
3.5 MATRIX NORMS AND BALLS	37
4.0 STRUCTURAL MODELING AND CONTROL OBJECTIVES	39
4.1 THE LUMPED PARAMETER MODEL	39
4.2 THE EULER-BERNOULLI BEAM FINITE ELEMENT MODEL	41
4.3 INTERCONNECTION STIFFNESS ELEMENT UNCERTAINTY	42
4.3.1 The Uncertain Interconnection Stiffness Element for the Full State Feed-back Case	42

4.3.2 The Uncertain Interconnection Stiffness Element for the Dynamic Output Feedback Case	42
4.3.3 Structured Norm-Bounded Uncertainty	45
4.3.4 Encapsulating the Structured Norm-Bounded Interconnection Uncertainty	46
4.3.5 Open-loop Response of the Uncertain Structures with Structured, Norm-bounded Uncertainty	48
4.3.6 Infinity Norm of the System Possessing Structured, Norm-Bounded Uncertainty	52
4.4 CONTROL OBJECTIVES	53
4.5 ACHIEVING CONTROL OBJECTIVES IN STATIC FULL-STATE FEEDBACK	55
4.5.1 Performance Output Function Design in Modal Coordinates	57
4.5.2 Frequency Weighting in Modal Coordinates	58
4.5.3 Decentralized Controller Architecture	63
4.5.4 A Probabilistic Robust Full State Feedback \mathcal{H}_∞ Controller	64
4.5.5 Probabilistic Robust Stability and Performance Metrics	64
4.6 ACHIEVING CONTROL OBJECTIVES IN DYNAMIC OUTPUT FEEDBACK	67
4.6.1 Performance Output Function Design in Modal Coordinates	69
4.6.2 Decentralized Controller Architecture	70

4.6.3 Probabilistic Robust Stability and Performance Metrics	72
4.7 CHAPTER SUMMARY	73
5.0 SCENARIO-BASED DECENTRALIZED FULL-STATE FEEDBACK CONTROL OF A LIGHTLY-DAMPED SYSTEM WITH RANDOM INTERCONNECTION UNCERTAINTY	74
5.1 THE SCENARIO APPROACH TO PROBABILISTIC ROBUST CONTROL	75
5.1.1 On sample size complexity and a priori probabilistic guarantees	77
5.1.2 Scenario-based Synthesis as a Semidefinite Program with LMI Con- straints	79
5.2 FULL-STATE FEEDBACK \mathcal{H}_∞ CONTROLLER SYNTHESIS USING LIN- EAR MATRIX INEQUALITIES	82
5.3 A USEFUL ISOMORPHISM BETWEEN \mathbb{C} AND \mathbb{R}	86
5.4 COMPLEX SEMIDEFINITE PROGRAMMING	90
5.4.1 Formulating the Equivalent Real-Valued Semidefinite Program	90
5.5 SCENARIO-BASED, DECENTRALIZED, PROBABILISTIC ROBUST SYN- THESIS FOR A SYSTEM REPRESENTED IN COMPLEX MODAL COOR- DINATES	92
5.5.1 Enforcing Sparsity Constraints on our Controller Variables	95
5.5.2 Frequency Weighting the Disturbance Input (B_1) and Performance Out- put (\tilde{C}_1) Matrices	96
5.5.3 Sample Bounds for this Problem	100

5.5.4 Pseudocode for this Optimization Problem	101
5.6 GUARANTEEING THAT THE CONTROLLER WILL BE STRICTLY REAL	101
5.7 RESULTS	109
5.7.1 Open Loop and Closed-Loop System Performance	109
5.7.2 Probabilistic Analyses	112
5.7.2.1 Stability and Performance Tests	112
5.7.2.2 Robust Stability and Performance Margins	114
5.8 CHAPTER SUMMARY	121
6.0 LOOP-AT-A-TIME DECENTRALIZED DYNAMIC OUTPUT FEEDBACK \mathcal{H}_∞ CONTROL USING μ-SYNTHESIS	122
6.1 LOOP-AT-A-TIME μ -SYNTHESIS IN DECENTRALIZED STRUCTURAL CONTROL	125
6.2 ROBUST CONTROL AND μ -SYNTHESIS	126
6.2.1 Uncertainty Representations in Robust Control	127
6.2.2 The Uncertainty Block, Δ	128
6.2.3 Uncertainty and Stability Margins	129
6.2.3.1 Construction of a Destabilizing Uncertainty Perturbation	132
6.2.4 Robust Stability Analysis	133

6.2.5 Robust Stability Tests Reduced to a Non-Singularity Test on the Imaginary Axis	133
6.2.6 The Central Test for Robust Stability	134
6.3 THE STRUCTURED SINGULAR VALUE (μ)	135
6.3.1 SSV Applied to Testing Robust Stability	137
6.3.2 Bounds on the SSV	139
6.3.3 Robust Performance	143
6.3.4 Testing Robust Performance	144
6.3.5 The Robust Stability and Robust Performance Test	149
6.3.6 Summary	149
6.4 μ -SYNTHESIS VIA D/K ITERATIONS	150
6.4.1 Scalings and Controller Iteration (D/K -iteration)	152
6.4.2 Step #1	153
6.4.3 Step #2	153
6.4.4 Step #3	155
6.4.5 Step #4	155
6.4.6 Examining Bounds on γ during Iterations	155
6.5 LOOP-AT-A-TIME FORMULATIONS AND μ -SYNTHESIS	157
6.5.1 System Descriptions	160

6.5.2	Collapsing the Systems during Different Stages of the Synthesis Process	163
6.5.3	First Step — No controller for G_1 , Synthesize Controller for G_2	164
6.5.4	Second Step — Controller Exists for G_2 , Synthesize Controller for G_1	167
6.5.5	Third Step — Controllers Exist for G_1, G_2 ; Performance Verification	172
6.5.6	Fourth Step — Iterative Controller Synthesis	174
6.5.7	Loop-at-a-Time μ -synthesis via D/K Iterations Algorithm	175
6.6	UNCERTAIN MAXIMUM SINGULAR VALUE PLOTS OF μ -SYNTHESIZED SEED SOLUTIONS	178
7.0	PROBABILISTIC DECENTRALIZED DYNAMIC OUTPUT FEEDBACK \mathcal{H}_∞ SYNTHESIS	182
7.1	THE TRANSFER FUNCTION MATRIX AND PERFORMANCE OBJECTIVES	184
7.2	STOCHASTIC OPTIMIZATION USING GENETIC ALGORITHMS	187
7.2.1	Steps in Genetic Algorithm-based Optimization	188
7.2.2	Stochastic Cost Functions and Genetic Algorithms	190
7.2.3	Theoretical Bounds on Probability Estimate Accuracy and Confidence	192
7.2.4	Genetic Algorithm Settings	195
7.3	FORMULATING THE PROBABILISTIC DECENTRALIZED DYNAMIC OUTPUT FEEDBACK SYNTHESIS PROBLEM AS A STOCHASTIC OPTIMIZATION PROBLEM SOLVED USING A GENETIC ALGORITHM	197

7.3.1 A Less Expensive \mathcal{H}_∞ -norm Performance Calculation	200
7.3.1.1 Selecting a Frequency Grid	200
7.3.2 Final Cost Function used for Synthesis	204
7.4 ON REDUCING THE NUMBER OF CONTROLLER VARIABLES	209
7.4.1 A Canonical Similarity Transform for Reducing the Number of Optimization Variables	210
7.4.2 Using Modal μ -Synthesized Seed Controllers for Stochastic Synthesis . .	213
7.5 RESULTS	215
7.5.1 Controlled System Performance	217
7.5.2 Stability and Performance Tests	220
7.5.3 Comments on Probabilistic Robust Solutions 1 and 2	221
7.5.4 Random Maximum Singular Value Plots of the Open and Closed Loop Systems	222
7.5.5 Degradation Functions of the Closed-Loop Systems	222
7.5.6 On Calculation of Probabilistic Robust Stability and Performance Margins	225
7.5.7 A Special Case: No Interconnection Stiffness Element	225
7.6 CHAPTER SUMMARY	231
8.0 CONCLUSIONS AND FUTURE WORK	233

8.1 SUMMARY OF CONTRIBUTIONS	236
8.2 FUTURE DIRECTIONS FOR PROBABILISTIC DECENTRALIZED ACTIVE VIBRATION CONTROL	237
APPENDIX A. FULL STATE FEEDBACK MODEL	240
A.1 SYSTEM MATRICES AND PARAMETER VALUES	241
APPENDIX B. DYNAMIC OUTPUT FEEDBACK MODEL	243
APPENDIX C. STABILIZABILITY AND DETECTABILITY OF LIGHTLY-DAMPED STRUCTURES	253
APPENDIX D. KYP LEMMA	256
APPENDIX E. KYP DUAL PROOF	259
APPENDIX F. PULLING OUT THE DELTA'S IN A PARAMETRICALLY-UNCERTAIN STATE SPACE SYSTEM	261
APPENDIX G. DEGRADATION FUNCTION DATA FOR THE PROBABILISTIC ROBUST DYNAMIC OUTPUT FEEDBACK CASE	265
BIBLIOGRAPHY	268

LIST OF TABLES

1	Initial Controller Population Resulting from μ -Synthesis	179
2	Genetic Algorithm Settings	196
3	Unique Controller Variables	213
4	Optimization algorithm performance and convergence.	216
5	Solutions #1 and #2 Performance	220
6	Input data for finite element Euler-Bernoulli beam and element creation. . . .	251
7	Input data for beam measurement, disturbance, and control input locations. Distances are with respect to the fixed-end boundary condition.	252
8	Resulting probability estimates for controller 1 as a function of variance inflation factor a . If the controlled system is found to be stable, it highly likely that it will also meet the performance specification for the systems and controllers designed in this research.	266
9	Resulting probability estimates for controller 2 as a function of variance inflation factor a . If the controlled system is found to be stable, it highly likely that it will also meet the performance specification for the systems and controllers designed in this research.	267

LIST OF FIGURES

1	Simplified difference between robust control and probabilistic robust control.	5
2	This figure is similar to those that appeared in Ray and Stengel's papers [1, 2] on stochastic robustness.	19
3	This figure is similar to those that appeared in Ray and Stengel's papers [1, 2] on stochastic robustness.	20
4	Generalized regulator framework.	34
5	Probabilistic decentralized active control conceptualization. Control inputs (u), measurements (y), disturbance inputs (w), performance outputs (z), and structure/interconnection forces/momenta and displacements/rotations (p, q) are depicted for substructures G_1 and G_2	40
6	Comparison of the uniform, structured norm-bounded uncertainty used for μ -synthesis with the normal distribution that has been defined for probabilistic robust synthesis.	49
7	Open loop $w \rightarrow z$ mapping.	50
8	Maximum singular value plot of beams coupled through a norm-bounded, uncertain interface stiffness element. Interface stiffness element modulus variability ranges between 5% and 150% of the nominal, or $E_\Delta \in [0.05E_0, 1.5E_0]$	50

9	Maximum singular value plot of beams coupled through a norm-bounded, uncertain interface stiffness element. Interface stiffness element modulus variability ranges between 1% and 200% of the nominal, or $E_\Delta \in [0.01E_0, 2E_0]$	51
10	Disturbance input and performance output filtering in a generalized plant setting.	59
11	Lightly damped linear system comparing disturbance input filter augmentation with input matrix scaling in modal coordinates. This figure depicts the open-loop, unfiltered system, the system with an augmented disturbance input filter, and the effects of magnitude scaling in modal coordinates. The filter that was augmented, and used for scaling, is also included on this figure. It is shown that magnitude scaling achieves a good filtered approximation near the system resonances.	62
12	Open loop maximum singular value plots, filtered and unfiltered, with the disturbance input and performance output filters used.	66
13	Initial generalized plant formulation used for K_1 controller synthesis.	71
14	Subsequent generalized plant formulation for K_2 controller synthesis.	71
15	Closed loop system for system analysis.	72
16	Frequency-weighted open and closed-loop lightly damped system with random interconnection uncertainty.	110
17	Random, unweighted maximum singular value plot of the $F_l(\hat{G}_\Delta, K_{\text{opt}})$ mapping.	111
18	Combined stability and performance degradation functions for the full-state feedback, probabilistic robust decentralized \mathcal{H}_∞ controller given by (5.123) for the uncertainty set (5.132) with $a \in [0, a_{\max}]$	117

19	Stability degradation function with the probabilistic stability margin (PSM) shown.	119
20	Performance degradation function with the probabilistic performance margin (PPM) shown.	120
21	Probabilistic decentralized active control conceptualization. Control inputs (u), measurements (y), disturbance inputs (w), performance outputs (z), and structure/interconnection forces/momenta and displacements/rotations (p, q) are depicted for substructures G_1 and G_2	123
22	Generic uncertain system.	128
23	Rewritten uncertain closed loop interconnection.	129
24	Uncertain closed loop interconnection with uncertainty block removed.	130
25	Condensed version of the uncertain system.	131
26	Condensed uncertain system, open loop.	131
27	Robustness test block diagram.	150
28	General system under consideration with labeled signals.	161
29	Posing the problem for synthesis of K_2	164
30	Intermediate step for loop at a time synthesis using μ synthesis via D/K iterations.	165
31	Stage in formulating system for μ -synthesis via D/K iterations.	166
32	Uncertain generalized regulator structure for G_3	167
33	Another stage in loop at a time synthesis process.	168

34	Intermediate closed loop system.	169
35	Intermediate collapsed subsystem.	171
36	The controlled global system.	172
37	Uncertain maximum singular value plot of open loop system and closed loop system for Controller Pair #2, synthesized with norm-bounded interconnection uncertainty $E_{\Delta,1} \in [0.01E_0, 2E_0]$	180
38	Uncertain maximum singular value plot of open loop system and closed loop system for Controller Pair #7, synthesized with norm-bounded interconnection uncertainty $E_{\Delta,2} \in [0.05E_0, 1.5E_0]$	181
39	Chernoff bounds as a parametric of accuracy (ϵ) and confidence ($1 - \delta$). This plot illustrates how accuracy is more expensive than confidence. Additionally, this plot aids in a later discussion on probability estimate accuracy and computational complexity.	194
40	Average \mathcal{H}_∞ -norm computation time versus state space order for a random, 2-input, 4-output, stable state space system.	199
41	Computation time comparison between Bruisma approach to \mathcal{H}_∞ -norm calculation with evaluation at lightly damped modes across the bandwidth of 2-input 4-output stable state space systems.	203
42	The set of systems with \mathcal{H}_∞ -norm below some scalar value γ is a subset of the stable systems, where both sets are generated by the same uncertainty distributions.	204
43	Probability estimate accuracy, 95% confidence, parametric with available computing cores and average computation time required to execute the cost function given by algorithm 4 for one Monte Carlo sample.	208

44	Reducing the seed controllers to a modal basis dramatically reduces the number of controller variables required during optimization.	212
45	Genetic algorithm based optimization was pursued around individual μ -synthesized seed controllers. Communication between computing nodes was not enabled. Eight seeds were used, meaning eight nodes, each with 24 cores, were involved in searching for probabilistic robust decentralized controllers in this research. . .	216
46	Solution #1, as described in table 4. These maximum singular value plots show the disturbance input/performance output mapping for the open-loop system and both the probabilisitic-robust and associated μ -synthesized seed closed-loop systems. These maximum singular value plots are for the nominal plant, where the interconnection stiffness modulus $E_0 = 200$ GPa. Around the nominal plant, with the exception of the second mode and a few modes in the mid-frequency range, the probabilistic robust solution tends to perform better than the μ -synthesized solution.	218
47	Solution #2, as described in table 4. These maximum singular value plots, mapping the disturbance inputs/performance outputs are around the nominal plant, where the interconnection stiffness modulus $E_0 = 200$ GPa. Similar to solution #1 shown in figure 46, the probabilistic robust solution out-performs the μ -synthesized solution with the exception to the second mode.	219

48	Solution #1, as described in table 4. This random maximum singular value plot was generated for both the open and closed-loop systems, for the first probabilistic robust solution featured in this chapter. Interconnection modulus uncertainty was generated from the distribution $\mathcal{N}(E_0, 0.16E_0^2)$, which was the uncertainty used for synthesis. This probabilistic robust solution was found to maintain stability 99.34% of the time, while maintaining the \mathcal{H}_∞ -norm below our objective of -45.4 dB for 99.34% of the random plants generated by this uncertainty. The equivalence between these probabilistic performance metrics implies that we only failed our performance requirements for those closed-loop plants that were unstable. This solution is probabilistically-robust against the random interconnection uncertainty that was defined for synthesis.	223
49	Solution #2, as described in table 4. Interconnection modulus uncertainty was generated from $\mathcal{N}(E_0, 0.16E_0^2)$ for synthesis and analysis. This probabilistic robust solution was found to maintain stability 99.33% of the time, while maintaining the \mathcal{H}_∞ -norm below our objective of -45.4 dB for 99.33% of the random plants generated by this uncertainty. The same insight is realized with respect to the conditional dependence between stability and performance as for solution #1. This solution is probabilistically-robust against the random interconnection uncertainty that was defined for synthesis.	224
50	Solution 1 degradation functions. The data that was used to construct this function is included in appendix G. These results show that if the system is stable it almost always meets the performance specification for the systems used in this research.	226
51	Solution 2 degradation functions. The data that was used to construct this function is included in appendix G.	227
52	Maximum Singular Value Plot of Uncoupled, Open and Closed-Loop Systems — Solution #1.	229

53	Maximum Singular Value Plot of Uncoupled, Open and Closed-Loop Systems — Solution #2.	230
54	Spring mass damper model with random interconnection stiffness.	240
55	Beam model.	244
56	Composite structure decomposed into substructures with uncertain interconnection element.	244
57	A single finite element statically loaded by forces and moments at ends, with associated elemental shape functions.	245
58	This figure depicts the relative location of control inputs (u_i), disturbance inputs (w_i), and measurements (y_i) along the length of each respective beam, with the approximate location of the uncertain interconnection stiffness element (e_Δ) shown.	251
59	Generalized regulator framework with controller and uncertainty block.	262

PREFACE

This work is dedicated to my wife, Emmeline, for her unwavering support during the writing of this dissertation. Her love and companionship motivates me to be the best person that I can be.

This research was performed under appointment to the Rickover Fellowship in Nuclear Engineering. This research was also supported in part by Pittsburgh Supercomputing Center grant number MSS180005P and also by the University of Pittsburgh Center for Research Computing through the resources provided.

1.0 INTRODUCTION

This research develops probabilistic decentralized active vibration control design and synthesis techniques for uncertain complex structures. The uncertainty and complexity of the structures studied in this thesis are concentrated at the point where two portions of a structure adjoin — the structural interconnection. This uncertainty is characterized using random variables. The controller design and synthesis approaches that are developed in this research lead to decentralized controller architectures while accounting for random uncertainty at structural interconnections. Ancillary to probabilistic robust controller design and synthesis is the development of analysis tools that enable the designer to evaluate the robust stability and robust performance of the synthesized controllers, given that the plant uncertainty is random.

The control approaches developed in this thesis fall into two distinct categories:

1. Full state feedback control design and synthesis for a lightly damped, lumped parameter model with random interconnection uncertainty.
2. Dynamic output feedback control design and synthesis for a lightly damped, high dimensional beam model derived using finite element theory with random interconnection element uncertainty.

For both the full state and dynamic output feedback control approaches that are developed in this research, the dynamic systems are modeled as generalized plants for control design and synthesis. Control laws that are decentralized, attenuate the disturbance input to performance output channels in an \mathcal{H}_∞ -norm sense, and that are robust against random interconnection uncertainty are then designed and synthesized. The models used in this re-

search are random, lightly damped structures. Control design philosophies and approaches are catered to, and exploit, properties specific to lightly damped structures.

1.1 RESEARCH OBJECTIVES

The act of decomposing large structures into a collection of many smaller ones is not new [3]. In fact, the elementary notion of breaking down a large structure, or system, into an interconnection of smaller ones has given rise to the fields of substructuring [3, 4] in structural dynamics and large scale system theory [5] in control theory. However, designing vibration controllers for each substructure and combining these controlled substructures to form a controlled superstructure that meets some global performance requirements still has several challenges.

One challenge is how uncertainty between substructures is quantified. The point where substructures are joined may be bolted, welded, or joined by some other means. These interconnections are not only difficult to model, but may experience changes in ways that differ from the main portions of the structure. To address this challenge, random stiffness elements are used to describe uncertainty at this interface. This uncertain interconnection between substructures can have a significant impact on the dynamics of the composite controlled structure — as shown in chapters 5 and 7 — and so techniques for evaluating the stability and performance of independently-controlled substructures are developed into a large scale structural control framework from the field of probabilistic robust control (PRC). Meeting this challenge resulted in the first objective of this research:

Objective #1: Evaluate stability and performance of a composite controlled structure possessing probabilistic interconnection uncertainty.

Developing methods to analyze the composite stability and performance of controlled substructures in the presence of probabilistic interconnection uncertainty provides the structural control engineer with powerful analysis tools, but methods for performing control design also are needed. Few techniques exist in the area of decentralized substructure control that en-

able the design of robust substructure controllers with attention to the types of uncertainty studied in this research [6, 7]. Furthermore, there are no techniques that use probabilistic interconnection uncertainty during decentralized substructure control design. Therefore, control design techniques that can achieve controlled substructure performance requirements in the presence of random interconnection uncertainty were needed. The second research objective is the following:

Objective #2: Achieve structural controller performance requirements when controlled substructures are joined in the presence of interconnection uncertainty.

A significant component of robustness analysis deals with robust stability and performance verification: for the amount of uncertainty present in the structural system model, will the given controller meet performance and stability requirements for all instances within the specified uncertainty set? Tools are developed in this research that allow the structural control engineer to do two things: verify robust stability and performance and find how much uncertainty can be tolerated by the controlled system before stability and performance guarantees degrade toward unacceptable levels. Therefore, the third objective of this research is the following:

Objective #3: Calculate probabilistic stability and performance margins.

In classical terms, these techniques translate into giving the structural control engineer ways to find the robust stability and performance margins for the superstructure that is joined by random interconnections.

1.2 RESEARCH APPROACH

An example application for the techniques that have been developed in this research is the design of vibration controllers that attenuate the transfer of low frequency vibrations between a marine engine compartment and hull. Due to the high dimension and complexity of the models used to describe the dynamics of components in the engine compartment and

hull, modeling endeavors for each subsystem may be pursued separately. Each subsystem can be considered to be a substructure and the composition of these substructures form the composite structure. For this type of system, sensing and actuation can be restricted to be local to the substructures. This constraint, which may exist for physical or design reasons, necessitates decentralized analysis and control strategies.

An additional challenge arises when we consider the dynamics at the point where substructures are interconnected. Whether this point in the structure is bolted, welded, or attached using some other means, the physics of this interconnection are complicated. Indeed, an active, burgeoning area of research now exists at the intersection of tribology, structural dynamics, and contact mechanics to better understand the dynamics across these portions of a structure — and how to model them [8].

This thesis does not study the physics at substructure interconnections explicitly. This thesis develops new controller design and synthesis techniques that allows engineers to synthesize decentralized controllers for structures while explicitly accounting for uncertainty in these interconnections. To capture the aggregate effects of: nonlinearities; material changes brought on by myriad phenomena; and other material or model anisotropies, the approaches developed in this thesis allow for the interconnection to be modeled as a *random system with uncertainty characterized by arbitrary probability density functions*.

The fields of control theory and active vibration control have developed techniques for designing and synthesizing controllers in the presence of interconnection uncertainty [7, 6, 9, 10]. These specific methods in active structural control, and control theory in general, are limited by design conservatism and potentially unrealistic expressions for substructure interconnection uncertainty. The way that uncertainty is characterized in existing methods, which is to model it as existing within some bounded ball of uncertainty, allows for the uncertainty to exist everywhere within this ball with equal probability. We then end up attempting to synthesize a controller for the theoretical worst-case plant configuration, even if this worst-case is not likely to represent the configuration of the plant “most of the time”. This notion has spurned the creation of an entire field within control theory: probabilistic robust control [11, 12, 13, 14]. The principal difference between these paradigms lies in

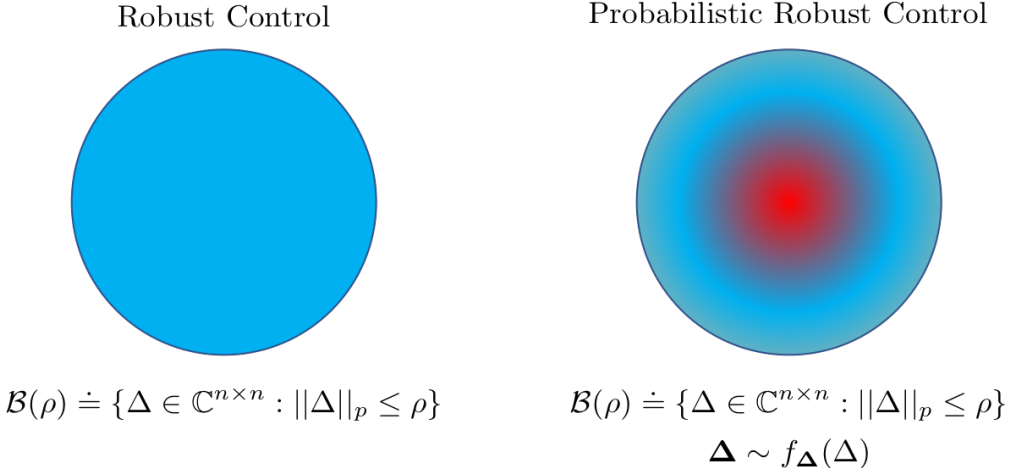


Figure 1: Simplified difference between robust control and probabilistic robust control.

how we characterize the system's uncertainty. And so we may consider the existence of two paradigms in robust control:

1. In **robust control**, norm-bounding uncertainty leads to asserting that the uncertain plant may exist anywhere within some ball of uncertainty. For robust controller design, the objective is to guarantee that stability and performance can be met for every member in the set.
2. In **probabilistic robust control**, the uncertainty may or may not be norm-bounded, and imposes a probability density function on the uncertainty. For probabilistic robust controller design, the objective is to guarantee, using some probability measure, that stability and robustness can be met for most members of the set.

A good way of visualizing these differences is shown in figure 1. Color, or a gradient, by way of a density function $f_{\Delta}(\Delta)$, is imposed onto the uncertainty set, as we attempt to find controllers that perform better for most members in a now focused uncertainty set.

Using the robust control approach to incorporating uncertainty into structural models, we are not able to incorporate precise information about the nature of the system's uncertainty during controller design and synthesis. At best, the traditional approach to bounding

uncertainty only permits a coarse characterization of uncertainty. Using the methods developed in this thesis, actual materials and test data can be translated into uncertainty inputs for use during controller design and synthesis.

This research provides the vibration control engineer with new techniques for analyzing the stability and performance of connected, controlled substructures where random uncertainty is concentrated in the interconnections. While accounting for random interconnection uncertainty, this research culminates in active control design and synthesis approaches that enforce a decentralized controller implementation. Techniques for evaluating the bounds on how much random uncertainty can be tolerated before performance degrades significantly, in a probabilistic sense, are also developed in this research. This research sets the stage for extending these techniques to the more complicated case of including uncertainty not only in the interconnections, but also in the substructures.

Two cases, using canonically studied models in vibration control, are features in this research:

1. The full-state feedback control case, which uses a simple lumped-parameter spring-mass-damper model;
2. The dynamic output feedback control case, which uses an Euler-Bernoulli beam derived from elementary finite element methods.

Novel, probabilistic robust, decentralized active vibration controller design and synthesis approaches are developed in this thesis for both the full-state feedback and dynamic output feedback control cases. Aside from their decentralized implementations, both of these approaches share a common feature: they are designed to attenuate the \mathcal{H}_∞ norm of disturbance input/performance output mapping for the structure below some level in the presence of random interconnection uncertainty. To achieve these ends in this research, two techniques have been developed that synthesize decentralized \mathcal{H}_∞ controllers for structural systems with random interconnection uncertainty through using techniques and tools such as:

1. Linear matrix inequalities/semidefinite programming and the scenario-based approach for the full-state feedback case [15, 16, 14];

2. μ -synthesis and genetic algorithms for solving a high-dimensional stochastic optimization problem for the dynamic output feedback case [17, 18].

These tools are developed, and then applied to solve the large scale structural control problem with attention paid to reducing controller design conservatism and computational complexity. The approaches for achieving this are the topics of chapters 5, 6, and 7.

Structural systems, especially those that operate in harsh environments, have specific mathematical and physical considerations that are highlighted during system modeling and controller design in this research, making the results of this research especially applicable to the structural dynamics and control community. These techniques may find application to problems in vibration control of large scale space structures and for marine structural vibration suppression.

1.3 CONTRIBUTIONS

This research develops probabilistic-robust, decentralized, structural control design techniques with tools for analyzing system stability and performance. Two controller design and synthesis approaches have been developed:

1. A decentralized, full state feedback \mathcal{H}_∞ control design and synthesis method where interconnection uncertainty is random;
2. A decentralized, dynamic output feedback \mathcal{H}_∞ control design and synthesis method where interconnection uncertainty is random, specifically catered to high dimensional models.

The main contributions to the field of structural dynamic control are the following:

1. Treating the interconnection terms randomly and coupling decentrally-controlled substructures in a generalized regulator framework is new.
2. A method for performing robust stability and performance tests and the definition and calculation of margins for controlled structures coupled by a probabilistically-uncertain interface stiffness matrix.

3. A controller design and synthesis approach that permits frequency-weighting of system models via complex-valued performance output functions and synthesis of a structure-constrained high-dimensional semidefinite program for achieving decentralized full-state feedback \mathcal{H}_∞ control in the presence of random interconnections.
4. A controller design and synthesis approach that permits frequency-weighting of system models, synthesis of robust controllers using loop-at-a-time μ -synthesis for the norm-bounded interconnection uncertainty case, and subsequent solution of stochastic optimization problems around the μ -synthesized solutions. This stochastic optimization problem is pursued after imposing an Gaussian distribution over the interconnection uncertainty, and is performed explicitly over the real and complex-parts of the μ -synthesized controllers for computational efficiency.
5. Application of these control approaches to lightly-damped, low and high-dimensional structure models.

This research sets the stage for extending these techniques to the more complicated case of including uncertainty not only in the interconnections, but also in the substructures themselves. In addition, these methods can be adapted to incorporate other types of controller performance objectives, such as those specific to \mathcal{H}_2 control.

1.4 THESIS OVERVIEW

The remainder of this thesis is organized in the following way: Chapter 2 is a review the state of the art along with associated limitations. Chapter 3 provides some mathematical preliminaries background, fundamental to the approaches developed and used in chapters 4, 5, 6 and 7. Chapter 4 discusses structural modeling and active control objectives. Chapter 5 develops a full-state feedback, decentralized, probabilistic-robust \mathcal{H}_∞ control approach using complex semidefinite programming and the scenario-based approach. Chapter 6 discusses and provides the methods and techniques used for decentralized robust \mathcal{H}_∞ controllers using loop-at-a-time μ -synthesis, where the interconnection uncertainty is real, parametric, and

norm-bounded. The output of chapter 6 is then used directly as input to chapter 7, where genetic algorithms and high-performance computing are used, along with careful construction of cost function and sample size for realizing the ultimate goal of this thesis: an approach to synthesizing probabilistically-robust, dynamic output feedback \mathcal{H}_∞ controllers for high-dimensional lightly-damped structures possessing random interconnection uncertainty. Finally, chapter 8 summarizes the research along with contributions made, advancements to the state of the art, and future directions for this research.

2.0 STATE OF THE ART AND CURRENT PRACTICE

2.1 A REVIEW OF DECENTRALIZED STRUCTURAL VIBRATION CONTROL

The field of structural control is well developed and has been an active field of research in excess of four decades. In the late 1980's and early 1990's the interdisciplinary field of control-structure interaction (CSI) was formed to bring structural dynamicists and control theorists together to exchange techniques, collaborate, and develop technology and methods in support of NASA's large space structures program. Within this timeframe and into the late 1990s, techniques were explored and developed for tackling large scale structural analysis and control problems.

Decomposing large structures into substructures and combining substructures to form large structures has been investigated since the early 1970's [3]. One idea behind decomposing large structures into substructures is obvious: structure decomposition into substructures allows for parallel computation of structural dynamic behavior, leading to computational savings and improved development time. Furthermore, substructures are sometimes designed and tested at different locations and by different organizations [19, 20]. This led researchers to develop ways to synthesize the dynamics of substructures, like the substructures that would comprise the International Space Station (ISS), in order to predict structural dynamic behavior.

Large scale structures, like the ISS, needed more than just a way to synthesize the open-loop dynamics of several substructures. Because the system is very lightly damped, they

needed a method to dissipate vibrational energy. One approach is active structural control. This let engineers use the actuators that are used to control the geometry of the structure to also control the structural vibrations. In response to this need, Su and Craig developed a substructure controller synthesis technique called controlled component synthesis (CCS) [21, 20]. This technique, which used elements directly from the field of large scale system theory, enabled engineers to design controllers for individual substructures and to synthesize these decentrally-designed controllers into a global controller [5, 10, 9]. This global controller synthesis approach accompanied existing techniques used for synthesizing substructures into a composite structure [3, 20]. A limitation of CCS is that there is no way to guarantee stability of the composite system. Composite system stability is also an issue for control design techniques germane to decentralized control [9].

In response to this limitation, Babuska developed a technique called the augmented physical component synthesis (APCS) method [7]. This method built off of the CCS technique by augmenting some of the dominant dynamics of adjacent substructures with the substructure under consideration [20]. A controller is then designed for the substructure, with augmented dynamics from neighboring substructures (components). Results were shown to be better than those for the CCS method; however, no guarantee of composite stability could be made, and the resulting composite controller had a centralized implementation [7].

A limitation to both CCS and ACPS methods is that no a priori guarantees for composite system stability could be made. A second limitation to these techniques is that they did not consider the fact that real structures would have uncertainty. The model used for control design does not perfectly match the actual dynamics of the structure.

In the dissertation authored by Babuska, he began to investigate a limitation to CCS and APCS. The question of interest was how to address uncertainty in the substructures and substructure interconnections [7]. In this investigation, he adapted a robust control approach for decentralized control of connected structures, where substructure interconnection uncertainty was modeled as an additive nonparametric uncertainty.

A limitation to the work by Babuska is that modeling interconnection uncertainty using an additive nonparametric approach is conservative [7, 17]. Furthermore, he did not make

connections to exactly how this nonparametric uncertainty quantification was physically related to the substructure interconnection. In his work, he made the open-ended assertion that “interconnection uncertainty could be modeled as a [nonparametric] internal feedback loop”.

The work by Lim, which was an extension of Babuska, formulated a robust control approach to substructure controller synthesis [6]. In Lim, multiple robust control design techniques were compared and contrasted where he used centralized and decentralized controller architectures for the substructure control problem. He also explicitly accounted for substructure interconnection uncertainty parametrically. Although Lim took a comprehensive approach to robust, decentralized controller design, his work is limited in two ways that will be addressed in this research:

1. Robust control design approaches, such as μ -synthesis, for systems with real parametric uncertainty lead to conservative control designs [14, 22, 23, 24, 13];
2. A finer approach to quantifying, and incorporating, information about the nature of the uncertainty into controller design and synthesis is possible.

Robust control treats system uncertainty as existing in some ball of uncertainty, where the actual system is allowed to exist with equal probability within this ball. Treatment of uncertainty in this manner is equivalent to giving system uncertainty uniform probability distributions, and it is this treatment of uncertainty that leads to conservative control designs [14]. Most real physical systems, such as structures, will more likely exist in certain regions of this ball and are less likely to exist in others.

If the limitations enumerated above can be overcome, then two inherently related benefits are achieved:

- A reduction in design conservatism;
- The inclusion of more realistic interconnection uncertainty descriptions is possible.

These benefits can be realized using techniques from the field of control theory called probabilistic robust control (PRC) [14]. PRC allows the enforcement of probability distributions on both nonparametric and parametric uncertainty in a system.

We will next review some specific, relevant research as it pertains to decentralized structural control. Some of these approaches account for substructure interconnection uncertainty; some do not. We will also review some of the limitations that exist in decentralized control — generally speaking — and will conclude with a review of some of the approaches germane to probabilistic robust control. Some of the approaches that will be reviewed from probabilistic robust control are used in this thesis, however, other methods have some limitations that must be highlighted, as certain decisions made along with approaches developed in this thesis were constructed to overcome some of these limitations.

2.2 A REVIEW OF SOME LIMITATIONS IN DECENTRALIZED CONTROL

Large scale system theory and decentralized represents a deep subset of research within control theory, and has been active for almost 40 years [5, 9]. An introduction to the basics behind this theory is needed, as elements of this theory arise in the decentralized control of substructures as approached by Babuska, Su, Craig, and Lim [7, 21, 20, 6]. The entire basis for the development of large scale system theory boils down to the development of techniques that allow for the decomposition of large systems into smaller ones for controller design, and for development of control techniques that rely on using only local measurements and actuators for regulation and tracking in large scale systems. By virtue of information and actuation signals being local, we are now examining control system architectures that are decentralized. A brief introduction to some central notions behind large scale systems theory will be provided.

Let us consider the LTI state space system

$$\dot{x} = Ax + Bu \quad (2.1)$$

$$y = Cx. \quad (2.2)$$

The system given by (2.1) and (2.2) can be partitioned into N subsystems, where each subsystem $i \in [1, N]$ can be represented as:

$$\mathcal{S}_i : \begin{cases} \dot{x}_i = A_i x_i + B_i u_i + \sum_{j=1}^N A_{ij} x_j \\ y_i = C_i x_i \end{cases} \quad (2.3)$$

where A_{ij} describes subsystem interconnections. In decentralized control, a most basic approach to design, synthesis, and implementation of decentralized control involves ignoring these interconnections and designing controllers for each subsystem \mathcal{S}_i (hence with $A_{i,j} = \mathbf{0}$ and each A_i, B_i, C_i of appropriate dimension). Decentralized control is achieved insomuch that the original system is controlled without sharing state information between these now “local” controllers. An adaptation of this method, coined the Substructure Component Synthesis (SCS) method by Craig [21] was created where substructure controllers are designed while ignoring interconnections; however, a global controller is formulated from the decentrally designed substructure controllers. Craig’s SCS technique is most applicable to situations where the interconnections are known with absolute certainty. Furthermore, this technique is good to use in situations where a component has varying or complicated variations in geometry, allowing for a reduction of the composite structure into substructures so that focus can be placed on individual substructure design and analysis.

In large scale system theory, the subsystems \mathcal{S}_i are typically of high dimension, and theory has been developed by [9] and others for finding the stability of the composite system using the Bellman-Matrosov concept of vector Lyapunov functions. This same theory is then used to find interconnection polyhedra¹ that guarantee stability of the interconnected system. As implied here, finding the stability boundary in this manner yields a hard, deterministic bound on stability in terms of the interconnection parameters. For this technique, there is no way to guarantee a priori stability of the decentrally controlled interconnected/composite system. One aspect of decentrally controlled systems that becomes evident is that the

¹Polyhedra is used, here, as Siljak’s theory enables one to find interconnection parameter bounds that may not be extrema, yet prove stability nonetheless. The optimal answer may be found but the transformations performed in doing so leads to loss in interconnection parameter physical interpretation. See Theorem 6.1 of [5] with associated proof. Probabilistic techniques could be used to aid the search for physically-meaningful interconnection parameter bounds that are “close” to the optimal answer, but this endeavor is not investigated in this thesis.

strength of the interconnections, given by $A_{i,j}$ in (2.3), can hint, slightly, at whether or not the composite system may be stable. Systems that are strongly coupled, like structures, make decentralized controller design and synthesis difficult. In what appears to be the first application of decentralized structural control in 1989, Young was quick to point this out [25].

In the 2008 review article written by Bakule, he covered the state of the art in decentralized control [26]. In this review, he covered controller synthesis for “strongly coupled systems”. Due to the intrinsic strength of the interconnections in structures, we almost always find ourselves dealing with what can be considered a strongly coupled system in the area of decentralized control. Synthesis of decentralized controllers for strongly coupled systems reduces to developing, or applying, decentralized control synthesis strategies that account for the neighboring subsystem’s dynamics. In this manner, controller synthesis for strongly coupled systems is really a co-synthesis strategy. We cannot decouple systems, synthesize controllers for each subsystem, and reconnect with the expectation that stability or performance requirements will be met in any way.

For the synthesis of decentralized controllers for strongly coupled systems with some norm-bounded interconnection uncertainty, Bakule did discuss that LMI-based techniques could be used to achieve this end. Indeed, a recent structural control application, for a lumped-parameter spring-mass-damper model in building earthquake control, was implemented by Wang in 2009 by enforcing sparsity constraints on decision variables in a full-state feedback \mathcal{H}_∞ synthesis problem [27]. Palacios-Quiñonero also applied decentralized, and semi-decentralized control techniques for structural vibration control; again, these models were lumped-parameter spring mass damper models, wherein techniques such as overlapping decompositions were used for achieving these ends [28, 29, 9]. The papers by Wang and Palacios-Quiñonero are highlighted here, as their techniques align a bit more closely with decentralized control, and less with the high-dimensional decentralized structural vibration control approaches discussed in section 2.1. Presently, no techniques exist in the area of decentralized control where the interconnection parameters are treated as having random uncertainty.

2.3 PROBABILISTIC ROBUST CONTROL: EVOLUTION OF THE FIELD AND SOME LIMITATIONS

This section provides an overview on how the field of probabilistic robust control came to fruition, including some of the threads within this field. Since this field’s inception, several prominent — and oft celebrated — techniques have been developed. These techniques will be briefly described, with some discussion on their positive attributes, as well as limitations, and how these attributes and limitations have guided the development of the control synthesis techniques in this thesis. Specifically, this section will cover:

- Stochastic robustness and evolutionary algorithms in probabilistic robust control [2, 1, 30, 31, 12, 32];
- Statistical learning theory in control [33, 34, 13, 35, 36];
- The scenario-based approach in probabilistic robust control [16, 14].

Development of PRC began in the early 1990’s through the work of Robert Stengel, where Stengel and colleagues began analyzing the robustness of uncertain, controlled systems using Monte Carlo methods [2, 1, 11]. What started out as a technique that just analyzed the “stochastic robustness” [30] of controlled systems gradually turned into using this probabilistic uncertainty during controller design and synthesis [31, 12, 32, 37, 38, 39]. Subsequently, researchers [14, 40, 16, 41] developed formal theory to support the use of PRC and drew direct connections to the field of robust control, [17] where in the monograph by Tempo, Calafiori, and Dabbene they showed how PRC addresses robust control limitations of conservatism and complexity [23, 42, 41, 14]. In addition to reducing design conservatism and computational complexity, the PRC paradigm gives rise to an alternative way of characterizing the stability and performance of controlled systems by quantifying the probability of stability and the probability of meeting performance.

By bridging the field of PRC to the robust substructure control techniques developed by Babuska and Lim almost 20 years earlier, limitations related to design conservatism and uncertainty quantification in the robust substructure control problems can be addressed, thereby advancing the state of the art.

2.3.1 Stochastic Robustness and Evolutionary Algorithms in Probabilistic Robust Control

Stengel's highly cited paper [2] addresses the basic concepts of stochastic robustness of linear time invariant systems. These basic concepts will be discussed, here, with acknowledgement toward the techniques that were birthed from this thread of research. In addition, a comparison between the fundamental, conceptual, differences between deterministic parameter bounding (robust control theory) and probabilistic robust control theory will be made.

The best system to motivate this subject with is the linear time-invariant, spring-mass-damper (SMD) equations of motion, whose characteristic equation is given by:

$$s^2 + 2\zeta\omega_n s + \omega_n^2 = 0. \quad (2.4)$$

For a real engineering system, it is known that the model of the plant is not going to match the true plant [17]. With that said, we know that the mass, stiffness, and damping of the SMD system will have some parameter uncertainty/variation. It is standard in robust control theory to treat parameter variations using linear fractional transformations (LFTs), where we would place hard bounds on the mass, stiffness, and damping coefficients [43]. Placing hard bounds on parameter coefficients can lead to overly-conservative designs, as we end up designing controllers for the worst-case plant configuration [33, 13, 14].

Probabilistic robust control theory instead associates some probability density functions, or distributions, with these parameter variations. In this framework, any probability density function could be used, but for motivating this topic we will focus on normal distributions.

For the standard characteristic equation given in (2.4) we can treat the damping and natural frequency as being statistically independent variables. By giving the damping coefficient and natural frequency the normal distributions:

$$\zeta \sim \mathcal{N}(0.1, 0.025) \quad \omega_n \sim \mathcal{N}(4.5, 0.5)$$

for the case where these parameters are normally distributed, and conversely describing them using the following uniform distributions:

$$\zeta \sim \mathcal{U}(0.07, 0.13) \quad \omega_n \sim \mathcal{U}(4, 5)$$

we can then sample from these distributions, solving for the system's eigenvalues at each iteration, and project the results for each distribution into the complex plane. The resulting pole-zero maps are shown in figure 2 and the associated bivariate histogram is shown in figure 3.

Modeling system uncertainty in this way introduces two alternative (probabilistic), system-theoretic notions: probability of stability and probability of meeting performance requirements. Stability is a binary condition: a system is stable or it is not. We also know that for the second-order system example our eigenvalues are described by $\lambda_{1,2} = \sigma \pm j\omega$ where asymptotic stability is described by all $\lambda_{1,2}$ whose real parts lie in the open left half of the complex plane. Since we know that the set of our systems, in terms of our binary metric of stability, has a probability of 1 of being stable or unstable (by virtue of a system's mere existence):

$$\Pr(\text{stability}) + \Pr(\text{instability}) = 1 \tag{2.5}$$

we can define the probability of instability in the following manner:

$$\Pr(\text{instability}) = 1 - \int_{-\infty}^0 \Pr(\text{Re}(\lambda) < 0) d\lambda \tag{2.6}$$

where $\Pr(\text{Re}(\lambda) < 0)$ is the joint probability that all real parts of the eigenvalues are in the left-half plane. $\Pr(\text{Re}(\lambda) < 0)$ does not necessarily have a closed-form solution. We can turn to Monte Carlo evaluation of the probability of stability by generating N instances of our

Eigenvalue Distributions for Stable Second Order System - Uniform vs. Normal Distributions

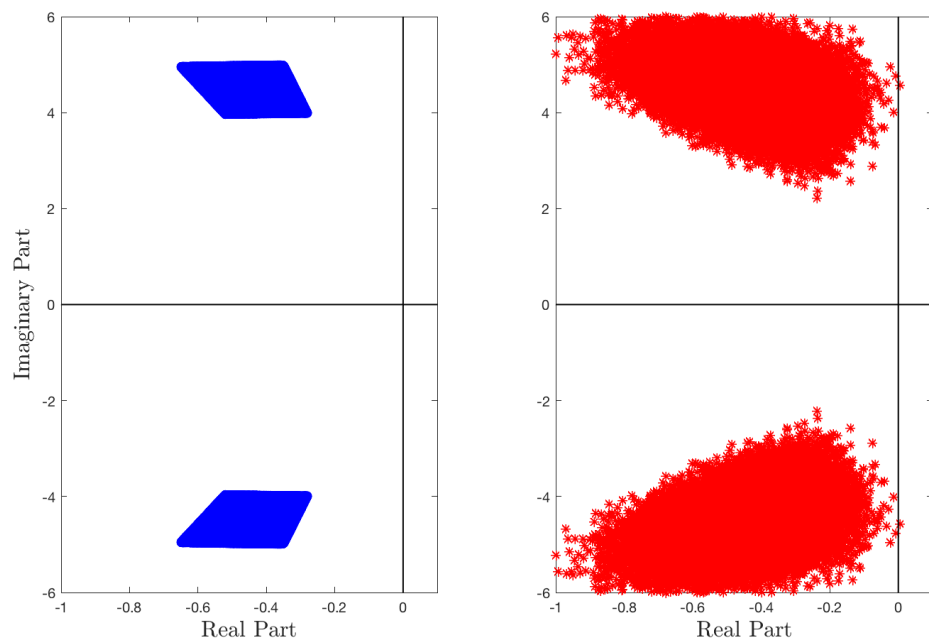


Figure 2: This figure is similar to those that appeared in Ray and Stengel's papers [1, 2] on stochastic robustness.

Bivariate Eigenvalue Histograms for Uniform and Normal Parameter Distributions

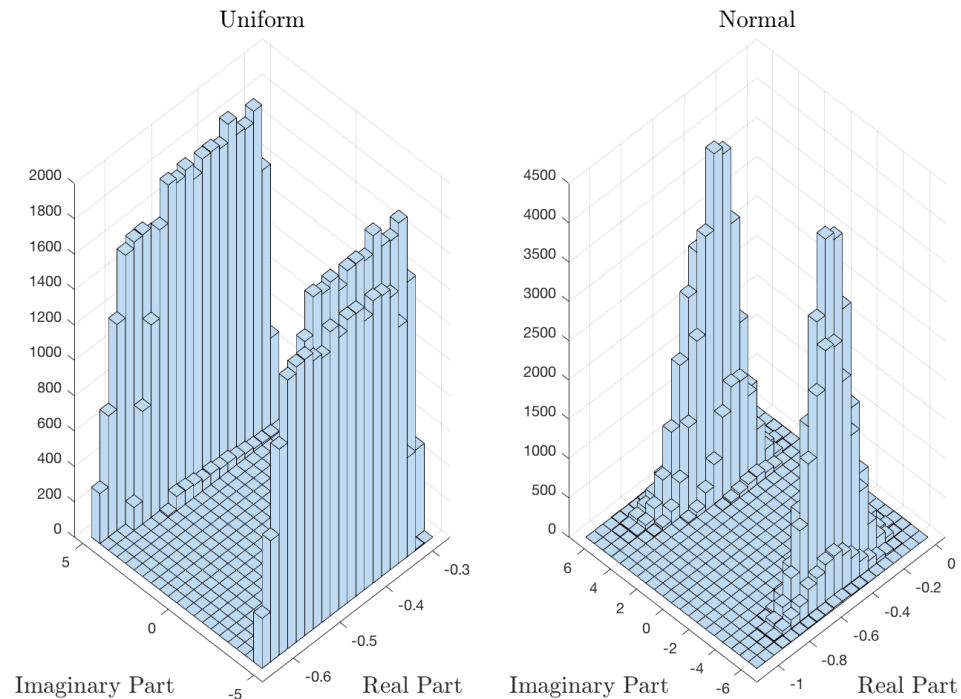


Figure 3: This figure is similar to those that appeared in Ray and Stengel's papers [1, 2] on stochastic robustness.

system (2.4) and equating the probability of stability by:

$$\int_{-\infty}^0 \Pr(\operatorname{Re}(\lambda) < 0) d\lambda = \lim_{N \rightarrow \infty} \frac{\sum_{i=1}^N \mathbb{I}_i(\Xi)}{N} \quad (2.7)$$

where $\mathbb{I}(\Xi)$ is the indicator function, given by

$$\mathbb{I}(\Xi) = \begin{cases} 1 & \operatorname{Re}(\lambda) < 0 \\ 0 & \text{otherwise.} \end{cases} \quad (2.8)$$

Something else that is clear about this problem and that is implicit is that we have a probability of instability that is conditioned on the parameter distributions. This is easily generalized for a closed-loop or high dimensional system.

We can likewise apply this technique to look at the conditional probability that the system will be both stable *and* meet some performance metrics. For instance, for the system we just examined with $\zeta \sim \mathcal{N}(0.05, 0.03)$, $\omega_n \sim \mathcal{N}(10, 1)$ we can impose that we are interested in the intersection of those systems that are stable and those systems that also have some settling time below some threshold: say $T_s = 6.824s$ (noting that for the nominal (mean) case, here, the settling time is 7.824s). With $T_s = -\frac{\ln(0.02)}{\omega_{n,0}\zeta_0}$, $\omega_{n,0} = 10 \text{ rad/s}$, and $\zeta_0 = 0.05$ we can examine, using Monte Carlo techniques:

$$\Pr(\text{stability}) \cap \Pr(0 < T_s \leq 6.824s). \quad (2.9)$$

For notational convenience we will refer to stability as the event s and meeting settling time performance as the event p . From probability calculus we know that the general multiplication rule can be expressed as:

$$\Pr(s \cap p) = \Pr(s|p)\Pr(p) = \Pr(p|s)\Pr(s). \quad (2.10)$$

We know that the only way for our system, here, to meet performance requirements is for the system to also be stable, meaning that the event, p , is a subset of the set of stable systems s . We see:

$$\Pr(s|p) = 1 \quad \text{since} \quad p \subseteq s, \quad (2.11)$$

allowing us to find the probability of meeting performance requirements:

$$\Pr(p) = \Pr(p|s)\Pr(s), \quad (2.12)$$

and so it follows that

$$\Pr(s \cap p) = \Pr(p). \quad (2.13)$$

This is an obvious link that we take for being implicit in deterministic settings. And so we can draw a link between these two, given prior knowledge about parameter distributions, to examine the conditional dependency of these dynamic system metrics in a probabilistic fashion: given that our system is stable, what is the probability that we'll meet performance requirements?

In this dynamic system framework it is interesting to think about this notion, which provides a probabilistic link between performance and stability. These two metrics are typically treated as being separate; that is, we prove stability and then we focus on meeting performance requirements. However, it is implicit that any system that meets some performance requirements must also be stable (unless it is desirable for our system to be unstable). This notion surrounding some basic probability calculus was not just provided as some academic exercise; the cost function constructed for solution of the controller synthesis/optimization problem in chapter 7 can be very expensive, especially for some of the high dimensional systems studied in this thesis, and so conditional dependencies between any stability or performance metrics are exploited when formulating these cost functions. As will be shown in this thesis, the computational complexity of the algorithms used for synthesis becomes important in this work.

For the example just discussed, the probability of meeting settling time requirements given that the system is stable, expressed by the term $\Pr(p|s)$, is evaluated to be 0.4201. And overall, $\Pr(p) = 0.3997$. These estimates used $N = 10,000$ Monte Carlo samples. This discussion on stochastic robustness was provided as a means of discussing the basic notions behind this framework. The researchers cited herein have extended these basic notions into control design and synthesis for both linear and nonlinear systems [44, 45, 11, 1, 30, 31].

So far, we have only introduced the notions of probability of stability and probability of meeting performance requirements, which should both be thought of as metrics describing probabilistic robustness. Next, we will briefly introduce probabilistic robust compensator design and synthesis [30, 12, 31, 37, 32]. The design of a probabilistic robust controller was approached by Morrison in the following way: probabilistic robust control can characterize compensator robustness by defining a probability, $\Pr(p)$, that the closed-loop system will have acceptable performance in the presence of parameter uncertainties. This probability, $\Pr(p)$, is characterized by:

$$\Pr(p) = \int_V \mathbb{I}[G(v), K] \Pr(v) dv \quad (2.14)$$

where G is the plant, K is some candidate controller, V is the space of possible parameter variations, $v \in V$ is a point in V , and $\Pr(v)$ is the probability density function over the parameter variations. $\mathbb{I}[\cdot]$ is the binary indicator function that equals 1 if $G(v)$ and K form an acceptable system and 0 if not.

A stochastic optimization problem is formulated by defining a cost function, J ,

$$J = f(\Pr(p_1), \dots, \Pr(p_n)), \quad j = 1 \dots n \quad (2.15)$$

where each element describes the probability that a given plant-controller pair meets some metric of importance to the designer. Recalling our motivating example from previous, we could have considered a static compensator design K and evaluated the probability of meeting stability and performance ($T_s = 6.824s$); obviously, this only examines one compensator configuration. A search over compensator configurations $K(d)$, $d \in D$ along with a cost evaluation, $J(K(d)) = f(\Pr_d(p_1), \dots, \Pr_d(p_n))$, $j = 1 \dots n$ allows for us to find the “best” compensator for our parametrically-uncertain plant. Now, $\Pr_d(p_j)$ arises from:

$$\Pr_d(p_j) = \int_V \mathbb{I}_j[G(v), K(d)] \Pr(v) dv \quad (2.16)$$

which can be evaluated using Monte Carlo techniques, turning this integral into the following summation to get an estimate of the integral's value as:

$$\hat{\Pr}_d(p_j) = \frac{1}{N} \sum_{m=1}^N \mathbb{I}_j[G(v_m), K(d)] \quad (2.17)$$

$$\hat{J}(K(d)) = f\left(\hat{\Pr}_d(p_1), \hat{\Pr}_d(p_2), \dots, \hat{\Pr}_d(p_n)\right), \quad j = 1 \dots n \quad (2.18)$$

and from the law of large numbers, we have that $\hat{J} \rightarrow J$ as $N \rightarrow \infty$ [12, 14]. A very attractive aspect to this general approach is the following: *the accuracy of the probability estimate is not dependent upon the order of the plant or candidate controller*. A drawback, however, is that we cannot make any a priori guarantees related to meeting stability or performance requirements using these methods. What we can guarantee, however, is that we place focus on searching over the stable controller configurations.

Stengel, Garrison, and Wang used genetic algorithms for searching over candidate controller variables for probabilistic robust synthesis of linear and nonlinear controllers, primarily for aircraft applications. Their systems had less than 10 states, however some of their cost functions had as many as 39 probability terms [12, 32]. In chapter 7, we deal with random plant/controller pairs that have over 400 state variables in a generalized regulator framework.

2.3.2 Statistical Learning Theory and Control

The probabilistic robust control paradigm has grown over the past several decades, and several elegant and powerful techniques have matured. We must point out the research that has been performed into statistical learning theory for controller design and synthesis, as pursued by Vidyasagar, Kolthcinskii, and others [33, 13, 34, 46, 13, 47, 36, 35, 14, 48]. And so a brief review of these techniques is provided, along with the identification of some limitations, which are especially onerous in the context of the specific problem pursued in this thesis.

In the work by Vidyasagar, he showed that statistical learning theory, via uniform convergence of empirical means (UCEM) can be used to establish sample bounds in a controller

synthesis process for finding controllers that satisfy performance constraints expressed as a finite family of boolean polynomial inequalities [34, 13]. Furthermore, using UCEM has the benefit of no longer focusing on the “worst-case” design that accompanies robust control methods (such as μ -synthesis), rather the focus is placed upon finding controllers that achieve performance “most of the time”. Mathematically, this performance constraint is

$$f(y) \doteq E_{P_x}[g(x, y)] \quad (2.19)$$

where $E_{P_x}[\cdot]$ is the expectation, with variables x distributed according to a probability distribution P_x . The function $g(x, y)$ is the performance function, which is dependent upon controller variables $y \in Y$ and plant variables $x \in X$. If we suppose that we select real parameters $\epsilon, \alpha, \delta > 0$, which are related to the accuracy (ϵ), level (α), and confidence ($1 - \delta$), the probability that the randomized algorithms fail to find what is called a “probably approximate near minimum” of the objective function $f(y)$ can be determined using the following algorithm from Vidyasagar [13]:

Algorithm 1. *Select integers n, m such that*

$$n \geq \frac{\log_{10}(2/\delta)}{\log_{10}[1/(1 - \alpha)]} \quad \text{and} \quad q(m, \epsilon; \mathcal{G}) \leq \delta/2. \quad (2.20)$$

Generate i.i.d. samples $y_1, \dots, y_n \in Y$ according to distribution P_y and $x_1, \dots, x_m \in X$ according to P_x . Define

$$\hat{f}_i \doteq \hat{f}_i(y_i) = \frac{1}{m} \sum_{j=1}^m f(x_j, y_i), \quad i = 1, \dots, n, \quad \text{and} \quad (2.21)$$

$$\hat{f}_0 \doteq \min_{1 \leq i \leq n} \hat{f}_i. \quad (2.22)$$

Then with confidence $1 - \delta$, it can be said that \hat{f}_0 is a probably approximate near minimum of $f(\cdot)$ to accuracy ϵ and level α .

The term $q(m, \epsilon; \mathcal{G})$ is related to a family of functions that has the UCEM property — these functions are those that are used for achieving some kind of performance with respect to our random system, and are special in that they possess what has been defined to be the Vapnik-Chervonenkis (VC-) dimension. The VC dimension is integral in determining an

upper-bound for choosing the integer m used in this algorithm. The integer, m , is related to the number of random plant samples required during controller synthesis. The VC dimension of a family of measurable functions \mathcal{A} that maps variables in X into $\{0, 1\}$, is denoted by $\text{VC-dim}(\mathcal{A})$. The VC-dimension leads to a definition of the largest integer m such that there exists a set of cardinality m that is shattered by \mathcal{A} . See [13] and specifically [49] for examples and further detail.

Choosing n, m for the robust stabilization problem, and for a system that approaches the size of that studied in chapter 7, will be highlighted momentarily. We now restate Theorem 1 without proof from Vidyasagar, which establishes bounds on m [13].

Theorem 1. *Suppose \mathcal{A} is a family of measurable functions X mapping into $\{0, 1\}$, and that $\text{VC-dim}(\mathcal{A}) \leq d < \infty$. Then \mathcal{A} has the UCEM property, whatever be the probability measure P_x . Moreover*

$$q(m, \epsilon; \mathcal{A}) \leq 4 \left(\frac{2em}{d} \right)^d \exp(-m\epsilon^2/8), \quad \forall m, \epsilon. \quad (2.23)$$

Moreover, $q(m, \epsilon; \mathcal{A}) \leq \delta$ provided

$$m \geq \max \left\{ \frac{16}{\epsilon^2} \log \frac{4}{\delta}, \frac{32d}{\epsilon^2} \log \frac{32e}{\epsilon^2} \right\}. \quad (2.24)$$

Proof. See the book by Vidyasagar [49].

At this point in time, two things must be recognized:

1. A probability distribution is defined over the possible controller variables Y , which may feel a bit unnatural (also pointed out by Tempo et. al. in [14]);
2. We see that we are choosing the best, or minimum, function value that is averaged over all random plant / controller combinations (which was a “disappointing” result pointed out by Vidyasagar in his papers [33, 13]). This result illustrates that we may have *many* plant/controller pairs to evaluate. At the same time, we still have an algorithm that is executable within polynomial time that permits a priori guarantees of meeting probabilistic stability and performance requirements, which is part of what has motivated the development of probabilistic techniques in control theory [23].

The theoretical details behind this algorithm are sparse here, as the intention here is to give a flavor for the complexity of this approach for high-dimensional control systems, such as those pursued in this thesis. To illustrate the complexity of this approach, we now focus our attention on one controller synthesis problem that can be solved using statistical learning theory: robust stabilization. Stated concisely, this canonical robust control problem is one where we wish to: find some controller, $K(y), y \in Y$, that stabilizes most of the plants $G(x)$ where $x \in X$, $X \sim P_x$.

In Vidyasagar [13], he defined the function

$$g_y(x) \doteq g(x, y) = \begin{cases} 1 & \text{if the pair } (G(x), K(y)) \text{ is unstable} \\ 0 & \text{otherwise.} \end{cases} \quad (2.25)$$

In the frequency domain, the plants $G(x, s)$ and controllers $K(y, s)$ were of the following form:

$$G(x, s) = \frac{n_G(x, s)}{d_G(x, s)}, \quad \forall x \in X \quad (2.26)$$

$$K(y, s) = \frac{n_K(y, s)}{d_K(y, s)}, \quad \forall y \in Y \quad (2.27)$$

where n_G, d_G are polynomials in x, s with degree in s at most α_s . He restricted the plant to be strictly proper. n_K, d_K are analogous, with the exception that he restricted $K(y, s)$ to be proper with McMillan degree β_s . Furthermore, he assumed that $n_K(y, s)$ and $d_K(y, s)$ were polynomials in y of degree no larger than β_y , and lastly that $X \subseteq \mathbb{R}^k, Y \subseteq \mathbb{R}^l$ for integers k, l . The integer l represents the number of “degrees of freedom” in the controller K . Under these assumptions, we restate Theorem 4 without proof from Vidyasagar [13]:

Theorem 2. *Under the assumptions given above, the family of binary-valued functions $\mathcal{G} \doteq \{g_y : y \in Y\}$ has finite VC-dimension. In particular,*

$$\text{VC-dim}(\mathcal{G}) \leq 2l \log[4e(\alpha_s + \beta_s)^2 \beta_y]. \quad (2.28)$$

If we assume that our plant is SISO with 400 states and that the controller is SISO with 400 states we get $\text{VC-dim}(\mathcal{G}) \leq d = 34,796$. If we choose “reasonable” values for ϵ, δ, α , such as

$\epsilon = 0.01, \delta = 0.05, \alpha = 0.01$, using equation 2.24 we have

$$m \geq 152,279,280,019. \quad (2.29)$$

And from algorithm 1, we get

$$n \geq 368. \quad (2.30)$$

Thus, we would have to sample into our controller space 368 times, and try each of these controllers with 152,279,280,019 samples from the random plant. Note that this approach assumes that the distribution and hypercube over the possible controller parameters is chosen judiciously, such that we even have a solution within the hypercube of controller parameters, and only applies for the case where we want a controller that is robustly stabilizing. The examples used by [13, 35] use controller parameter intervals where solutions are known to exist. In addition, the sample bounds provided above are for a SISO plant/controller pair. In chapter 7, we are dealing with a MIMO generalized regulator structure.

Some limitations must be pointed out with respect to statistical learning theory. These limitations by no means denigrate these approaches — they are pointed out to highlight their unsuitability for the decentralized, dynamic output feedback \mathcal{H}_∞ control of high-dimensional lightly-damped structures:

1. Sample complexity. This is dependent upon the VC-dimension, which is directly related to the dimension of the plant, controller, and number of “free” controller variables.
2. Bounding or choosing a hypercube for constraining the optimization parameters can lead to an inadvertent “leaving out” of good portions of a solution space, or will make it so large that randomly sampling a “good” plant is highly improbable. Statistical learning theory is also predicated on imposing a probability distribution over the controller variables. Aside from choosing a uniform distribution, making a good choice for a high-dimensional system would be very difficult and feels somewhat unnatural.
3. Despite the fact that the number of plant samples is divorced from the number of controller samples, we still have to try every plant-controller pair, and choose the best one.

The theoretical elegance and sophistication of this technique cannot be downplayed, and numerous researchers have been working to develop machinery for obtaining less-conservative estimates of the VC-dimension for specific families of boolean-polynomials (see [46, 13, 47, 36, 35]). However, for the high-dimensional problem pursued in this work, pursuing such techniques was deemed to be impractical. Even with advances in determining reduced sample sizes, for plants and controllers of several hundred states, this technique would still suffer from the limitations enumerated above.

2.3.3 Some Results from Probabilistic Robust Structural Control

Researchers have broached probabilistic robust structural control in the past. Several of the more significant pieces of research are highlighted, here, however, the work in this thesis is distinguished from their research in the following ways:

- This research focuses on decentralized controller design, synthesis, and implementation.
- We focus on random interconnection uncertainty, and not uncertainty distributed over the entirety of the structural model’s parameter space.
- High dimensional structural models and controllers are considered, here, with attention paid to the computational efficiency of the algorithms developed.
- For both the full-state feedback, as well as dynamic output feedback controller cases, \mathcal{H}_∞ control objectives are featured.

Guo, in [50], developed a technique that has \mathcal{H}_∞ control objectives and uses an LMI-based approach for controller synthesis. However, a decentralized architecture with focus on interconnection uncertainty is not pursued. The method developed in chapter 5 differs from this approach in that we demonstrate that a complex performance output function can be formulated, permitting control design and frequency-weighting in complex modal coordinates, and we also show how a decentralized control architecture can be incorporated using sparsity constraints in the decision variables of a semidefinite program.

Crespo, in [51, 52], used both time and frequency-domain metrics for achieving a probabilistic robust solution, with a focus on “reliability control synthesis,” which is a synthesis

approach that is very similar to the approaches discussed in section 2.3.1, and is implicit in the approach developed in chapter 7. Basically, the cost function is penalized for exceeding some specified value, which are termed as “failure boundaries” in Crespo’s work. This focus, which uses a “reliability” metric, is similar to a definition that Guo also used in [50]. Crespo demonstrated his technique using low order models for satellite attitude control. Decentralized control architectures were not considered, nor were \mathcal{H}_∞ performance objectives. In this thesis, it is also demonstrated that control design and synthesis can be performed directly over the field of complex numbers of a state space system for achieving the end of synthesizing low-order, static, probabilistically robust decentralized full-state feedback \mathcal{H}_∞ controllers and also high-order, dynamic, probabilistically robust dynamic output-feedback \mathcal{H}_∞ controllers.

May, in his dissertation titled “Probabilistic Robust Control: Theory and Applications”, developed approaches for probabilistic robust control of low-order, lumped parameter, civil structures [44]. His control objectives did not involve \mathcal{H}_∞ performance. His thesis involved the development of static output and full-state feedback controllers using “failure probability” and \mathcal{H}_2 performance measures. His performance measures, being that he was interested in civil engineering applications, were related to the minimization of inter-story drift, absolute acceleration at certain points in the structure, and the magnitude of the base shear between the structure and its foundation. A “probabilistically reliable” design ends up being related to the probability that certain thresholds, as they are related to these metrics, are not exceeded. His probabilistic robust control synthesis approach involved asymptotic approximation of probability integrals for estimating total failure probability, which during optimization, is a method whose computation time grows exponentially with the number of uncertain parameters. For this reason, high-dimensional control synthesis would be very difficult. May did not focus on dynamic compensator synthesis, a decentralized control architecture, \mathcal{H}_∞ control objectives, or frequency domain-based design, which are all features of this research.

3.0 PRELIMINARIES

This background section is meant to introduce some of the general mathematics and notation used throughout this thesis. These tools and definitions are used in chapters 4, 5, 6, and 7.

3.1 SCALAR, VECTOR, AND MATRIX NOMENCLATURE

Scalar and vector-valued variables will be lowercase. These variables will be distinguished by pointing out their size. For example, given $x_s \in \mathbb{R}$, $x_v \in \mathbb{R}^n$, x_s is a scalar, real-valued variable and x_v is a real-valued vector of length n . Similarly, we will also deal with scalars and vectors that exist over the field of complex numbers. These will be denoted as $x_s \in \mathbb{C}$, $x_v \in \mathbb{C}^n$. Matrices will be represented using upper-case letters, with sizes denoted as

$$A_r \in \mathbb{R}^{n \times n}, \quad A_c \in \mathbb{C}^{n \times n}. \quad (3.1)$$

Some matrix, A , that is in the cone of symmetric matrices will be denoted $A \in \mathbb{S}^{n \times n}$. If A is complex and symmetric it is hermitian, which will be denoted by $A \in \mathbb{H}^{n \times n}$.

3.1.1 Positive and Negative (Semi)Definiteness

A matrix, Q , is positive definite if and only if (iff) for any vector $x \neq 0$,

$$x^H Q x > 0. \quad (3.2)$$

If a matrix is positive definite, the following properties also hold:

$$Q = Q^H, \quad \text{Re}(\lambda(Q)) > 0, \quad \text{Im}(\lambda(Q)) = 0 \quad (3.3)$$

where Q^H denotes the hermitian transpose. Q may be a real or complex matrix. The $\lambda(Q)$ refers to the eigenvalues of Q . $\text{Re}(\cdot)$ specifically refers to the real parts and $\text{Im}(\cdot)$ specifically refers to the imaginary parts of the matrix. For a matrix to be positive definite, it must be symmetric and all eigenvalues must be real and strictly positive. Positive definiteness is indicated by $Q > 0$.

A matrix, Q , is positive semidefinite iff for any vector $x \neq 0$,

$$x^H Q x \geq 0. \quad (3.4)$$

If a matrix is positive semidefinite, the following properties also hold:

$$Q = Q^H, \quad \text{Re}(\lambda(Q)) \geq 0, \quad \text{Im}(\lambda(Q)) = 0 \quad (3.5)$$

which says that the conditions of positive definiteness are relaxed by permitting Q to have eigenvalues that are equal to zero. There are other (equivalent) properties that characterize positive definiteness of matrices, however, these two properties are all that are really needed here.

Negative (semi)definiteness has the same requirements, however, we have that for some $Q = Q^H$ and $x \neq 0$ that

$$x^H Q x < (\leq) 0 \quad (3.6)$$

and that $\text{Re}(\lambda(Q)) < (\leq) 0$.

3.2 SYSTEM REPRESENTATIONS

All system model will be represented as generalized plants in state space form or, as will be shown to be equivalent, transfer function matrices. That is, a system will have the description

$$\begin{aligned}\dot{x} &= Ax + B_1 w + B_2 u \\ z &= C_1 x + D_{11} w + D_{12} u \\ y &= C_2 x + D_{21} w + D_{22} u.\end{aligned}\tag{3.7}$$

These system matrices have the sizes $A \in \mathbb{R}^{n \times n}$, $B_1 \in \mathbb{R}^{n \times r_1}$, $B_2 \in \mathbb{R}^{n \times r_2}$, $C_1 \in \mathbb{R}^{m_1 \times n}$, $C_2 \in \mathbb{R}^{m_2 \times n}$. The sizes of the vectors x, w, u, z, y and matrices $D_{11}, D_{12}, D_{21}, D_{22}$ are all implied by the sizes given.

By defining

$$B = \begin{bmatrix} B_1 & B_2 \end{bmatrix}; \quad C = \begin{bmatrix} C_1 \\ C_2 \end{bmatrix}; \quad D = \begin{bmatrix} D_{11} & D_{12} \\ D_{21} & D_{22} \end{bmatrix}; \quad u_g = \begin{bmatrix} w \\ u \end{bmatrix}; \quad y_g = \begin{bmatrix} z \\ y \end{bmatrix}\tag{3.8}$$

it is quickly seen that the transfer function matrix that maps $u_g \rightarrow y_g$ is given by

$$G(s) = D + C(sI - A)^{-1}B, \quad s = j\omega, \omega \in [0, \infty) \cup \{\infty\}.\tag{3.9}$$

As is typical in robust control, the shorthand for indicating this transformation which describes the equivalent time domain/frequency domain system representations will be adopted [17]. That is,

$$G(s) \sim \left[\begin{array}{c|c} A & B \\ \hline C & D \end{array} \right] = D + C(sI - A)^{-1}B, \quad s = j\omega.\tag{3.10}$$

3.2.1 The Linear Fractional Transformation (LFT)

Let $P(s)$ denote a 2×2 transfer function matrix that relates inputs u_1 and u_2 to outputs y_1 and y_2 :

$$\begin{bmatrix} y_1 \\ y_2 \end{bmatrix} = \begin{bmatrix} P_{11} & P_{12} \\ P_{21} & P_{22} \end{bmatrix} \begin{bmatrix} u_1 \\ u_2 \end{bmatrix}.\tag{3.11}$$

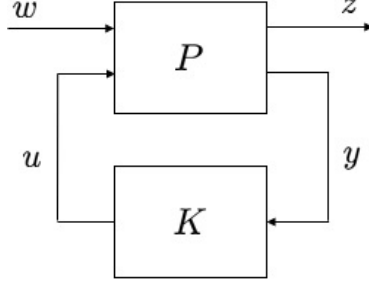


Figure 4: Generalized regulator framework.

Given some controller K , that connects y_2 to u_2 , we have

$$\begin{aligned} y_1 &= \left[P_{11} + P_{12}K(I - P_{22}K)^{-1}P_{21} \right] u_1 \\ &\doteq F_l(P, K)u_1 \end{aligned} \quad (3.12)$$

where $F_l(P, K)$ is called the lower linear fractional transformation (LFT) of P and K . In a similar manner, the upper linear fractional transformation, denoted $F_u(P, K)$ can be formed if we instead had $u_1 = Ky_1$. State space realizations of LFTs can also be formed, and will be explained next.

3.2.2 State-Space Realizations of LFTs

Given the two systems

$$P \sim \begin{bmatrix} P_{11} & P_{12} \\ P_{21} & P_{22} \end{bmatrix} = \left[\begin{array}{c|cc} A_1 & B_1 & B_2 \\ \hline C_1 & D_{11} & D_{12} \\ C_2 & D_{21} & D_{22} \end{array} \right], \quad K \sim \left[\begin{array}{c|c} A_3 & B_3 \\ \hline C_3 & D_3 \end{array} \right] \quad (3.13)$$

with interconnection described by figure 4, the lower LFT $F_l(P, K)$ is

$$F_l(P, K) = \left[\begin{array}{cc|c} A_1 + B_2FD_3C_2 & B_2FC_3 & B_1 + B_2FD_3D_{21} \\ B_3EC_2 & A_3 + B_3ED_{22}C_3 & B_3ED_{21} \\ \hline C_1 + D_{12}FD_3C_2 & D_{12}FC_3 & D_{11} + D_{12}FD_3D_{21} \end{array} \right] \quad (3.14)$$

where $E = (I - D_{22}D_3)^{-1}$ and $F = (I - D_3D_{22})^{-1}$. LFTs of systems and controllers are used throughout chapters 5, 6, and 7 of this thesis.

3.3 SIGNAL AND SYSTEM NORMS

Certain signal and system norms are defined here, with aid from the book by Doyle, Francis, and Tannenbaum [53].

3.3.1 Norms for signals

A signal is some $u(t) : \mathbb{R} \rightarrow \mathbb{R}$ where \mathbb{R} describes the field of real numbers. A signal may be zero for time $t < 0$. A norm must have the following four properties:

1. $\|u\| \geq 0$
2. $\|u\| = 0 \Leftrightarrow u(t) = 0, \quad \forall t$
3. $\|au\| = |a| \|u\|, \quad \forall a \in \mathbb{R}$
4. $\|u + v\| \leq \|u\| + \|v\|$

From this, we introduce the following useful signal norms:

2-Norm The 2-norm of $u(t)$ is given by

$$\|u\|_2 \doteq \left(\int_{-\infty}^{\infty} u(t)^2 dt \right)^{1/2}. \quad (3.15)$$

∞ -Norm The ∞ -norm of a signal is the least upper bound of its absolute value:

$$\|u\|_{\infty} \doteq \sup_t |u(t)|. \quad (3.16)$$

3.3.2 Norms for systems

Considering a linear time-invariant, causal, finite-dimensional system, which we will call G , we can give the time domain input-output equation for such a system via the convolution integral

$$y = G * u = \int_{-\infty}^{\infty} G(t - \tau)u(\tau)d\tau. \quad (3.17)$$

Letting $\hat{G}(s)$ denote the transfer function matrix of this system, which is the Laplace transform of the impulse response matrix $G(t)$, the ∞ -norm is given by

$$\|\hat{G}\|_{\infty} \doteq \sup_{\omega} \bar{\sigma}(\hat{G}(j\omega)), \quad \omega \in [0, \infty] \quad (3.18)$$

where $\bar{\sigma}(\hat{G}(j\omega))$ denotes the maximum singular value of the transfer function matrix $\hat{G}(j\omega)$.

A useful relationship is the following:

$$\|y\|_2 \leq \|\hat{G}\|_{\infty} \|u\|_2 \quad (3.19)$$

which can also be written as

$$\frac{\|y\|_2}{\|u\|_2} \leq \|\hat{G}\|_{\infty} \quad (3.20)$$

which shows, roughly, that the ∞ -norm of the system can be thought of as the maximum input/output signal amplification across all frequencies. A derivation for this relationship is provided in Doyle [53].

3.4 VECTOR NORMS AND BALLS

Letting $x \in \mathbb{F}^n$ where \mathbb{F} is either the real or complex field, the l_p norm of x is defined as

$$\|x\|_p \doteq \left(\sum_{i=1}^n |x_i|^p \right)^{1/p}, \quad p \geq 1. \quad (3.21)$$

The l_∞ norm of the vector x is defined as

$$\|x\|_\infty \doteq \max_i |x_i|. \quad (3.22)$$

The ball of radius ρ in the l_p norm is defined as

$$\mathcal{B}_{\|\cdot\|_p}(\rho, \mathbb{F}^n) \doteq \{x \in \mathbb{F}^n : \|x\|_p \leq \rho\} \quad (3.23)$$

with the boundary of this ball defined as

$$\partial \mathcal{B}_{\|\cdot\|_p}(\rho, \mathbb{F}^n) \doteq \{x \in \mathbb{F}^n : \|x\|_p = \rho\}. \quad (3.24)$$

3.5 MATRIX NORMS AND BALLS

Two classes of matrix norms are introduced. The first is the so-called Hilbert-Schmidt norm which is based on the isomorphism between the matrix space $\mathbb{F}^{n \times m}$ and the vector space \mathbb{F}^{nm} .

Hilbert-Schmidt Matrix Norm The Hilbert-Schmidt l_p norm of a matrix $X \in \mathbb{F}^{n \times m}$ is defined as

$$\|X\|_p \doteq \left(\sum_{i=1}^n \sum_{k=1}^m |X_{i,k}|^p \right)^{1/p}, \quad p \in [0, \infty) \quad (3.25)$$

$$\|X\|_\infty \doteq \max_{i,k} |X_{i,k}| \quad (3.26)$$

where $X_{i,k}$ is the (i, k) entry of the matrix X . Also introduced is the matrix column vectorization operator. Given a matrix $X \in \mathbb{F}^{n,m}$ the vectorization operator is given by

$$\text{vec}(X) \doteq \begin{bmatrix} c_1 \\ \vdots \\ c_m \end{bmatrix} \quad (3.27)$$

where c_1, \dots, c_m are the columns of X . Then, using (3.25), the Hilbert-Schmidt l_p norm of X can be described by

$$\|X\|_p = \|\text{vec}(X)\|_p. \quad (3.28)$$

Then, the l_p Hilbert-Schmidt norm ball in $\mathbb{F}^{n,m}$ of radius ρ is defined as

$$\mathcal{B}_{\|\cdot\|_p}(\rho, \mathbb{F}^{n,m}) \doteq \{X \in \mathbb{F}^{n,m} : \|X\|_p \leq \rho\}. \quad (3.29)$$

These matrix norm and ball definitions will become useful when we are discussing uncertainty descriptions, and particularly when the idea of degradation functions are introduced in chapters 5 and 7. Other definitions and concepts will be introduced as needed within chapters 4, 5, 6, and 7.

4.0 STRUCTURAL MODELING AND CONTROL OBJECTIVES

In this chapter, we will discuss the models, assumptions that are made, how interconnection uncertainty is characterized, and control objectives. Two models are used in this work: a random lumped parameter spring mass damper model; and a random Euler-Bernoulli beam model, which was modeled using finite element methods. Both of these models are detailed in separate appendices. The lumped parameter model is detailed in appendix [A](#). The finite element model is detailed in appendix [B](#).

For both cases, a generalization of the input/output (I/O), controller architecture, and interconnection with associated uncertainty is provided in figure [5](#). The lumped parameter model is used for developing the decentralized control techniques in chapter [5](#). The finite element beam model is used for developing the decentralized control techniques in chapters [6](#) and [7](#).

4.1 THE LUMPED PARAMETER MODEL

The model that is used for full-state feedback controller design and synthesis is a simple one: a, lightly damped, fixed-fixed lumped parameter spring mass damper model. Although this type of model may be hard-pressed to find application for controller design, synthesis, and analysis of a complicated piping system, other applications could find some of these developed techniques to be attractive. Areas such as: building earthquake structural dynamics and active control; automotive active suspension control; robotic manipulator control; and

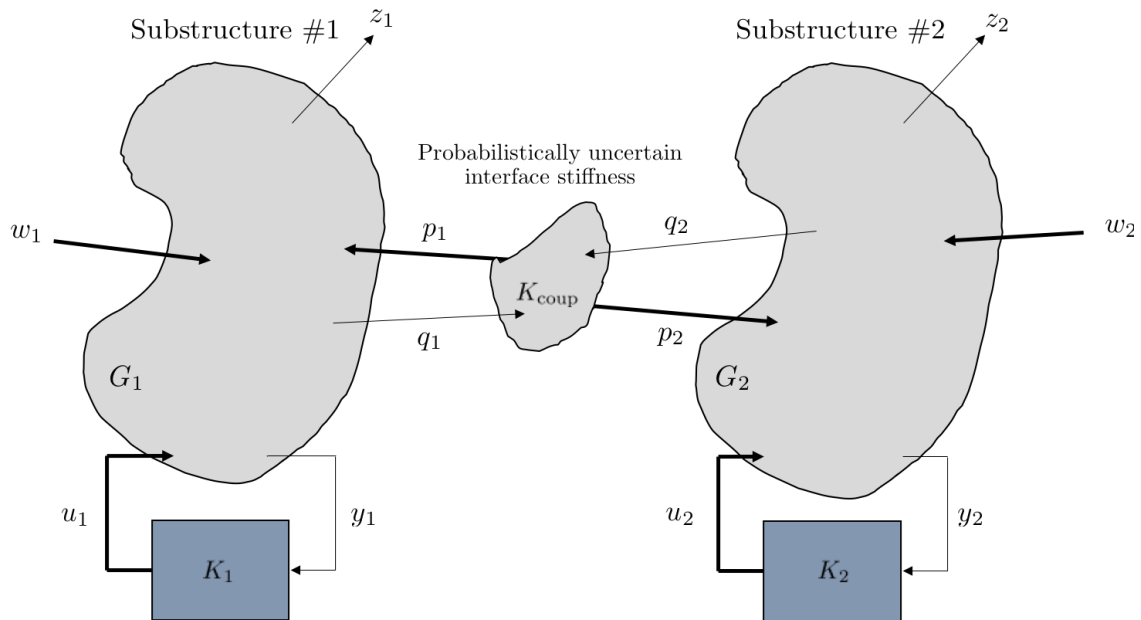


Figure 5: Probabilistic decentralized active control conceptualization. Control inputs (u), measurements (y), disturbance inputs (w), performance outputs (z), and structure/interconnection forces/momenta and displacements/rotations (p, q) are depicted for substructures G_1 and G_2 .

microgrid power system control may find applications for these approaches. A few of these areas fall under the large umbrella of active vibration control.

We will consider the lumped model in appendix A, shown in figure 54, which depicts a four-mass system that is coupled by some spring k_Δ , with the subscript Δ indicating that this spring is an uncertain element. This system has disturbance inputs w_1, w_2 and control inputs u_1, u_2 entering the system in the locations shown. One thing that will become important when we get into discussing controller objectives and design is the fact that there is no dissipative element included between masses 2 and 3. By modeling the system in this way, we cannot have proportional damping. This model structure leads to a situation where the eigenvectors of this system will be complex. Details behind this model can be found in appendix A.

The lumped parameter model, as a generalized plant, has the representation

$$G \sim \left[\begin{array}{c|cc} A & B_1 & B_2 \\ \hline C_1 & D_{11} & D_{12} \\ I & 0 & 0 \end{array} \right] \quad (4.1)$$

with inputs $[w \ u]^T$ and outputs $[z \ y]^T$.

4.2 THE EULER-BERNOULLI BEAM FINITE ELEMENT MODEL

This particular structural model is derived using elementary finite element analysis/structural dynamic theory. We are able to treat certain system parameters as being random variables. Specifically, we can account for geometric nonlinearities (length, area moment of inertia in a generalized beam model) and material anisotropies and uncertainty directly and on an elemental basis (elastic modulus, mass density). Only the elastic modulus of an interconnecting element is treated as having random uncertainty in this research. We only consider transverse (bending) deflection in this model. Details behind this model can be found in appendix B.

The beam model, as a generalized plant, has the representation

$$G \sim \left[\begin{array}{c|cc} A & B_1 & B_2 \\ \hline C_1 & D_{11} & D_{12} \\ C_2 & D_{21} & D_{22} \end{array} \right] \quad (4.2)$$

with inputs $[w \ u]^T$ and outputs $[z \ y]^T$. This generalized plant has a random interconnection stiffness element embedded within the dynamics matrix A .

4.3 INTERCONNECTION STIFFNESS ELEMENT UNCERTAINTY

We must discuss two different cases for random interconnection uncertainty in this research. The first case is specific to the lumped parameter model/full-state feedback case. This definition does not require very much discussion. The second case is specific to the finite element model/dynamic output feedback case. This case requires more discussion related to the random uncertainty that was modeled for this case, as well as an associated structured, norm-bounded uncertainty for the interconnection stiffness matrix.

4.3.1 The Uncertain Interconnection Stiffness Element for the Full State Feedback Case

For k_Δ , the interconnection stiffness adjoining substructures in the lumped parameter model, we have chosen that the uncertainty be normally-distributed with mean of 100 and standard deviation of 15: $k_\Delta \sim \mathcal{N}(100, 15^2)$.

4.3.2 The Uncertain Interconnection Stiffness Element for the Dynamic Output Feedback Case

Uncertainty in the interconnection stiffness element must be characterized in two ways:

1. As a random variable;

2. As an uncertain element satisfying some structured norm-bound.

The first uncertainty characterization stands at the crux of this dissertation — how can we synthesize a control law that is decentralized and robustly meets performance and stability requirements in the presence of random interconnection uncertainty? The second uncertainty characterization, in addition to being borne out of the elegant field of robust control, is actually used as a mechanism to give us good starting points in a large-scale stochastic optimization problem to solve the controller synthesis problem for the first uncertainty characterization. Thus, we must define, and set the stage, for both of these uncertainty cases.

An uncertain stiffness interface is introduced that connects the substructure systems G_1 and G_2 shown in figure 5. This formulation is recast, perhaps a bit more neatly/formally, in figures 13, 14, and 15. The uncertainty in the elastic modulus in the interconnection stiffness matrix will be characterized using a normal distribution. The random, uncertain interconnection stiffness matrix is given by

$$\mathbf{K}_\Delta = \begin{bmatrix} K_{\Delta,11} & K_{\Delta,12} \\ K_{\Delta,21} & K_{\Delta,22} \end{bmatrix} = - \left(\frac{E_\Delta I}{L^3} \right) \left[\begin{array}{cc|cc} 12 & 6L & -12 & 6L \\ * & 4L^2 & -6L & 2L^2 \\ \hline * & * & 12 & -6L \\ * & * & * & 4L^2 \end{array} \right], \quad E_\Delta \sim \mathcal{N}(E_0, 0.16E_0^2) \quad (4.3)$$

where $E_0 = 200$ GPa.

As the control objectives in this research focus on low frequency vibration attenuation, probabilistic parametric modeling is adequate for capturing dynamical system uncertainty [54]. Results from the fields of computational stochastic mechanics and stochastic finite element methods have shown that the parametric probabilistic approach is quite effective at capturing uncertainty in both the low and mid-frequency ranges [54, 55, 56].

To moderate the amount complexity that we introduce into the development of these techniques and through a recognition that these techniques can be generalized to more complicated cases, we focus on the situation where only one parameter of the interconnection stiffness element is uncertain — the elastic modulus. We will assume that the random

uncertainty in the elastic modulus can be characterized by a normal distribution. The scalar case for the normal distribution is given by

$$f(E | \mu, \sigma^2) = \frac{1}{\sqrt{2\pi\sigma^2}} e^{-\frac{(E-\mu)^2}{2\sigma^2}} \quad (4.4)$$

where E corresponds to the uncertain elastic modulus specific to the uncertain interconnection stiffness element, μ is the mean, and σ^2 is the variance¹. As a general note, we could similarly declare that the element length, elastic modulus, width, and height were all uncertain, thereby enabling us to characterize their uncertainty using a multivariate distribution, such as the multivariate normal:

$$f_{K_{\text{coup}}}(k_1, \dots, k_p) = \frac{\exp\left(-\frac{1}{2}(\mathbf{k} - \boldsymbol{\mu})^T \boldsymbol{\Sigma}^{-1} (\mathbf{k} - \boldsymbol{\mu})\right)}{2\pi^{p/2} |\boldsymbol{\Sigma}|^{1/2}} \quad (4.5)$$

where \mathbf{k} is a p -dimensional column vector, $\boldsymbol{\Sigma} > 0$ is the covariance matrix, and $\boldsymbol{\mu}$ is the p -dimensional mean vector. The aggregate effect of the uncertainty in all of these terms could very well result in an uncertain dynamic response that looks almost identical to that specific to the case where only the elastic modulus is uncertain. As a part of this thesis, wherein we generate stability/performance degradation functions that are a function of the amount of uncertainty in the system, these cases differ in how we either:

- Scale the variance on the univariate normal distribution as a measure for the amount of uncertainty;
- Scale the covariance matrix and decompose the “size” of this matrix into a scalar value, such as the Frobenius norm, as a measure for the amount of uncertainty.

Thus, it is with no detriment to the development of the techniques in this thesis that we consider only the scalar case of uncertainty on the elastic modulus for one interconnection stiffness element.

¹Throughout this thesis, we typically use σ to denote the singular value of a matrix, and μ to describe the structured singular value of an uncertain dynamic system, as defined in robust control. However, μ is used in a few other places, mainly within this chapter, to denote the mean.

A normal distribution, similarly, was an arbitrary choice. Probabilistic robust control techniques, as applied in this research, do not have to be implemented on systems that have analytic types of uncertainty associated with them. Any distribution, especially those derived from actual plant uncertainty data, can be used with the techniques developed in this thesis [14].

4.3.3 Structured Norm-Bounded Uncertainty

We have stated that the random interconnection element uncertainty has an uncertain elastic modulus characterized by $E_\Delta \sim \mathcal{N}(E_0, 0.16E_0^2)$. In order to solve for seed solutions using techniques from robust control, we must construct uncertainty structures that are “similar” to our desired random uncertainty distribution. Doing so requires that we define these uncertainty characterizations to be structured and norm-bounded.

Defining structured norm-bounded uncertainty is common in robust control, where the elegant theory behind doing so has demonstrated good results on practical engineering systems [57, 17]. However, part of this research is motivated by the notion that norm-bounding uncertainty can lead to conservative results — indeed, this notion has motivated other researchers to further investigate probabilistic robust control methods [14, 30, 12].

We define the following structured, norm-bounded interconnection uncertainty for the elastic modulus in the interconnection stiffness element:

- $E_{\Delta,1} \in [0.01E_0, 2E_0]$
- $E_{\Delta,2} \in [0.05E_0, 1.5E_0]$

These choices were facilitated by comparing them to the normal distribution that we had imposed on our interconnection uncertainty.

4.3.4 Encapsulating the Structured Norm-Bounded Interconnection Uncertainty

We chose $E_\Delta \sim \mathcal{N}(E_0, 0.16E_0^2)$ for the random uncertainty on the interconnection stiffness modulus. We also defined some structured, norm-bounded uncertainty sets $E_{\Delta,1}$ and $E_{\Delta,2}$, that will characterize the uncertainty used during loop-at-a-time μ -synthesis for generating an initial population/starting point in a stochastic optimization problem.

It now becomes insightful to examine how the random uncertainty set compares to the structured, norm-bounded uncertainty set, which can be equivalently thought of as being characterized using uniform probability distributions. This section is meant to show how we can compare these two sets, along with some considerations around how uniform bounds can be selected and analyzed against random distributions of arbitrary shape.

The first thing that we note is that $E_{\Delta,2} \subset E_{\Delta,1}$. This implies that $\mu(E_{\Delta,2}) \in E_{\Delta,1}$. We can therefore analyze the normal distribution with respect to the set $E_{\Delta,1}$. We can also see that this normal distribution also has the effect of weighting the structured norm-bounded uncertainty ball — this explains the notion that probabilistic robust control can have the effect of weighting us toward a solution that can be less conservative/better-performing for the “most-likely” plants in a structured norm-bounded uncertainty set.

The cumulative distribution function, adjunct to any density, is given by

$$\Pr[a \leq E_\Delta \leq b] = \int_a^b f(E_\Delta | \mu, \sigma^2) dE_\Delta \quad (4.6)$$

where we recall that

$$E_\Delta \sim \mathcal{N}(E_0, 0.16E_0^2) \Leftrightarrow E_\Delta \sim f(E | E_0, 0.16E_0^2) = \frac{1}{\sqrt{2\pi}0.16E_0^2} e^{-\frac{(E-E_0)^2}{0.32E_0^2}}. \quad (4.7)$$

To understand how we have “encapsulated” the norm-bounded uncertainty using $E_\Delta \sim \mathcal{N}(E_0, 0.16E_0^2)$, we want to calculate:

$$\Pr[0.01E_0 \leq E_\Delta \leq 2E_0] = \int_{0.01E_0}^{2E_0} f(E_\Delta | \mu, \sigma^2) dE_\Delta. \quad (4.8)$$

It is a well-known result from probability calculus, that for the univariate normal kernel, that

$$\Pr[E_\Delta \leq L] = \frac{1}{2} \left[1 + \operatorname{erf} \left(\frac{L - E_0}{\sqrt{2}(0.4E_0)} \right) \right] \quad (4.9)$$

where erf is the “error function”. A closed-form solution to the error function is not known, however, using a series expansion this function can be approximated by

$$\operatorname{erf}(x) = \frac{2}{\sqrt{\pi}} \sum_{n=0}^{\infty} \frac{(-1)^n x^{2n+1}}{n! (2n+1)} \approx \frac{2}{\sqrt{\pi}} \left(x - \frac{x^3}{3} + \frac{x^5}{10} - \frac{x^7}{42} + \frac{x^9}{216} - \dots \right). \quad (4.10)$$

Now, we have

$$\Pr[0.01E_0 \leq E_\Delta \leq 2E_0] = \frac{1}{2} \left[1 + \operatorname{erf} \left(\frac{2E_0 - E_0}{\sqrt{2}(0.4E_0)} \right) \right] - \frac{1}{2} \left[1 + \operatorname{erf} \left(\frac{0.01E_0 - E_0}{\sqrt{2}(0.4E_0)} \right) \right] \quad (4.11)$$

$$= \frac{1}{2} \left[\operatorname{erf} \left(\frac{2E_0 - E_0}{\sqrt{2}(0.4E_0)} \right) - \operatorname{erf} \left(\frac{0.01E_0 - E_0}{\sqrt{2}(0.4E_0)} \right) \right] \quad (4.12)$$

$$= 0.9871. \quad (4.13)$$

Thus, we have shown that the probability of E_Δ being sampled to be within the range $[0.01E_0, 2E_0]$ is 98.71%. This implies that $E_\Delta \sim \mathcal{U}(0.01E_0, 2E_0) \subset E_\Delta \sim \mathcal{N}(E_0, 0.16E_0^2)$. Furthermore,

$$1 - \Pr[0.01E_0 \leq E_\Delta \leq 2E_0] = 0.0129, \quad (4.14)$$

meaning that 1.29% of the $E_\Delta \sim \mathcal{N}(E_0, 0.16E_0^2)$ will fall outside of the range $[0.01E_0, 2E_0]$. In this manner, it is safe to say that the selected distribution used for probabilistic synthesis — and analysis — in chapter 7 encapsulates the norm bounded range, while simultaneously allowing us to “focus” our analysis and synthesis on the most-likely portions of the uncertainty set.

For completeness, for $E_\Delta \sim \mathcal{N}(E_0, 0.16E_0^2)$,

$$\Pr[0.05E_0 \leq E_\Delta \leq 1.5E_0] = 0.8856. \quad (4.15)$$

We note that as $\Pr[aE_0 \leq E_\Delta \leq bE_0] \rightarrow 1$ for scalar values of (a, b) , denoting the upper and lower bounds, we find ourselves in a situation where the norm-bounded set actually encapsulates the normally-distributed set. It is with this logic, then, that we make the claim

that our random uncertainty encapsulates the norm-bounded uncertainty. Converse to this situation, one can also choose some (a, b) such that $\Pr[aE_0 \leq E_\Delta \leq bE_0] \rightarrow 0$. This implies one of two things:

1. Significant “mean bias”: the means of the distribution and norm-bounded sets are chosen to be very far away from one another, or
2. Significant “variance bias”: The interval width characterizing (a, b) and the “width” of the distribution, given by its variance, were chosen to be very different. This can arise if a very large variance is imposed over a very small interval width.

Either of these conditions imply that the distribution chosen to encapsulate/color some norm-bounded uncertainty set is not a good one. Therefore, the designer must choose the distribution and associated norm-bounded sets in a meaningful way. No further guidance is given in this thesis, aside from the quantified differences and discussion above.

An alternative view is depicted in figure 6, where histograms of the norm-bounded (uniformly-distributed) versus normally-distributed interconnection modulus are contrasted.

4.3.5 Open-loop Response of the Uncertain Structures with Structured, Norm-bounded Uncertainty

We also examined the random maximum singular value plots to get a feel for how the response spectra was affected by this uncertainty — see figures 8 and 9. These figures depict the mapping

$$\begin{bmatrix} w_1 \\ w_2 \end{bmatrix} \rightarrow \begin{bmatrix} z_1 \\ z_2 \end{bmatrix},$$

as shown in figure 7 for the two norm-bounded uncertainty cases given above.

The low-mid frequency region for these uncertain systems appear to have enough uncertainty to potentially be useful in some practical structural control problems. A cursory analysis of variability that we have in the maximum singular value plot for $E_{\Delta,1} \in [0.01E_0, 2E_0]$ (figure 9) shows us that the second mode’s frequency $\omega_2 \in [3.2, 3.8]$ Hz. Since we have norm-bounded this uncertainty within the range mentioned earlier, we can assert that this

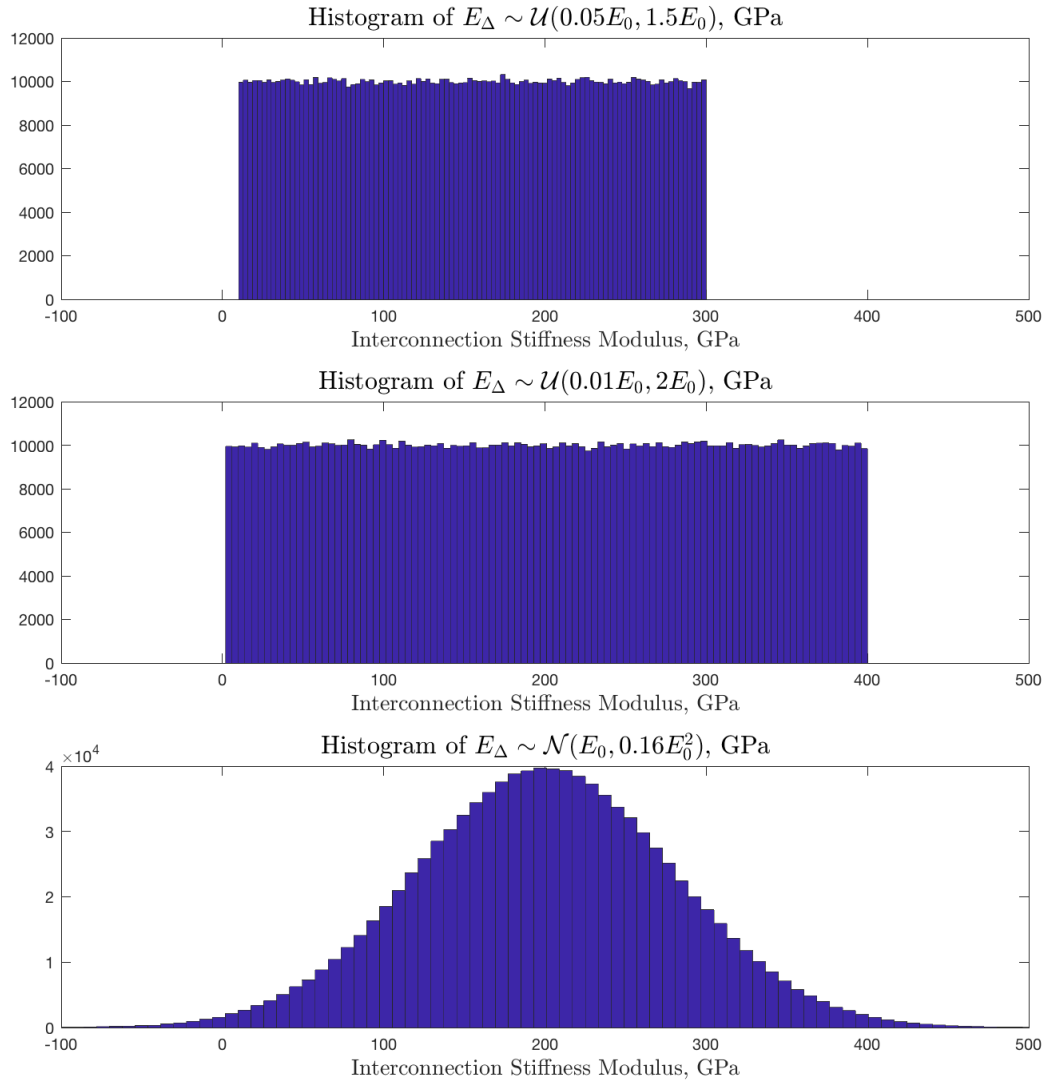


Figure 6: Comparison of the uniform, structured norm-bounded uncertainty used for μ -synthesis with the normal distribution that has been defined for probabilistic robust synthesis.

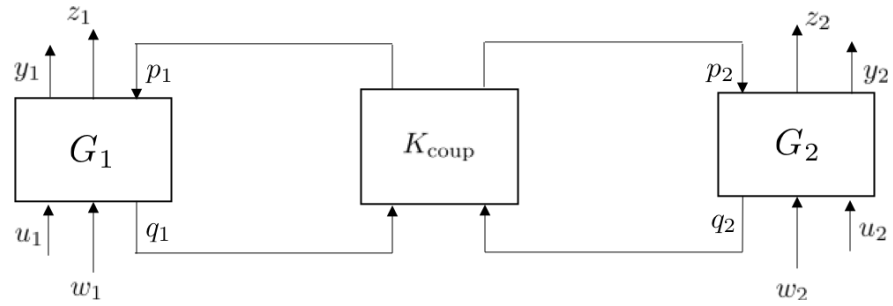


Figure 7: Open loop $w \rightarrow z$ mapping.

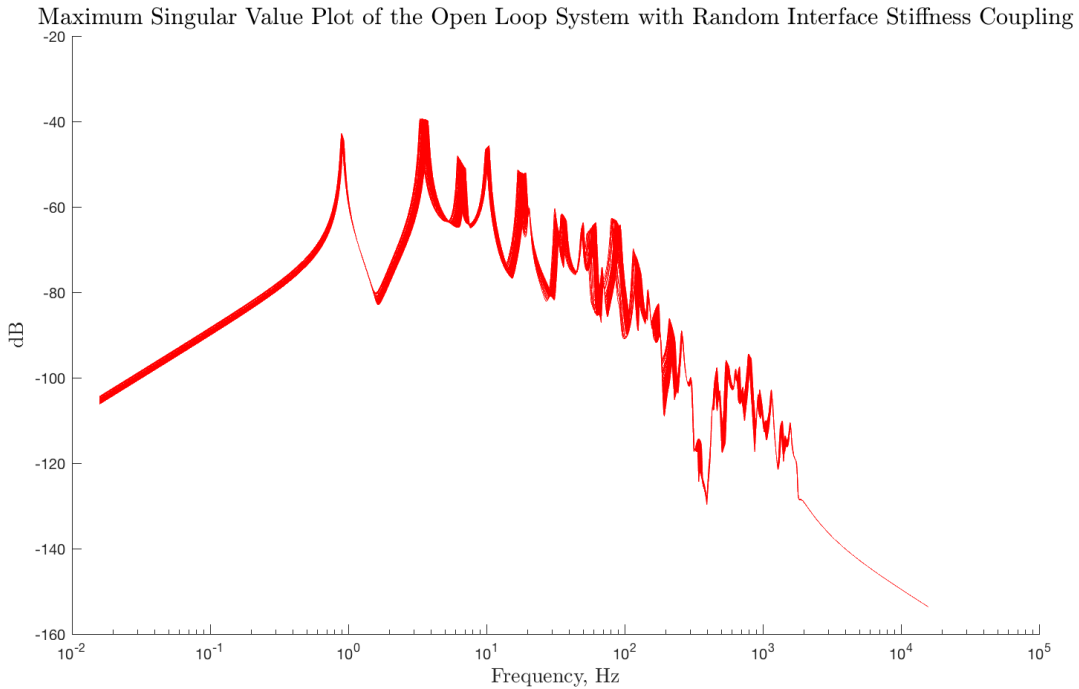


Figure 8: Maximum singular value plot of beams coupled through a norm-bounded, uncertain interface stiffness element. Interface stiffness element modulus variability ranges between 5% and 150% of the nominal, or $E_\Delta \in [0.05E_0, 1.5E_0]$.

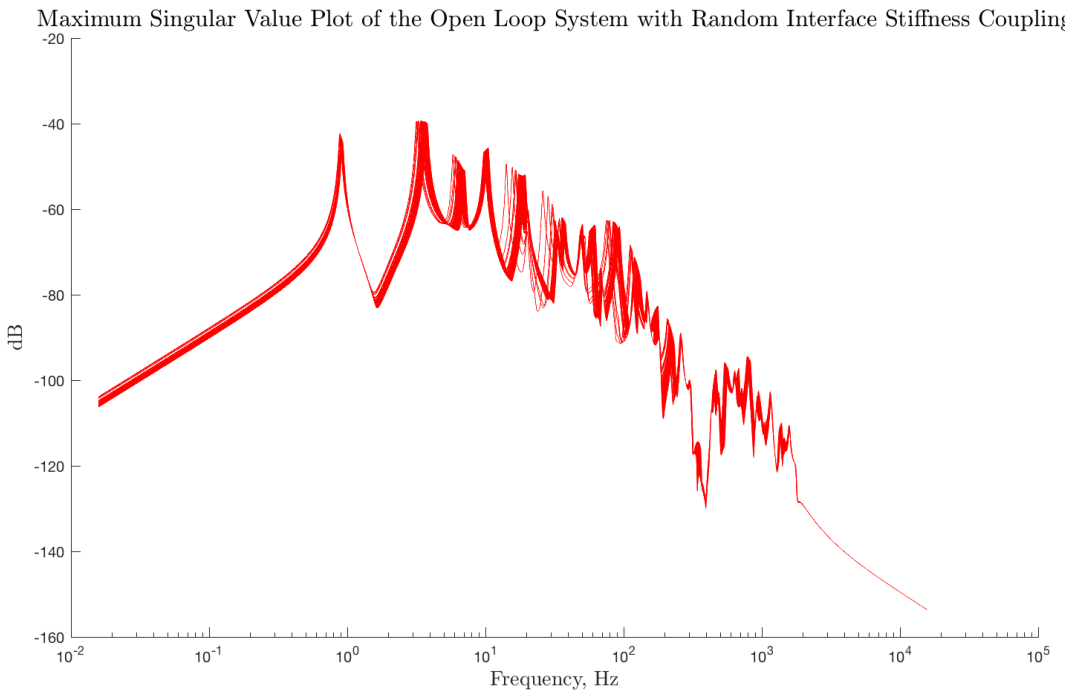


Figure 9: Maximum singular value plot of beams coupled through a norm-bounded, uncertain interface stiffness element. Interface stiffness element modulus variability ranges between 1% and 200% of the nominal, or $E_\Delta \in [0.01E_0, 2E_0]$.

mode can exist within the range just given with equal probability (uniform distribution over this range). Therefore, we can say that the average $\mu(\omega_2) = 3.5$ Hz. This implies that we have approximately $\pm 9\%$ uncertainty around this mode.

Variability around other modes is different. This mode was chosen for additional study so that we can make one statement: this amount of uncertainty, and the associated variability in natural frequencies, will make for a formidable controller synthesis problem, while also allowing for us to capture a high degree of variability in the interconnection stiffness.

4.3.6 Infinity Norm of the System Possessing Structured, Norm-Bounded Uncertainty

Randomized algorithms were used to evaluate the infinity norm of the open-loop, norm-bounded uncertain system. This open-loop system is represented by the mapping

$$\begin{bmatrix} w_1 \\ w_2 \end{bmatrix} \rightarrow \begin{bmatrix} z_1 \\ z_2 \end{bmatrix},$$

which we will call G_Δ for the time being, and is depicted in figure 7. The intent of this step was to determine the approximate worst-case infinity norm of the open-loop system so that a probabilistic robust control performance objective could be crystallized. Due to how random interconnection uncertainty was defined, we can have some members of the uncertainty set that are unstable, since the normal distribution is unbounded. Although unlikely, we wanted to examine the portion of the uncertainty set that will occur 98.71% of the time — that portion that is bounded between $0.01E_0$ and $2E_0$.

Note that by even using μ methods, it is not possible to find the *exact* infinity norm within this continuous uncertainty set [58, 59]; this fact further motivated the use of probabilistic methods [41]. Thus, 150 instances of this uncertain system were sampled and the infinity norm of each system was evaluated. Then,

$$\bar{\gamma} \doteq \max_i \sup_{\omega} \bar{\sigma}(G_{\Delta,i}(j\omega)), \quad \omega \in [0, \infty) \cup \{\infty\}, \quad i = 1, \dots, 150 \quad (4.16)$$

which says that $\bar{\gamma}$ is the approximate worst-case ∞ -norm within the uncertain plant set,

with uncertainty in the plant $G_\Delta(j\omega)$ characterized by $E_\Delta \in [0.01E_0, 2E_0]$.

Using this approach and the data generated from it, we observe that the approximate maximum is $\bar{\gamma} = -39.4$ dB. We do not perform a rigorous evaluation for estimating the probability that this norm serves as the upper-bound for the entire set. Instead, this cursory evaluation is sufficient so that we can reasonably select some level below this value as we move into solving the stochastic optimization problem in our chapter 7.

With that statement being made, we can declare that we wish to find a probabilistically robust dynamic output feedback, decentralized controller pair that maintains the \mathcal{H}_∞ norm of this system 6 dB less than this “worst case” norm. Therefore, our desired performance shall be declared to be

$$\gamma^* = \bar{\gamma} - 6 = -45.4 \text{ dB}. \quad (4.17)$$

One thing that we have to recognize, here, is that we are dealing with a random/uncertain system. This makes achieving aggressive performance targets more difficult. This leads us into discussing our control objectives.

4.4 CONTROL OBJECTIVES

The control objectives are very similar for both models and methods developed in this research. The approaches to achieving these control objectives are different and will be discussed in this section. The overarching control objectives that we seek to achieve in this work are:

- **Objective #1: Disturbance Attenuation at Low Frequencies** We want to find decentralized control laws, which we can call K , such that the \mathcal{H}_∞ -norm of the LFT mapping the disturbance inputs to performance outputs is attenuated below some level, especially at the low frequency modes of the structure. Mathematically, we want

$$\left\| F_l(G, K) \right\|_\infty \leq \gamma. \quad (4.18)$$

Designing the approaches to focus control effort on low frequency modes will be discussed in this chapter. The attenuation that we want to achieve for the lumped-parameter and finite-element models are different, as these models, and their parameters, are different.

- **Objective #2: Decentralized Controller Architecture** Decentralization is with respect to enforcing both sensing and actuation constraints on the controllers. That is, a controller K_1 can only use measurements specific to the portion of the structure where it is located. Similarly, it can only issue commands to the actuators local to the portion of the structure where it is located. The same is true for another controller for this structure, K_2 . Figure 5 generalizes this architecture for both the full-state as well as output feedback cases.

The approaches to achieving decentralized controller implementations for the full-state and dynamic output feedback cases are quite different. These approaches will be touched upon in this present chapter, with the details behind the implementations in chapters 5, 6, and 7.

- **Objective #3: Robustness Against Random Interconnection Uncertainty** Lastly, we want our approach to be able to incorporate information about, and result in a controller that is robust against, random interconnection uncertainty. This is a problem that has not been addressed by the decentralized control community, resulting in a contribution of this research [26].

This robustness is with respect to the two fundamental metrics that we use for evaluating the effectiveness of a controller: stability and performance. If we suggest that the random uncertainty in our system is characterized by some Δ , robustness against Δ becomes:

$$\hat{\Pr}(\text{stable} \mid \Delta) \geq 1 - \epsilon_s \quad (4.19)$$

$$\hat{\Pr}\left(\left\|F_l(G, K)\right\|_{\infty} \leq \gamma \mid \Delta\right) \geq 1 - \epsilon_p \quad (4.20)$$

which says, in probability, that we want the volume of “good” decentrally-controlled systems to be greater than $1 - \epsilon_s$ for stability and $1 - \epsilon_p$ for performance with respect to the random systems generated by the interconnection uncertainty, described by Δ .

4.5 ACHIEVING CONTROL OBJECTIVES IN STATIC FULL-STATE FEEDBACK

For the full-state feedback case, we will now discuss how control objectives will be achieved vis-à-vis control approach and design. The overarching control objective is to synthesize decentralized controllers that attenuate the maximum of the system's response across all disturbance input/performance output channels at low-frequencies while being robust against random uncertainty in the interconnection stiffness element.

We are also interested in the attenuation of low-frequency disturbance inputs at low frequencies. There are many ways to achieve this, however, some model bases have theoretical benefits that are attractive and intuitive. An approach is developed in modal coordinates, which is a basis that is attractive in the structural control community.

We recall that the eigenvectors of our system are complex, which arises from how we have defined our interconnection stiffness and damping matrices (see equation (A.5)). This research will show how we can divorce ourselves from the canonically-used proportional damping assumption, allowing us to pursue control design and synthesis over the field of complex numbers.

The system is modeled as a full-information generalized plant, with the form

$$\begin{aligned}\dot{x} &= Ax + B_1 w + B_2 u \\ z &= C_1 x + D_{11} w + D_{12} u \\ y &= Ix\end{aligned}\tag{4.21}$$

where the equation y implies that we can measure/sense all state variables, and the equation z is termed the performance output equation. This should be viewed as a virtual output, as we use it to achieve our specific performance objectives. The traditional full-information \mathcal{H}_∞ control problem that one would want to solve is to find some $u = Kx$ such that the ∞ -norm of the transfer function matrix

$$\frac{\|z(s)\|_2}{\|w(s)\|_2} \doteq \|F_c(s)\|_\infty \leq \gamma\tag{4.22}$$

where

$$F_c(s) = \left[\begin{array}{c|c} A + B_2 K & B_1 \\ \hline C_1 + D_{12} K & D_{11} \end{array} \right]. \quad (4.23)$$

Controller synthesis can be achieved by solving algebraic Riccati equations, or alternatively, by solving a semidefinite program (SDP) with linear matrix inequality (LMI) constraints [17, 60]. To achieve the macroscopic control objectives listed previously, we must employ several techniques and approaches which are discussed in chapter 5. These approaches involve solving the full-information \mathcal{H}_∞ synthesis problem as an SDP with LMI constraints. The LMI constraint in this synthesis problem is:

$$\begin{bmatrix} QA^T + AQ + Y^T B_2 + B_2 Y & B_1 & QC_1^T + Y^T D_{12}^T \\ B_1^T & -\gamma I & D_{11}^T \\ C_1 Q + D_{12} Y & D_{11} & -\gamma I \end{bmatrix} < 0 \quad (4.24)$$

$$Q > 0, Y \in \mathbb{R}^{r_2 \times n}$$

with the controller given by $K = YQ^{-1}$.

There are some assumptions that we must make about the system that we are studying in this thesis. First, some definitions are required.

Definition 1 (Stabilizability). *A linear system (continuous or discrete) is stabilizable if all unstable modes are controllable.*

Definition 2 (Detectability). *A linear system (continuous or discrete) is detectable if all unstable modes are observable.*

For full-state feedback \mathcal{H}_∞ synthesis using linear matrix inequalities, we have made the following assumptions about our system:

- (i) (A, B_1) is stabilizable and (C_1, A) is detectable;
- (ii) (A, B_2) is stabilizable;

and we have enforced that

$$D_{12}^T \begin{bmatrix} C_1 & D_{12} \end{bmatrix} = \begin{bmatrix} 0 & r_z I \end{bmatrix} \quad (4.25)$$

where $r_z > 0$. The linear dynamic, lightly damped structures that we study in this thesis are both stabilizable and detectable. Since we are interested primarily in lightly-damped structural dynamic systems that do not have rigid body modes, this assumption is automatically satisfied, as these types of systems do not have any unstable modes. See appendix C for a theorem and proof that shows this.

4.5.1 Performance Output Function Design in Modal Coordinates

Recall that we want to develop a technique that:

1. attenuates the system response at low frequencies due to disturbance inputs; and
2. allows us to perform control design in a modal basis with non-proportional damping.

When we are dealing with a system that does not have proportional damping, the mass, stiffness, and damping matrices may not all be diagonalized. In that case, the resulting modal damping matrix will be non-diagonal. When this is the case, the way to talk about the system modes tends to be more complicated and must be done in state space. Nevertheless, the modal form, in state space, can still be intuitive — the system modes still correspond with specific natural frequencies in the structure.

This basis is attractive when used in the context of the full-information \mathcal{H}_∞ control design and synthesis problem; rather than limiting ourselves to considering the original, physical displacements and velocities of our masses, we are now considering the modes of the system, making the definition of some $z = C_1 q + D_{11} w + D_{12} u$ very intriguing, as the \mathcal{H}_∞ controller seeks to make $\frac{\|z\|_2}{\|w\|_2}$ small. We can now, quite intuitively, target specific system modes when designing our control law. Indeed, we can define some C_1 such that we attempt to attenuate, or find some controller that, maintains the ∞ -norm of the $w \rightarrow z$ mapping below some level for only the first two modes of the system.

We chose to perform control design in complex modal coordinates, yet perform synthesis in the physical state space system. Doing so allowed us to achieve a decentralized controller directly in the physical state space and helped to avoid other complications that arise with using the scenario approach in probabilistic robust control.

For design, we transform to a complex modal basis where we can define our performance output function to look like:

$$\begin{aligned} z &= \hat{C}_1 q + D_{11} w + D_{12} u \\ &= \begin{bmatrix} I_{n \times n} \\ 0_{r_2 \times n} \end{bmatrix} q + \begin{bmatrix} 0_{(n+r_2) \times r_1} \end{bmatrix} w + \begin{bmatrix} 0_{n \times r_2} \\ I_{r_2 \times r_2} \end{bmatrix} u. \end{aligned} \quad (4.26)$$

Performing design and probabilistic robust synthesis in a complex modal space while preserving a decentralized structure in the physical space was a challenge that was not pursued directly in this research. Even if a modal basis that preserved a decentralized structure in our physical coordinate system was found, we would have to map the synthesized controller back through the basis transformation used to get into complex modal coordinates. Mapping back through such a transformation has implications on the scenario-approach to probabilistic robust synthesis that is used to achieve the end of finding a probabilistic robust \mathcal{H}_∞ controller for the full-state feedback case; by solving a high-dimensional SDP with LMIs representing random instances of the plant, we end up with many basis transformations that can be used to map back into a physical controller space. A question, then is related to how we go about choosing which basis transformation to use in order to transform our controller into a decentralized physical one.

Performing synthesis in the physical basis, with a modal performance output function, avoids these challenges related to finding, and choosing, a basis that allows control design and synthesis to only be performed in complex modal coordinates.

Decentralization of controller variables in the physical state space is discussed in section 4.5.3 and the scenario approach is discussed in chapter 5.

4.5.2 Frequency Weighting in Modal Coordinates

Another attractive feature of performing control design in a modal basis, especially for lightly-damped systems, is related to a simple method that allows us to frequency-shape our disturbance input and performance output matrices. This is a practice that is already

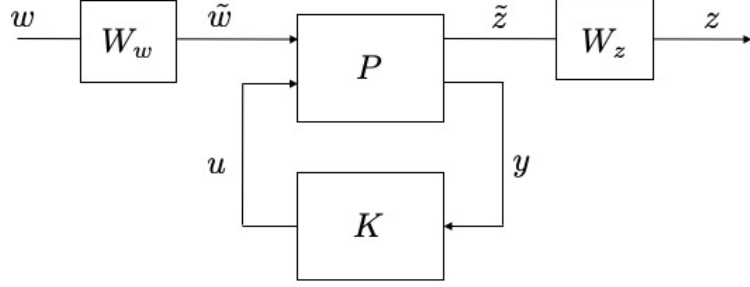


Figure 10: Disturbance input and performance output filtering in a generalized plant setting.

used in active structural control, and is another component of this research [61]. Part of the attractiveness behind this practice is the fact that we are able to preserve the order of our plant during controller synthesis.

Frequency weighting either the disturbance input or performance output allows us to incorporate knowledge about the spectral content of disturbances entering the system and allows us to target low frequency modes by filtering the performance output prior to controller synthesis. The input and output filters are augmented with the generalized plant as shown in figure 10.

We exploit properties that lightly-damped structures possess to achieve frequency weighting without augmenting filters to the generalized plant. Due to the presence of these lightly-damped modes, we can achieve the approximate result that input or output filtering has on the plant by multiplying the corresponding rows/columns of the input/output matrices, while in modal coordinates, by the magnitude of a smooth filter function at each resonant frequency.

This approximation is by no means an equivalence. However, the approximation works well at the system resonances, thereby making the \mathcal{H}_∞ -norm approximately equal for the case where the entire filter is augmented and for the case where we are scaling the modes by the magnitude of the filter function at each resonance.

We provide the following property to show how this is the case and refer to Gawronski for additional details [61].

Property 1 (\mathcal{H}_∞ Norm of a structure with a filter). *Given a system G and a smooth filter F , the \mathcal{H}_∞ norm of a structure with a smooth filter is equal to the \mathcal{H}_∞ norm of the structure with scaled modes.*

$$\|GF\|_\infty \approx \max_i(\|G_i\alpha_i\|_\infty), \quad i = 1, \dots, n \quad (4.27)$$

and the norm of the i th mode with a smooth filter is approximately equal to the norm of the scaled mode

$$\|G_i F\|_\infty \approx \|G_i \alpha_i\|_\infty, \quad (4.28)$$

where the scaling factor α_i is defined

$$\alpha_i = |F(\omega_i)| = \sqrt{F(\omega_i)^H F(\omega_i)}. \quad (4.29)$$

G_i corresponds to the i th mode's transfer function. A diagonal $F(\omega)$ of order s represents input filters without cross-coupling between the inputs. Similarly, a diagonal $F(\omega)$ of order r represents the output filter without cross coupling between the outputs. This approximation holds only for smooth input or output filters.

To demonstrate this approximation, we note that for a smooth filter the transfer function GF preserves the notion that the structural transfer function at the i th natural frequency is approximately equal to the i th modal transfer function at this frequency (see property 2.1 of Gawronski [61]);

$$\|GF\|_\infty = \sup_{\omega} \bar{\sigma}(G(\omega)F(\omega)) \approx \max_i \bar{\sigma}(G(\omega_i)F(\omega_i)) \quad (4.30)$$

$$\approx \max_i \bar{\sigma}(G_i(\omega_i)\alpha_i) = \max_i(\|G_i\alpha_i\|_\infty). \quad (4.31)$$

In the approximation just provided, the fact that $\sigma_k(GF) = \sigma_k(G|F|)$ is used, which is shown by

$$\sigma_k^2(GF) = \lambda_k(F^H G^H GF) = \lambda_k(FF^H G^H G) \quad (4.32)$$

$$= \lambda_k(|F|^2 G^H G) = \lambda_k(|F|G^H G|F|) = \sigma_k^2(G|F|) \quad (4.33)$$

which says that the norm of a smooth filter in series with a flexible structure is approximately equal to the norm of a structure scaled by the filter gains at the natural frequencies. This property can also be shown for a structure with a filter at the output.

For a given diagonal bank of input or output filters, where all filters are the same, we can achieve this modal input or output scaling by:

$$\tilde{B}_1 = \Phi W_w \Phi^{-1} B_1 \quad (4.34)$$

$$\tilde{C}_1 = C_1 \Phi W_z \Phi^{-1} \quad (4.35)$$

with Φ representing the eigenvectors of the state space system matrix A , and where

$$W_w = \text{diag}(\alpha_1^B, \alpha_1^B, \dots, \alpha_n^B, \alpha_n^B) \quad (4.36)$$

$$W_z = \text{diag}(\alpha_1^C, \alpha_1^C, \dots, \alpha_n^C, \alpha_n^C) \quad (4.37)$$

where each α_i corresponds to the magnitude of the filter at that particular system natural frequency. The left/right multiplication is shown since we are able to compactly scale the rows/columns of the disturbance input/performance output using this approach, and provided the diagonal filters are all equivalent. See Gawronski for additional information on using this approximation for filter approximation in lightly-damped structures, and how the the 2 and Hankel norms can similarly be approximated by scaling [61].

To illustrate the effectiveness of this approximation, an example is provided wherein the disturbance input matrix, B_1 , is scaled by the magnitude of a smooth filter at the system's resonances, with this comparison made to an open-loop unfiltered system along with the open-loop system with an input filter augmented. See figure 11. In figure 11, an input filter $W_w(s) = \frac{\omega_c}{s+\omega_c}$ where $\omega_c = 10 \text{ rad/s}$ was used. This figure was created for the system depicted in figure 54 of appendix A, but only represents a single I/O mapping between a disturbance entering the first mass and the velocity of the first mass. It is purely used to illustrate the effect of frequency weighting in the manner discussed. For the full-state feedback problem, we have chosen to frequency weight both the disturbance input and performance output matrices to achieve the end of low-frequency response attenuation while accounting for frequency content in disturbance inputs.

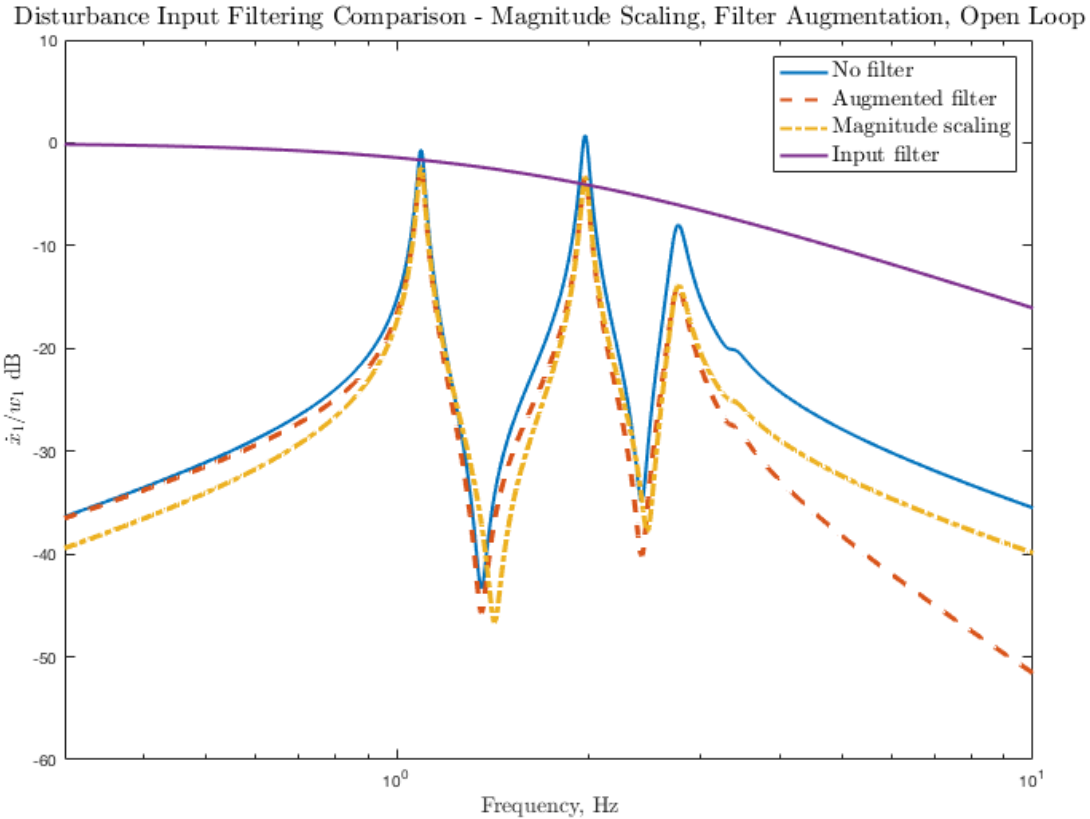


Figure 11: Lightly damped linear system comparing disturbance input filter augmentation with input matrix scaling in modal coordinates. This figure depicts the open-loop, unfiltered system, the system with an augmented disturbance input filter, and the effects of magnitude scaling in modal coordinates. The filter that was augmented, and used for scaling, is also included on this figure. It is shown that magnitude scaling achieves a good filtered approximation near the system resonances.

So far, we have sketched out how control objectives would be met for achieving the attenuation of low frequency structural modes due to exogenous disturbances entering our system. In order to do this, we approach the problem from three directions:

1. Pursue the synthesis of a full-state feedback \mathcal{H}_∞ controller, since this type of controller has appeal in its ability to attenuate some virtual performance output in the presence of broad-band exogenous inputs in some ∞ -norm sense;
2. Define the performance output function in modal coordinates, which allows us to target specific, or all, modes in the system directly during control design;
3. Frequency-shape the disturbance input and performance output B_1 and C_1 matrices, in modal coordinates.

There are two other objectives that we strive to meet:

1. A decentralized controller architecture;
2. A controller that is probabilistically-robust against random interconnection uncertainty.

We will now discuss how we will achieve these specific ends, before moving into our discussion on the model used for dynamic output feedback controller design and synthesis.

4.5.3 Decentralized Controller Architecture

A decentralized controller implementation is very straightforward to achieve when controller synthesis is pursued as a semidefinite program [60]. A decentralized controller architecture is achieved by enforcing sparsity constraints on the decision variables in the semidefinite program used to solve this type of controller synthesis problem. The full state feedback controller, denoted by K , is constructed as

$$u = Kx = YQ^{-1}x \quad (4.38)$$

where Y and Q are the decision variables in an SDP and our state vector, $x = [x_{(1)} \ x_{(2)}]^T$, with $x_{(1)}$ corresponding to only those states specific to subsystem 1, and $x_{(2)}$ corresponding

only to those states specific to subsystem 2. By enforcing that

$$Q = \begin{bmatrix} Q_1 & 0 \\ 0 & Q_2 \end{bmatrix}, \quad Y = \begin{bmatrix} Y_1 & 0 \\ 0 & Y_2 \end{bmatrix} \Rightarrow K = \begin{bmatrix} Y_1 Q_1^{-1} & 0 \\ 0 & Y_2 Q_2^{-1} \end{bmatrix} \quad (4.39)$$

we pose the optimization problem such that the off-diagonal terms in the decision variables are set to zero, and only search only over the block-diagonal terms, leading to a decentralized controller architecture.

4.5.4 A Probabilistic Robust Full State Feedback \mathcal{H}_∞ Controller

Robustness against the random interconnection uncertainty for the lumped parameter model used for the full state feedback case is addressed using the scenario approach in robust control [14, 16]. The full-information \mathcal{H}_∞ synthesis problem, solved as an SDP with LMI constraints, can be used in the scenario approach. This approach, with many considerations surrounding controller design and analysis, is the topic of chapter 5.

4.5.5 Probabilistic Robust Stability and Performance Metrics

The fact that we have random uncertainty tells us a few things. Stability and performance objectives are no longer deterministic. Therefore, we must define acceptable probability estimates that reflect our confidence that a certain amount of stability or performance can be guaranteed. Since our open loop system has random uncertainty, we need to evaluate the open loop performance through a similar probabilistic lens, which is how we can crystallize our desired probabilistic performance. It was previously discussed that part of the approach to achieving low-frequency performance was through frequency-shaping of the disturbance input and performance output matrices in modal coordinates.

Since controller synthesis will be performed on the filtered system, figure 12 is useful for understanding the effects that the interconnection uncertainty has on the resonance peaks that occur across the system's spectrum. Using the open-loop, random maximum singular value plot of the filtered and unfiltered system in figure 12, our objective was to achieve at

least a 20 dB reduction in the open-loop \mathcal{H}_∞ -norm of the disturbance input to performance output mapping. According to figure 12, the filtered \mathcal{H}_∞ -norm is approximately 10 dB.

By defining (4.26) frequency-scaling in modal coordinates, and transforming back into our physical coordinate system, our performance output equation is now defined to be

$$z = \begin{bmatrix} W_z \Phi^{-1} \\ 0 \end{bmatrix} x + \begin{bmatrix} 0_{(n+r_2) \times r_1} \end{bmatrix} w + r_z \begin{bmatrix} 0_{n \times r_2} \\ I_{r_2 \times r_2} \end{bmatrix} u. \quad (4.40)$$

We declare that we want to find a control law, $u = Kx$, such that the \mathcal{H}_∞ -norm of the LFT

$$\left\| F_l(\tilde{G}, K) \right\|_\infty \leq -10 \text{ dB} \quad (4.41)$$

where the \tilde{G} is the frequency-scaled plant, with disturbance input filter W_w and performance output filter W_z approximated by scaling the B_1 and C_1 matrices in modal coordinates. Using the magnitude scaling shown previously, this system is

$$F_l(\tilde{G}, K) \sim \left[\begin{array}{c|c} A + B_2 K & \tilde{B}_1 \\ \hline \tilde{C}_1 + D_{12} K & D_{11} \end{array} \right] \quad (4.42)$$

where \tilde{B}_1 is the “physical” version of B_1 after being scaled in modal coordinates by the magnitude of the filter function $W_w(s)$ at each $s = j\omega_i$ open-loop resonant frequency. The \tilde{C}_1 matrix, likewise, was scaled using $W_z(s)$ at each $s = j\omega_i$ resonant frequency.

Thus, the probabilistic robust controller that we find, if one exists, will have a priori guarantees on the probability of meeting this performance objective on the filtered system. A posteriori analyses around the unfiltered (actual) system are carried out, as is done for other systems that are frequency-shaped for controller synthesis [17].

We can now state our performance objectives as it relates to having probabilistic guarantees. We want our decentralized controller to meet performance objectives 97% of the time with 95% confidence in this estimate. This allows us to arrive at our desired probabilistic robust performance requirement.

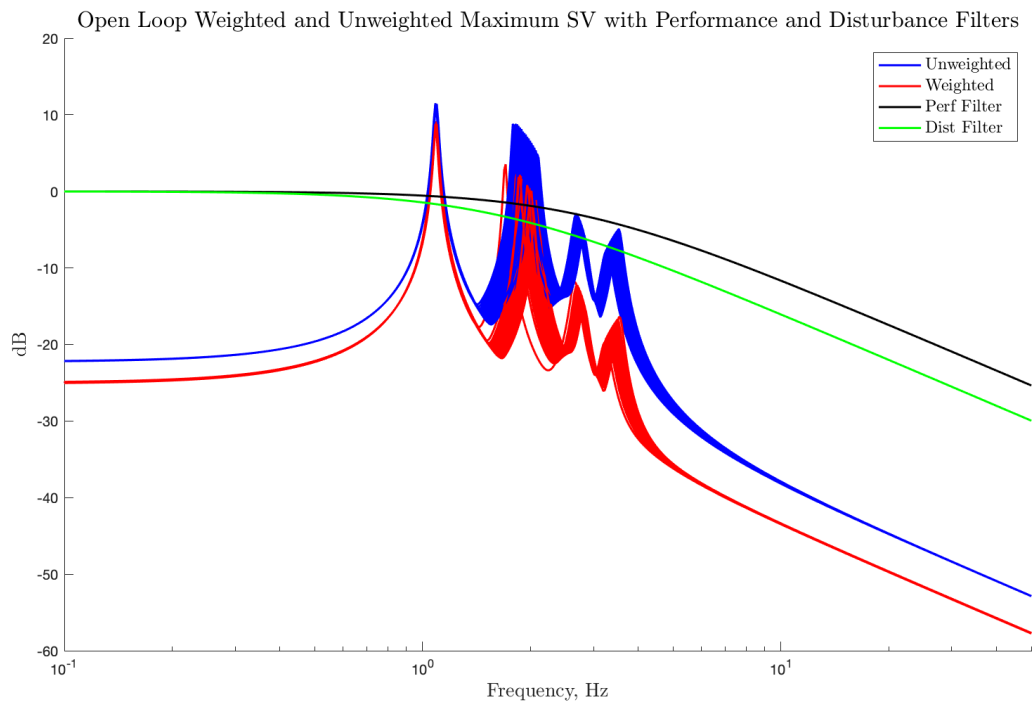


Figure 12: Open loop maximum singular value plots, filtered and unfiltered, with the disturbance input and performance output filters used.

Probabilistic Robust Performance: The probabilistic robust performance test for the full-state feedback case is given by:

$$P_{\text{test}} \doteq \hat{\Pr} \left(\left\| F_l(\tilde{G}_\Delta, K) \right\|_\infty \leq \gamma \mid \Delta \right) \geq 0.97 \quad (4.43)$$

with 95% confidence in this a priori probability estimate and with $\gamma = -10$ dB. The \tilde{G}_Δ and conditional dependence upon Δ implies that we are evaluating the performance of random instances of the controlled system, with samples being drawn from the prescribed probability distribution. A system is asymptotically stable if and only if it has a finite infinity norm, and so stability is implied by this performance requirement. This implies that a system that meets these performance requirements exists within the subset of stable plant/controller configurations. This conditional dependency, although somewhat obvious, was briefly discussed in chapter 2. This allows us to arrive at our desired probabilistic robust stability requirement.

Probabilistic Robust Stability: The probabilistic robust stability test for the full-state feedback case is given by:

$$S_{\text{test}} \doteq \hat{\Pr} \left(\operatorname{Re} \left(\lambda(A_\Delta + B_2 K) \right) < 0 \mid \Delta \right) \geq 0.99 \quad (4.44)$$

with 95% confidence in this a priori probability estimate. The A_Δ , along with the Δ , implies that we are evaluating the stability of random instances of the controlled system, with samples being drawn from the prescribed probability distribution.

4.6 ACHIEVING CONTROL OBJECTIVES IN DYNAMIC OUTPUT FEEDBACK

We also want to design and synthesize dynamic output feedback controllers that are robust against random model uncertainty while attenuating the system's excitation at low-frequencies due to broadband disturbance inputs. Furthermore, we want a decentralized controller architecture. This means that controllers are synthesized that can only use those

spatially-local measurements and actuators for achieving overarching control objectives. This situation is depicted by figure 5.

We want to synthesize probabilistic-robust \mathcal{H}_∞ controllers for the substructures in this research. In order to do this, and as is well-known from the field of robust control and \mathcal{H}_∞ , a generalized model of the plant must be constructed. Recalling the generalized plant representation for the finite element modeled beams,

$$G \sim \left[\begin{array}{c|cc} A & B_1 & B_2 \\ \hline C_1 & D_{11} & D_{12} \\ C_2 & D_{21} & D_{22} \end{array} \right], \quad (4.45)$$

we make the following assumptions, which are specifically relevant for the loop-at-a-time μ -synthesis approaches in chapter 6:

- (i) (A, B_1) and (A, B_2) are stabilizable;
- (ii) (C_1, A) and (C_2, A) are detectable;
- (iii) $D_{12}^T D_{12} = I$;
- (iv) $D_{21} D_{21}^T = I$;
- (v) $D_{11} = 0$, $D_{22} = 0$.

Note that in order to satisfy (iii) and (iv), D_{12} must have no more columns than rows and D_{21} no more rows than columns. Generally, if D_{12} and D_{21} have full rank, scaling matrices can always be found to make sure (iii) and (iv) are satisfied. These scalings preserve the system's ∞ -norm. See the lecture notes by Dailey for additional details [62]. We note that when using the LMI approach to \mathcal{H}_∞ synthesis, we only have the requirement that (A, B_2) be stabilizable, (C_2, A) be detectable, and $D_{22} = 0$ [63]. To achieve the objectives in this thesis, however, we have designed D_{12} and D_{21} to be full rank matrices, with D_{12} having more rows than columns, and D_{21} more columns than rows.

For the plant given by (4.45), we want to find some control law $u = Ky$, where

$$K \sim \left[\begin{array}{c|c} A_k & B_k \\ \hline C_k & D_k \end{array} \right] \quad (4.46)$$

that renders

$$\left\| F_l(G, K) \right\|_{\infty} \leq \gamma \quad (4.47)$$

where this LFT is mapping the disturbance inputs to the performance outputs for this structure.

Very generally, we have just covered what the objective that a controller must attenuate the system \mathcal{H}_{∞} -norm below some level. Controller synthesis approaches will be covered in both chapters 6 and 7, as we develop an approach to synthesizing multiple robust controllers using μ -synthesis, and use these controllers as starting points in a stochastic optimization problem. We will now continue our discussion on this system model and how we are going about designing the controller.

4.6.1 Performance Output Function Design in Modal Coordinates

To achieve performance output attenuation at low frequencies, the C_1 performance output matrices are defined to be frequency-weighted versions of the measured position and velocity at measurement locations. Thus, the performance output equations are constructed as

$$z = \begin{bmatrix} C_2 \Phi W_z \Phi^{-1} \\ 0 \end{bmatrix} x + D_{11} w + D_{12} u, \quad i = 1, \dots, n \quad (4.48)$$

where each $W_z = \text{diag}(\alpha_1^C, \alpha_1^C, \dots, \alpha_n^C, \alpha_n^C)$, $i = 1 \dots n$ is a diagonal matrix of positive scalings equal to the magnitude of a smooth filter function at each resonance frequency. The coefficients of W_z are determined by evaluating the following filter at each resonant frequency of the system:

$$\alpha_i = |W_z(s_i)| = \left| \frac{500}{s_i + 500} \right|, \quad s_i = j\omega_i, \quad i = 1, \dots, n \quad (4.49)$$

where n is equal to the dimension of our state space system. Since the fixed-fixed beam, determined using the parameters in table 6, has a first fundamental frequency at approxi-

mately 5.8 rad/s (0.9 Hz), filtering the performance outputs with the filter (4.49) was chosen to attempt to achieve the end of attenuating the system's response at low frequencies. The open-loop, uncertain maximum singular value plot of the coupled system was shown in figures 8 and 9.

4.6.2 Decentralized Controller Architecture

To achieve the end of synthesizing decentralized, robust controllers that attenuate the system's \mathcal{H}_∞ -norm below some level while achieving the attenuation of low frequency modes, we combine a technique known as loop-at-a-time controller synthesis with μ -synthesis via D/K iterations [6, 17]. This means that different $w \rightarrow z$ mappings are required during loop formulations and controller synthesis. The details of this approach are included in chapter 6, however, we present the high-level approach at this juncture. To start, we formulate the mapping

$$\begin{bmatrix} w_1 \\ w_2 \end{bmatrix} \rightarrow z_1$$

where w_1 is the disturbance entering substructure #1 and w_2 is the disturbance entering substructure #2. z_1 is the frequency-weighted, measured positions and velocities specific to substructure #1. The generalized plant block diagram depicting this open-loop formulation is shown in figure 13. The K_{coup} block represents the structured, norm-bounded uncertain interconnection stiffness element. We then synthesize the controller K_1 for this configuration, using only the control inputs u_1 and measurements y_1 . Next, we move toward formulating the next open loop interconnection for synthesis of controller K_2 . This involves formulating the mapping

$$\begin{bmatrix} w_1 \\ w_2 \end{bmatrix} \rightarrow z_2,$$

where w_1 and w_2 are as defined before, with z_2 as a frequency-weighted version of the measured positions and velocities specific to substructure #2. This case becomes even more interesting, however; the controller K_1 is collapsed into G_1 , meaning frequency-weighting of z_2 at the system's resonances includes the closed-loop dynamics produced by having the

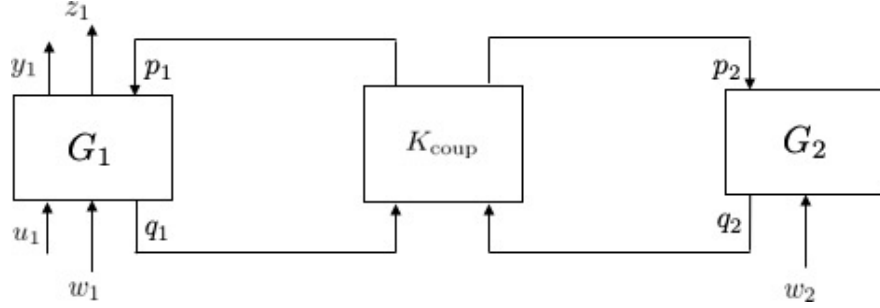


Figure 13: Initial generalized plant formulation used for K_1 controller synthesis.

controller K_1 active. This system is depicted in figure 14. Synthesis around this system is performed, using only control inputs u_2 and measurements y_2 for synthesis of K_2 .

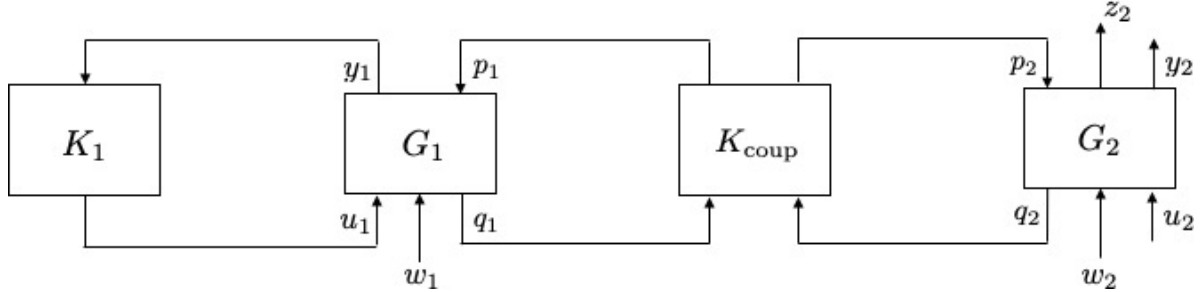


Figure 14: Subsequent generalized plant formulation for K_2 controller synthesis.

Lastly, we arrive at the final system configuration that we use for assessing the performance of our closed loop system. We are finally interested in the mapping

$$\begin{bmatrix} w_1 \\ w_2 \end{bmatrix} \rightarrow \begin{bmatrix} z_1 \\ z_2 \end{bmatrix}$$

where z_1 and z_2 are no longer frequency-weighted versions of the measured positions and velocities specific to each substructure. Rather, these are now just the positions and velocities at measurement locations, with these measurements only being particular to each substructure. The controllers K_1 and K_2 are wrapped around substructures G_1 and G_2 as shown in figure 15.

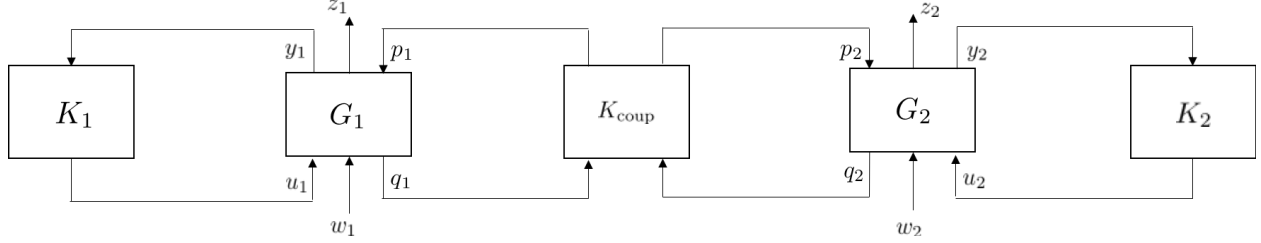


Figure 15: Closed loop system for system analysis.

The controllers resulting from loop-at-a-time μ -synthesis, if they are found to exist while achieving good performance at low frequencies, will be used as seed solutions in a stochastic optimization problem as we search for solutions that achieve a 6 dB reduction in the open-loop \mathcal{H}_∞ norm of the uncertain plant.

4.6.3 Probabilistic Robust Stability and Performance Metrics

The performance test is given by:

$$P_{\text{test}} \doteq \hat{\Pr} \left(\|F_l(G, K)\|_\infty \leq \gamma^* \mid \mathbf{K}_\Delta \right) \geq 1 - \epsilon_p \quad (4.50)$$

where we chose $\gamma^* = -45.4$ dB and $\epsilon_p = 0.05$. Probability estimate accuracy and confidence is detailed in chapter 7.

The stability test is given by:

$$S_{\text{test}} \doteq \hat{\Pr} \left(F_l(G, K) \text{ stable} \mid \mathbf{K}_\Delta \right) \geq 1 - \epsilon_s \quad (4.51)$$

where we chose $\epsilon_s = 0.02$. Probability estimate accuracy and confidence is detailed in chapter 7. The robust stability test says that we want our system to be stable for some prescribed volume $(1 - \epsilon_s)$ of our set. Clearly, and using the logic/arguments presented in section 2.3.1, $\epsilon_s \leq \epsilon_p$, since the \mathcal{H}_∞ -norm of a system is finite if and only if the system is stable.

A critical statement must be made, now. The approaches developed in chapter 7 do not allow us to make an a priori guarantees for passing our stability (S_{test}) or performance (P_{test}) for given volumes $1 - \epsilon_s$ and $1 - \epsilon_p$, respectively. This fact is what makes the scenario-based approach and statistical learning theory attractive in probabilistic robust control, as discussed in chapter 2. Thus, we will say that a satisfactory solution will be one for which:

- S_{test} passes for an $\epsilon_s = 0.02$;
- P_{test} passes for an $\epsilon_p = 0.05$.

In words, we want 98% of our random, decentrally-controlled structures to be stable, and for 95% of these random plants to have a $w \rightarrow z$ mapping with \mathcal{H}_∞ -norm less than or equal to γ^* .

4.7 CHAPTER SUMMARY

In this chapter we have discussed and developed the following:

- The lumped parameter model, with quantified random interconnection uncertainty, for the full-state feedback control case;
- The finite element model, with quantified random interconnection uncertainty, for the dynamic output feedback control case;
- Control objectives for the probabilistic robust, decentralized, full-state feedback \mathcal{H}_∞ problem that we solve in chapter 5;
- Control objectives for the probabilistic robust, decentralized, dynamic-output feedback \mathcal{H}_∞ problem that we solve in chapters 6 and 7.

We now move into chapter 5, which develops a scenario-based decentralized full-state feedback control technique for lightly-damped system with random interconnection uncertainty.

5.0 SCENARIO-BASED DECENTRALIZED FULL-STATE FEEDBACK CONTROL OF A LIGHTLY-DAMPED SYSTEM WITH RANDOM INTERCONNECTION UNCERTAINTY

For the field of probabilistic controller design and synthesis for dynamical systems, a powerful, contemporary development pioneered by Calafiore et al., is the scenario approach [16]. Perhaps the most attractive aspects of this approach are that it is both computationally tractable and straightforward in its implementation. This approach also enables the incorporation of real, complex, structured and unstructured uncertainties into the system model.

In this chapter, we show how scenario design can be used to synthesize decentralized \mathcal{H}_∞ controllers where the system interconnections are real, random variables, and where our performance objectives are complex-valued. An advantage to this technique is that global system performance objectives can be defined and met, where controller synthesis accounts for the random interconnections and adjoining system dynamics, yet is completely decentralized in implementation. In addition, we show how a real-valued control law can be synthesized with control design performed in a complex modal basis.

Several techniques and concepts are brought together to achieve the end of synthesizing a decentralized, probabilistically-robust, full-state feedback \mathcal{H}_∞ controller for the light, non-proportionally damped model with random interconnection uncertainty introduced in chapter 4. This chapter is structured as follows:

- The scenario approach to probabilistic robust control will be detailed;

- Representing the full-state feedback \mathcal{H}_∞ problem as a semidefinite program with linear matrix inequality constraints will be detailed, hence showing that this is a convex program amenable to the scenario approach;
- Primal and dual forms of semidefinite programs will be presented, as the dual form is fundamental to understanding complex semidefinite programming;
- A little abstract algebra: how complex numbers can be represented as real matrices, and some important properties that are preserved through this transformation;
- Complex semidefinite programming, and how the transformation between complex and real matrices is used to represent this problem as a real semidefinite program;
- Scenario-based, decentralized, complex, full-state feedback \mathcal{H}_∞ synthesis for a lightly damped system model possessing random interconnection uncertainty;
- The stability and performance of the resulting decentralized, probabilistic robust \mathcal{H}_∞ controller is analyzed.

5.1 THE SCENARIO APPROACH TO PROBABILISTIC ROBUST CONTROL

This section is provided as an overview to the scenario approach, which was developed by Calafiori et al. in [16, 64]. A good overview of the approach is provided in the monograph by Tempo et al. [14].

In the scenario approach, if we consider some nominal plant given by G where it is known that certain physical parameters of this plant G are uncertain, we can represent G as a finite collection of plants, denoted by $\mathcal{G}_N = \{G^{(1)}, \dots, G^{(N)}\}$. If the number of scenarios, equal to N , is chosen properly during controller design and subsequently for controller synthesis, a specified level of probabilistic robustness can be achieved [14].

We denote $\Delta \in \mathcal{B}_\Delta$ to represent the random uncertainty that is affecting our system. The set \mathcal{B}_Δ assumes the form

$$\mathcal{B}_\Delta(a) \doteq \{\Delta \in \mathbb{R}^{n \times m} : \Delta \sim f_\Delta(a)\} \quad (5.1)$$

where

$$f_\Delta(a) = \mathcal{N}(\mu, a\sigma_0), \quad a \in [0, a_{\max}], \quad a_{\max} \in \mathbb{R}_+. \quad (5.2)$$

For probabilistic robust synthesis, a is chosen to be equal to unity. Note that through using this approach, the distribution does not have to be normal, uniform, or any other analytic distribution. The uncertainty can be characterized in any way, allowing the designer to incorporate uncertainty information derived from test data or other means.

For analysis, and for the construction of stability and performance degradation functions, a will be allowed to vary in some set that is upper-bounded by some scalar a_{\max} , which is what will allow us to construct these probabilistic analogues to the structured singular value from robust control [17].

We also denote $\theta \in \Theta \subseteq \mathbb{R}^{n_\theta}$ to be the controller variables that we must find. Thus, the set Θ is the domain of optimization variables.

We state the following assumption, which is an assumption upon which the scenario-based approach to controller synthesis is based [14]:

Assumption 1 (Convexity). *The performance function, which we denote $g(\Delta, \Theta)$, is convex in Θ for any fixed value of $\Delta \in \mathcal{B}_\Delta$.*

Under satisfaction of the Assumption 1 given above, the scenario design problem amounts to determining some $\theta \in \Theta$, for some randomly extracted scenarios $\Delta^{(1, \dots, N)}$, that solves

$$\begin{aligned} \min_{\theta} \quad & c^T \theta \\ \text{s.t.} \quad & g(\Delta_i, \theta) \leq \rho^*, \quad i = 1, \dots, N. \end{aligned} \quad (5.3)$$

The scenario design problem form, with its underlying convexity assumption, opens up our ability to use it for many control synthesis problems. One such problem is the synthesis of full-state feedback \mathcal{H}_∞ controllers. This type of synthesis approach is possible using

scenario design since the controller variables are convex in the problem's constraints. It is well-established that this problem is convex and is solvable as a semidefinite program [15]. This will be detailed later on in this chapter.

5.1.1 On sample size complexity and a priori probabilistic guarantees

Perhaps one of the most powerful aspects to the scenario approach is that by using a finite number of constraints, one can make an a priori probabilistic guarantee on meeting performance requirements with specified accuracy. For the \mathcal{H}_∞ synthesis problem, this approach involves solving a semidefinite program with finite number of LMI constraints. We then see that the algorithms used to synthesize controllers are of polynomial complexity [14].

We will now discuss how bounds are determined using the scenario approach, leading to our ability to guarantee a priori the probability that a given solution will meet specified performance requirements with specified accuracy. For a multisample $\Delta^{(1,\dots,N)} \in \mathcal{B}_\Delta^N$, the events in this multisample are measured by a product probability $\Pr_{\Delta^{(1,\dots,N)}}$. For any multisample $\Delta^{(1,\dots,N)}$ for which the problem in (5.3) is feasible, a unique optimal solution is attained, which is due to Θ being a convex and compact set. Then, $\mathcal{B}_\Delta^{*N} \subseteq \mathcal{B}_\Delta^N$ describes those multisamples that lead to feasible solutions.

Given some multisample extraction drawn from \mathcal{B}_Δ^{*N} , the optimal solution is denoted as $\hat{\theta}_N$, which is itself a random variable. Since the set \mathcal{B}_Δ^{*N} corresponds to an extraction wherein no constraints are violated, and since sampling into \mathcal{B}_Δ^N to form some random multiextraction $\Delta^{(1,\dots,N)}$ can lead to formulation of a problem where constraints are violated, we must define the constraint violation probability as we move toward establishing sample bounds using the scenario approach. The constraint violation probability is given by

$$V(\hat{\theta}_N) = \begin{cases} \Pr \left\{ g(\Delta, \hat{\theta}_N) > \rho^* \right\}, & \text{if } \Delta^{(1,\dots,N)} \in \mathcal{B}_\Delta^{*N} \\ 1, & \text{otherwise.} \end{cases} \quad (5.4)$$

$V(\hat{\theta}_N)$ is a random variable in the interval $[0, 1]$, with events in $V(\hat{\theta}_N)$ measured by the product probability $\Pr_{\Delta^{(1,\dots,N)}}$. In line with the nomenclature in Tempo et al. [14], the

reliability of a scenario solution is given by $R(\hat{\theta}_N) = 1 - V(\hat{\theta}_N)$. Thus, we can write

$$R(\hat{\theta}_N) = \Pr \left\{ g(\Delta, \hat{\theta}_N) \leq \rho^* \right\} \times \mathbb{I}_{\mathcal{B}_\Delta^{*N}} \Delta^{(1, \dots, N)}, \quad (5.5)$$

where $\mathbb{I}_{\mathcal{B}_\Delta^{*N}}$ is the indicator function. We now state Theorem 12.1 from [14]:

Theorem 3. *Let Assumption 1 on convexity be satisfied, and let Θ be a convex and compact set. Also assume that when (5.3) is feasible, we attain a unique, optimal solution. Let $\epsilon \in (0, 1)$ be a given probability level and let $N \geq n_\theta + 1$. Then it holds that*

$$\Pr_{\Delta^{(1, \dots, N)}} \left\{ \left\{ V(\hat{\theta}_N) > \epsilon \right\} \cap \mathcal{B}_\Delta^{*N} \right\} \leq B_{N, \epsilon}(n_\theta) \quad (5.6)$$

where $B_{N, \epsilon}(n_\theta)$ is the binomial distribution,

$$B_{N, \epsilon}(n_\theta) = \sum_{k=0}^{n_\theta} \binom{N}{k} \epsilon^k (1 - \epsilon)^{N-k}. \quad (5.7)$$

The proof behind this theorem is extensive and can be found in Calafiore [64]. Importantly, the following corollary, which accompanies this result, gives us a straightforward means for bounding sample complexity for a probabilistically robust convex program.

Corollary 4. *Let the assumptions of Theorem 3 be met, and let positive scalars $\epsilon, \delta \in (0, 1)$ be given probability levels. If N is an integer such that*

$$N \geq \frac{2}{\epsilon} \left(\log \frac{1}{\delta} + n_\theta \right) \quad (5.8)$$

then it holds that

$$\Pr_{\Delta^{(1, \dots, N)}} \left\{ \left\{ V(\hat{\theta}_N) > \epsilon \right\} \cap \mathcal{B}_\Delta^{*N} \right\} \leq \delta. \quad (5.9)$$

This result says that if the number of scenarios, N , is selected according to the bound given in (5.8), then the unique, optimal solution — if one exists — to the scenario approach has with probability $1 - \delta$, a level of accuracy $1 - \epsilon$.

5.1.2 Scenario-based Synthesis as a Semidefinite Program with LMI Constraints

Semidefinite programs with linear matrix inequalities are convex [15]. Some nomenclature will now be introduced and the primal and dual forms of semidefinite programs will be presented. This discussion will aid with some of the machinery used later for:

- Achieving a decentralized control architecture by enforcing sparsity constraints in an SDP with LMI constraints, and
- Transforming the scenario-based synthesis problem into a complex semidefinite program, for achieving the end of synthesizing a controller with complex performance output equations that were designed in modal coordinates.

We now start with introducing linear matrix inequalities. We refer to the monograph by Boyd [15] for a comprehensive review of LMIs and how they are used throughout system and control theory.

If we let $x \in \mathbb{R}^m$, an LMI condition on x is the following:

$$F(x) > 0 \quad (5.10)$$

where (5.10) indicates that the matrix function is positive definite. Moreover, $F(x)$ actually has the representation

$$F(x) = F_0 + \sum_{i=1}^m x_i F_i \quad (5.11)$$

where $F_i \in \mathbb{S}^{n \times n}$, $i = 0, \dots, m$ are symmetric matrices. We note that if $F_{(1)}(x)$ and $F_{(2)}(x)$ are both LMIs in x , then

$$F_{(1,2)}(x) = \begin{bmatrix} F_{(1)}(x) & 0 \\ 0 & F_{(2)}(x) \end{bmatrix} \quad (5.12)$$

is also an LMI.

In many control synthesis and analysis problems, linear matrix inequalities are used as the constraints in semidefinite programs. These problems are cast as

$$\begin{aligned} \min_x \quad & c^T x \\ \text{s.t.} \quad & F(x) < 0. \end{aligned} \tag{5.13}$$

A semidefinite program has both a primal and a dual form. Introducing these forms now will be useful as we get into a discussion on complex semidefinite programming later on in this chapter.

We consider a semidefinite program in primal inequality form

$$\begin{aligned} \min_x \quad & c^T x \\ \text{s.t.} \quad & x_1 F_1 + \cdots + x_m F_m + F_0 \leq 0 \end{aligned} \tag{5.14}$$

where $F_1, \dots, F_m, F_0 \in \mathbb{S}^{n \times n}$. $x \in \mathbb{R}^m$ is the variable and $c^T \in \mathbb{R}^m$.

We can associate with the constraint a dual variable or multiplier $Z \in \mathbb{S}^{n \times n}$ so that the Lagrangian is

$$L(x, Z) = c^T x + \text{Tr}((x_1 F_1 + \cdots + x_m F_m + F_0)Z) \tag{5.15}$$

which is affine in x . The dual function is given by

$$h(Z) = \inf_x L(x, Z) = \begin{cases} \text{Tr}(F_0 Z) & \text{Tr}(F_i Z) + c_i = 0, \quad i = 1, \dots, m \\ -\infty & \text{otherwise} \end{cases} \tag{5.16}$$

which can be written as:

$$\begin{aligned} \max \quad & \text{Tr}(F_0 Z) \\ \text{s.t.} \quad & \text{Tr}(F_i Z) + c_i = 0, \quad i = 1, \dots, m \\ & Z \geq 0. \end{aligned} \tag{5.17}$$

This form is important when we get into discussing complex semidefinite programming later on in this chapter.

What we see at this point is that semidefinite programming is performed over real-valued decision variables and cones of symmetric matrices. See Boyd for more details on LMIs and convex optimization [15, 65].

We return to discussing the scenario-based problem. The problem given by (5.3) can be solved as an SDP with multiple linear matrix inequality constraints. In primal form, this looks like

$$\begin{aligned} \min_{\theta} \quad & c^T \theta \\ \text{s.t.} \quad & F_1(\theta) \leq 0 \\ & F_2(\theta) \leq 0 \\ & \vdots \\ & F_N(\theta) \leq 0 \end{aligned} \tag{5.18}$$

which is a convex (semidefinite) program with N linear matrix inequality constraints. In this work we set $c = 0$, turning this into a feasibility problem: that is, we search over the set $\theta \in \Theta$ for the existence of some θ^* that satisfies all N linear matrix inequality constraints which represent a multisample of the random plant set. Numerically, this optimization problem is solved with the use of open-source optimization parsing software, Yalmip [66], and the commercially-available (yet free to university researchers) conic optimization solver MOSEK©.

Something powerful and elegant about the scenario approach is that we are able to formulate high-dimensional stochastic optimization problems that are convex. Furthermore, this approach permits the leveraging of any available computing resources. Many conic solvers, such as MOSEK©, are internally parallelized.

It is well-known that the full-state feedback \mathcal{H}_∞ problem can be represented as a semidefinite program with linear matrix inequality constraints; this makes this specific controller synthesis problem amenable to the scenario-based approach, as we can aggregate a finite collection of linear matrix inequality constraints, each containing samples from the random

plant data, into the form given by (5.18) [60]. Prior to actually doing this, we will present the theory behind full-state feedback \mathcal{H}_∞ synthesis, as some results through this presentation will be useful later on in this chapter.

5.2 FULL-STATE FEEDBACK \mathcal{H}_∞ CONTROLLER SYNTHESIS USING LINEAR MATRIX INEQUALITIES

We will now show how the full-state feedback \mathcal{H}_∞ problem is formulated as a semidefinite program with linear matrix inequality constraints. Some of this derivation becomes quite useful in a result that we will derive later on. The formulations provided were compiled with the aid of [60, 67].

In the full-state feedback \mathcal{H}_∞ formulation, we want to find the existence of some control law $u = Kx$ for the system

$$G \sim \left[\begin{array}{c|cc} A & B_1 & B_2 \\ \hline C_1 & D_{11} & D_{12} \\ I & 0 & 0 \end{array} \right] \quad (5.19)$$

and controller

$$\bar{K} \sim \left[\begin{array}{c|c} 0 & 0 \\ \hline 0 & K \end{array} \right] \quad (5.20)$$

leading to the LFT mapping $w \rightarrow z$

$$F_l(G, \bar{K}) = \left[\begin{array}{c|c} A + B_2K & B_1 \\ \hline C_1 + D_{12}K & D_{11} \end{array} \right]. \quad (5.21)$$

By the Kalman-Yakubovich-Popov (KYP) Lemma (also known as the Bounded Real Lemma), $\|F_l(G, \bar{K})\|_\infty < \gamma$ if and only if there exists some $X > 0$ such that

$$\begin{bmatrix} (A + B_2K)^T X + X(A + B_2K) & XB_1 \\ B_1^T X & -\gamma I \end{bmatrix} + \gamma^{-1} \begin{bmatrix} (C_1 + D_{12}K)^T \\ D_{11}^T \end{bmatrix} \begin{bmatrix} (C_1 + D_{12}K) & D_{11} \end{bmatrix} < 0. \quad (5.22)$$

The KYP condition is given by the following equivalency.

Lemma 1 (The KYP Lemma, also known as the Bounded Real Lemma). *Suppose*

$$G \sim \left[\begin{array}{c|c} A & B \\ \hline C & D \end{array} \right] \quad (5.23)$$

Then the following are equivalent:

1. $\|G\|_\infty \leq \gamma$
2. There exists a $X > 0$ such that

$$\begin{bmatrix} A^T X + XA & XB \\ B^T X & -\gamma I \end{bmatrix} + \gamma^{-1} \begin{bmatrix} C^T \\ D^T \end{bmatrix} \begin{bmatrix} C & D \end{bmatrix} < 0. \quad (5.24)$$

The proof to this lemma is provided in appendix D.

A fundamental concept from linear algebra is the Schur Complement of a block matrix. The Schur Complement is used to prove the bounded real lemma, for formulating the full-state feedback \mathcal{H}_∞ synthesis problem, and used for a proof surrounding controller synthesis for complex performance output equations in this thesis. Although the Schur Complement is fundamental to linear algebra, we refer to [68] for the proof.

Theorem 5 (Schur Complement). *For any $M \in \mathbb{S}^{n \times n}$, $Q \in \mathbb{S}^{m \times m}$, and $R \in \mathbb{R}^{n \times m}$, the following are equivalent:*

1. $\begin{bmatrix} M & R \\ R^T & Q \end{bmatrix} < 0$
2. $Q < 0$ and $M - RQ^{-1}R^T < 0$

For the case specific to the KYP Lemma, let

$$Q = -\gamma^{-1}I < 0, \quad M = \begin{bmatrix} A^T X + XA & XB \\ B^T X & -\gamma I \end{bmatrix}, \quad R = \begin{bmatrix} C & D \end{bmatrix}^T, \quad (5.25)$$

thus, using the Schur complement we get

$$\begin{bmatrix} A^T X + XA & XB \\ B^T X & -\gamma I \end{bmatrix} + \gamma^{-1} \begin{bmatrix} C^T \\ D^T \end{bmatrix} \begin{bmatrix} C & D \end{bmatrix} < 0 \quad (5.26)$$

if and only if

$$\begin{bmatrix} A^T X + XA & XB & C^T \\ B^T X & -\gamma I & D^T \\ C & D & -\gamma I \end{bmatrix} < 0. \quad (5.27)$$

We notice that we have made the LMI larger, in this case. This leads to the full-state feedback condition for the system given by equation (5.21):

$$\begin{bmatrix} (A + B_2 K)^T X + X(A + B_2 K) & XB_1 & (C_1 + D_{12} K)^T \\ B_1^T X & -\gamma I & D_{11}^T \\ (C_1 + D_{12} K) & D_{11} & -\gamma I \end{bmatrix} < 0 \quad (5.28)$$

where the above LMI is now bilinear in X and K . We want to use a variable substitution trick to formulate an LMI that is linear in its controller variables. To do so, we must apply the Dual KYP Lemma, which says:

Lemma 2 (KYP Dual). *Suppose*

$$G \sim \left[\begin{array}{c|c} A & B \\ \hline C & D \end{array} \right], \quad (5.29)$$

then the following are equivalent:

- $\|G\|_\infty \leq \gamma$
- there exists a $Q > 0$, s.t.

$$\begin{bmatrix} QA^T + AQ & B & QC^T \\ B^T & -\gamma I & D^T \\ CQ & D & -\gamma I \end{bmatrix} < 0. \quad (5.30)$$

We let $X = Q^{-1}$. Then,

$$\begin{bmatrix} QA^T + AQ & B & QC^T \\ B^T & -\gamma I & D^T \\ CQ & D & -\gamma I \end{bmatrix} < 0 \quad \text{and} \quad Q > 0 \quad \text{iff} \quad X > 0 \quad (5.31)$$

and

$$\begin{bmatrix} Q^{-1} & 0 & 0 \\ 0 & I & 0 \\ 0 & 0 & I \end{bmatrix} \begin{bmatrix} QA^T + AQ & B & QC^T \\ B^T & -\gamma I & D^T \\ CQ & D & -\gamma I \end{bmatrix} \begin{bmatrix} Q^{-1} & 0 & 0 \\ 0 & I & 0 \\ 0 & 0 & I \end{bmatrix} = \begin{bmatrix} A^T Q + QA & QB & C^T \\ B^T Q & -\gamma I & D^T \\ C & D & -\gamma I \end{bmatrix} < 0. \quad (5.32)$$

By a Schur complement, this is equivalent to

$$\begin{bmatrix} A^T X + XA & XB \\ B^T X & -\gamma I \end{bmatrix} + \gamma^{-1} \begin{bmatrix} C^T \\ D^T \end{bmatrix} \begin{bmatrix} C & D \end{bmatrix} < 0 \quad (5.33)$$

and by the KYP lemma this is equivalent to $\|G\|_\infty \leq \gamma$. This result can now be applied to the full state feedback problem.

Theorem 6. *The following are equivalent:*

- There exists an K such that $\|F_l(G, \bar{K})\|_\infty \leq \gamma$
- There exists a $Q > 0$ and Y such that

$$\begin{bmatrix} QA^T + AQ + Y^T B_2 + B_2 Y & B_1 & QC_1^T + Y^T D_{12}^T \\ B_1^T & -\gamma I & D_{11}^T \\ C_1 Q + D_{12} Y & D_{11} & -\gamma I \end{bmatrix} < 0. \quad (5.34)$$

Then $K = YQ^{-1}$.

Proof. See appendix E.

These derivations and results were provided to achieve the following ends:

1. Provide some background into LMIs and SDP, as this background is built into complex semidefinite programming (CSDP).
2. Show that the full-state feedback \mathcal{H}_∞ synthesis problem, cast as an SDP with LMI constraints, is convex and thus amenable to the scenario approach.
3. Introduce the Schur Complement and show how it is used with full-state feedback \mathcal{H}_∞ LMIs, as it is used later to prove a result related to guaranteeing real-valued controllers for complex performance output equations using the scenario approach.

5.3 A USEFUL ISOMORPHISM BETWEEN \mathbb{C} AND \mathbb{R}

One of the contributions of this thesis is the following: a controller design and synthesis approach that permits frequency-weighting of system models with complex-valued performance output functions, and the synthesis of a structure-constrained high-dimensional semidefinite program for achieving decentralized full-state feedback \mathcal{H}_∞ control in the presence of random interconnections.

Before getting into complex semidefinite programming, an isomorphism between \mathbb{C} and \mathbb{R} must be detailed, as this isomorphism is useful for CSDP, as well as for a theorem and proof that is developed later in this chapter.

Complex-coefficient systems in control is a topic that is receiving attention within the controls community as of late [69]. Using the approaches developed in this chapter, in conjunction with the scenario approach to probabilistic robust control, could lead to some exciting developments for those investigating controller design, synthesis, and analysis for complex-coefficient systems.

We begin by observing that one way to construct the field of complex numbers is the following:

$$\mathbb{C} = \left\{ \begin{bmatrix} a & -b \\ b & a \end{bmatrix} \mid a, b \in \mathbb{R} \right\} = \left\{ a \begin{bmatrix} 1 & 0 \\ 0 & 1 \end{bmatrix} + b \begin{bmatrix} 0 & -1 \\ 1 & 0 \end{bmatrix} \mid a, b \in \mathbb{R} \right\}. \quad (5.35)$$

Formally, this is called a commutative subring of $\mathcal{M}_2(\mathbb{R})$. This construction identifies the number 1 with I , which is the identity of size 2, a real number a with the diagonal matrix aI , and the imaginary number i with the matrix $J = \begin{bmatrix} 0 & -1 \\ 1 & 0 \end{bmatrix}$, which is justified by the fact that $J^2 = -I$.

The matrix representation of a complex number, using this construction, is an isomorphism. Standard properties for matrix operations hold: associativity, commutativity, distributivity. This is very powerful and enables us to manipulate complex numbers using linear

algebra over the field of real numbers. What this means, then, is that

$$aI + bJ = \begin{bmatrix} a & -b \\ b & a \end{bmatrix} \quad (5.36)$$

behaves exactly like $a + jb$ under addition, subtraction, multiplication, complex conjugation/transposition. This means that an isomorphic map exists from \mathbb{C} to the set of skew-symmetric matrices $aI + bJ$. This isomorphism is what makes complex semidefinite programming possible.

This transformation will now be applied to a complex matrix. We can take a complex matrix that we will call Z , given by

$$Z = \begin{bmatrix} z_{11} & z_{12} \\ z_{21} & z_{22} \end{bmatrix} \quad (5.37)$$

we can map this complex matrix $Z \in \mathbb{C}^{2 \times 2}$ into a real matrix $\in \mathbb{R}^{4 \times 4}$ by replacing each $z_{i,j}$ with 2 by 2 matrices that look like the matrix given in (5.35). Let us further examine this by substituting $z_{i,j} = a_{i,j} + ib_{i,j}$. So, we have

$$Z = \begin{bmatrix} a_{11} + ib_{11} & a_{12} + ib_{12} \\ a_{21} + ib_{21} & a_{22} + ib_{22} \end{bmatrix} \quad (5.38)$$

where we perform the transformation outlined in this section to get a block 2×2 matrix

$$\tilde{Z} = \left[\begin{array}{cc|cc} a_{11} & -b_{11} & a_{12} & -b_{12} \\ b_{11} & a_{11} & b_{12} & a_{12} \\ \hline a_{21} & -b_{21} & a_{22} & -b_{22} \\ b_{21} & a_{21} & b_{22} & a_{22} \end{array} \right]. \quad (5.39)$$

This matrix can then be mapped through a similarity transform into

$$\mathcal{T}(Z) \doteq T^{-1}\tilde{Z}T = \begin{bmatrix} \text{Re}(Z) & -\text{Im}(Z) \\ \text{Im}(Z) & \text{Re}(Z) \end{bmatrix}. \quad (5.40)$$

This transformation is important, at this stage, for showing that a complex semidefinite program (CSDP) is equivalent to a semidefinite program (SDP). We shall denote $\mathcal{T}(Z)$ as the

transformation that is used in converting a complex matrix into a real one of the form given in (5.40), with $\dim(\mathcal{T}(Z)) = 2\dim(Z)$. We can then carry out block matrix multiplication between the real and imaginary blocks given by (5.40). There are a few properties, preserved through this transformation, that are important in the context of this work.

Theorem 7 (Eigenvalue and Eigenvector Preservation under $\mathcal{T}(\cdot)$). *The eigenvalues of a complex matrix Z are preserved through the isomorphism $\mathcal{T}(Z)$.*

Proof. For a complex matrix $Z \in \mathbb{C}^{n \times n}$, let

$$Z = X + jY, \quad X, Y \in \mathbb{R}^{n \times n}. \quad (5.41)$$

We have that $\mathcal{T}(Z)$ is the isomorphic transformation given by (5.40), meaning this is a real matrix $\mathcal{T}(Z) \in \mathbb{R}^{2n \times 2n}$:

$$\mathcal{T}(Z) = \begin{bmatrix} X & -Y \\ Y & X \end{bmatrix}. \quad (5.42)$$

Lemma 3. *If Z is Hermitian, $Z = Z^H$, then X is symmetric, $X = X^T$ and Y is skew-symmetric, $Y = -Y^T$.*

Proof.

$$X + jY = (X + jY)^H = X^T - jY^T \quad (5.43)$$

equating real and imaginary parts, $X = X^T$ and $Y = -Y^T$.

Lemma 4. *If Z is Hermitian $Z = Z^H$, then*

$$\mathcal{T}(Z) = \begin{bmatrix} X & -Y \\ Y & X \end{bmatrix} \quad \text{is symmetric.} \quad (5.44)$$

Proof.

$$\mathcal{T}(Z)^T = \begin{bmatrix} X & -Y \\ Y & X \end{bmatrix}^T = \begin{bmatrix} X^T & Y^T \\ -Y^T & X^T \end{bmatrix} = \begin{bmatrix} X & -Y \\ Y & X \end{bmatrix} = \mathcal{T}(Z)^T. \quad (5.45)$$

We point out that Z and $\mathcal{T}(Z)$ have real eigenvalues since they are hermitian.

Lemma 5. *The hermitian matrix Z has an eigenvalue λ with eigenvector $u + jv$ if and only if $\mathcal{T}(Z)$ has eigenvalue of multiplicity two with real eigenvectors $\hat{\Phi}_1 = \begin{bmatrix} u \\ v \end{bmatrix}$ and $\hat{\Phi}_2 = \begin{bmatrix} v \\ -u \end{bmatrix}$.*

Proof.

$$Z\Phi = \lambda\Phi \quad (5.46)$$

$$(X + jY)(u + jv) = \lambda(u + jv) \quad (5.47)$$

$$(Xu - Yv) = j(Yu + Xv) = \lambda u + j\lambda v \quad (5.48)$$

$$\text{real } Xu - Yv = \lambda u \quad (5.49)$$

$$\text{imag } Yu + Xv = \lambda v \quad (5.50)$$

$$\begin{bmatrix} X & -Y \\ Y & X \end{bmatrix} \begin{bmatrix} u \\ v \end{bmatrix} = \lambda \begin{bmatrix} u \\ v \end{bmatrix} \quad (5.51)$$

$$\mathcal{T}(Z)\hat{\Phi}_1 = \lambda\hat{\Phi}_1. \quad (5.52)$$

Now, proving the equality in the other direction is straightforward. Showing that this result holds for the eigenvector $\begin{bmatrix} v \\ -u \end{bmatrix}$ is also straightforward. We have therefore shown that if λ is an eigenvalue with eigenvector $u + jv$ of the complex, hermitian matrix A , then it is an eigenvalue of multiplicity two with eigenvectors $\begin{bmatrix} u \\ v \end{bmatrix}$ and $\begin{bmatrix} v \\ -u \end{bmatrix}$ of the matrix $\mathcal{T}(A)$.

Q.E.D.

This leads us to the following corollary:

Corollary 8. *Positive and negative (semi)definiteness are preserved under the transformation given by $\mathcal{T}(\cdot)$, which follows immediately from theorem 7:*

$$A > 0 \Leftrightarrow \lambda(A) > 0 \Leftrightarrow \lambda(\mathcal{T}(A)) > 0 \Leftrightarrow \mathcal{T}(A) > 0. \quad (5.53)$$

We will now use these results to discuss complex semidefinite programming.

5.4 COMPLEX SEMIDEFINITE PROGRAMMING

Goemans and Williamson [70] showed that complex semidefinite programs can be reduced to semidefinite programs, which is achievable by using linear transformations that map $\mathbb{H}^{n \times n}$ matrices to $\mathbb{S}^{2n \times 2n}$ matrices. These transformations were the topic of section 5.3.

In a complex semidefinite program, the linear matrix inequalities are given by

$$\tilde{F}(\tilde{x}) = \tilde{F}_0 + \sum_{i=1}^n \tilde{x}_i \tilde{F}_i, \quad (5.54)$$

where $\tilde{x} \in \mathbb{C}^m$ and $\tilde{F}_0, \tilde{F}_i \in \mathbb{H}^{n \times n}$. This means that the program that we are trying to solve, in the dual form, looks like

$$\begin{aligned} \max \quad & \text{Tr}(\tilde{F}_0 Z) \\ \text{s.t.} \quad & \text{Tr}(\tilde{F}_i Z) + c_i = 0, \quad i = 1, \dots, m \\ & Z \geq 0 \\ & Z \in \mathbb{H}^{n \times n}. \end{aligned} \quad (5.55)$$

It may be obvious from the discussion in section 5.3 what we will be doing to convert this problem into an equivalent real-valued semidefinite program. This will now be discussed.

5.4.1 Formulating the Equivalent Real-Valued Semidefinite Program

Given two complex, Hermitian matrices A , and B , the inner product of these matrices is given by

$$A \bullet B = \text{Tr}(AB^H). \quad (5.56)$$

By mapping both A and B through the transformation given by (5.40), the inner product is

$$\mathcal{T}(A) \bullet \mathcal{T}(B) = \text{Tr} \left(\begin{bmatrix} \text{Re}A & -\text{Im}A \\ \text{Im}A & \text{Re}A \end{bmatrix} \begin{bmatrix} \text{Re}B & \text{Im}B \\ -\text{Im}B & \text{Re}B \end{bmatrix} \right) \quad (5.57)$$

$$= 2\text{Tr}(\text{Re}B\text{Re}A + \text{Im}B\text{Im}A) = 2A \bullet B. \quad (5.58)$$

This is important to note, as we can now examine the canonical, dual form of a semidefinite program for the complex case. And we now consider the following SDP

$$\max \quad \text{Tr}(\tilde{\mathcal{F}}_0 Y) \quad (5.59)$$

$$\text{s.t.} \quad \text{Tr}(\tilde{\mathcal{F}}_i Y) + 2c_i = 0, \quad i = 1, \dots, m \quad (5.60)$$

$$\text{Tr} \left(\begin{bmatrix} E_{ij} & 0 \\ 0 & -E_{ij} \end{bmatrix} Y \right) = 0, \quad i, j = 1, \dots, n, i \leq j \quad (5.61)$$

$$\text{Tr} \left(\begin{bmatrix} 0 & E_{ij} \\ E_{ij} & 0 \end{bmatrix} Y \right) = 0, \quad i, j = 1, \dots, n, i \leq j \quad (5.62)$$

$$Y \geq 0 \quad (5.63)$$

$$Y \in \mathbb{S}^{2n \times 2n} \quad (5.64)$$

where e_i is the i th unit vector, and $E_{ij} = e_i e_j^T + e_j e_i^T$ — this matrix has unity in positions (i, j) and (j, i) and zeros everywhere else. The two constraints (5.61) and (5.62) ensure that our decision matrix Y has the form

$$Y = \begin{bmatrix} L & -M \\ M & L \end{bmatrix} \quad (5.65)$$

for some symmetric L and skew-symmetric M . We see that for Y of this form that $\mathcal{T}^{-1}(Y) = Z$ is unique and well-defined.

The SDP is equivalent to the CSDP. Given some feasible solution Z to the CSDP, $\mathcal{T}(Z)$ is also a feasible solution for the SDP with objective function that is twice that of the CSDP. If Y is a feasible solution to the SDP, then $\mathcal{T}^{-1}(Z)$ is also a feasible solution to the CSDP with objective function equal to one half of that of the SDP [70].

Lastly, using theorem 7 and corollary 8, we have that $Y > 0 \Rightarrow Z > 0$, and that these matrices have the same eigenvalues.

We are now prepared to discuss how the scenario approach to probabilistic robust controller synthesis is used to find a decentralized controller for a lightly-damped SMD model with complex performance output function, where control design was performed in a complex modal basis.

5.5 SCENARIO-BASED, DECENTRALIZED, PROBABILISTIC ROBUST SYNTHESIS FOR A SYSTEM REPRESENTED IN COMPLEX MODAL COORDINATES

In this section we consider control design and synthesis of a lightly-damped, uncertain structure for the case of non-proportional damping where controller design and synthesis is performed in a modal basis. This section brings together the topics that were discussed in the preceding sections of this chapter:

- The scenario approach;
- Representation of the \mathcal{H}_∞ synthesis SDP as a CSDP since control design is performed in complex modal coordinates.

Analyzing lightly damped systems, including controller design, in the modal basis is both attractive and intuitive to the vibration control engineer. Implicit to this basis is the fact that we have decoupled modes, enabling us to analyze specific modes and frequencies during controller design and synthesis.

The system model, controller design approach, and control objectives for this section were discussed in chapter 4. The specifics about the system model are included in appendix A.

State space control design and synthesis approaches are typically approached in \mathbb{R} . That is, we usually look at the system

$$G \sim \left[\begin{array}{c|cc} A & B_1 & B_2 \\ \hline C_1 & D_{11} & D_{12} \\ I & 0 & 0 \end{array} \right] \quad (5.66)$$

with the sizes of this matrices defined in chapter 3. One thing that we know is that for any $A \in \mathbb{R}^{n \times n}$ that we can solve

$$A\Phi = \Phi\Lambda \quad (5.67)$$

which is the generalized eigenvalue problem for any square matrix, A . Then,

$$\Phi^{-1}A\Phi = \Lambda = \text{diag}(\lambda_1, \dots, \lambda_n) \quad (5.68)$$

is a diagonal matrix containing the eigenvalues of our original matrix A , provided A has eigenvalues that are distinct and nonzero. It almost goes without saying that Φ is our matrix of eigenvectors.

It is common practice for the vibration control engineer to examine, model, and synthesize controllers in the modal space. That is, our modal coordinates are given by $q = \Phi^{-1}x$, meaning the similarity transformation $x = \Phi q$, leads our system to be described as

$$\tilde{G} \sim \left[\begin{array}{c|cc} \Phi^{-1}A\Phi & \Phi^{-1}B_1 & \Phi^{-1}B_2 \\ \hline C_1\Phi & D_{11} & D_{12} \\ \Phi & 0 & 0 \end{array} \right] = \left[\begin{array}{c|cc} \Lambda & \Phi^{-1}B_1 & \Phi^{-1}B_2 \\ \hline C_1\Phi & D_{11} & D_{12} \\ \Phi & 0 & 0 \end{array} \right]. \quad (5.69)$$

Now we can see why this would be an attractive basis. All of our states are decoupled in the dynamics matrix. Control design and system analysis in modal coordinates can be both powerful and very intuitive in this basis, and is fundamental in the study of lightly damped structures [61].

Placing the system into the coordinate system described by (5.69) does not exactly inhibit the interpretability of the physics. Although most transformations involve assuming proportional damping (leading to the use of bases with real-valued eigenvectors), we still have that each eigenvalue, or natural frequency, is associated with a given eigenvector, thereby

assigning a magnitude (natural frequency) to the rotation (mode shape) of our similarity transformation as we get our system into its new, modal form. In this form we have

$$\Lambda = \begin{bmatrix} -\sigma_1 + j\omega_1 & 0 & 0 & 0 & 0 & 0 \\ 0 & -\sigma_1 - j\omega_1 & 0 & 0 & 0 & 0 \\ 0 & 0 & \ddots & 0 & 0 & 0 \\ 0 & 0 & 0 & \ddots & 0 & 0 \\ 0 & 0 & 0 & 0 & -\sigma_n + j\omega_n & 0 \\ 0 & 0 & 0 & 0 & 0 & -\sigma_n - j\omega_n \end{bmatrix} \quad (5.70)$$

where, clearly, our complex conjugate pairs are associated with the natural frequencies by $\omega_{n,i} = |\sigma_i \pm j\omega_i|$, with each natural frequency corresponding with their respective mode shapes. In this state space, we can target specific modes/frequencies all-the-same.

To do so, we define our z -equations while in modal coordinates:

$$z = \tilde{C}_1 q + D_{11} w + D_{12} u$$

$$z = \begin{bmatrix} I_{n \times n} \\ 0_{r_2 \times n} \end{bmatrix} q + \begin{bmatrix} 0_{(n+r_2) \times r_1} \end{bmatrix} w + r_z \begin{bmatrix} 0_{n \times r_2} \\ I_{r_2 \times r_2} \end{bmatrix} u. \quad (5.71)$$

By defining the performance output function while in modal coordinates, the mapping is now an explicit expression that maps disturbance inputs to the system modes. Even though the system matrices specific to this realization are complex, it is perfectly acceptable to examine the magnitude and phase of this transfer function matrix, as any transfer function matrix is a complex function, anyway. With this being said, it is worthwhile to highlight the property of transfer function invariance under non-singular similarity transformations. Because of the basis in which \tilde{C}_1 is defined, our physical state space will still have complex matrices.

In order to map back into our physical coordinate system, we know that we use the similarity transform $q = \Phi^{-1}x$. This will bring our system into the form

$$\hat{G} \sim \left[\begin{array}{c|cc} A & B_1 & B_2 \\ \hline \tilde{C}_1 \Phi^{-1} & D_{11} & D_{12} \\ I & 0 & 0 \end{array} \right] \quad (5.72)$$

where we see, right away, that the term $\tilde{C}_1\Phi^{-1} \in \mathbb{C}^{(n+r_2) \times n}$. Now, if we suppose that we synthesize a control law $u = Ky = Kx \in \mathbb{R}^{r_2 \times n}$ such that $\left\| F_l(\hat{G}, K) \right\|_\infty \leq \gamma$, where

$$F_l(\hat{G}, K) \sim \begin{bmatrix} A + B_2K & B_1 \\ \tilde{C}_1\Phi^{-1} + D_{12}K & D_{11} \end{bmatrix} \quad (5.73)$$

then the same \mathcal{H}_∞ -norm is achieved when the controlled system is also in (complex) modal coordinates.

Now, under the non-singular similarity transformation $x = \Phi q$, we have

$$\tilde{G} \sim \begin{bmatrix} \Phi^{-1}A\Phi & \Phi^{-1}B_1 & \Phi^{-1}B_2 \\ \tilde{C}_1 & D_{11} & D_{12} \\ \Phi & 0 & 0 \end{bmatrix} \quad (5.74)$$

and that the control law $u = K\Phi q$. Since any system is invariant under any nonsingular similarity transform, we have that $\hat{G} = \tilde{G}$, leading to the conclusion that $F_l(\tilde{G}, K) = F_l(\hat{G}, K)$.

5.5.1 Enforcing Sparsity Constraints on our Controller Variables

The essence of this idea is straightforward. This is achieved by choosing a block-diagonal basis for the controller variables in the semidefinite program. This was briefly described in equation (4.39) in chapter 4. Parsing this structure for the decentralized full state feedback \mathcal{H}_∞ scenario-based synthesis is achieved using the software YALMIP [66]. We will show how this structure-enforced optimization is carried out for a simple problem.

This is most easily seen for the Lyapunov Inequality for a 2×2 stable system matrix, A . Given some $A \in \mathbb{R}^{2 \times 2}$, $\text{Re}(\lambda(A) < 0)$, we know that the Lyapunov Inequality states that A is stable if some $P > 0$ exists that satisfies

$$A^T P + PA < 0. \quad (5.75)$$

This equation is easily posed as the semidefinite feasibility problem

$$\begin{aligned} \min_x & \quad 0 \\ \text{s.t.} & \quad A^T P + PA < 0, \quad P > 0. \end{aligned} \tag{5.76}$$

To cast this problem into it's canonical form with sparsity constraints enforced on a candidate diagonal $P > 0$ we write the matrix inequality as

$$\sum_{i=1}^2 x_i \begin{bmatrix} P_i & 0 \\ 0 & -A^T P_i - P_i A \end{bmatrix} > 0 \tag{5.77}$$

where

$$P_1 = \begin{bmatrix} 1 & 0 \\ 0 & 0 \end{bmatrix}, \quad P_2 = \begin{bmatrix} 0 & 0 \\ 0 & 1 \end{bmatrix}. \tag{5.78}$$

And so it is as simple as choosing a diagonal, or block diagonal basis for our controller variables in a semidefinite program. The one drawback to enforcing sparsity constraints is that we restrict our feasible search space from $\frac{1}{2}n(n+1)$ to $\frac{1}{2}n(\frac{n}{2}+1)$ variables to search over (for problems where we deal with only one symmetric matrix). This can lead to a higher chance of infeasibility in SDPs since we are constricting our search space. For the scenario approach, however, we are reducing the number of unique controller variables, thus requiring fewer samples to achieve some specified level of accuracy and confidence in a solution.

5.5.2 Frequency Weighting the Disturbance Input (B_1) and Performance Output (\tilde{C}_1) Matrices

Frequency weighting of lightly-damped structures for control design was covered in section 4.5.2. It is implemented on the disturbance input (B_1) and performance output (\tilde{C}_1) matrices for controller design in this chapter.

In this aspect of the research we have elected to focus on the attenuation of low-frequency disturbance inputs. A first-order disturbance input filter transfer function matrix that looks like

$$W_w(s) = \text{diag} \left(\frac{\omega_{wc}}{(s + \omega_{wc})_1}, \dots, \frac{\omega_{wc}}{(s + \omega_{wc})_{r_1}} \right) \tag{5.79}$$

is constructed with $\omega_{wc} = 1.6 \text{ Hz}$ (10 rad/s) chosen as the cutoff frequency in this filter. A first order filter was chosen to promote rolloff at high frequencies, thus placing the greatest emphasis on those low-frequency disturbances that enter the system, and hence, placing the greatest amount of emphasis on controller synthesis in the low frequency range. To implement this filtering strategy using the scaling methods detailed in chapter 4, which are particular to lightly-damped systems, the disturbance input matrix rows are scaled by the magnitude of the filter function at each resonant frequency in modal coordinates. This means that the frequency scaled disturbance input matrix is

$$\tilde{B}_1^* = \Phi W_w \Phi^{-1} B_1 \quad (5.80)$$

where W_w was defined in equation (4.36) in chapter 4. Note that the term $\Phi W_w \Phi^{-1} B_1$ is guaranteed to be real since W_w is only row scaling the matrix $\Phi^{-1} B_1$, which is the disturbance input matrix in modal coordinates. Thus, by left multiplying by Φ after this scaling, we still map back into \mathbb{R} since $B_1 \in \mathbb{R}^{r_2 \times n}$.

Each pair of elements in (4.36) represents the magnitude of the input filters at each system resonance. Since all transfer functions in (5.79) are equal, we end up with the diagonal structure W_w , as indicated, which gives rise to the row scaling in (5.80).

In similar order, we presume that we are most interested in the attenuation of low-frequency structural modes. As a slight variant to our disturbance input filtering, we will augment our performance output function with a first-order transfer function with unity DC-gain. In this manner, we get -20 dB/decade rolloff at frequencies beyond our cutoff frequency. This means that our performance output, for controller synthesis, will be filtered through some transfer function matrix that looks like

$$W_z(s) = \text{diag} \left(\frac{\omega_{zc}}{(s + \omega_{zc})_1}, \dots, \frac{\omega_{zc}}{(s + \omega_{zc})_n} \right), \quad (5.81)$$

with $\omega_{zc} = 2.7 \text{ Hz}$ (17 rad/s). A diagonal matrix results from evaluating $W_z(s)$ at each resonant frequency, as shown in equation (4.37) in chapter 4.

We saw from previous that when in our modal coordinate system, we defined

$$\tilde{C}_1 = \begin{bmatrix} I_{n \times n} \\ 0_{r_2 \times n} \end{bmatrix} \quad (5.82)$$

where the zeros, with rows equal to the number of control inputs, are appended since we have included nonzero D_{12} terms for control design and synthesis, as we want to avoid actuator singularities at high frequencies and also want the ability to trade off control input energy.

Performance output matrix scaling in modal coordinates serves as a good approximation of this filtering that we've just discussed, without increasing the order of the plant. Our frequency-weighted performance output matrix in modal coordinates will now look like:

$$\tilde{C}_1^* = \begin{bmatrix} W_z \\ 0_{r_2 \times n} \end{bmatrix}, \quad W_z = \begin{bmatrix} \alpha_1^C & 0 & \dots & 0 & 0 \\ 0 & \alpha_1^C & \dots & 0 & 0 \\ 0 & 0 & \ddots & 0 & 0 \\ 0 & 0 & \dots & \alpha_p^C & 0 \\ 0 & 0 & 0 & 0 & \alpha_p^C \end{bmatrix}, \quad p = n/2 \quad (5.83)$$

where each α_i^C is the magnitude of the filter functions at each resonant frequency.

These scalings, with performance output functions defined and scaled in modal coordinates, leads our system to have the representation (in physical coordinates):

$$\bar{G} \sim \left[\begin{array}{c|cc} A & \tilde{B}_1^* & B_2 \\ \hline \tilde{C}_1^* \Phi^{-1} & D_{11} & D_{12} \\ I & 0 & 0 \end{array} \right]. \quad (5.84)$$

The system given by (5.84) is the nominal open-loop system that we are using for synthesis. However, as the title of this chapter (and thesis) imply, we are interested in synthesizing a controller that is robust against random interconnection uncertainty. In chapter 4 we declared that the interconnection stiffness, $k_\Delta \sim \mathcal{N}(100, 15^2)$. By removing the interconnection stiffness terms from the dynamics matrix A and denoting this system, with interconnection stiffness terms removed A_0 , we can represent our uncertain system as having real, random,

affine parametric uncertainty entering the system. That is,

$$A_\Delta = A_0 + \Delta \quad (5.85)$$

where Δ has the support

$$\mathcal{B}_\Delta(a) \doteq \{\Delta \in \mathbb{R}^{n \times n} : \Delta \sim f_\Delta(a)\} \quad (5.86)$$

with $a = 1$ and $f_\Delta(a) = \mathcal{N}(100, a15^2)$ for synthesis.

The matrix Δ , as shown in appendix A, has the structure:

$$\Delta = \begin{bmatrix} 0 & 0 & 0 & 0 \\ 0 & k_\Delta & -k_\Delta & 0 \\ 0 & -k_\Delta & k_\Delta & 0 \\ 0 & 0 & 0 & 0 \end{bmatrix} \quad (5.87)$$

$$k_\Delta \sim f_\Delta(a) = \mathcal{N}(100, a15^2). \quad (5.88)$$

Now, this means is that the \mathcal{H}_∞ synthesis problem, as a CSDP, becomes

$$\min_{Q,Y} 0 \quad (5.89)$$

$$\text{s.t. } \begin{bmatrix} QA_\Delta^H + A_\Delta Q + Y^H B_2^H & \tilde{B}_1^* & Q(\tilde{C}_1^* \Phi^{-1})^H + Y^H D_{12}^H \\ \tilde{B}_1^{*H} & -\gamma I & D_{11}^H \\ \tilde{C}_1^* \Phi^{-1} Q + D_{12} Y & D_{11} & -\gamma I \end{bmatrix} < 0 \quad (5.90)$$

$$Q = \begin{bmatrix} Q_1 & 0 \\ 0 & Q_2 \end{bmatrix} > 0 \quad (5.91)$$

$$Y = \begin{bmatrix} Y_1 & 0 \\ 0 & Y_2 \end{bmatrix} \text{ free} \quad (5.92)$$

$$Q \in \mathbb{H}^{n \times n}, \quad Y \in \mathbb{C}^{r_2 \times n} \quad (5.93)$$

which is our scenario-based feasibility problem, solved for some level γ . Recall in chapter 4 that $\gamma = -10 \text{ dB} = 0.3162$. We notice a few more things:

- Hermitian transposes are used since $\tilde{C}_1^* \Phi^{-1}$ is complex.

- Our decision variables are over the field of complex numbers.
- We have enforced sparsity/decentralization constraints on the decision variables.
- This LMI now has a random matrix, A_Δ , and hence, the system's eigenvectors Φ also have random uncertainty.

We are now prepared to discuss the sample bounds used in the scenario approach.

5.5.3 Sample Bounds for this Problem

The scenario based approach to control synthesis enables us to establish a priori sample size bounds guaranteeing that, if a solution exists, it will meet stability and performance requirements with prescribed probability and confidence in this probability estimate [14]. We recall from equation (5.8), that these bounds are given by

$$N \geq \frac{2}{\epsilon} \left(\log \frac{1}{\delta} + n_\theta \right) \quad (5.94)$$

where this bound states that if the number of scenarios is selected in this manner, then the optimal solution has, with probability $1 - \delta$, a guaranteed level of accuracy $1 - \epsilon$. We also note that the number of decision variables is included in this bound, which is given by n_θ . For the full-state feedback \mathcal{H}_∞ problem, we know that this is tied to two things:

1. Dimension of our plant dynamics matrix
2. Number of control inputs

In full-state feedback \mathcal{H}_∞ control where synthesis is achieved via semidefinite programming, we have two matrix variables in our optimization problem: some $Q > 0 \Rightarrow Q = Q^T$ and some $Y \in \mathbb{R}^{r_2 \times n}$. This implies that we have

$$n_\theta = \frac{1}{2}n(n + 2r_2 + 1) \quad (5.95)$$

optimization variables. However, we have restricted our decision variables to have a block-diagonal structure, such that $Q_1, Q_2 \in \mathbb{H}^{4 \times 4}$ and $Y_1, Y_2 \in \mathbb{C}^{1 \times 4}$. This implies that $n_\theta = 28$. We choose $\epsilon = 0.03, \delta = 0.005$, requiring $N \geq 2,220$.

5.5.4 Pseudocode for this Optimization Problem

The pseudocode for decentralized, scenario-based synthesis with disturbance input/performance output weighting in modal coordinates is provided in algorithm 2. Now, if a solution has been found, can it be guaranteed that it is real? For the design that we have conceived in this chapter, $K = YQ^{-1} \in \mathbb{R}^{r_2 \times n}$. We discuss, and prove this, in the next section.

5.6 GUARANTEEING THAT THE CONTROLLER WILL BE STRICTLY REAL

We see that our physical system is real. Intuitively, one would probably think that the controller, K , must be strictly real. But how can this be guaranteed? Indeed, we can find some $K \in \mathbb{C}^{r_2 \times n}$ such that $A + B_2 K$ is stable, and that $\|F_l(\bar{G}, K)\|_\infty \leq \gamma$. Since we must solve a complex semidefinite program that searches over the real and complex parts of the candidate controller solutions, can we guarantee that the controller that we find for this case will be real — and therefore implementable?

For our problem, we have that $A \in \mathbb{R}^{n \times n}$ and $B_2 \in \mathbb{R}^{n \times r}$. This is an important fact. We will use part of the KYP Dual Lemma, presented previously, in a moment.

Theorem 9. *For a system with the realization*

$$G \sim \left[\begin{array}{c|cc} A & B_1 & B_2 \\ \hline C_1 & D_{11} & D_{12} \\ I & 0 & 0 \end{array} \right] \quad (5.97)$$

with A, B_1, B_2 real, C_1 complex, and all of appropriate dimension, a full-state feedback \mathcal{H}_∞ controller synthesized via Complex Semidefinite Programming (CSDP) will yield a real-valued full-state feedback control law, $u = Kx$, that stabilizes the system and maintains the system's \mathcal{H}_∞ -norm below some prescribed, real, scalar level γ .

Algorithm 2 Formulation and Solution of the Scenario Synthesis Problem

- 1: **procedure** COMPLEX DECENTRALIZED SCENARIO-BASED SYNTHESIS
 - 2: Establish sample bounds, N , using (5.8).
 - 3: Set some performance level γ , for which it is desired that $\left\| F_l(\bar{G}, K) \right\|_\infty \leq \gamma$.
 - 4: Establish a convex, compact hypercube for decision variables, such that $Q, Y \in \Theta \subseteq \mathbb{C}^{n_\theta}$.
 - 5: **for** $i = 1 : N$ **do**
 - 6: Generate a k_Δ from $\mathcal{N}(100, 15^2)$ and form the random interconnection matrix Δ .
 - 7: Form $A_\Delta = A_0 + \Delta$.
 - 8: Solve $A_\Delta \Phi = \Phi \Lambda$.
 - 9: Form \tilde{C}_1^* and \tilde{B}_1^* as in (5.83) and (5.80), since the system's resonant frequencies will change due to the randomness in the dynamics matrix.
 - 10: Form the complex matrix:
- $$F_i(\theta) \doteq \begin{bmatrix} QA_\Delta^H + A_\Delta Q + Y^H B_2^H & \tilde{B}_1^* & Q(\tilde{C}_1^* \Phi^{-1})^H + Y^H D_{12}^H \\ \tilde{B}_1^{*H} & -\gamma I & D_{11}^H \\ \tilde{C}_1^* \Phi^{-1} Q + D_{12} Y & D_{11} & -\gamma I \end{bmatrix} \quad (5.96)$$
- with sparsity constraints enforced on the decision variables Q, Y .
- 11: Map each matrix within this matrix inequality through the isomorphism $\mathcal{T}(\cdot)$ discussed in section 5.3, equation (5.40), thus converting this matrix inequality into a real-valued matrix inequality.
 - 12: Append this real-valued matrix inequality as a constraint in the SDP that is to be solved. Note: Using parsing software such as YALMIP is highly recommended, as this software is also capable of handling complex constraints and interfaces with many different solvers [66].
 - 13: **end for**
-

14: Solve the SDP:

$$\begin{aligned} & \min_{\theta} \quad 0 \\ \text{s.t.} \quad & F_1(\theta) < 0 \\ & F_2(\theta) < 0 \\ & \vdots \\ & F_N(\theta) < 0 \\ Q = & \begin{bmatrix} Q_1 & 0 \\ 0 & Q_2 \end{bmatrix} > 0 \\ Y = & \begin{bmatrix} Y_1 & 0 \\ 0 & Y_2 \end{bmatrix} \\ Q \in \mathbb{H}^{n \times n}, \quad & Y \in \mathbb{C}^{r_2 \times n} \end{aligned}$$

15: If a solution exists, then the controller is given by $K = YQ^{-1}$, and it meets performance requirements with probability at least $1 - \epsilon$ and confidence $1 - \delta$ in this estimate.

16: **end procedure**

Proof. Suppose that solutions $Q > 0, Q \in \mathbb{H}^{n \times n}$ and $Y \in \mathbb{C}^{r_2 \times n}$ are found and satisfy the following complex-valued matrix inequality:

$$\begin{bmatrix} QA^H + AQ + Y^H B_2^H + B_2 Y & B_1 & QC_1^H + Y^H D_{12}^H \\ B_1^H & -\gamma I & D_{11}^H \\ C_1 Q + D_{12} Y & D_{11} & -\gamma I \end{bmatrix} < 0. \quad (5.98)$$

We start by introducing a definition:

Definition 3 (Schur Complement of a Block Matrix). *Given a block matrix $M \in \mathbb{C}^{(p+q) \times (p+q)}$ comprised of the blocks $A \in \mathbb{C}^{p \times p}, B \in \mathbb{C}^{p \times q}, C \in \mathbb{C}^{q \times p}$, and $D \in \mathbb{C}^{q \times p}$*

$$M \doteq \begin{bmatrix} A & B \\ C & D \end{bmatrix}, \quad (5.99)$$

the Schur complement of M with respect to D , abbreviated as M/D , is given by:

$$M/D \doteq A - BD^{-1}C. \quad (5.100)$$

Following definition 3, we also have, which is proven in [68],

Definition 4 (Schur Complement of a Matrix $X = X^H < 0$). *Given a matrix*

$$X \doteq \begin{bmatrix} A & B \\ B^H & C \end{bmatrix}, \quad (5.101)$$

The Schur Complement of X with respect to C is given by

$$X/C \doteq A - BC^{-1}B^H \quad (5.102)$$

and

$$X < 0 \Leftrightarrow A < 0, A - BC^{-1}B^H < 0 \quad (5.103)$$

We take the Schur complement of the LMI given by (5.98) to get

$$\begin{bmatrix} QA^H + AQ + Y^H B_2^H + B_2 Y & B_1 \\ B_1^H & -\gamma I \end{bmatrix} + \gamma^{-1} \begin{bmatrix} QC_1^H + Y^H D_{12}^H \\ D_{11}^H \end{bmatrix} \begin{bmatrix} C_1 Q + D_{12} Y & D_{11} \end{bmatrix} < 0 \quad (5.104)$$

which, when multiplying out the RHS, is

$$\begin{aligned} & \begin{bmatrix} QA^H + AQ + Y^H B_2^H + B_2 Y & B_1 \\ B_1^H & -\gamma I \end{bmatrix} \\ & + \gamma^{-1} \begin{bmatrix} QC_1^H C_1 Q + QC_1^H D_{12} Y + Y^H D_{12}^H C_1 Q + Y^H D_{12}^H D_{12} Y & QC_1^H D_{11} + Y D_{12}^H D_{11} \\ D_{11}^H C_1 Q + D_{11}^H D_{12} Y & D_{11}^H D_{11} \end{bmatrix} < 0 \end{aligned} \quad (5.105)$$

where, since we assume that we have found solutions Q and Y to this problem, and using definition 4 that we have that

$$\begin{bmatrix} QA^H + AQ + Y^H B_2^H + B_2 Y & B_1 \\ B_1^H & -\gamma I \end{bmatrix} < 0. \quad (5.106)$$

We find that the Schur complement of (5.106) is

$$QA^H + AQ + Y^H B_2^H + B_2 Y + \gamma^{-1} B_1 B_1^H < 0 \quad (5.107)$$

which, we know is true for the Q, Y , found and γ for this problem. We recall that A, B_1, B_2, γ are all real for this problem. This implies that Q and Y are both real. We will now show why.

Multiplication of complex numbers/matrices in this transformed space preserves the nature of the multiplication, which was shown in section 5.3. We return our attention to (5.107) where we map each real complex matrix through the transformation $\mathcal{T}(\cdot)$.

This means that the matrices Q and A will have representations

$$\mathcal{T}(Q) = \begin{bmatrix} \operatorname{Re}(Q) & -\operatorname{Im}(Q) \\ \operatorname{Im}(Q) & \operatorname{Re}(Q) \end{bmatrix}, \quad \mathcal{T}(A) = \begin{bmatrix} \operatorname{Re}(A) & 0 \\ 0 & \operatorname{Re}(A) \end{bmatrix}. \quad (5.108)$$

We shall declare the transformed version of (5.107) where each matrix is mapped through $\mathcal{T}(\cdot)$ as

$$\tilde{Q}^T \tilde{A}^T + \tilde{A} \tilde{Q} + \tilde{Y}^T \tilde{B}_2^T + \tilde{B}_2 \tilde{Y} + \gamma^{-1} \tilde{B}_1 \tilde{B}_1^T < 0. \quad (5.109)$$

Hence, the tilde notation implies $\tilde{Q} = \mathcal{T}(Q)$. Noting that negative definiteness is preserved under this transformation, as shown earlier. This arises from the fact that the eigenvalues

are invariant. We will now expand these matrices out and will perform the block matrix multiplications as we move forward in this proof.

What we get when we expand (5.109) is the following:

$$\begin{aligned}
& \begin{bmatrix} \operatorname{Re}(Q) & \operatorname{Im}(Q) \\ -\operatorname{Im}(Q) & \operatorname{Re}(Q) \end{bmatrix} \begin{bmatrix} \operatorname{Re}(A)^T & 0 \\ 0 & \operatorname{Re}(A)^T \end{bmatrix} \\
& + \begin{bmatrix} \operatorname{Re}(A) & 0 \\ 0 & \operatorname{Re}(A) \end{bmatrix} \begin{bmatrix} \operatorname{Re}(Q) & -\operatorname{Im}(Q) \\ \operatorname{Im}(Q) & \operatorname{Re}(Q) \end{bmatrix} \\
& + \begin{bmatrix} \operatorname{Re}(Y)^T & \operatorname{Im}(Y)^T \\ -\operatorname{Im}(Y)^T & \operatorname{Re}(Y)^T \end{bmatrix} \begin{bmatrix} \operatorname{Re}(B_2)^T & 0 \\ 0 & \operatorname{Re}(B_2)^T \end{bmatrix} \\
& + \begin{bmatrix} \operatorname{Re}(B_2) & 0 \\ 0 & \operatorname{Re}(B_2) \end{bmatrix} \begin{bmatrix} \operatorname{Re}(Y) & -\operatorname{Im}(Y) \\ \operatorname{Im}(Y) & \operatorname{Re}(Y) \end{bmatrix} \\
& + \gamma^{-1} \begin{bmatrix} \operatorname{Re}(B_1)\operatorname{Re}(B_1)^T & 0 \\ 0 & \operatorname{Re}(B_1)\operatorname{Re}(B_1)^T \end{bmatrix} < 0
\end{aligned} \tag{5.110}$$

which is equal to

$$\begin{aligned}
& \begin{bmatrix} \operatorname{Re}(Q)\operatorname{Re}(A)^T & \operatorname{Im}(Q)\operatorname{Re}(A)^T \\ -\operatorname{Im}(Q)\operatorname{Re}(A)^T & \operatorname{Re}(Q)\operatorname{Re}(A)^T \end{bmatrix} + \begin{bmatrix} \operatorname{Re}(A)\operatorname{Re}(Q) & -\operatorname{Re}(A)\operatorname{Im}(Q) \\ \operatorname{Re}(A)\operatorname{Im}(Q) & \operatorname{Re}(A)\operatorname{Re}(Q) \end{bmatrix} \\
& + \begin{bmatrix} \operatorname{Re}(Y)^T\operatorname{Re}(B_2)^T & \operatorname{Im}(Y)^T\operatorname{Re}(B_2)^T \\ -\operatorname{Im}(Y)^T\operatorname{Re}(B_2)^T & \operatorname{Re}(Y)^T\operatorname{Re}(B_2)^T \end{bmatrix} \\
& + \begin{bmatrix} \operatorname{Re}(B_2)\operatorname{Re}(Y) & -\operatorname{Re}(B_2)\operatorname{Im}(Y) \\ \operatorname{Re}(B_2)\operatorname{Im}(Y) & \operatorname{Re}(B_2)\operatorname{Re}(Y) \end{bmatrix} \\
& + \gamma^{-1} \begin{bmatrix} \operatorname{Re}(B_1)\operatorname{Re}(B_1)^T & 0 \\ 0 & \operatorname{Re}(B_1)\operatorname{Re}(B_1)^T \end{bmatrix} < 0
\end{aligned} \tag{5.111}$$

which is equal to

$$F = \begin{bmatrix} F_{11} & F_{12} \\ F_{21} & F_{22} \end{bmatrix} < 0 \tag{5.112}$$

with

$$F_{11} = \operatorname{Re}(Q)\operatorname{Re}(A)^T + \operatorname{Re}(A)\operatorname{Re}(Q) + \operatorname{Re}(Y)^T\operatorname{Re}(B_2)^T + \operatorname{Re}(B_2)\operatorname{Re}(Y) + \gamma^{-1}\operatorname{Re}(B_1)\operatorname{Re}(B_1)^T \quad (5.113)$$

$$F_{12} = \operatorname{Im}(Q)\operatorname{Re}(A)^T - \operatorname{Re}(A)\operatorname{Im}(Q) + \operatorname{Im}(Y)^T\operatorname{Re}(B_2)^T - \operatorname{Re}(B_2)\operatorname{Im}(Y) \quad (5.114)$$

$$F_{21} = -\operatorname{Im}(Q)\operatorname{Re}(A)^T + \operatorname{Re}(A)\operatorname{Im}(Q) - \operatorname{Im}(Y)^T\operatorname{Re}(B_2)^T + \operatorname{Re}(B_2)\operatorname{Im}(Y) \quad (5.115)$$

$$F_{22} = \operatorname{Re}(Q)\operatorname{Re}(A)^T + \operatorname{Re}(A)\operatorname{Re}(Q) + \operatorname{Re}(Y)^T\operatorname{Re}(B_2)^T + \operatorname{Re}(B_2)\operatorname{Re}(Y) + \gamma^{-1}\operatorname{Re}(B_1)\operatorname{Re}(B_1)^T. \quad (5.116)$$

We know that for any square matrix that

$$\operatorname{Tr}(F) = \sum_i^n \lambda_i(F), \quad F \in \mathbb{H}^{n \times n}. \quad (5.117)$$

We see that for this problem, both F_{11} and F_{22} , which are the block diagonal components of this transformed, real-valued complex linear matrix inequality, are only comprised of the real parts of Q and Y . The imaginary parts of Q and Y do not have an impact on our ability to satisfy the constraints in this SDP. Because of this, we can also say that negative definiteness of (5.106) is not determined by these imaginary parts, which also implies the same for (5.105). During this optimization, then, the variables entering the linear matrix inequalities that correspond to the imaginary parts of Q and Y do not affect our ability to satisfy these constraints, and therefore do not lead to the generation of a solution that renders (5.105) satisfied. When solving the CSDP under discussion, since the complex parts of the solution variables Q and Y have no effect on our ability to satisfy the LMI constraints in our problem, when associating this problem with its dual form, non-zero complex parts of Q and Y will lead to no change in the objective function value. What we find, then, is that these variables remain at zero, leading to purely-real Q and Y .

Since negative definiteness of F implies that negative definiteness of (5.107) is not affected by any of the imaginary parts of Q or Y , we can conclude that negative definiteness of (5.98), despite the fact that we have a complex C_1 . If this were not the case, we could

arbitrarily choose the imaginary components of Q and Y such that we rendered (5.107) positive definite, thereby violating the solution that we achieved by solving (5.98), as stated in the beginning of this theorem.

We also know that the closed loop system is embedded in (5.107) by the dual KYP Lemma. That is,

$$QA^T + AQ + Y^T B_2^T + B_2 Y + \gamma^{-1} B_1 B_1^T < 0 \quad (5.118)$$

is equivalent to

$$Q(A + B_2 K)^T + (A + B_2 K)Q + \gamma^{-1} B_1 B_1^T < 0 \quad (5.119)$$

by simply performing the substitution $Y = KQ$. From our theory behind full-state feedback \mathcal{H}_∞ controller synthesis using linear matrix inequalities via solving a semidefinite program, we see that the controller, K , is recovered from $K = YQ^{-1}$. Since we can take $\text{Im}(Q), \text{Im}(Y) = 0$ without any loss in generality, this complex semidefinite program does not need to admit a controller solution that has complex parts.

This would not be the case if any of A, B_1, B_2 has complex parts. By performing the first multiplication shown in (5.109) for the case where the matrix A is complex, we see

$$\begin{aligned} & \begin{bmatrix} \text{Re}(Q) & \text{Im}(Q) \\ -\text{Im}(Q) & \text{Re}(Q) \end{bmatrix} \begin{bmatrix} \text{Re}(A)^T & \text{Im}(A)^T \\ -\text{Im}(A)^T & \text{Re}(A)^T \end{bmatrix} \\ &= \begin{bmatrix} \text{Re}(Q)\text{Re}(A)^T + \text{Im}(Q)\text{Im}(A)^T & \text{Re}(Q)\text{Im}(A)^T + \text{Im}(Q)\text{Re}(A)^T \\ -\text{Im}(Q)\text{Re}(A)^T - \text{Re}(Q)\text{Im}(A)^T & \text{Im}(Q)\text{Im}(A)^T + \text{Re}(Q)\text{Re}(A)^T \end{bmatrix} \end{aligned} \quad (5.120)$$

where we see, immediately, that the trace of this matrix is now dependent upon the imaginary components of Q , thereby suggesting that the imaginary components of Q, Y in this complex semidefinite program will now affect the negative definiteness of the solution, leading to the admission of a complex-valued controller. This may seem obvious, since our state matrix is now complex. Nevertheless, this had to be shown, since we endeavored to prove that even with a complex-valued performance output function that is mapped through $C_1 \in \mathbb{C}$ (of appropriate dimension) we end up with a real-valued controller. **Q.E.D.**

5.7 RESULTS

5.7.1 Open Loop and Closed-Loop System Performance

A probabilistic robust, decentralized full state feedback \mathcal{H}_∞ controller was found such that

$$\hat{\Pr}\left(\left\|F_l(\bar{G}_\Delta, K_{\text{opt}})\right\|_\infty \leq -10\text{dB}\right) \geq 0.97. \quad (5.121)$$

where

$$F_l(\bar{G}_\Delta, K_{\text{opt}}) \sim \begin{bmatrix} A_\Delta + B_2 K_{\text{opt}} & \tilde{B}_1^* \\ \tilde{C}_1^* \Phi^{-1} + D_{12} K_{\text{opt}} & D_{11} \end{bmatrix}. \quad (5.122)$$

Indeed, we did better than these a priori bounds for controller that was synthesized, as will be shown from the a posteriori robustness analysis that is performed in this chapter. The synthesized controller is

$$K_{\text{opt}} = \begin{bmatrix} 669.7 & -7763.5 & -197.4 & -216.4 & 0 & 0 & 0 & 0 \\ 0 & 0 & 0 & 0 & 13635 & -24713.9 & -2475.1 & -952.7 \end{bmatrix}. \quad (5.123)$$

Since the controller was synthesized for a weighted version of the plant, we present the random, weighted open and closed-loop maximum singular value plots in figure 16. It is only appropriate to perform this analysis for this weighted version of the plant, which was pursued in an effort to shape the synthesis process with a focus on low frequency disturbance attenuation, with similar focus on the low frequency modes of the system. Like other loop shaping approaches in multivariable control, it is also appropriate that we examine the closed-loop response of the unfiltered system. Of course, probabilistic robustness of the unweighted system is possible, and can certainly be done with respect to stability. Performance, on the other hand, would not be a fair comparison. It is noted that the eigenvalues of the weighted and unweighted closed-loop, random systems are equivalent. This is evidenced by observing

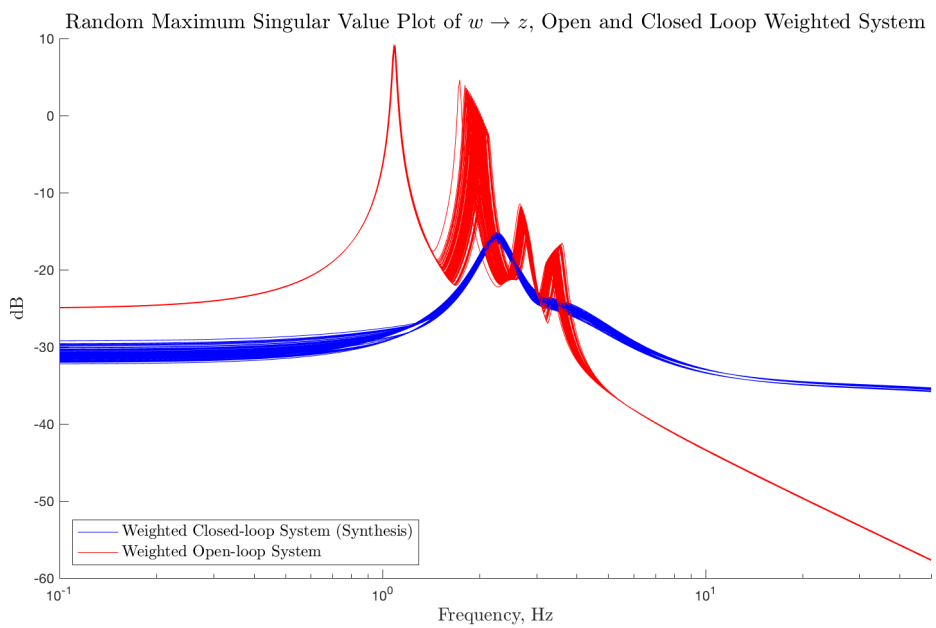


Figure 16: Frequency-weighted open and closed-loop lightly damped system with random interconnection uncertainty.

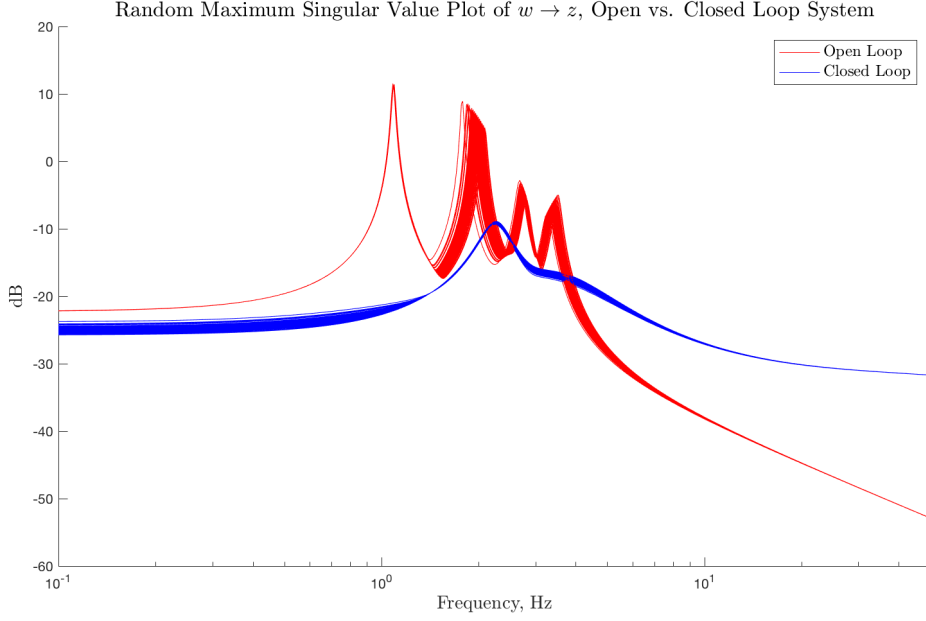


Figure 17: Random, unweighted maximum singular value plot of the $F_l(\hat{G}_\Delta, K_{\text{opt}})$ mapping.

the following:

$$F_l(\bar{G}_\Delta, K_{\text{opt}}) \sim \left[\begin{array}{c|c} A_\Delta + B_2 K_{\text{opt}} & \tilde{B}_1^* \\ \hline \tilde{C}_1^* \Phi^{-1} + D_{12} K_{\text{opt}} & D_{11} \end{array} \right], \quad F_l(\hat{G}_\Delta, K_{\text{opt}}) \sim \left[\begin{array}{c|c} A_\Delta + B_2 K_{\text{opt}} & B_1 \\ \hline \tilde{C}_1 \Phi^{-1} + D_{12} K_{\text{opt}} & D_{11} \end{array} \right] \quad (5.124)$$

where \bar{G} and \hat{G} are those system realizations given by equations (5.84) and (5.72), respectively, with the subscript Δ indicating that random uncertainty is included. Although a somewhat obvious result, we see that scaling has no effect on the eigenvalues of the system.

What we can observe from figure 16 is that the weighted closed-loop system has infinity norm below -10 dB. The unweighted maximum singular value plot, which depicts the maximum singular values of the linear fractional transformation $F_l(\hat{G}_\Delta, K_{\text{opt}})$ is shown in figure 17. These results may be slightly less than exciting, however, a contribution of this research is that a loop shaping method is now possible by way of scaling the magnitudes

of disturbance input and performance output matrices in modal coordinates for achieving a probabilistic robust, decentralized, \mathcal{H}_∞ controller.

Next, we will evaluate the probabilistic robustness of the controller given by (5.123).

5.7.2 Probabilistic Analyses

Since the uncertainty in our system is random, nondeterministic tools must be developed, and used, for evaluating the effectiveness of our controller. This section on probabilistic analyses is separated into the following evaluations:

1. Stability and performance tests.
2. Robust stability and performance margins.

These tools represent a contribution of this thesis for lightly-damped structural systems, and are adjunct to evaluating the probabilistic robust controllers that are synthesized. These tests and evaluations will now be performed for the controller found, and given by (5.123), for the uncertain lightly-damped system featured in this chapter.

5.7.2.1 Stability and Performance Tests The robust stability test is a probabilistic test that measures, using a probability estimate, whether or not some percentage of all system configurations will be stable. This percentage is defined by a level parameter, $\epsilon_s \in [0, 1]$. This test involves generating samples from the distribution that describes the interconnection stiffness, forming the composite system, and evaluating stability. A probability estimate of composite system stability replaces the classic notion of deterministic system stability and the test amounts to evaluating whether or not the probability of stability is greater than the threshold defined by the level parameter:

$$\hat{\Pr}(\text{stable}) = \frac{1}{\hat{N}} \sum_{i=1}^{\hat{N}} \mathbb{I}\left(\text{stable} \mid (A_\Delta + B_2 K_{\text{opt}})\right), \quad S_{\text{test}} \doteq \hat{\Pr}(\text{stable}) \geq 1 - \epsilon_s. \quad (5.125)$$

The term \hat{N} is the total number of controlled structure configurations analyzed, and \mathbb{I} is the indicator function. This robust stability test is carried out using established Monte Carlo methods where \hat{N} is appropriately chosen [14]. Note that the $\hat{\Pr}(\cdot)$ nomenclature is used to denote that these are probability estimates, and not exact probabilities.

Recall that the “nominal” uncertainty used during synthesis was characterized by $f_\Delta(a_0) = \mathcal{N}(100, 15^2)$. Using established Monte Carlo approaches (which are detailed in chapter 7), we chose $\hat{N} = 100,000$, a level parameter of $\epsilon_s = 0.01$, which is equal to the original ϵ_s chosen in chapter 4 (and is admittedly a lax requirement since the performance test is also ingrained in this a priori probabilistic performance parameter), to find that

$$\hat{\Pr}(\text{stable}) = 1 \Rightarrow \pi_{s,0} = 0 \quad (5.126)$$

which says that we have passed the stability test. The variable $\pi_{s,0}$ represents the probability of instability specific to the amount of uncertainty included during synthesis. Using $\hat{N} = 100,000$ in our a posteriori Monte Carlo evaluations leads to a probability estimate accuracy of $\epsilon = 0.0051$ with confidence of 99% ($1 - \delta$) in the probability estimates generated by (5.125) and (5.129). These estimates, and confidence in this estimate, are derived using Chernoff Bounds [14]:

$$\hat{N} \geq \frac{1}{2\epsilon^2} \log \frac{2}{\delta}. \quad (5.127)$$

For the case where we want 99% confidence in our estimate, choosing $\hat{N} = 100,000$ will lead to

$$\left| \hat{\Pr}(\text{stable}) - \Pr(\text{stable}) \right| \leq \epsilon. \quad (5.128)$$

The same confidence and accuracy applies for the performance test. The details, and theory, behind these probability bounds and estimates is a subject of chapter 7, and so they are spared here. In chapter 7, these Chernoff Bounds are also used during controller synthesis, as more accurate probability estimates tend to smooth out the “noise” generated during the synthesis process developed in that chapter.

The performance test is given by

$$\hat{\Pr}(\text{performance}) = \frac{1}{\hat{N}} \sum_{i=1}^{\hat{N}} \mathbb{I}\left(\text{performance} \mid (\bar{G}_{\Delta,i}, K_{\text{opt}})\right), \quad P_{\text{test}} = \hat{\Pr}(\text{performance}) \geq 1 - \epsilon_p, \quad (5.129)$$

where

$$\text{performance} \doteq \left\| F_l(\bar{G}_{\Delta}, K_{\text{opt}}) \right\|_{\infty} \leq -10 \text{ dB} \quad (5.130)$$

which was the originally-specified performance, with level parameter $\epsilon_p = 0.03$ defined in chapter 4. Using the same $\hat{N} = 100,000$, we found

$$\hat{\Pr}(\text{performance}) = 1 \Rightarrow \pi_{p,0} = 0 \quad (5.131)$$

where $\pi_{p,0}$ represents the probability of not meeting performance for the amount of uncertainty included for synthesis. Using the level parameter ϵ_p , we can say that the probabilistic robust controller K_{opt} passed the stability and performance tests for our random system quite handily. Of course, these tests are with respect to the nominal amount of uncertainty, where the interconnection stiffness element is characterized by $f_{\Delta}(a_0) = \mathcal{N}(100, 15^2)$.

5.7.2.2 Robust Stability and Performance Margins Another contribution of this research is that a method for finding probabilistic stability and performance margins for controlled structures coupled by a probabilistically-uncertain interface stiffness matrix is developed. These margins can be thought of as a probabilistic analogue to the structured singular value [17].

To find probabilistic robust stability and performance margins, we construct degradation functions [14]. Degradation functions are simple to construct: simply choose some metrics against which we would like to measure/evaluate our system, and establish an approach to increasing the amount of random uncertainty present in our model. At discrete points, these metrics are evaluated using Monte Carlo techniques, thus evaluating the probability of violation at these discrete points. The probability of violation then becomes a function of how the model uncertainty is changed.

The ball that characterized the uncertainty in our model used for synthesis is given by

$$\mathcal{B}_\Delta(a_0) \doteq \{\Delta \in \mathbb{R}^{n \times n} : \Delta \sim f_\Delta(a_0)\} \quad (5.132)$$

$$f_\Delta(a_0) \sim \mathcal{N}(100, a_0 15^2) \quad (5.133)$$

where $a_0 = 1$ for synthesis. We could have built this set to be

$$\mathcal{B}_\Delta(a, \rho) \doteq \{\Delta \in \mathbb{R}^{n \times n} : \Delta \sim f_\Delta(a), \|\Delta\|_p \leq \rho\} \quad (5.134)$$

$$f_\Delta(a) \sim \mathcal{N}(100, a 15^2) \quad (5.135)$$

$$a \in [0, a_{\max}], \quad a_{\max} \in \mathbb{R}_+ \quad (5.136)$$

$$\rho \in \mathbb{R}_+ \quad (5.137)$$

where we see that the ball now is now bounded in some norm-sense, where we could choose p to be the a norm of our choice: Frobenius, 2, ∞ , etc. For synthesis and analysis, we chose not to bound this set, as illustrated by (5.132). Note that the probability estimates generated by not bounding the set are not a consequence of absence of a bound — imposing a hard bound would retain the validity of this approach. However, it was chosen not to use a hard bound, as a more exhaustive, and perhaps exciting, search of the solution space would be possible during synthesis. Moreover, rather than just coloring a norm-bound, which is a bit of an incremental step beyond the robust control approach, we are able to color the uncertainty set and give it fuzzy edges.

When constructing these degradation functions, we must therefore change the uncertainty that is characterizing our random system while performing probabilistic analyses. For this present chapter, and for the full state feedback case, degradation functions were constructed defining the set given in (5.132) with $a_{\max} = 10$. Clearly, we are just scaling the standard deviation/variance of our uncertainty. At points along the line $a \in [0, a_{\max}]$, the probability of stability and having ∞ -norm less than γ , as given by equations (5.129) and (5.125) were calculated with $\hat{N} = 100,000$, yielding the same accuracy and confidence that resulted from performing these evaluations for the nominal case, $a_0 = 1$.

The resulting degradation functions, depicting the probability of instability and performance violation, for the *filtered* systems, are shown in figure 18. We are now prepared to discuss what is meant by probabilistic margins, as it pertains to a contribution of this research.

Definition 5 (Probabilistic Margin). *Probabilistic stability and performance margins are extractions of a degradation function, and provide a measure for the amount of random uncertainty that can be tolerated before the probabilistic levels for failure become unacceptable to the designer. By defining the nominal amount of uncertainty that was used for controller synthesis as a_0 , and the amount of uncertainty that corresponds with an unacceptable probabilistic level of failure as a_1 , the probabilistic margin, PM , is*

$$PM \doteq \frac{a_1}{a_0}. \quad (5.138)$$

The probabilistic stability and performance margins are extractions from the degradation functions given in figure 18. For the stability degradation function shown in figure 19, we see that a given $a \in [0, a_{\max}]$ is associated with a specific probability of instability. That is,

$$\begin{aligned} \text{degrade}(a_{s,1}) = \pi_1 &\Rightarrow a_{s,1} = \text{degrade}^{-1}(\pi_{s,1}) \\ \text{degrade}(a_{s,0}) = \pi_0 &\Rightarrow a_{s,0} = \text{degrade}^{-1}(\pi_{s,0}). \end{aligned} \quad (5.139)$$

where we recall from (5.126) that $\pi_{s,0} = 0$. If we declare that we are willing to accept a 1% chance of instability, then $\pi_{s,1} = 0.01$. The probabilistic stability margin, referred to as PSM in figure 19, is then given by

$$\text{PSM} = \frac{a_{s,1}}{a_{s,0}} \approx 4.9. \quad (5.140)$$

Using the way that we have defined our uncertainty set, given by (5.132), we can scale the standard deviation on the original uncertainty by approximately $4.9 \times$ before encountering unacceptable levels of instability, in a probability sense.

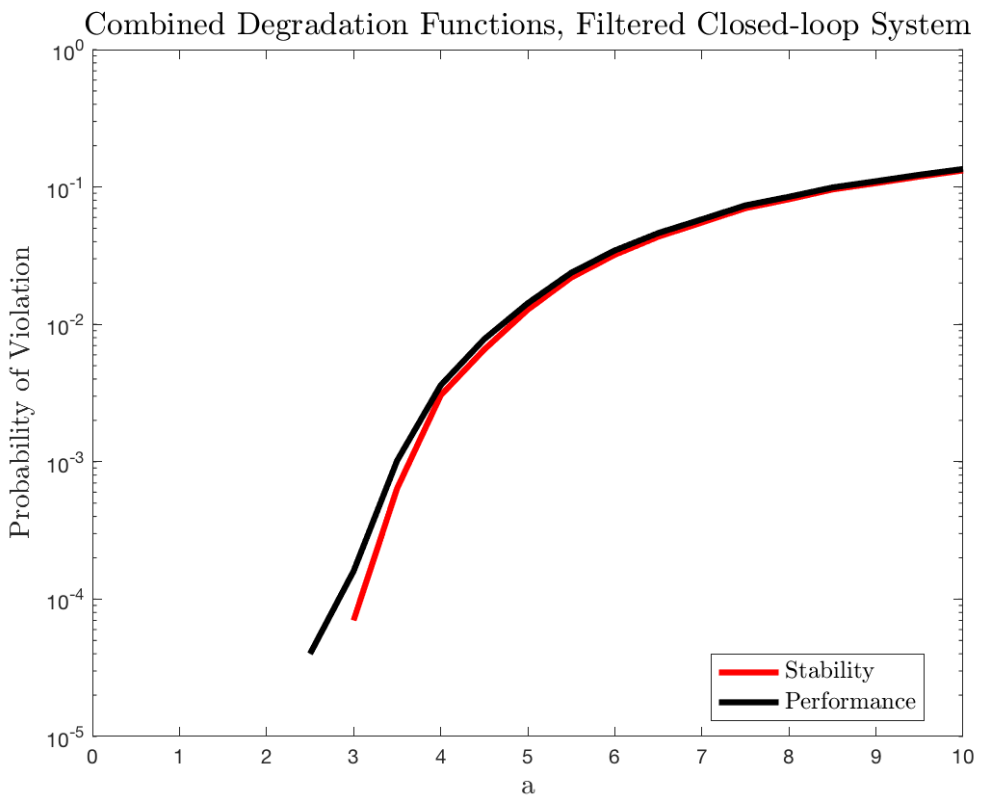


Figure 18: Combined stability and performance degradation functions for the full-state feedback, probabilistic robust decentralized \mathcal{H}_∞ controller given by (5.123) for the uncertainty set (5.132) with $a \in [0, a_{\max}]$.

By the same token, we analyze the probabilistic performance margin (PPM). Refer to figure 20. Recalling that $\pi_{p,0} = 0$ from equation 5.131, and by positing that we are willing to accept a 1% chance of performance violation, we have

$$\begin{aligned}\text{degrade}(a_{p,1}) = \pi_1 &\Rightarrow a_{p,1} = \text{degrade}^{-1}(\pi_{p,1}) \\ \text{degrade}(a_{p,0}) = \pi_0 &\Rightarrow a_{p,0} = \text{degrade}^{-1}(\pi_{p,0}).\end{aligned}\tag{5.141}$$

leading to

$$\text{PPM} = \frac{a_{s,1}}{a_{s,0}} \approx 4.75,\tag{5.142}$$

which says that we can scale the standard deviation on the original uncertainty by approximately $4.75\times$ before encountering an unacceptable probability of performance violation.

This can be a powerful design tool, as engineers or operators can now make decisions regarding how long active vibration controllers should remain in operation before re-tuning. In harsh environments where structures are subjected to radiation and experience fatigue, such as in space, uncertainty in structure parameters will inevitably increase over time.

Using probabilistic robust control to analyze the probability of stability and probability of meeting performance objectives for the composite, decentrally-controlled structural system not only allows the structural control engineer to capture interconnection uncertainty in a way that represents structural dynamic uncertainty, [71] it relaxes the conservatism and computational complexity associated with traditional robust control approaches to quantifying robust stability and performance [14]. It has been shown that using randomized algorithms for testing robust stability and performance are more computationally efficient than those used in traditional robust control since they can be executed in polynomial time. Traditional robust stability algorithms have been shown to be NP-hard [42, 41, 14, 24, 23].

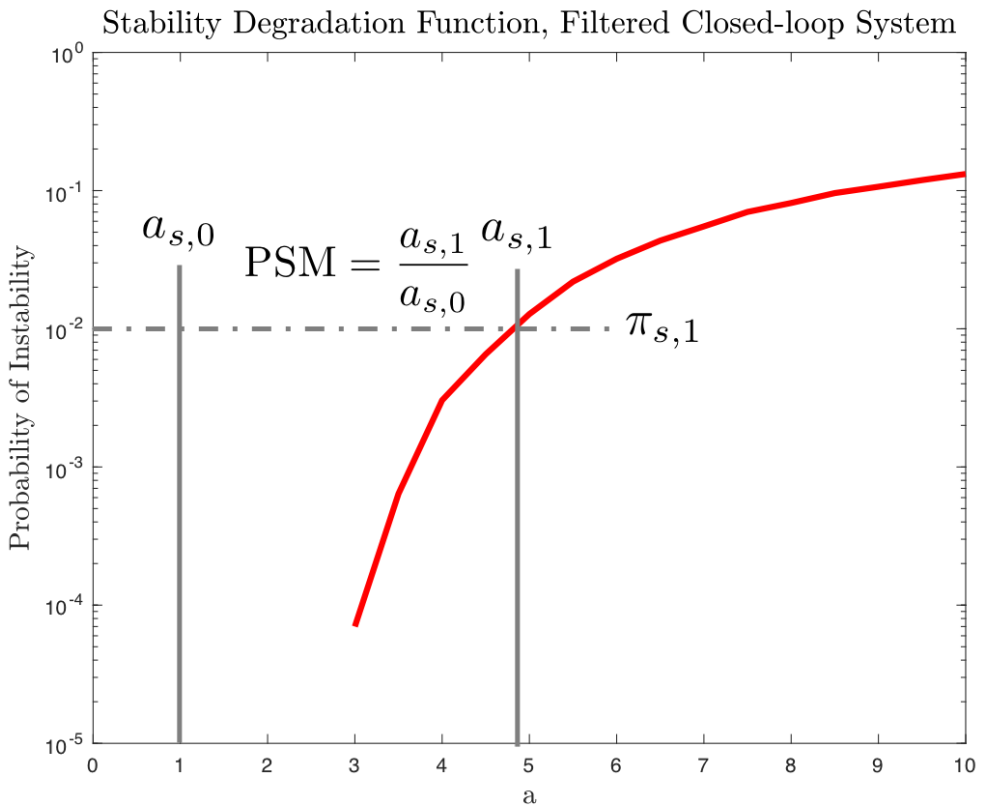


Figure 19: Stability degradation function with the probabilistic stability margin (PSM) shown.

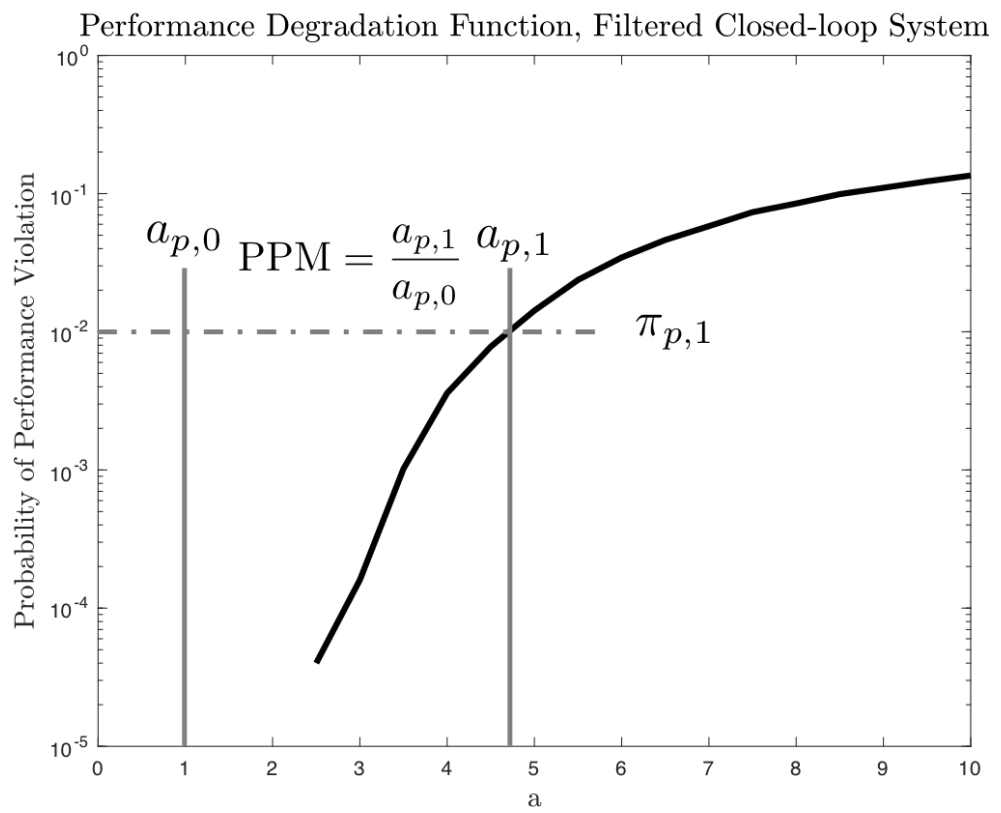


Figure 20: Performance degradation function with the probabilistic performance margin (PPM) shown.

A designer can define an increased probability of instability or performance violation that they are willing to accept in exchange for greater uncertainty. Engineers or operators can now make decisions regarding how long active vibration controllers should remain in operation before re-tuning or decommissioning. In harsh environments where structures are subjected to radiation and experience mechanical fatigue, such as in space, uncertainty in structure parameters will inevitably increase over time.

5.8 CHAPTER SUMMARY

In this chapter, we developed the following techniques with associated results:

1. A way of enforcing sparsity constraints in a scenario-based full state feedback \mathcal{H}_∞ synthesis problem, allowing for the incorporation of random interconnection uncertainty.
2. A method, with theorem and proof, for showing how control design can be performed in frequency-weighted complex modal coordinates, with performance output equation defined in complex modal coordinates, that results in a real-valued controller using the scenario approach.
3. Stability and performance tests and the concept of probabilistic stability and performance margins for decentrally-controlled systems possessing random interconnection uncertainty.
4. Application of these approaches to a lightly-damped system possessing random uncertainty.

We will now move into chapter 6 as we set up the control design and synthesis approach for a high-order, dynamic output feedback case.

6.0 LOOP-AT-A-TIME DECENTRALIZED DYNAMIC OUTPUT FEEDBACK \mathcal{H}_∞ CONTROL USING μ -SYNTHESIS

This chapter provides a discussion into μ -synthesis techniques, and thereafter shows how μ -synthesis is used in a loop-at-a-time synthesis process to achieve a collection decentralized, robust controllers. The plurality of controllers is emphasized, as the output of this process is used as input to the approach developed in chapter 7.

As we will discuss, the μ -synthesis process is both elegant and powerful, with the resulting controllers guaranteed to be robust against the structured or unstructured uncertainty defined during controller design and synthesis. Unfortunately, μ -synthesis is not guaranteed to achieve an optimal answer, and modeling uncertainty using approaches specific to robust control tend to be overly-conservative [57, 14]. Despite some of these drawbacks, μ -synthesis has demonstrated great success in practice, and we demonstrate that its inherent sub-optimality and conservatism work in our favor in chapter 7.

Philosophically-speaking, all control design and synthesis processes are iterative. That is, we always pursue the following steps:

- Step #1:** Model the plant with associated uncertainty;
- Step #2:** Determine control objectives;
- Step #3:** Design the controller;
- Step #4:** Synthesize the controller;
- Step #5:** Check nominal stability/performance, robust stability/performance;
- Step #6:** If “acceptable”, you’re done. If “unacceptable”, return to **Step #3**.

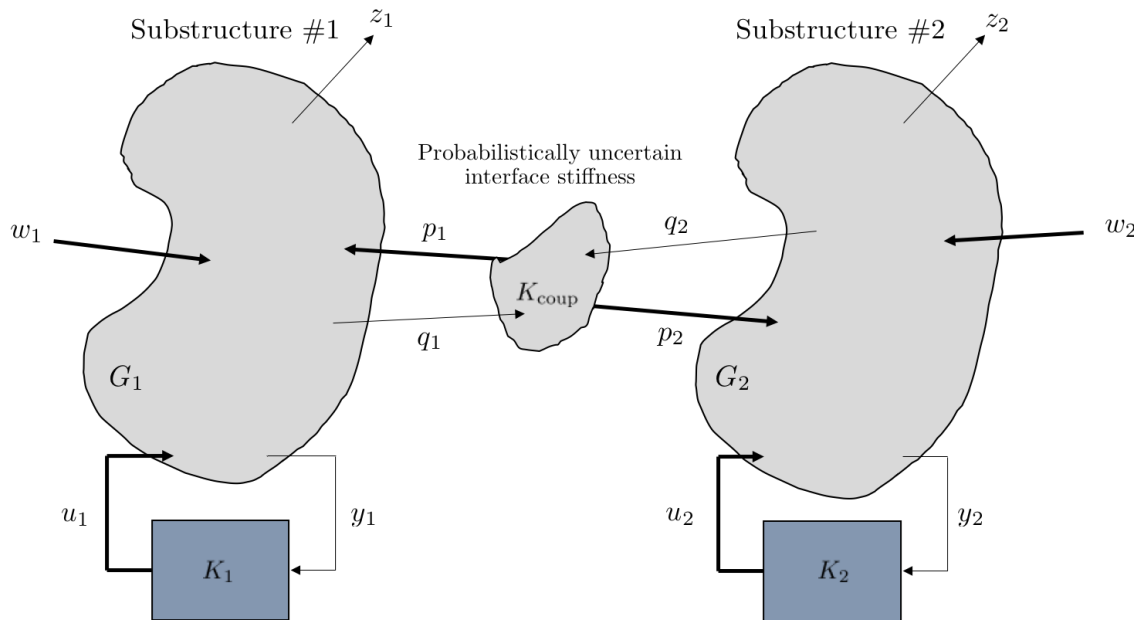


Figure 21: Probabilistic decentralized active control conceptualization. Control inputs (u), measurements (y), disturbance inputs (w), performance outputs (z), and structure/interconnection forces/moments and displacements/rotations (p, q) are depicted for substructures G_1 and G_2 .

In the same way that PID control design is often iterated, we iterate using μ -synthesis. If objectives are not met, either uncertainty weightings/models are adjusted, disturbance input/performance output weightings are adjusted, or control objectives are retooled altogether. A difference between these techniques, of course, is related to the machinery used for control design and synthesis.

In our pursuit of excellence or perfection, we may end up discarding controllers that are good in step #6, because they may not be as excellent as we wish for them to be. However, controllers that are synthesized using μ -synthesis are robust against some prescribed structured norm-bounded uncertainty. Due to the conservatism and sub-optimality inherent to μ -synthesis via D/K iterations, these solutions may exist near probabilistically-robust solutions. Therefore, we will use this synthesis process to generate good starting points for a high-dimensional stochastic optimization problem.

The goal of this research was to develop an approach for designing and synthesizing probabilistically robust, decentralized controllers that achieved specified performance objectives in the presence of random interconnection uncertainty. The controllers that are synthesized in this chapter allow us to find seed solutions for the high-dimensional, non-convex, stochastic optimization problem posed, and solved, in chapter 7 in order to achieve the overarching goal of this research.

A discussion on robust control and μ -synthesis is provided in this chapter. Going into some depth will serve the following purposes:

1. Reveal the conservatism of μ -synthesis and in estimating the structured singular value.
This helps with motivating the use of probabilistic robust techniques.
2. To show how we are able to extract multiple robust controllers from μ -synthesis via D/K iterations, subsequently leading to good, initial solutions spaces to search in chapter 7.

6.1 LOOP-AT-A-TIME μ -SYNTHESIS IN DECENTRALIZED STRUCTURAL CONTROL

Loop-at-a-time μ -synthesis for decentralized structural control was a technique that Kyong Lim implemented, where he modeled interconnection uncertainty as possessing real, parametric uncertainty, and modeled uncertainty in the structures, especially at high frequencies, as additive uncertainties [6]. This chapter makes contributions to loop-at-a-time μ -synthesis beyond how Lim originally pursued these methods:

1. Lim pioneered loop-at-a-time synthesis for the robust decentralized control of coupled Euler-Bernoulli beams, where he was explicit about the interconnection stiffness matrix having norm-bounded, parametric uncertainty. Lim did not work out the loop formulations for controller design and synthesis. This thesis works out these manipulations. The results are very general, and hopefully makes this approach even more accessible to the vibration control engineer. A virtue of this generality, of course, is that other control approaches can be adapted into these loop formulations/synthesis steps and subsequently used with the approaches in chapter 7.
2. In the context of loop-at-a-time μ -synthesis for the decentralized robust control of coupled substructures, this thesis provides a new controller design approach. Frequency-weighting of performance output matrices in modal coordinates is pursued, which does not increase the overall model order. This is now a common design practice for lightly-damped structures [72, 61].
3. By virtue of how D/K iterations occur, we end up with multiple (possibly robust) controllers on our way to minimizing the infinity norm of our uncertain system. In other words, the third contribution is the identification that we are able to assemble a collection of good robust controllers in our high-dimensional solution space. Then, we can use this collection as initial members of a population in a genetic/evolutionary algorithm for searching for probabilistic-robust controllers.

This chapter is structured as follows:

1. A discussion on robust control and μ -synthesis is provided.
2. Loop-at-a-time formulations, with interconnection stiffness terms explicitly identified, are provided for all of the cases used during loop-at-a-time μ -synthesis.
3. An algorithm that condenses controller design, loop formulations, and μ -synthesis is formulated.
4. The performance of the resulting robust controllers are highlighted. Closed-loop maximum singular value plots for those controllers that ended up working very well as initial solution seeds for the techniques developed in chapter 7 are shown.

6.2 ROBUST CONTROL AND μ -SYNTHESIS

In sections 6.2, 6.3, and 6.4 we will discuss the following topics:

- general uncertainty representations in robust control;
- the structured singular value;
- robust stability and performance tests and evaluations using the structured singular value;
- μ -synthesis via D/K iterations.

Subsequently, we will discuss how μ -synthesis is used in the context of this thesis and how loop-at-a-time synthesis is performed. During D/K iterations, we are able to capture multiple controller starting points for use in the stochastic optimization problem formulated in chapter 7.

μ -synthesis via D/K iterations is an approach that has been in existence for over 30 years. The machinery behind this approach is well understood, and the discussion in this section was put together with the aid of several sources [57, 17, 59]. During loop-at-a-time μ -synthesis, Matlab's Robust Control Toolbox was used for synthesizing the controllers used as input to chapter 7 [73, 74].

6.2.1 Uncertainty Representations in Robust Control

Uncertainty is unavoidable. The actual dynamic system almost always has some variation in its physical parameters. This uncertainty can be captured using several modeling techniques.

In robust control, we represent the model-controller-uncertainty triplet using the generalized regulator framework shown in figure 22, where the plant is given by P , controller by K , and uncertainty by Δ . The signals are u - control input; w - disturbance/reference input; w_Δ - uncertainty inputs; y - measured outputs; z - performance output; and z_Δ - uncertainty outputs.

The uncertain inputs and outputs, along with the system given by Δ are pure modeling constructs. Through certain modeling choices, we elect to pull them out of P for analysis and controller synthesis purposes. At this point, it is worthwhile to discuss the details behind Δ before getting into our discussion on the structured singular value.

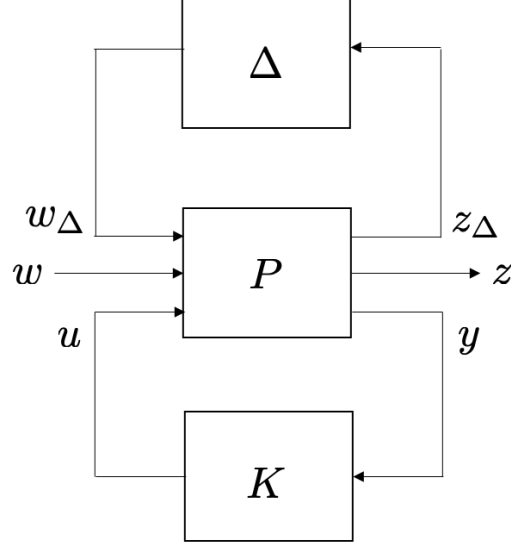


Figure 22: Generic uncertain system.

6.2.2 The Uncertainty Block, Δ

Generally, the uncertainty set Δ is described by

$$\Delta_c = \text{diag} (p_1 I, \dots, p_{n_r} I, \delta_1 I, \dots, \delta_{n_c} I, \Delta_1, \dots, \Delta_{n_f}) \quad (6.1)$$

whose elements satisfy

- $p_j \in \mathbb{R}$ with $|p_j| < 1$, $j = 1, \dots, n_r$
- $\delta_j \in \mathbb{C}$ with $|\delta_j| < 1$, $j = 1, \dots, n_c$
- $\Delta_j \in \mathbb{C}^{p_j \times q_j}$ with $\|\Delta_j\| < 1$, for $j = 1, \dots, n_f$

where $p_j I$ is a real repeated block, $\delta_j I$ is a complex repeated block, and Δ_j is a full complex block.

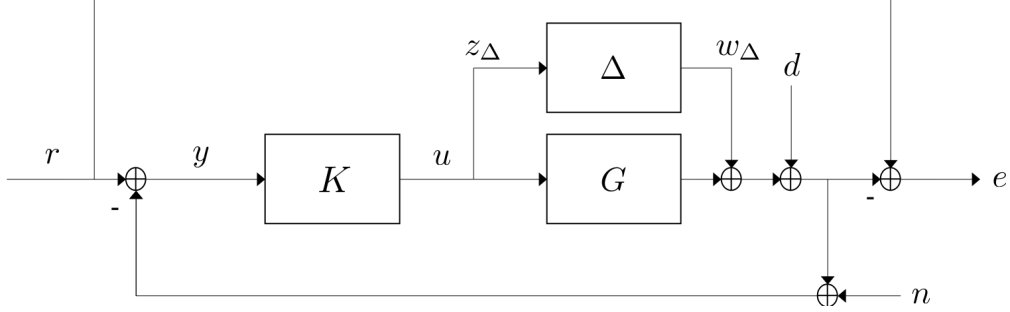


Figure 23: Rewritten uncertain closed loop interconnection.

The expanded, open-loop equations of the system depicted in figure 22 are given here:

$$\begin{pmatrix} z_\Delta \\ z \\ y \end{pmatrix} = \begin{pmatrix} P_{11} & P_{12} & P_{13} \\ P_{21} & P_{22} & P_{23} \\ P_{31} & P_{32} & P_{33} \end{pmatrix} \begin{pmatrix} w_\Delta \\ w \\ u \end{pmatrix}. \quad (6.2)$$

The upper or lower linear fractional transformation of this uncertain, controlled system, mapping $w \rightarrow z$ can be formed by substituting $w_\Delta = \Delta z_\Delta$ and $u = Ky$. The significance of these mappings will become evident as we get further into this discussion on μ -synthesis.

6.2.3 Uncertainty and Stability Margins

This discussion will help with setting a stage to discuss the structured singular value, whose upper/lower bounds arise in μ -synthesis. Furthermore, a discussion on traditional robust stability/performance is insightful for illustrating its conservatism.

The uncertainty can be pulled out of an uncertain system $G + \Delta$ to get the rewritten uncertain system shown in figure 23. Next, we can remove the uncertainty block in order to get the transfer function that is seen by the uncertainty block. That is, the transfer function $w_\Delta \rightarrow z_\Delta$. This interconnection is shown in figure 24. For this interconnection, the transfer function is given by

$$M = -(I + KG)^{-1}K. \quad (6.3)$$

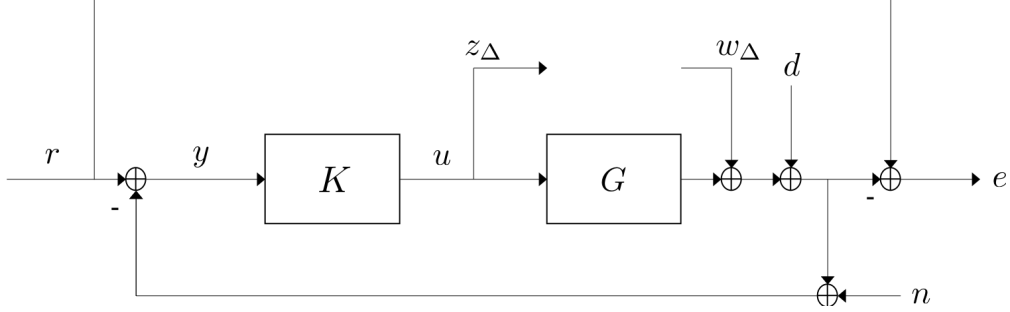


Figure 24: Uncertain closed loop interconnection with uncertainty block removed.

For robust stability, we will show that the loop remains stable for a specific Δ if $I - M\Delta$ has a proper and stable inverse.

Recalling figure 24, we set $z = e$ and collect d, n, r into $w = [d \ n \ r]^T$. From here, we correspond figure 24 to figure 26. Our signals can then be related by

$$\begin{pmatrix} z_\Delta \\ z \end{pmatrix} = \begin{pmatrix} N_{11} & N_{12} \\ N_{21} & N_{22} \end{pmatrix} \begin{pmatrix} w_\Delta \\ w \end{pmatrix} = \begin{pmatrix} M & N_{12} \\ N_{21} & N_{22} \end{pmatrix} \begin{pmatrix} w_\Delta \\ w \end{pmatrix}. \quad (6.4)$$

We notice that the transfer matrix seen by Δ in this structure is $N_{11} = M$, which is what was shown by (6.3). By reconnecting the uncertainty by

$$w_\Delta = \Delta z_\Delta \quad (6.5)$$

we arrive at the linear fractional transformation mapping $w \rightarrow z$

$$z = [N_{22} + N_{21}\Delta(I - M\Delta)^{-1}N_{12}]w. \quad (6.6)$$

Since we know that the controller that was designed, K , is stabilizing, $N_{11} = M$, N_{12} , N_{21} , N_{22} are all proper and stable. It is through $(I - M\Delta)^{-1}$ that instability or improprieness occurs. We end up having to verify that

$$I - M\Delta = I + (I + KG)^{-1}K\Delta \quad (6.7)$$

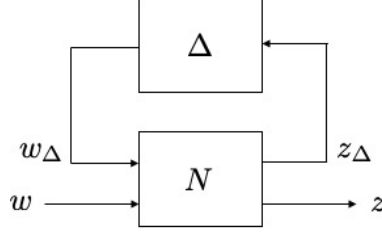


Figure 25: Condensed version of the uncertain system.

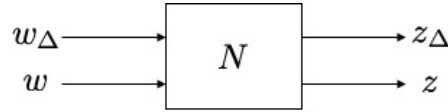


Figure 26: Condensed uncertain system, open loop.

has a proper, stable inverse with the requirement that $\|\Delta\| < 1$. The Nyquist criterion can now be applied. Since both $M = -(I + KG)^{-1}K$ and Δ are stable, this is true if the curve

$$\omega \rightarrow -M(j\omega)\Delta(j\omega) = \left(I + K(j\omega)G(j\omega) \right)^{-1} K(j\omega)\Delta(j\omega) \quad (6.8)$$

does not encircle -1 . This is true if

$$\left| M(j\omega)\Delta(j\omega) \right| = \left| \left(I + K(j\omega)G(j\omega) \right)^{-1} K(j\omega)\Delta(j\omega) \right| < 1 \quad \forall \quad \omega \in \mathbb{R} \cup \{\infty\}. \quad (6.9)$$

Due to the requirement that $\|\Delta\| < 1$, (6.9) is implied by

$$\left| M(j\omega) \right| = \left| \left(I + K(j\omega)G(j\omega) \right)^{-1} K(j\omega) \right| \leq 1 \quad \forall \quad \omega \in \mathbb{R} \cup \{\infty\}. \quad (6.10)$$

So, if (6.10) is valid, then the transfer function matrix $I - M\Delta = I + (I + KG)^{-1}K\Delta$ has a proper, stable inverse for all stable Δ , with $\|\Delta\| < 1$, allowing us to conclude that no uncertainties contained within Δ will be destabilizing.

Using the results derived above, we can move forward with discussing how we may go about constructing a destabilizing uncertainty perturbation. After doing so, we will set the stage for introducing the structured singular value (SSV), before getting into μ -synthesis.

6.2.3.1 Construction of a Destabilizing Uncertainty Perturbation A destabilizing uncertainty is one for which a Δ causes $(I - M\Delta)^{-1}$ to have a right-half plane pole, or alternatively, for $I - M\Delta$ to have a right-half plane zero. We can look for a zero, $j\omega_0$, on the imaginary axis. This would require that

$$M(j\omega_0)\Delta(j\omega_0) = 1. \quad (6.11)$$

Put another way, if we choose some ω_0 such that $|M(j\omega_0)| > 1$, then the complex number

$$\Delta_0 \doteq \frac{1}{M(j\omega_0)} \quad (6.12)$$

leads to $M(j\omega_0)\Delta_0 = 1$, therefore destabilizing the loop. Recalling (6.10), and relaxing the requirement that $\|\Delta\| < 1$, we can have that

$$\left| M(j\omega) \right| = \left| \left(I + K(j\omega)G(j\omega) \right)^{-1} K(j\omega) \right| \leq \gamma_0 \quad \forall \omega \in \mathbb{R} \cup \{\infty\} \quad (6.13)$$

meaning that this equality will hold, and the system will be stable for, all Δ that satisfy

$$|\Delta(j\omega)| < \frac{1}{\gamma_0} \quad \forall \omega \in \mathbb{R} \cup \{\infty\} \quad (6.14)$$

where we see that this bound is directly related to the inverse of the infinity norm of M . That is,

$$\frac{1}{\gamma_0} = \left(\sup_{\omega \in \mathbb{R} \cup \{\infty\}} |M(j\omega)| \right)^{-1} = \|M\|_{\infty}^{-1} \quad (6.15)$$

which illustrates how we can analyze, and establish bounds, on the robust stability of some system M subjected to uncertainty Δ .

6.2.4 Robust Stability Analysis

Our discussion on general uncertainty and stability margin has set the stage for us to discuss robust stability analysis, and thereafter robust performance analysis. Afterward, we will be able to move into a discussion on the structured singular value. Before doing so, it is worthwhile to state the well-known robust stability analysis and synthesis problems.

Robust Stability Analysis For a given, fixed controller K , test whether K robustly stabilizes $F_u(\Delta, P)$ against all uncertainties within a given set Δ .

Robust Stability Synthesis Find a controller K that robustly stabilizes $F_u(\Delta, P)$ against all uncertainties in Δ . We introduce the notation

$$F_l(P, K) = N = \begin{pmatrix} N_{11} & N_{12} \\ N_{21} & N_{22} \end{pmatrix} = \begin{pmatrix} M & N_{12} \\ N_{21} & N_{22} \end{pmatrix} \quad (6.16)$$

where we recall that M is the block that is “seen” by the uncertainty. This brings us to the following theorem, which is provided without proof, on robust stability.

Theorem 10. *If K stabilizes P , and if $I - M\Delta$ has a proper and stable inverse for all $\Delta \in \Delta$, then K robustly stabilizes $F_u(\Delta, P)$ against Δ .*

6.2.5 Robust Stability Tests Reduced to a Non-Singularity Test on the Imaginary Axis

We need to verify whether $I - M\Delta$ has a proper and stable inverse. To do so, as discussed previously, we would check that the matrix $I - M\Delta$ does not have any zeros in the closed right half plane, including infinity. This check amounts to

$$\det(I - M(s)\Delta(s)) \neq 0 \quad \forall s \in \mathbb{C}^0 \cup \mathbb{C}^+ \cup \{\infty\}, \Delta \in \Delta \quad (6.17)$$

This is challenging to do, since the entirety of the right half plane must be evaluated and the test must be performed for every $\Delta \in \Delta$.

The proceeding result, taken from the lecture notes by Scherer [59], shows that it is sufficient to test that $I - M(s)\Delta_c$ is nonsingular only on the $j\omega$ axis. We note that $\Delta_c \subset \Delta$ are those members of Δ along the imaginary axis, only. The following theorem states this.

Theorem 11. *Suppose M is a proper and stable transfer function matrix. If*

$$\det(I - M(j\omega)\Delta_c) \neq 0 \quad \forall \quad \Delta_c \in \Delta_c, \omega \in \mathbb{R} \cup \{\infty\}, \quad (6.18)$$

then $I - M\Delta$ has a proper stable inverse for all $\Delta \in \Delta$.

Proof. See Scherer, page 68 [59].

6.2.6 The Central Test for Robust Stability

Through combining theorems 10 and 11, we arrive at the fundamental robust stability test for controlled systems/interconnections.

Corollary 12. *If K stabilizes P , and if*

$$\det(I - M(j\omega)\Delta_c) \neq 0 \quad \forall \quad \Delta_c \in \Delta_c, \omega \in \mathbb{R} \cup \{\infty\}, \quad (6.19)$$

then K robustly stabilizes $F_u(\Delta, P)$ against Δ .

6.3 THE STRUCTURED SINGULAR VALUE (μ)

Thus far, we have discussed uncertainties whose values on the imaginary axis assume the following structure

$$\Delta_c = \text{diag} (p_1 I, \dots, p_{n_r} I, \delta_1 I, \dots, \delta_{n_c} I, \Delta_1, \dots, \Delta_{n_f}) \quad (6.20)$$

whose elements satisfy

- $p_j \in \mathbb{R}$ with $|p_j| < 1$, $j = 1, \dots, n_r$
- $\delta_j \in \mathbb{C}$ with $|\delta_j| < 1$, $j = 1, \dots, n_c$
- $\Delta_j \in \mathbb{C}^{p_j \times q_j}$ with $\|\Delta_j\| < 1$, for $j = 1, \dots, n_f$

where $p_j I$ is a real repeated block, $\delta_j I$ is a complex repeated block, and Δ_j is a full complex block.

When the uncertainty, Δ_c takes on the structure given by (6.1), the size of the blocks can be expressed as $\|\Delta_c\| < 1$. Furthermore, the set $r\Delta_c$ consists of all complex matrices Δ_c that take the same structure as (6.1) and whose blocks are bounded in size by r . That is, $\|\Delta_c\| < r$. The scaling factor, r , will be very relevant to our discussion on the structured singular value.

Recalling theorem 11, we know that the robust stability test is given by the following:

$$I - M(j\omega)\Delta_c \quad \text{is non-singular for all } \Delta_c \in \Delta_c \quad (6.21)$$

which is a problem of linear algebra [59]. Now we get into formally introducing the structured singular value. Given the complex matrix $M \in \mathbb{C}^{q \times p}$ and the set of complex matrices $\Delta_c \subset \mathbb{C}^{p \times q}$, we must decide whether

$$I - M\Delta_c \quad \text{is non-singular for all } \Delta_c \in \Delta_c. \quad (6.22)$$

We modify this test by considering the scaled set $r\Delta_c$ in which every element of Δ_c is being scaled by r . The robust stability test can now be modified into a new one: *Determine the largest r such that $I - M\Delta_c$ is nonsingular for all Δ_c in the set $r\Delta_c$. We denote this largest value of r as r_* .*

Formally, we want to calculate

$$r_* = \sup \left\{ r \mid \det(I - M\Delta_c) \neq 0 \quad \forall \quad \Delta_c \in r\Delta_c \right\}. \quad (6.23)$$

Using r as a scaling factor, we are inflating or shrinking the set $r\Delta_c$. r_* is the finite critical value for which we are able to claim that the set $r\Delta_c$ is nonsingular. Conversely, r_* also equals the smallest r such that we find the existence of some $\Delta_c \in r\Delta_c$ that renders $I - M\Delta_c$ singular. We are now prepared to define the structured singular value.

Definition 6. *The structured singular value (SSV) of the matrix M with respect to the set Δ_c is*

$$\mu_{\Delta_c}(M) = \frac{1}{r_*} = \frac{1}{\sup \left\{ r \mid \det(I - M\Delta_c) \neq 0 \quad \forall \quad \Delta_c \in r\Delta_c \right\}}. \quad (6.24)$$

We now assume that the SSV can be calculated. Thereafter we can decide whether or not (6.22) is true by checking whether $\mu_{\Delta_c}(M) \leq 1$. We provide the following theorem that supports this test, with proof contained within the lecture notes by Scherer [59].

Theorem 13. *Let M be a complex matrix and Δ_c be an arbitrary, open set of complex matrices. Then*

- $\mu_{\Delta_c}(M) \leq 1$ implies that $I - M\Delta_c$ is non-singular for all $\Delta_c \in \Delta_c$.
- $\mu_{\Delta_c}(M) > 1$ implies that there exists a $\Delta_c \in \Delta_c$ for which $I - M\Delta_c$ is singular.

Unfortunately, computation of the SSV is a difficult task. It is a task that we cannot perform exactly for problems of moderate size. What is done, instead, is a calculation of the upper and lower bounds on the SSV. Upper and lower bounds are used when performing robust performance/stability analyses, as well as during robust controller synthesis. Bounds on the SSV can be interpreted by letting M be a complex matrix and Δ_c an arbitrary (open) set of complex matrices.

Then,

- $\mu_{\Delta_c}(M) \leq \gamma_1$ implies that $I - M\Delta_c$ is non-singular for all $\Delta_c \in \gamma_1^{-1}\Delta_c$.
- $\mu_{\Delta_c}(M) > \gamma_2$ implies that there exists a $\Delta_c \in \gamma_2^{-1}\Delta_c$ for which $I - M\Delta_c$ is singular.

Given some scalar α , this is a consequence of the following:

$$\alpha\mu_{\Delta_c}(M) = \mu_{\Delta_c}(\alpha M) = \mu_{\alpha\Delta_c}(M). \quad (6.25)$$

We have that a scaling by some scalar α of the SSV is the same as scaling either M or the set Δ_c by the same amount.

6.3.1 SSV Applied to Testing Robust Stability

At this point, we have mentioned that we are relinquished to calculating the upper and lower bounds of the SSV. See Newlin for a more thorough discussion on this topic [75]. These bounds may or may not be tight — they are nonetheless approximations. This fact is part of the reason why probabilistic robustness evaluations have found acceptance and have developed within the controls community [14].

For robust stability to hold, we must have that the SSV of $M(j\omega)$, calculated with respect to the set Δ_c is smaller than 1. Since this must be true for all $\omega \in \mathbb{R}$, we arrive at the most fundamental result related to the SSV and robust stability testing: *$I - M\Delta$ has a proper and stable inverse for all $\Delta \in \Delta$ iff*

$$\mu_{\Delta_c}(M(j\omega)) \leq 1 \quad \text{for all } \omega \in \mathbb{R} \cup \{\infty\}. \quad (6.26)$$

We also can formulate the following corollary, resulting from theorems 10 and the small gain theorem to obtain the robust stability test for the general interconnection [17, 59]:

Corollary 14. *If K stabilizes P , and if*

$$\mu_{\Delta_c}(M(j\omega)) \leq 1 \quad \text{for all } \omega \in \mathbb{R} \cup \{\infty\}, \quad (6.27)$$

then K robustly stabilizes $F_u(\Delta, P)$ against Δ .

The robust stability tests are applied by simply calculating the number $\mu_{\Delta_c}(M(j\omega))$ for a finite number of frequencies. Practically-speaking, this would amount to plotting the function

$$\omega \rightarrow \mu_{\Delta_c}(M(j\omega)) \quad (6.28)$$

and verifying that the curve remains below one for all frequency. If it does not, we can move toward finding the destabilizing perturbation. As a somewhat useful aside, by plotting upper bound of $\mu_{\Delta_c}(M(j\omega))$ over the frequency ω , we can determine some $\gamma > 0$ such that

$$\mu_{\Delta_c}(M(j\omega)) \leq \gamma \quad \text{for all } \omega \in \mathbb{R} \cup \{\infty\} \quad (6.29)$$

is satisfied. Robust stability can be concluded for the uncertainty set

$$\left\{ \frac{1}{\gamma} \Delta \mid \Delta \in \Delta \right\} \quad (6.30)$$

where the above set admits the same structure as those in Δ , but that are bounded by $\frac{1}{\gamma}$ instead of one. By varying γ , the largest set $\frac{1}{\gamma}\Delta$ is obtained with the smallest γ for which (6.29) is valid. This value is

$$\gamma_* = \sup_{\omega \in \mathbb{R} \cup \{\infty\}} \mu_{\Delta_c}(M(j\omega)). \quad (6.31)$$

This number is called the stability margin since γ_*^{-1} is the largest inflating factor for the given set of uncertainties.

6.3.2 Bounds on the SSV

This subsection discusses how we go about calculating bounds on the SSV. The fact that we can only calculate bounds, even if they are tight, on the SSV shows that we are introducing additional conservatism into our analysis, and thereafter synthesis process by using μ -techniques. The entire purpose of this chapter, and using μ -techniques for establishing an initial search space for probabilistic robust, decentralized controller synthesis, is that we are hypothesizing that this conservatism will benefit our search. Indeed, this hypothesis, and approach, did work in our favor. This is detailed in chapter 7. For now, we continue this exposition into robust control and μ -methods.

Given two sets of complex matrices Δ_1 and Δ_2 such that

$$\Delta_1 \subset \Delta_2 \quad (6.32)$$

then we can say that

$$\mu_{\Delta_1}(M) \leq \mu_{\Delta_2}(M). \quad (6.33)$$

Now, we introduce the sets

$$\Delta_1 \doteq \left\{ pI \in \mathbb{R}^{p \times q} \mid |p| < 1 \right\} \quad (6.34)$$

$$\Delta_2 \doteq \left\{ pI \in \mathbb{C}^{p \times q} \mid |p| < 1 \right\} \quad (6.35)$$

$$\Delta_3 \doteq \left\{ \Delta_c \in \mathbb{C}^{p \times q} \mid \|\Delta_c\| < 1 \right\} \quad (6.36)$$

where these sets correspond to one real repeated block, one complex repeated block, and one full block. For each of these structures, the SSV can be computed explicitly [59]:

$$\mu_{\Delta_1}(M) = \rho_{\mathbb{R}}(M) \quad (6.37)$$

$$\mu_{\Delta_2}(M) = \rho(M) \quad (6.38)$$

$$\mu_{\Delta_3}(M) = \|M\| \quad (6.39)$$

where $\rho_{\mathbb{R}}(M)$ is the real spectral radius of M , which is defined as

$$\rho_{\mathbb{R}}(M) = \max \left\{ |\lambda| \mid \lambda \text{ is a real eigenvalue of } M \right\}. \quad (6.40)$$

The complex spectral radius has the same definition, with the exception that λ is complex. Generally, we have that

$$\Delta_1 \subset \Delta_c \subset \Delta_3, \quad (6.41)$$

which implies that

$$\mu_{\Delta_1}(M) \leq \mu_{\Delta_c}(M) \leq \mu_{\Delta_3}(M). \quad (6.42)$$

If there are no real blocks, then we have

$$\mu_{\Delta_2}(M) \leq \mu_{\Delta_c}(M) \leq \mu_{\Delta_3}(M). \quad (6.43)$$

This leads to the following lemma from Scherer [59]:

Lemma 6. *In general,*

$$\rho_{\mathbb{R}}(M) \leq \mu_{\Delta_c}(M) \leq \|M\| \quad (6.44)$$

and if the number of real blocks, $n_r = 0$, then

$$\rho(M) \leq \mu_{\Delta_c}(M) \leq \|M\| \quad (6.45)$$

These bounds are coarse. Computational approaches are used to refine the bounds in getting close to the actual value of the SSV. These computational approaches are not discussed here.

Lower Bounds on the SSV: If we can compute some

$$\Delta_0 \in \frac{1}{\gamma} \Delta_c \quad \text{that renders } I - M\Delta_0 \text{ singular,} \quad (6.46)$$

then we can conclude that

$$\gamma \leq \mu_{\Delta_c}(M). \quad (6.47)$$

Upper Bounds on the SSV: If we can compute

$$\text{for all } \Delta_c \in \frac{1}{\gamma} \Delta_c \quad \text{the matrix } I - M\Delta_c \text{ is non-singular} \quad (6.48)$$

then we can conclude that

$$\mu_{\Delta_c}(M) \leq \gamma. \quad (6.49)$$

Previously, we saw that $\|M\| \leq \gamma$ is a sufficient condition for (6.48) to hold. So, we move toward refining this condition.

Simple Scalings: We assume that all full blocks of the general uncertainty structure are square, meaning that $p_j = q_j$. Supposing that D is a non-singular matrix that satisfies

$$D\Delta_c = \Delta_c D \quad \text{for all } \Delta_c \in \frac{1}{\gamma} \Delta_c. \quad (6.50)$$

Given the condition that

$$\|D^{-1}MD\| < \gamma \quad (6.51)$$

it is implied that

$$I - [D^{-1}MD]\Delta_c \quad (6.52)$$

is non-singular for all $\Delta_c \in \frac{1}{\gamma} \Delta_c$. By exploiting $D\Delta_c = \Delta_c D$, (6.52) can be written as

$$I - D^{-1}[M\Delta_c]D = D^{-1}[I - M\Delta_c]D \quad (6.53)$$

which means that we not only have that $I - M\Delta_c$ is nonsingular, but that γ is also an upper bound for $\mu_{\Delta_c}(M)$.

To find the smallest upper bound, we need to minimize the norm

$$\|D^{-1}MD\| \quad (6.54)$$

over the set of matrices D satisfying equation (6.50). This marks the beginning of D/K iterations. Since, $D = I$ is in the class of these commutative matrices, the minimal value is better than $\|M\|$, meaning that this upper bound can be refined through introduction of extra variables D . We are interested in a scaled version, $D^{-1}MD$ of M , meaning these variables D are called *scalings*. This brings us to the following lemma from Scherer [59]:

Lemma 7. *We have*

$$\mu_{\Delta_c}(M) \leq \inf_{D \text{ satisfies (6.50) and is non-singular}} \|D^{-1}MD\|. \quad (6.55)$$

To find the best upper bound we want to minimize the RHS of the inequality above. Fortunately, this problem is convex and is furthermore amenable to being cast as a semidefinite program. One thing that we recognize is that (6.50) holds if and only if D admits the structure

$$D = \text{diag}(D_1, \dots, D_{n_r}, D_{n_r+1}, \dots, D_{n_r+n_c}, d_1 I, \dots, d_{n_f} I) \quad (6.56)$$

where n_r is the number of real repeated blocks, n_c is the number of the complex repeated blocks, and n_f is the number of full complex blocks. Furthermore, D_j is a non-singular complex matrix and d_j is a non-zero complex scalar. In the next step of this scaling approach, we transform $\|D^{-1}MD\| < \gamma$ into an LMI. We see that this is equivalent to

$$[D^{-1}MD][D^{-1}MD]^H < \gamma^2 I. \quad (6.57)$$

By left multiplication with D and right multiplication with D^H we get

$$D[D^{-1}MD][D^{-1}MD]^H D^H < \gamma^2 D D^H \quad (6.58)$$

$$D D^{-1} M D D^H M D^{-H} D^H < \gamma^2 D D^H \quad (6.59)$$

$$M D D^H M < \gamma^2 D D^H. \quad (6.60)$$

By introducing the Hermitian matrix

$$Q \doteq D D^H \quad (6.61)$$

the last inequality above becomes

$$M Q M^H < \gamma^2 Q \quad (6.62)$$

where Q has the structure

$$Q = \text{diag}(Q_1, \dots, Q_{n_r}, Q_{n_r+1}, \dots, Q_{n_r+n_c}, q_1 I, \dots, q_{n_f} I) \quad (6.63)$$

where Q_j , given the structure that has been imposed, is Hermitian and positive definite, and q_j is a real positive scalar. This is a semidefinite program. This semidefinite program can be cast with the objective of minimizing γ , allowing us to find the best upper bound. A larger class of scalings can be considered, allowing more freedom and ability to approach the actual value of the SSV. For a brief discussion on this topic, refer to Scherer's notes [59].

6.3.3 Robust Performance

The robust performance test is very similar to that pursued for robust stability. Performance signals are identified, uncertainties are pulled out, and weightings for the uncertainties are introduced such that the preceding framework is mirrored.

In the robust performance framework, performance weightings are incorporated to turn the desired performance into an \mathcal{H}_∞ norm bound on the virtual output/performance channel. As mentioned previously, the controlled uncertain system is given by

$$\begin{pmatrix} z_\Delta \\ z \\ y \end{pmatrix} = \begin{pmatrix} P_{11} & P_{12} & P_{13} \\ P_{21} & P_{22} & P_{23} \\ P_{31} & P_{32} & P_{33} \end{pmatrix} \begin{pmatrix} w_\Delta \\ w \\ u \end{pmatrix}, \quad u = Ky, \quad w_\Delta = \Delta z_\Delta, \quad \Delta \in \Delta \quad (6.64)$$

we now provide the following hypothesis from Scherer [59]:

Hypothesis 1. *P is a generalized plant, and*

- *The set of uncertainties is given as*

$$\Delta \doteq \left\{ \Delta \in \mathcal{RH}_\infty \mid \Delta(j\omega) \in \Delta_c \right\} \quad \text{for all } \omega \in \mathbb{R} \cup \{\infty\} \quad (6.65)$$

where Δ_c is the set of all matrices Δ_c structured as given by (6.1) and satisfying $\|\Delta_c\| < 1$.

- *The direct feed-through P_{11} and Δ_c are such that*

$$I - P_{11}(\infty)\Delta_c \quad (6.66)$$

is non-singular for all $\Delta_c \in \Delta_c$.

- The performance of the system is as desired if the \mathcal{H}_∞ norm of the $w \rightarrow z$ channel is smaller than 1.

Using the notation

$$P_\Delta = F_u(\Delta, P) = \begin{bmatrix} P_{22} & P_{23} \\ P_{32} & P_{33} \end{bmatrix} + \begin{bmatrix} P_{21} \\ P_{32} \end{bmatrix} \Delta(I - P_{11}\Delta)^{-1} \begin{bmatrix} P_{12} & P_{13} \end{bmatrix} \quad (6.67)$$

for the uncertain open-loop interconnection, we have the open-loop interconnection without uncertainty

$$P_0 = F_u(0, P) = \begin{bmatrix} P_{22} & P_{23} \\ P_{32} & P_{33} \end{bmatrix}. \quad (6.68)$$

If K stabilizes P and if

$$\left\| F_u(P_0, K) \right\|_\infty \leq 1 \quad (6.69)$$

we can say that K achieves nominal performance for P . Robust performance is achieved if

$$K \text{ stabilizes } P_\Delta = F_u(\Delta, P) \text{ and } \left\| F_u(P_\Delta, K) \right\|_\infty \leq 1 \text{ for all } \Delta \in \Delta$$

allowing us to say that

$$K \text{ achieves robust performance for } F_u(\Delta, P) \text{ against } \Delta.$$

6.3.4 Testing Robust Performance

The SSV of a complex matrix equals its norm if the uncertainty structure consists of just one full block. This was given in (6.39). Recalling this: given $\Delta_3 \doteq \left\{ \Delta_c \in \mathbb{C}^{p \times q} \mid \|\Delta_c\| < 1 \right\}$ we had that $\mu_{\Delta_3}(M) = \|M\|$. We assume throughout that the controller K stabilizes P , implying that $N \doteq F_l(P, K)$ is stable. Introducing the partition:

$$\begin{pmatrix} z_\Delta \\ z \end{pmatrix} = F_l(P, K) \begin{pmatrix} w_\Delta \\ w \end{pmatrix} = N \begin{pmatrix} w_\Delta \\ w \end{pmatrix} = \begin{pmatrix} M & N_{12} \\ N_{21} & N_{22} \end{pmatrix} \begin{pmatrix} w_\Delta \\ w \end{pmatrix} \quad (6.70)$$

the inference can be made that

$$F_l(P_\Delta, K) = F_u(\Delta, N) = N_{22} + N_{21}\Delta(I - M\Delta)^{-1}N_{12}, \quad (6.71)$$

leading us to conclude robust performance if the robust stability condition

$$\mu_{\Delta_c}(M(j\omega)) \leq 1 \quad \forall \omega \in \mathbb{R} \cup \{\infty\} \quad (6.72)$$

$$\Leftrightarrow \det(I - M(j\omega)\Delta_c) \neq 0 \quad \forall \Delta_c \in \Delta_c, \omega \in \mathbb{R} \cup \{\infty\} \quad (6.73)$$

and furthermore that the performance bound

$$\left\| N_{22} + N_{21}\Delta(I - M\Delta)^{-1}N_{12} \right\| \leq 1 \quad \forall \Delta \in \Delta \quad (6.74)$$

$$\Leftrightarrow \left\| N_{22}(j\omega) + N_{21}(j\omega)\Delta(j\omega)(I - M(j\omega)\Delta(j\omega))^{-1}N_{12}(j\omega) \right\| \leq 1 \quad \forall \Delta \in \Delta, \quad (6.75)$$

$$\omega \in \mathbb{R} \cup \{\infty\}$$

$$\Leftrightarrow \left\| N_{22}(j\omega) + N_{21}(j\omega)\Delta_c(j\omega)(I - M(j\omega)\Delta_c(j\omega))^{-1}N_{12}(j\omega) \right\| \leq 1 \quad \forall \Delta_c \in \Delta_c, \quad (6.76)$$

$$\omega \in \mathbb{R} \cup \{\infty\}$$

all hold true.

Just as for the robust stability tests, for each frequency within some grid that we have defined, we end up with linear algebraic problems to solve. To show this, we introduce the main loop theorem. After this has been shown, we will be fully prepared to discuss μ -synthesis via D/K iterations. Given the set Δ_c and the complex matrix

$$N_c = \begin{pmatrix} M & N_{12} \\ N_{21} & N_{22} \end{pmatrix} \quad \text{with} \quad N_{22} \in \mathbb{C}^{r_1 \times m_1} \quad (6.77)$$

we need to test whether or not the two conditions hold:

$$\det(I - M\Delta_c) \neq 0 \quad (6.78)$$

$$\left\| N_{22}(j\omega) + N_{21}(j\omega)\Delta_c(j\omega)(I - M(j\omega)\Delta_c(j\omega))^{-1}N_{12}(j\omega) \right\| \leq 1 \quad \forall \Delta_c \in \Delta_c. \quad (6.79)$$

What has been referred to as a “fundamental trick” is used to solve this problem [59]. The structured singular value is equal to the norm of a complex matrix for the case where the

uncertainty is a full block matrix. The condition

$$\left\| N_{22} + N_{21}\Delta_c(I - M\Delta_c)^{-1}N_{12} \right\| = \left\| F_u(\Delta_c, N_c) \right\| \leq 1 \quad (6.80)$$

is equivalent to

$$\det(I - F_u(\Delta_c, N_c)\hat{\Delta}_c) \neq 0 \quad \forall \quad \hat{\Delta}_c \in \mathbb{C}^{p_2 \times q_2}, \|\hat{\Delta}_c\| < 1. \quad (6.81)$$

Again, this uses the fact that the SSV of a full complex matrix equals its norm if the uncertainty structure is just one full block. It is noticed that the term $\hat{\Delta}_c$ has now appeared. This is defined as

$$\hat{\Delta}_c = \left\{ \hat{\Delta}_c \in \mathbb{C}^{p_2 \times q_2} \mid \|\hat{\Delta}_c\| < 1 \right\} \quad (6.82)$$

and infer that, for all $\Delta_c \in \Delta_c$, that

$$\det(I - M\Delta_c) \neq 0 \quad \text{and} \quad \left\| F_u(\Delta_c, N_c) \right\| \leq 1 \quad (6.83)$$

iff for all $\Delta_c \in \Delta_c$ and $\hat{\Delta}_c \in \hat{\Delta}_c$, we have that both

$$\det(I - M\Delta_c) \neq 0 \quad \text{and} \quad \det(I - F_u(\Delta_c, N_c)\hat{\Delta}_c) \neq 0 \quad (6.84)$$

iff for all $\Delta_c \in \Delta_c$, that

$$\det \begin{pmatrix} I - M\Delta_c & -N_{12}\hat{\Delta}_c \\ -N_{21}\Delta_c & I - N_{22}\hat{\Delta}_c \end{pmatrix} \neq 0 \quad (6.85)$$

iff for all $\Delta_c \in \Delta_c$,

$$\det \left(I - \begin{pmatrix} M & N_{12} \\ N_{21} & N_{22} \end{pmatrix} \begin{pmatrix} \Delta_c & 0 \\ 0 & \hat{\Delta}_c \end{pmatrix} \right) \neq 0 \quad (6.86)$$

where these arguments arise from the Schur formula for the determinant of a block matrix. That is, given

$$M \doteq \begin{bmatrix} A & B \\ C & D \end{bmatrix} \quad (6.87)$$

we know that M/A gives us

$$M/A \doteq D - CA^{-1}B \quad (6.88)$$

and that $\det(M)$, using this formula, can be found from

$$\det(M) = \det(A)\det(D - CA^{-1}B). \quad (6.89)$$

For our specific case we require that $\det(I - M\Delta_c) \neq 0$. Thoroughly, we have

$$\begin{aligned} \det\left(I - F_u(\Delta_c, N_c)\hat{\Delta}_c\right) &= \det\left(I - [N_{22} + N_{21}\Delta_c(I - M\Delta_c)^{-1}N_{12}]\hat{\Delta}_c\right) = \\ &= \det\left([I - N_{22}\hat{\Delta}_c] - [N_{21}\Delta_c](I - M\Delta_c)^{-1}[N_{12}\hat{\Delta}_c]\right) = \det\begin{pmatrix} I - M\Delta_c & -N_{12}\hat{\Delta}_c \\ -N_{21}\Delta_c & I - N_{22}\hat{\Delta}_c \end{pmatrix}. \end{aligned} \quad (6.90)$$

This derivation and discussion motivates the introduction of what have been termed the set of **extended** matrices [59]:

$$\Delta_e \doteq \left\{ \begin{pmatrix} \Delta_c & 0 \\ 0 & \hat{\Delta}_c \end{pmatrix} : \Delta_c \in \Delta_c, \hat{\Delta}_c \in \mathbb{C}^{p_2 \times q_2}, \|\hat{\Delta}_c\| < 1 \right\}. \quad (6.91)$$

The original uncertainty structure has been augmented with one full, complex block uncertainty. The derivation above has just proven the **Main Loop Theorem**, which is stated:

Theorem 15 (Main Loop Theorem). *The two conditions*

$$\mu_{\Delta_c}(M) \leq 1 \quad \text{and} \quad \left\| F_u(\Delta_c, N_c) \right\| \leq 1 \quad \text{for all } \Delta_c \in \Delta_c \quad (6.92)$$

are equivalent to

$$\mu_{\Delta_e}(N_c) \leq 1. \quad (6.93)$$

Thus, this result reduces the desired condition to another SSV test on the matrix N_c with respect to the extended structure Δ_e ! Now, we will complete our discussion on this topic. Typically, a computation of $\mu_{\Delta_e}(N_c)$ will lead to an inequality

$$\mu_{\Delta_e}(N_c) \leq \gamma \quad (6.94)$$

with bound $\gamma > 0$ different from one. We can easily re-scale. That is,

$$\mu_{\Delta_e} \left(\frac{1}{\gamma} N_c \right) \leq 1. \quad (6.95)$$

This is equivalent to

$$\mu_{\Delta_c} \left(\frac{1}{\gamma} M \right) \leq 1 \quad (6.96)$$

and

$$\left\| \frac{1}{\gamma} N_{22} + \frac{1}{\gamma} N_{21} \Delta_c \left(I - \frac{1}{\gamma} M \Delta_c \right)^{-1} \frac{1}{\gamma} N_{12} \right\| \leq 1 \quad \text{for all } \Delta_c \in \Delta_c \quad (6.97)$$

showing us that both conditions are just

$$\mu_{\Delta_c}(M) \leq \gamma \quad (6.98)$$

and

$$\left\| N_{22} + N_{21} \frac{1}{\gamma} \Delta_c \left(I - M \frac{1}{\gamma} \Delta_c \right)^{-1} N_{12} \right\| \leq \gamma \quad \text{for all } \Delta_c \in \Delta_c \quad (6.99)$$

leading us to arrive at

$$\det(I - M \Delta_c) \neq 0 \quad \text{for all } \Delta_c \in \frac{1}{\gamma} \Delta_c \quad (6.100)$$

and

$$\left\| N_{22} + N_{21} \Delta_c (I - M \Delta_c)^{-1} N_{12} \right\| \leq \gamma \quad \text{for all } \Delta_c \in \frac{1}{\gamma} \Delta_c, \quad (6.101)$$

showing us that a bound γ , different from one, leads to stability and a performance bound γ for the scaled complex matrices $\frac{1}{\gamma} \Delta_c$.

6.3.5 The Robust Stability and Robust Performance Test

By combining the main loop theorem with our robust performance test, we arrive at the main theorem for robust stability and performance testing.

Theorem 16. Let $N = \begin{pmatrix} M & N_{12} \\ N_{21} & N_{22} \end{pmatrix}$ be a proper and stable transfer matrix. For all $\Delta \in \Delta$,

$$(I - M\Delta)^{-1} \in R\mathcal{H}_\infty \quad \text{and} \quad \left\| F_u(\Delta, N) \right\|_\infty \leq 1 \quad (6.102)$$

iff

$$\mu_{\Delta_e}(N(j\omega)) \leq 1 \quad \text{for all } \omega \in \mathbb{R} \cup \{\infty\}. \quad (6.103)$$

This leads us to a fundamental corollary in structured singular value theory:

Corollary 17. If K stabilizes P , and if

$$\mu_{\Delta_e}(N(j\omega)) \leq 1 \quad \text{for all } \omega \in \mathbb{R} \cup \{\infty\} \quad (6.104)$$

the K achieves robust performance for $F_u(\Delta, P)$ against all $\Delta \in \Delta$.

6.3.6 Summary

Figure 27 will aid this discussion. Supposing that some controller K stabilizes the plant P and supposing that the controlled, uncertain system is given by

$$\begin{pmatrix} z_\Delta \\ z \end{pmatrix} = F_l(P, K) \begin{pmatrix} w_\Delta \\ w \end{pmatrix} = N \begin{pmatrix} w_\Delta \\ w \end{pmatrix} = \begin{pmatrix} M & N_{12} \\ N_{21} & N_{22} \end{pmatrix} \begin{pmatrix} w_\Delta \\ w \end{pmatrix}, \quad w_\Delta = \Delta z_\Delta \quad (6.105)$$

with proper and stable Δ satisfying

$$\Delta(j\omega) \in \Delta_c \quad \text{for all } \omega \in \mathbb{R} \cup \{\infty\}, \quad (6.106)$$

then the controller K achieves:

- Robust stability if

$$\mu_{\Delta_c}(M(j\omega)) \leq 1 \quad \text{for all } \omega \in \mathbb{R} \cup \{\infty\}; \quad (6.107)$$

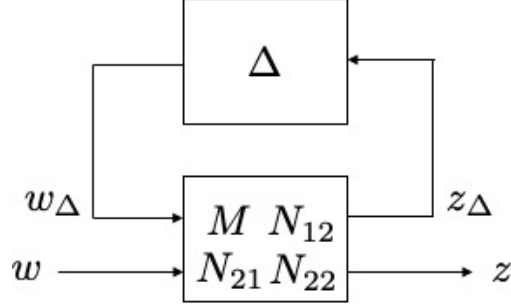


Figure 27: Robustness test block diagram.

- Nominal performance if

$$\left\| N_{22}(j\omega) \right\| \leq 1 \quad \text{for all } \omega \in \mathbb{R} \cup \{\infty\}; \quad (6.108)$$

- Robust performance if

$$\mu_{\Delta_e} \left(N(j\omega) \right) \leq 1 \quad \text{for all } \omega \in \mathbb{R} \cup \{\infty\}. \quad (6.109)$$

Referring back to figure 27, robust stability is guaranteed by an SSV-test on the block M of $N = F_l(P, K)$; nominal performance by an SSV-test on the block N_{22} , and robust performance is guaranteed by an SSV-test on the whole N , with respect to the **extended block uncertainty structure** Δ_e .

6.4 μ -SYNTHESIS VIA D/K ITERATIONS

The design of controllers that achieve robust stability and performance amounts to minimizing the SSV, with respect to a certain uncertainty structure, of the controlled system over all frequencies. Another name for D/K -iteration is actually scalings/controller-iteration.

We consider the uncertain, controlled system:

$$\begin{pmatrix} z_\Delta \\ z \\ y \end{pmatrix} = \begin{pmatrix} P_{11} & P_{12} & P_{13} \\ P_{21} & P_{22} & P_{23} \\ P_{31} & P_{32} & P_{33} \end{pmatrix} \begin{pmatrix} w_\Delta \\ w \\ u \end{pmatrix}, \quad u = Ky, \quad w_\Delta = \Delta z_\Delta, \quad \Delta \in \Delta \quad (6.110)$$

and again use the notation, $P_\Delta \doteq F_u(\Delta, P)$. The goal of D/K iteration is to design a controller, K , that stabilizes P_Δ and leads to the condition that

$$\left\| F_l(P_\Delta, K) \right\| \leq 1 \quad \text{for all } \Delta \in \Delta. \quad (6.111)$$

In order to do this, we turn, again, to the extended uncertainty block structure, which looks like

$$\Delta_e \doteq \left\{ \begin{pmatrix} \Delta_c & 0 \\ 0 & \hat{\Delta}_c \end{pmatrix} : \Delta_c \in \Delta_c, \hat{\Delta}_c \in \mathbb{C}^{r_1 \times m_1}, \|\hat{\Delta}_c\| < 1 \right\} \quad (6.112)$$

where r_1/m_1 are the lengths of the w/z channels, respectively. A controller K achieves robust performance if it stabilizes the nominal system and satisfies the condition

$$\mu_{\Delta_e} (F_l(P, K)(j\omega)) \leq 1 \quad \text{for all } \omega \in \mathbb{R} \cup \{\infty\}. \quad (6.113)$$

Finding a controller that achieves (6.113) directly cannot be done [76]. We cannot even compute the SSV directly in most practical cases [75]. To achieve (6.113) we want to guarantee that a computable upper bound on the SSV is smaller than one for all frequencies.

Recalling that the set of scalings \mathbf{D} corresponding to Δ_c for computing an upper bound look like

$$D = \text{diag}(D_1, \dots, D_{n_r}, D_{n_r+1}, \dots, D_{n_r+n_c}, d_1 I, \dots, d_{n_f} I) \quad (6.114)$$

with each D_j matrix being Hermitian and positive definite and each d_j real, positive scalars. The class of scalings corresponding to the extended uncertainty structure Δ_e is then

$$\mathbf{D}_e \doteq \left\{ \begin{pmatrix} D & 0 \\ 0 & I \end{pmatrix} > 0 \mid D \in \mathbf{D} \right\}. \quad (6.115)$$

This class of scalings has the property that

$$\mu_{\Delta_e} \left(F_l(P, K)(j\omega) \right) \leq \inf_{D \in \mathbf{D}_e} \left\| D^{-1} F_l(P, K)(j\omega) D \right\|. \quad (6.116)$$

which means that any stabilizing controller K that leads to

$$\inf_{D \in \mathbf{D}_e} \left\| D^{-1} F_l(P, K)(j\omega) D \right\| \leq 1 \quad \text{for all } \omega \in \mathbb{R} \cup \{\infty\} \quad (6.117)$$

guarantees that (6.113) will be met. Thus, we are actually minimizing the upper bound of the SSV — not the SSV, directly. Put another way, we are actually performing “upper bound design”. It helps to reformulate (6.117) slightly — we can say that there exists a frequency-dependent scaling $D(\omega) \in \mathbf{D}_e$ such that

$$\left\| D(\omega)^{-1} F_l(P, K)(j\omega) D(\omega) \right\| < 1 \quad \text{for all } \omega \in \mathbb{R} \cup \{\infty\} \quad (6.118)$$

which leads us to the problem that we want to solve:

$$\min \sup_{\omega \in \mathbb{R} \cup \{\infty\}} \left\| D(\omega)^{-1} F_l(P, K)(j\omega) D(\omega) \right\| \quad (6.119)$$

over all controllers stabilizing K , and over all frequency-dependent scalings $D(\omega) \in \mathbf{D}_e$. If the minimal value is found to be smaller than one, our controller synthesis problem is complete. We meet (6.117), which implies that we meet (6.113)! The procedure fails if the minimal value is found to be greater than one.

6.4.1 Scalings and Controller Iteration (D/K -iteration)

Scaling/controller iteration is pursued via two, iterative steps:

1. Fix the scaling function $D(\omega)$ and minimize (6.119) over all stabilizing controllers. This amounts to solving the \mathcal{H}_∞ problem, which can be pursued by solving a semidefinite program or by solving indefinite algebraic Riccati equations [63, 17].
2. Fix the stabilizing controller K and minimize (6.119) over all scaling functions $D(\omega)$.

We can now turn to the distinct steps behind this method.

6.4.2 Step #1

Set

$$D_1(\omega) = I \quad (6.120)$$

and minimize

$$\sup_{\omega \in \mathbb{R} \cup \{\infty\}} \left\| D_1(\omega)^{-1} F_l(P, K)(j\omega) D_1(\omega) \right\| = \left\| F_l(P, K) \right\|_{\infty} \quad (6.121)$$

over all stabilizing controllers. We note that this is just the standard \mathcal{H}_{∞} problem. We suppose that the optimal value is found to be smaller than some γ_1 , denoting K_1 as the controller that achieves this optimal bound.

6.4.3 Step #2

Find, through a separate optimization process, another diagonal $D_2(\omega)$ such that $D_2(\omega)$ and $D_2^{-1}(\omega)$ are stable and such that we minimize

$$\inf_{D_2 \in \mathbf{D}_e} \left\| D_2^{-1} F_l(P, K_1)(j\omega) D_2 \right\| \quad (6.122)$$

at each frequency. In this sense, we are attempting to minimize the upper bound of our estimate of the SSV. We recall that this minimization can be cast as a semidefinite program described by

$$\min_{Q, \gamma} \quad \gamma \quad (6.123)$$

$$\text{s.t.} \quad M Q M^H - \gamma^2 Q < 0 \quad (6.124)$$

$$Q > 0, \quad \gamma > 0 \quad (6.125)$$

where $Q \doteq D D^H$, with this SDP being solved at each frequency. This exact problem is also covered in section 3.3 of Boyd [15].

As a result of solving this optimization problem, we arrive at two new spots in our D/K iteration:

- Some new bound $\hat{\gamma}_1$
- D_2

That is, this step leads to a scaling function $D_2(\omega)$ such that

$$\sup_{\omega \in \mathbb{R} \cup \{\infty\}} \left\| D_2(\omega)^{-1} F_l(P, K_1)(j\omega) D_2(\omega) \right\| < \hat{\gamma}_1 \quad (6.126)$$

One thing that we notice here is that we've calculated new upper bounds on some $D_2(\omega)$, but that this collection of matrices do not represent some real rational transfer function matrix. Therefore, we must fit these matrices to some real-rational transfer function matrix $\hat{D}_2(s)$, such that

$$\left\| D_2(\omega) - \hat{D}_2(s) \right\| \leq \epsilon \quad \forall \quad \omega \in \mathbb{R} \cup \{\infty\} \quad (6.127)$$

for some small, prescribed error ϵ . This step can be achieved using several approaches to fitting data to transfer function matrices, for instance, see the interpolation problem posed in section 10.5.3 of Boyd [15].

Once this fitting has been completed, we are prepared to proceed to the next step. That is, we are now prepared to solve the \mathcal{H}_∞ problem, again, with our real rational $\hat{D}_2(s)$ that was just found.

6.4.4 Step #3

We now solve

$$\inf_{K \text{ stabilizes } P} \left\| \hat{D}_2(j\omega)^{-1} F_l(P, K)(j\omega) \hat{D}_2(j\omega) \right\|_\infty \quad (6.128)$$

to find another “almost” optimal controller, which we call K_2 . This step leads us to the condition such that

$$\sup_{\omega \in \mathbb{R} \cup \{\infty\}} \left\| D_2(\omega)^{-1} F_l(P, K_2)(j\omega) D_2(\omega) \right\| < \gamma_2 \quad (6.129)$$

where this controller, K_2 , now holds for some new bound γ_2 . We have arrived at (6.126) and can now iterate.

6.4.5 Step #4

Return to step #1, replacing $K_1 \rightarrow K_k \rightarrow K_{k+1}$ as we iterate, and $D_1(\omega) \rightarrow D_k(\omega) \rightarrow D_{k+1}(\omega)$.

These approaches are implicit to the μ -synthesis tools used by Matlab and Matlab’s Robust Controls toolbox [77, 74]. This toolbox was used for achieving the collection of robust controllers that are subsequently in chapter 7 in order to search for probabilistic robust, decentralized dynamic output feedback controllers.

6.4.6 Examining Bounds on γ during Iterations

One thing that is interesting about these iterations is that during our scaling iterations, we are guaranteed that each new bound $\hat{\gamma}_k$ can be chosen such that $\hat{\gamma}_k < \gamma_k$. This is insightful, since if our desired robust performance is such that we want some $\gamma_k < \gamma_0$, then all controllers subsequent to γ_k will be both robustly stabilizing and robustly performing. These controllers, which we find on our way to solving the overarching mini-max problem in μ -synthesis, are still useful in the larger context of this research.

What we may find, however, is that the value of (6.126) cannot be made significantly smaller than γ_k at some frequency. If this is the case, the new bound $\hat{\gamma}_k$ is very close to γ_k , and the algorithm is stopped. Otherwise, if we have that $\hat{\gamma}_k$ is significantly smaller than γ_k and the algorithm proceeds.

We will now show that during each iteration, $\gamma_{k+1} < \gamma_k$. This is important to show, since by proceeding in this manner during synthesis, we are able to extract useful solutions for input into a larger stochastic optimization problem that we wish to solve.

During controller iteration, we see that the scaling function $D_k(\omega)$ is fit to a real rational $\hat{D}_k(s)$ uniformly over all frequencies. If ϵ is small, it can be inferred that

$$\sup_{\omega \in \mathbb{R} \cup \{\infty\}} \left\| \hat{D}^{-1}(j\omega) F_l(P, K)(j\omega) \hat{D}(j\omega) \right\| \approx \sup_{\omega \in \mathbb{R} \cup \{\infty\}} \left\| D_{k+1}(\omega) F_l(P, K)(j\omega) D_{k+1}(j\omega) \right\| \quad (6.130)$$

for both $K = K_k$ and K_{k+1} . We can infer from (6.129) that

$$\sup_{\omega \in \mathbb{R} \cup \{\infty\}} \left\| \hat{D}^{-1}(j\omega) F_l(P, K_k)(j\omega) \hat{D}(j\omega) \right\| \leq \hat{\gamma}_k. \quad (6.131)$$

Since K_{k+1} is found by solving an \mathcal{H}_∞ -optimization problem, we can choose that

$$\left\| \hat{D}^{-1}(j\omega) F_l(P, K_{k+1})(j\omega) \hat{D}(j\omega) \right\|_\infty \leq \left\| \hat{D}^{-1}(j\omega) F_l(P, K)(j\omega) \hat{D}(j\omega) \right\|_\infty \quad (6.132)$$

which implies that

$$\sup_{\omega \in \mathbb{R} \cup \{\infty\}} \left\| \hat{D}^{-1}(j\omega) F_l(P, K_{k+1})(j\omega) \hat{D}(j\omega) \right\| < \hat{\gamma}_k. \quad (6.133)$$

If the approximation of the scaling is good, this leads to

$$\sup_{\omega \in \mathbb{R} \cup \{\infty\}} \left\| \hat{D}_{k+1}^{-1}(j\omega) F_l(P, K_{k+1})(j\omega) \hat{D}_{k+1}(j\omega) \right\| < \hat{\gamma}_k. \quad (6.134)$$

which means that the bound γ_{k+1} can be taken smaller than $\hat{\gamma}_k$, allowing us to conclude

$$\gamma_{k+1} < \hat{\gamma}_k < \gamma_k. \quad (6.135)$$

During iterations, if we find that γ_{k+1} is not much smaller than γ_k , the algorithm stops.

We will now discuss how μ -synthesis via D/K iterations is used using an approach that has been called loop-at-a-time synthesis to achieve a collection of robust, decentralized controllers. A collection of controllers is obtained using this process and are subsequently as initial starting points, or seeds for the stochastic optimization problem that is posed and solved in chapter 7, for achieving the end of developing a controller design and synthesis approach that results in probabilistically-robust, decentralized, dynamic output feedback controllers.

6.5 LOOP-AT-A-TIME FORMULATIONS AND μ -SYNTHESIS

Loop-at-a-time synthesis is pursued so that we can achieve a decentralized controller architecture. This approach yields several benefits:

- The dynamics of the adjoining substructure are included during controller synthesis.
- After the first controller is synthesized, synthesis of the second controller accounts for the closed loop dynamics of the adjoining substructure.
- The resulting controllers are decentralized. Measurements and performance outputs are specific to the substructures.

Recall that the beam model that is used for controller design and synthesis in this chapter, as well as in chapter 7, was described in chapter 4. A schematic of this beam, with uncertain interconnection element shown, was given in figure 58, with beam data detailed in table 6, input/output locations in table 7, and the structured norm-bounded interconnection uncertainty described in section 4.3.3.

At a high level, loop at a time synthesis is described by the following steps:

1. Design controller K_2 to be robust against uncertainty and attenuate the ∞ -norm of the $\begin{bmatrix} w_1 & w_2 \end{bmatrix}^T \rightarrow z_2$ mapping at low frequencies.
2. Design controller K_1 to be robust against uncertainty and attenuate the ∞ -norm of the $\begin{bmatrix} w_1 & w_2 \end{bmatrix}^T \rightarrow z_1$ mapping at low frequencies while accounting for the closed-loop dynamics due to the presence of K_2 .
3. Check the stability and performance of the $\begin{bmatrix} w_1 & w_2 \end{bmatrix}^T \rightarrow \begin{bmatrix} z_1 & z_2 \end{bmatrix}^T$ mapping.
4. If acceptable, exit. Otherwise, set $K_2 = 0$, holding K_1 constant, and return to step 1. Alternate this iteration on K_1 and K_2 until acceptable performance and stability is achieved.

At the end of this process, we will achieve a controller structure, like that conceptualized in figure 21, that is robust against some structured norm-bounded interconnection uncertainty.

Now, we will recall the model, some of the design parameters, and the uncertainty descriptions that were defined in chapter 4. Then, we will develop the loops, algebraically, showing the state-space/transfer function matrices used for loop-at-a-time synthesis.

Loop-at-a-time μ -synthesis via D/K iterations was performed for the following uncertainty cases, which specify the parametric uncertainty in the interconnection stiffness elastic modulus:

- $E_{\Delta,1} \in [0.01E_0, 2E_0]$
- $E_{\Delta,2} \in [0.05E_0, 1.5E_0]$

Controller objectives and performance output function definition are similarly given in chapter 4. Stated again, we wanted to synthesize controllers, using μ -synthesis via D/K iterations, that were robust against the structured norm-bounded uncertainty $E_{\Delta,1}$ and $E_{\Delta,2}$, and attenuated the magnitudes of the displacement and velocity of each substructure, as sensed at measurement locations. Frequency-weighting was performed by scaling the performance output matrices, given by C_1 , in modal coordinates by the magnitude of a smooth first-order filter with cutoff frequency of 80 Hz (500 rad/s), which was also discussed in chapter 4.

Recall from chapter 4 and appendix B that a model stiffness element, as given by (B.10), is

$$\mathbf{k}_e = \left(\frac{EI}{L^3} \right) \begin{bmatrix} 12 & 6L & -12 & 6L \\ * & 4L^2 & -6L & 2L^2 \\ * & * & 12 & -6L \\ * & * & * & 4L^2 \end{bmatrix}. \quad (6.136)$$

We have said that the elastic modulus, given by E , has structured norm-bounded uncertainty characterized by either $E_{\Delta,1}$ or $E_{\Delta,2}$ as described earlier, where $E_0 = 200$ GPa. As an aside, we recognize that this interconnection stiffness element is actually just an uncertain static gain. This will become evident when the entire system is modeled in a multi-loop generalized plant architecture, which is iteratively collapsed during loop-at-a-time synthesis.

Seeing that the interconnection stiffness matrix is uncertain, with single uncertain parameter given by $E_{\Delta,i}$, $i = 1, 2$, this system is perfectly amenable to being cast into the uncertain generalized regulator framework discussed earlier in this chapter. For real-valued parametric uncertainty, the process of pulling out this uncertainty is straightforward. We show how this is done in appendix F for real-valued, parametric uncertainty and state that Matlab's Robust Control Toolbox was used to perform this step for μ -synthesis [74, 73]. During loop formulations, we must carry around the fact that the interconnection stiffness element is uncertain (which amounts to a fair amount of bookkeeping for high-dimensional systems). This is where computer-aided design software, such as Matlab's Robust Control Toolbox, aid in this endeavor.

The resulting robust, decentralized controllers are used as warm start points in a stochastic optimization problem, where we search for controllers of a similar-structure in a now-random space, as the interconnection is colored by random uncertainty and relatively unbounded — recall section 4.3. Thus, we will not explicitly analyze the nominal stability, performance, and robust stability and performance of the controllers that are obtained through this synthesis process. These controllers serve as a means to the end that is achieved in

chapter 7. Recall that our probabilistic robust performance objective, detailed in chapter 4 and given by (4.50), was

$$P_{\text{test}} \doteq \Pr \left(\left\| F_l(G, K) \right\|_{\infty} \leq \gamma^* \mid \mathbf{K}_{\Delta} \right) \geq 1 - \epsilon_p \quad (6.137)$$

where we chose $\gamma^* = -45.4$ dB and $\epsilon_p = 0.05$. The random transfer function matrix maps both disturbance inputs into the structure to both performance outputs of the structure. This implies that we wanted to find robust controllers using μ -synthesis via D/K iterations that attenuated the structure's response to disturbance inputs at low frequencies, yet did not necessarily achieve the 6 dB reduction below the open-loop response that was used to determine γ^* for all members of the norm-bounded plant uncertainty set. Theoretically, we could have iterated on our design and synthesis scheme using μ -synthesis to hopefully find a solution that achieved this, however, the goal of this research was to develop a probabilistic robust decentralized design and synthesis approach for structures that have random interconnection uncertainty. This chapter, and its approaches, are steps to achieving this end.

6.5.1 System Descriptions

For this section we shall define equations, along with the systems, that comprise figure 28. Going from left to right we will describe each system. We will then move toward closing the loop, as we transform the system toward achieving the end of loop-at-a-time synthesis.

The Controller, K_1 : The first controller, using shorthand notation, is described by

$$K_1 \sim \left[\begin{array}{c|c} A_{k,1} & B_{k,1} \\ \hline C_{k,1} & D_{k,1} \end{array} \right] \quad (6.138)$$

The equations for this dynamic compensator are given by

$$\dot{x}_{k,1} = A_{k,1}x_{k,1} + B_{k,1}u_{k,1} \quad (6.139)$$

$$y_{k,1} = C_{k,1}x_{k,1} + D_{k,1}u_{k,1}. \quad (6.140)$$

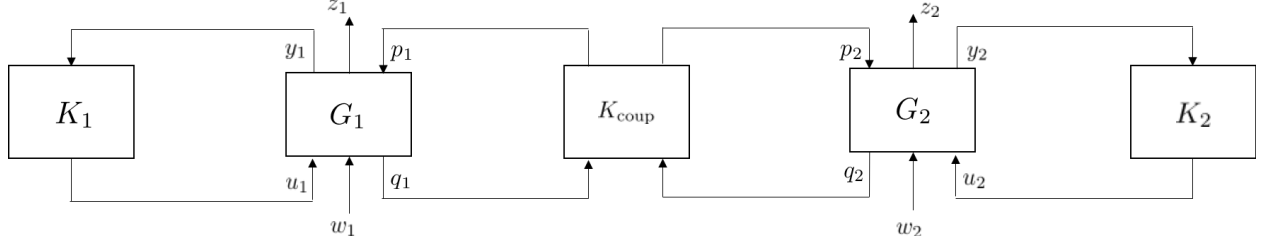


Figure 28: General system under consideration with labeled signals.

The Substructure, G_1 : The first substructure's dynamics are described by

$$G_1 \sim \left[\begin{array}{c|ccc} A_1 & B_{w,1} & B_{u,1} & B_{p,1} \\ \hline C_{z,1} & 0 & D_{12,1} & 0 \\ C_{y,1} & D_{21,1} & 0 & 0 \\ C_{q,1} & 0 & 0 & 0 \end{array} \right] \quad (6.141)$$

These equations are given by

$$\dot{x}_1 = A_1 x_1 + B_{w,1} w_1 + B_{u,1} u_1 + B_{p,1} p_1 \quad (6.142)$$

where w_1 is the disturbance input vector, u_1 is the control input vector, and p_1 represents the interconnection forces / moments that are acting on G_1 . The other salient equations that characterize this system's outputs are

$$z_1 = C_{z,1} x_1 + D_{12,1} u_1 \quad (6.143)$$

$$y_1 = C_{y,1} x_1 + D_{21,1} w_1 \quad (6.144)$$

$$q_1 = C_{q,1} x_1 \quad (6.145)$$

where (6.143) describes the performance output function defined for control design; (6.144) are the measurements made (transverse displacements and velocities); and (6.145) are the displacements and rotations at the interconnection stiffness interface.

At this point, it is appropriate to define the interconnection stiffness matrix and how it is incorporated into the model.

The Interconnection Stiffness, K_{coup} : In terms of realizing the interconnection stiffness as a dynamic system, the first thing that we notice is that this system component is actually just a static gain. That is,

$$K_{\text{coup}} \sim \left[\begin{array}{c|c} 0 & 0 \\ \hline 0 & \mathbf{K} \end{array} \right] \quad (6.146)$$

where

$$\mathbf{K} = \begin{bmatrix} K_{11} & K_{12} \\ K_{21} & K_{22} \end{bmatrix} = - \left(\frac{EI}{L^3} \right) \left[\begin{array}{cc|cc} 12 & 6L & -12 & 6L \\ * & 4L^2 & -6L & 2L^2 \\ \hline * & * & 12 & -6L \\ * & * & * & 4L^2 \end{array} \right] \quad (6.147)$$

where E, I, L are the modulus, area moment of inertia, and length of the stiffness element, respectively. From this, we see that interface forces/moment are related to displacements/rotations through

$$\begin{bmatrix} p_1 \\ p_2 \end{bmatrix} = \mathbf{K} \begin{bmatrix} q_1 \\ q_2 \end{bmatrix} \quad (6.148)$$

with q_1 describing the displacement and rotation on one side of the element, and q_2 describing the displacement and rotation on the other. Correspondingly, the $p_i, i = 1, 2$ are the forces/moment exerted due to displacements/rotations in the element. And so we can expand these equations, which will be useful in the derivations to follow, as

$$p_1 = K_{11}q_1 + K_{12}q_2 \quad (6.149)$$

$$p_2 = K_{21}q_1 + K_{22}q_2. \quad (6.150)$$

The Substructure, G_2 : Very similar to the first substructure (and included here for completeness and since the equations will be uniquely manipulated), the second substructure's

dynamics are captured by

$$G_2 \sim \left[\begin{array}{c|ccc} A_2 & B_{w,2} & B_{u,2} & B_{p,2} \\ \hline C_{z,2} & 0 & D_{12,2} & 0 \\ C_{y,2} & D_{21,2} & 0 & 0 \\ C_{q,2} & 0 & 0 & 0 \end{array} \right]. \quad (6.151)$$

The associated equations for this subsystem are

$$\dot{x}_2 = A_2 x_2 + B_{w,2} w_2 + B_{u,2} u_2 + B_{p,2} p_2 \quad (6.152)$$

The output equations, in an almost identical manner, are given by

$$z_2 = C_{z,2} x_2 + D_{12,2} u_2 \quad (6.153)$$

$$y_2 = C_{y,2} x_2 + D_{21,2} w_2 \quad (6.154)$$

$$q_1 = C_{q,2} x_2 \quad (6.155)$$

The Controller, K_2 : Finally, the last controller is given by

$$K_2 \sim \left[\begin{array}{c|c} A_{k,2} & B_{k,2} \\ \hline C_{k,2} & D_{k,2} \end{array} \right], \quad (6.156)$$

explicitly:

$$\dot{x}_{k,2} = A_{k,2} x_{k,2} + B_{k,2} u_{k,2} \quad (6.157)$$

$$y_{k,2} = C_{k,2} x_{k,2} + D_{k,2} u_{k,2} \quad (6.158)$$

6.5.2 Collapsing the Systems during Different Stages of the Synthesis Process

The steps, along with the algebra, for putting the systems into a form for loop-at-a-time synthesis are provided here. Figures accompany these operations for clarity. Once the controllers K_1 and K_2 have been synthesized, we will enter an iteration loop, if necessary, until we are satisfied with the closed-loop system's performance.

6.5.3 First Step — No controller for G_1 , Synthesize Controller for G_2

Our first step is to attempt to find a robust controller using μ -synthesis for the situation where G_1 is uncontrolled, where this controller's measurements and performance outputs are spatially-local to the subsystem G_2 .

In order to pose this problem in a form that is amenable to controller synthesis, we must collapse G_1 and K_{coup} into G_2 . The mathematics behind this operation are not complicated, but the algebra is slightly tedious. We will go through some of these derivations for this case now. This case is depicted in figure 29. For this case, there is no controller specific to G_1

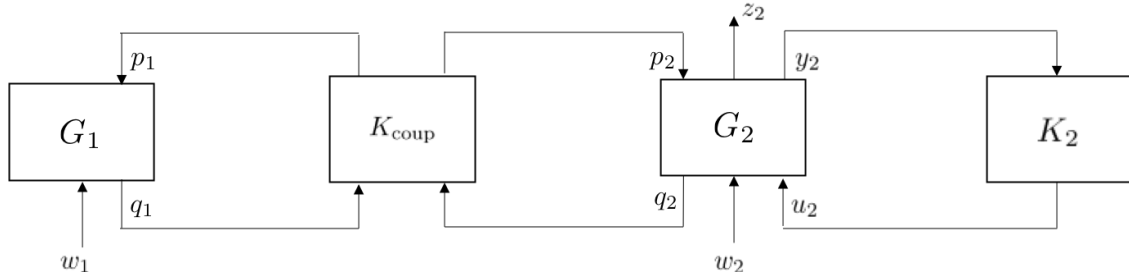


Figure 29: Posing the problem for synthesis of K_2 .

and so the $B_{u,1}$ term of (6.142) is omitted along with (6.144). Similarly, we are no longer interested in the virtual performance output equation given by (6.143). This means that our redefined dynamics for G_1 are

$$\dot{x}_1 = A_1 x_1 + B_{w,1} w_1 + B_{p,1} p_1 \quad (6.159)$$

with the interface stiffness output still given by (6.145). We recall that the interface stiffness coupling is given by equations (6.149) and (6.150). To close the loop, we begin by eliminating the variables q_1, p_1 . If we substitute (6.149) and (6.145) into (6.159) we get

$$\dot{x}_1 = A_1 x_1 + B_{w,1} w_1 + B_{p,1} K_{11} C_{q,1} x_1 + B_{p,1} K_{12} q_2 \quad (6.160)$$

We can also substitute (6.145) into (6.150) to get

$$p_2 = K_{21} C_{q,1} x_1 + K_{22} q_2 \quad (6.161)$$

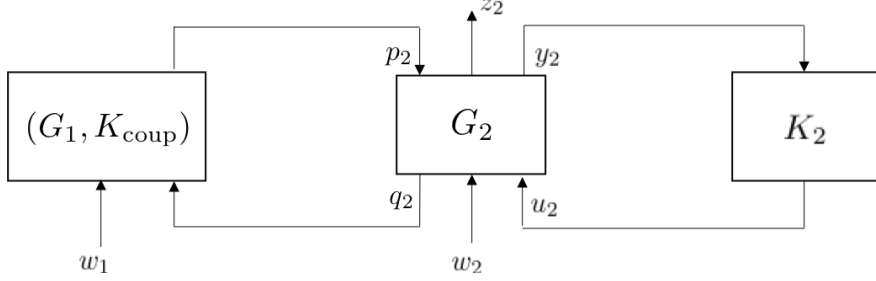


Figure 30: Intermediate step for loop at a time synthesis using μ synthesis via D/K iterations.

and so we see that we have eliminated q_1, p_1 by closing the loop around the pair (G_1, K_{coup}) . We are presently have the system depicted by figure 30. We need to continue this process for the displacement/rotation and force/moment interactions between the interface stiffness element and G_2 , now. To do this, we must similarly eliminate the terms q_2, p_2 .

This is easily accomplished by substituting (6.161) and (6.155) into (6.152), yielding

$$\dot{x}_2 = (A_2 + B_{p,2}K_{22}C_{q,2})x_2 + B_{w,2}w_2 + B_{u,2}u_2 + B_{p,2}K_{21}C_{q,1}x_1. \quad (6.162)$$

We recall that (6.160) still has a q_2 term. Substituting (6.155) into (6.160) gives us

$$\dot{x}_1 = (A_1 + B_{p,1}K_{11}C_{q,1})x_1 + B_{w,1}w_1 + B_{p,1}K_{12}C_{q,2}x_2. \quad (6.163)$$

Our resulting system is now depicted by figure 31. Note that the connections for y_2 and u_2 are still open — the controller K_2 is not yet included in our closed-loop equations. The controller is included in these figures to indicate it's presence as we move toward formulating the open-loop system around this controller. We can now aggregate our system in terms of exogenous inputs and outputs. That is, inputs $[w_1 \ w_2 \ u_2]^T$ and outputs $[z_2 \ y_2]^T$.

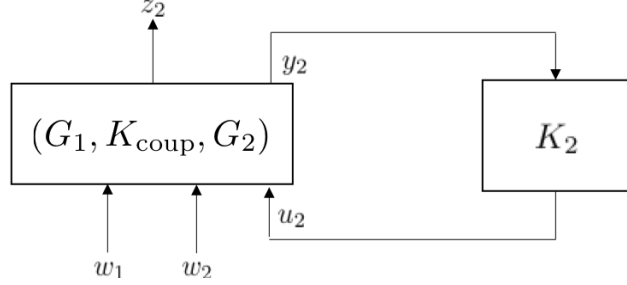


Figure 31: Stage in formulating system for μ -synthesis via D/K iterations.

Defining $G_3 \doteq (G_1, K_{\text{coup}}, G_2)$, our system has the representation

$$G_3 \sim \left[\begin{array}{cc|ccc} A_1 + B_{p,1}K_{11}C_{q,1} & B_{p,1}K_{12}C_{q,2} & B_{w,1} & 0 & 0 \\ B_{p,2}K_{21}C_{q,1} & A_2 + B_{p,2}K_{22}C_{q,2} & 0 & B_{w,2} & B_{u,2} \\ \hline 0 & C_{z,2} & 0 & 0 & D_{12,2} \\ 0 & C_{y,2} & 0 & D_{21,2} & 0 \end{array} \right]. \quad (6.164)$$

We note that this derivation was performed for the nominal case. There is uncertainty in the elements contained within the coupling stiffness interface previously given by \mathbf{K} . Thus, and for the first step of μ -synthesis, we can isolate the uncertain terms in our system and cast this uncertain generalized regulator problem into the familiar form shown in figure 32. Control synthesis is then performed around this structure using μ -synthesis via D/K iterations.

Assuming a robust controller was found, we now have our K_2 . The K_2 assumes the form given by the equations (6.157) and (6.158). Depending upon controller order, we either perform a balanced reduction of the controller or proceed with closing the loop in the opposite direction for pursuing synthesis of K_1 . In this thesis, the model order was retained since model reduction inevitably leads to decreased robustness and performance [17]. Concurrently, we want to develop techniques that are applicable for high-order systems.

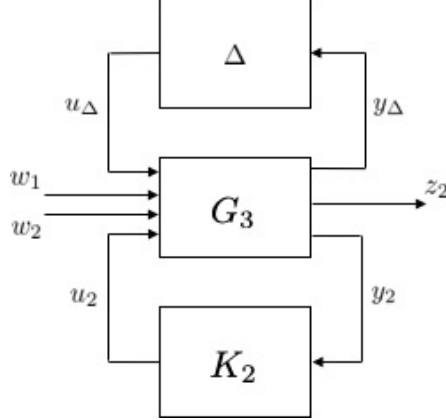


Figure 32: Uncertain generalized regulator structure for G_3 .

6.5.4 Second Step — Controller Exists for G_2 , Synthesize Controller for G_1

At this step, we begin by formulating the controlled subsystem (G_2, K_2) . This amounts to finding the lower linear fractional transformation that maps the interconnection input p_2 to the interconnection output q_2 (see [17] for a review of LFTs). This is essentially what we are doing, repeatedly, as we converge toward a collapsed version of the system for performing loop-at-a-time synthesis. Nevertheless, we go through the algebra, here. We stress that the definition and frequency scaling of the performance output matrix $C_{z,1}$ includes the closed loop dynamics of the adjoining substructure. Although construction of this performance output matrix is derived from the displacement and velocity measurements on substructure #1, we are calculating the eigenvectors of the entire closed loop system, and are frequency scaling across the bandwidth of the entire structure, when constructing this $C_{z,1}$.

Recalling the K_2 equations given by (6.157) and (6.158), we see that

$$y_{k,2} = u_2 \quad (6.165)$$

$$u_{k,2} = y_2. \quad (6.166)$$

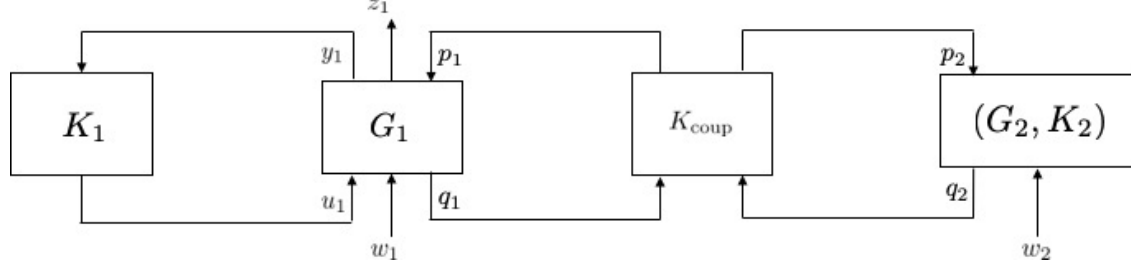


Figure 33: Another stage in loop at a time synthesis process.

To close the loop, we seek to eliminate u_2 and y_2 from our G_2 system equations. By substituting (6.154) into (6.157) and (6.158) we get

$$\dot{x}_{k,2} = A_{k,2}x_{k,2} + B_{k,2}C_{y,2}x_2 + B_{k,2}D_{21,2}w_2 \quad (6.167)$$

$$y_{k,2} = C_{k,2}x_{k,2} + D_{k,2}C_{y,2}x_2 + D_{k,2}D_{21,2}w_2. \quad (6.168)$$

We then substitute (6.168) into (6.152) to get:

$$\dot{x}_2 = (A_2 + B_{u,2}D_{k,2}C_{y,2})x_2 + B_{u,2}C_{k,2}x_{k,2} + (B_{w,2} + B_{u,2}D_{k,2}D_{21,2})w_2 + B_{p,2}p_2 \quad (6.169)$$

which is accompanied by (6.167) and the interface output equation given by (6.155). Our (G_2, K_2) , system is realized by the transfer function matrix

$$(G_2, K_2) \sim \left[\begin{array}{cc|cc} A_2 + B_{u,2}D_{k,2}C_{y,2} & B_{u,2}C_{k,2} & B_{w,2} + B_{u,2}D_{k,2}D_{21,2} & B_{p,2} \\ B_{k,2}C_{y,2} & A_{k,2} & B_{k,2}D_{21,2} & 0 \\ \hline C_{q,2} & 0 & 0 & 0 \end{array} \right] \quad (6.170)$$

where our exogenous inputs are given by $\begin{bmatrix} w_2 & p_2 \end{bmatrix}^T$ and outputs is q_2 . Clearly, our augmented state vector is $\begin{bmatrix} x_2 & x_{k,2} \end{bmatrix}^T$. This system is depicted on the far right in figure 33. We recall that the static interconnection stiffness coupling is described by (6.149) and (6.150). To close the loop on K_{coup} , we want to eliminate p_2 and q_2 . To achieve this end, we first insert (6.155) into (6.150) to get

$$p_2 = K_{21}q_1 + K_{22}C_{q,2}x_2 \quad (6.171)$$

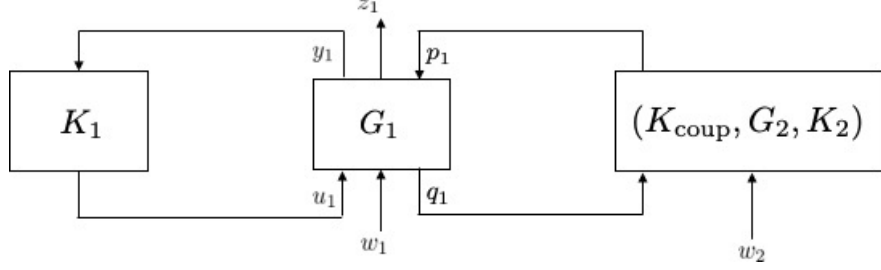


Figure 34: Intermediate closed loop system.

and then insert (6.171) into (6.169) to get

$$\dot{x}_2 = (A_2 + B_{u,2}D_{k,2}C_{y,2} + B_{p,2}K_{22}C_{q,2})x_2 + B_{u,2}C_{k,2}x_{k,2} + (B_{w,2} + B_{u,2}D_{k,2}D_{21,2})w_2 + B_{p,2}K_{21}q_1. \quad (6.172)$$

Inserting (6.155) into (6.149) we get

$$p_1 = K_{11}q_1 + K_{12}C_{q,2}x_2 \quad (6.173)$$

meaning that at this intermediate step we now have

$$\begin{aligned} \dot{x}_2 &= (A_2 + B_{u,2}D_{k,2}C_{y,2} + B_{p,2}K_{22}C_{q,2})x_2 + B_{u,2}C_{k,2}x_{k,2} + (B_{w,2} + B_{u,2}D_{k,2}D_{21,2})w_2 \\ &\quad + B_{p,2}K_{21}q_1 \end{aligned} \quad (6.174)$$

$$\dot{x}_{k,2} = A_{k,2}x_{k,2} + B_{k,2}C_{y,2}x_2 + B_{k,2}D_{21,2}w_2 \quad (6.175)$$

$$p_1 = K_{11}q_1 + K_{12}C_{q,2}x_2 \quad (6.176)$$

which are given by equations (6.172), (6.167), and (6.173), respectively. This system is depicted on the far right in figure 34. Finally, we want to close the loop between G_1 and $(K_{\text{coup}}, G_2, K_2)$. To do this, we want to eliminate p_1 and q_1 .

Recall the system equations given by (6.142), (6.143), (6.144), and (6.145). Since we want to eliminate p_1 and q_1 , we systematically approach this similar to previous. First, we

insert (6.145) into (6.173) to get

$$p_1 = K_{11}C_{q,1}x_1 + K_{12}C_{q,2}x_2. \quad (6.177)$$

We then insert (6.177) into (6.142) and (6.145) into (6.172) to get

$$\begin{aligned} \dot{x}_2 &= (A_2 + B_{u,2}D_{k,2}C_{y,2} + B_{p,2}K_{22}C_{q,2})x_2 + B_{u,2}C_{k,2}x_{k,2} + (B_{w,2} + B_{u,2}D_{k,2}D_{21,2})w_2 \\ &\quad + B_{p,2}K_{21}C_{q,1}x_1 \end{aligned} \quad (6.178)$$

$$\dot{x}_1 = (A_1 + B_{p,1}K_{11}C_{q,1})x_1 + K_{12}C_{q,2}x_2 + B_{w,1}w_1 + B_{u,1}u_1 \quad (6.179)$$

We can aggregate (6.179), (6.178), (6.167), (6.143), and (6.144) as our closed-loop system:

$$\dot{x}_1 = (A_1 + B_{p,1}K_{11}C_{q,1})x_1 + B_{p,1}K_{12}C_{q,2}x_2 + B_{w,1}w_1 + B_{u,1}u_1 \quad (6.180)$$

$$\begin{aligned} \dot{x}_2 &= (A_2 + B_{u,2}D_{k,2}C_{y,2} + B_{p,2}K_{22}C_{q,2})x_2 + B_{u,2}C_{k,2}x_{k,2} + (B_{w,2} + B_{u,2}D_{k,2}D_{21,2})w_2 \\ &\quad + B_{p,2}K_{21}C_{q,1}x_1 \end{aligned} \quad (6.181)$$

$$\dot{x}_{k,2} = A_{k,2}x_{k,2} + B_{k,2}C_{y,2}x_2 + B_{k,2}D_{21,2}w_2 \quad (6.182)$$

$$z_1 = C_{z,1}x_1 + D_{12,1}u_1 \quad (6.183)$$

$$y_1 = C_{y,1}x_1 + D_{21,1}w_1. \quad (6.184)$$

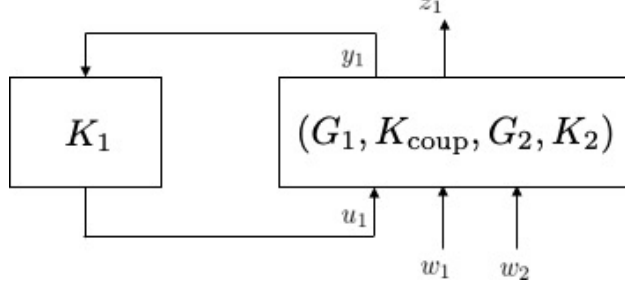


Figure 35: Intermediate collapsed subsystem.

This collapsed system is shown in figure 35. Calling $G_4 \doteq (G_1, K_{\text{coup}}, G_2, K_2)$, we have the transfer matrix representation

$$G_4 \sim \left[\begin{array}{c|c} A_4 & B_4 \\ \hline C_4 & D_4 \end{array} \right] \quad (6.185)$$

where

$$A_4 = \begin{bmatrix} A_1 + B_{p,1}K_{11}C_{q,1} & B_{p,1}K_{12}C_{q,2} & 0 \\ B_{p,2}K_{21}C_{q,1} & A_2 + B_{u,2}D_{k,2}C_{y,2} + B_{p,2}K_{22}C_{q,2} & B_{u,2}C_{k,2} \\ 0 & B_{k,2}C_{y,2} & A_{k,2} \end{bmatrix}, \quad (6.186)$$

$$B_4 = \begin{bmatrix} B_{w,1} & B_{u,1} & 0 \\ 0 & 0 & B_{w,2} + B_{u,2}D_{k,2}D_{21,2} \\ 0 & 0 & B_{k,2}D_{21,2} \end{bmatrix}, \quad (6.187)$$

$$C_4 = \begin{bmatrix} C_{z,1} & 0 & 0 \\ C_{y,1} & 0 & 0 \end{bmatrix}, \quad D_4 = \begin{bmatrix} 0 & D_{12,1} & 0 \\ D_{21,1} & 0 & 0 \end{bmatrix}, \quad (6.188)$$

with the exogenous inputs $[w_1 \ u_1 \ w_2]^T$ and outputs $[z_1 \ y_1]^T$. We note that the uncertain interconnection terms are embedded as affine terms within the G_4 dynamics matrix — meaning that these parametrically uncertain terms can be easily extracted during controller synthesis. It is around this system — the mapping from $[w_1 \ w_2]^T$ to z_1 that we try to synthesize a robust controller around using μ -synthesis via D/K iterations.

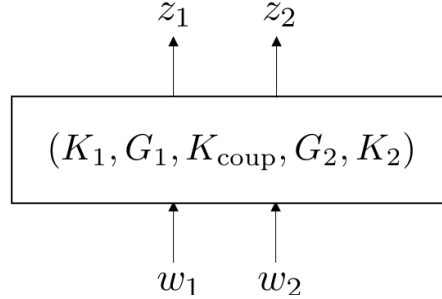


Figure 36: The controlled global system.

6.5.5 Third Step — Controllers Exist for G_1, G_2 ; Performance Verification

Under the presumption that we find a K_1 that is robust against this parametric interconnection uncertainty, which exists in the presence of the controlled substructure pair (G_2, K_2) , we want to formulate the composite closed loop system. The derivation for the closed loop systems, with controllers included, can be inferred from the steps that we have followed through with previously. Therefore, we will provide the resulting system, which we will call G_{global} . G_{global} is depicted in figure 36, where we see that for the performance verification step, we are interested in the $\begin{bmatrix} w_1 & w_2 \end{bmatrix}^T \rightarrow \begin{bmatrix} z_1 & z_2 \end{bmatrix}^T$ mapping. Recall from chapter 4 that the D_{12} and D_{21} terms meet certain properties. To do this, measurement disturbance inputs were defined and appended to the measurement equations (y_i 's) and additional actuator performance output functions were appended, thus adding rows to the C_1 matrices and creating a nonzero performance feedforward matrix D_{12} . These modeling choices were made more for synthesis purposes. However, an additional benefit to appending these terms, especially with respect to the D_{12} matrices which enter as feedforward terms in the performance output equations, is that we are given an additional knob to turn during synthesis. Generally, the performance output equations are defined as:

$$z = \begin{bmatrix} C_2 \Phi W_z \Phi^{-1} \\ 0 \end{bmatrix} x + r_z \begin{bmatrix} 0 \\ I \end{bmatrix} u \quad (6.189)$$

where r_z is chosen to be a small positive scalar. By choosing r_z to be larger, we are both penalizing excess control and preventing actuator singularities at high frequencies from occurring during \mathcal{H}_∞ controller synthesis. Similarly,

$$y = C_2 x + r_y \begin{bmatrix} 0 & I \end{bmatrix} w \quad (6.190)$$

where r_y is chosen to be a small positive scalar and the size of I is equal to the number of sensor measurements being made (which is two for each substructure). For every instance of D/K iteration, $r_y = 10^{-5}$. Thus, we have presumed that we have accurate sensor measurements.

For analysis of the resulting controllers that were obtained through the loop-at-a-time μ -synthesis we are principally interested in how the disturbance inputs to the system affect the displacements and velocities, at low frequencies, at the measurement locations. Thus, we eliminate the augmented terms in the z -equations by setting each D_{12} term to zero. Furthermore, we are also now considering the unweighted version of the system. The modal-magnitude scaling used on the performance output matrices C_1 , as covered in chapter 4, is removed, and we are just examining the unfiltered displacements and velocities at measurement locations. Thus, the maximum singular value plots are generated for the following system:

$$G_{\text{global}} \sim \left[\begin{array}{c|c} A_{\text{global}} & B_{\text{global}} \\ \hline C_{\text{global}} & D_{\text{global}} \end{array} \right] \quad (6.191)$$

where the input, output, and state vectors are given by

$$u = \begin{bmatrix} w_1 \\ w_2 \end{bmatrix}, \quad y = \begin{bmatrix} z_1 \\ z_2 \end{bmatrix}, \quad x = \begin{bmatrix} x_1 \\ x_2 \\ \vdots \\ x_{k,1} \\ x_{k,2} \end{bmatrix}. \quad (6.192)$$

Thus, we have

$$A_{\text{global}} = \begin{bmatrix} A_1 + B_{u,1}D_{k,1}C_{y,1} + B_{p,1}K_{11}C_{q,1} & B_{p,1}K_{12}C_{q,2} & B_{u,1}C_{k,1} & 0 \\ B_{p,2}K_{21}C_{q,1} & A_2 + B_{u,2}D_{k,2}C_{y,2} + B_{p,2}K_{22}C_{q,2} & 0 & B_{u,2}C_{k,2} \\ B_{k,1}C_{y,1} & 0 & A_{k,1} & 0 \\ 0 & B_{k,2}C_{y,2} & 0 & A_{k,2} \end{bmatrix} \quad (6.193)$$

$$B_{\text{global}} = \begin{bmatrix} B_{w,1} + B_{u,1}D_{k,1}D_{21,1} & 0 \\ 0 & B_{w,2} + B_{u,2}D_{k,2}D_{21,2} \\ B_{k,1}D_{21,1} & 0 \\ 0 & B_{k,2}D_{21,2} \end{bmatrix} \quad (6.194)$$

$$C_{\text{global}} = \begin{bmatrix} C_{z,1} + D_{12,1}D_{k,1}C_{y,1} & 0 & D_{12,1}C_{k,1} & 0 \\ 0 & C_{z,2} + D_{12,2}D_{k,2}C_{y,2} & 0 & D_{12,2}C_{k,2} \end{bmatrix} \quad (6.195)$$

$$D_{\text{global}} = \begin{bmatrix} D_{12,1}D_{k,1}D_{21,1} & 0 \\ 0 & D_{12,2}D_{k,2}D_{21,2} \end{bmatrix}. \quad (6.196)$$

6.5.6 Fourth Step — Iterative Controller Synthesis

The fourth step in loop-at-a-time μ -synthesis via D/K iterations is invoked if we find that a controller K_1 does not exist, or if we are not at all satisfied with how the robust, closed-loop system is performing within our bandwidth of interest. If this is the case, we essentially reverse the process derived in section 6.5.4. Otherwise, we proceed with candidate controller solutions to be used for probabilistic-robust decentralized \mathcal{H}_∞ controller synthesis. These acceptable controllers are robust decentralized controllers that were synthesized using loop-at-a-time μ -synthesis/ D/K iterations. These robust controllers will serve as a starting

points for our search for a probabilistically-robust controllers. That is, we will now incorporate random uncertainty into this problem and pursue stochastic optimization to find probabilistically-robust decentralized \mathcal{H}_∞ controllers.

6.5.7 Loop-at-a-Time μ -synthesis via D/K Iterations Algorithm

We will now cover how loop-at-a-time μ -synthesis via D/K iterations is executed. This procedure is described in algorithm 3. Note that it does not really matter which controller we initiate with. The derivations provided in this thesis are specific to starting with $K_1 = 0$, and attempting to first synthesize K_2 . We easily could have starting by attempting to synthesize K_1 , first, without any loss in generality. In line with several other chapters in this thesis, we provide the following algorithm.

Algorithm 3 Loop at a Time μ -synthesis via D/K Iterations

1: **procedure** LOOP AT A TIME μ -SYNTHESIS VIA D/K ITERATIONS

- 2: Form the open-loop system given by G_3 , given by (6.164), as we prepare to design and synthesize controller K_2 , with

$$G_3 \sim \left[\begin{array}{c|c} A_3 & B_3 \\ \hline C_3 & D_3 \end{array} \right]$$

- 3: Calculate $A_3\Phi_3 = \Phi_3\Lambda_3$

- 4: Form $C_{z,1} = C_{y,1}\Phi_3 W_z \Phi_3^{-1}$, as performed in chapter 4, through construction of the diagonal F_z which represents the magnitude of a first-order filter function with cutoff frequency of 500 rad/s at each A_3 system resonance. This magnitude scaling is performed for the nominal plant in the uncertainty set. That is, for an interconnection stiffness modulus $E_0 = 200$ GPa.

- 5: Ensure that norm-bounded interconnection uncertainty is appropriately captured in the model, and attempt to synthesize a controller using μ -synthesis via D/K iterations.

- 6: Assuming a controller K_2 was found, form system G_4 , given by (6.185), so that we can prepare to synthesize controller K_1 , with

$$G_4 \sim \left[\begin{array}{c|c} A_4 & B_4 \\ \hline C_4 & D_4 \end{array} \right]$$

- 7: Calculate $A_4\Phi_4 = \Phi_4\Lambda_4$

- 8: Form $C_{z,2} = C_{y,2}\Phi_4 W_z \Phi_4^{-1}$, as performed in chapter 4 and using the same first-order filter for magnitude scaling. Notice that magnitude scaling accounts for the closed-loop substructure dynamics, as well. This magnitude scaling is performed for the nominal plant in the uncertainty set. That is, for an interconnection stiffness modulus $E_0 = 200$ GPa.

- 9: Ensure that norm-bounded interconnection uncertainty is appropriately captured in the model, and attempt to synthesize a controller using μ -synthesis via D/K iterations.
-

10: Assuming K_1 and K_2 exist, form the composite system for performance analysis.

This composite system is given by G_{global} in (6.191),

$$G_{\text{global}} \sim \left[\begin{array}{c|c} A_{\text{global}} & B_{\text{global}} \\ \hline C_{\text{global}} & D_{\text{global}} \end{array} \right]$$

11: Define a frequency grid $\omega = [0, \omega_{\max}]$ and calculate instances of the curve

$$f(\omega) = \bar{\sigma}(G_{\text{global}})$$

which is a plot of the maximum singular value of the G_{global} mapping. Instances are plants drawn from the norm-bounded uncertainty set.

12: **if** K_1 and K_2 are robust (e.g. with SSV < 1) and perform relatively well within the bandwidth of interest, **then**

13: Proceed to use these candidate solutions as starting points in the stochastic optimization problem developed in chapter 7.

14: **else**

15: Set $K_2 = 0$ and perform this procedure again, forming the appropriate system for synthesis of a new K_2 with K_1 held constant.

16: **end if**

17: **end procedure**

6.6 UNCERTAIN MAXIMUM SINGULAR VALUE PLOTS OF μ -SYNTHESIZED SEED SOLUTIONS

Eight candidate decentralized controller pairs were synthesized using loop-at-a-time μ -synthesis via D/K iterations. After synthesis of K_1 , formulation of the loop equations for design and synthesis of K_2 , and synthesis of K_2 , it was judged that the collection of controllers obtained through this synthesis process would be adequate for pursuing the stochastic optimization problem in chapter 7 with all candidate solutions. Therefore, subsequent loop iterations were not needed. All of these controllers share a common quality: they are all robust against some amount of structured norm-bounded uncertainty. As discussed in section 6.4, \mathcal{H}_∞ -norm minimization, using an approach such as a bisection method, is pursued after the D -scalings iteration, meaning that the robust performance *levels* of all of these controllers are different. What we are looking for are controllers that are robust and attenuate low frequency modes in our system. (As an aside: this thesis is about developing an approach, and not finding the optimal way to control Euler-Bernoulli beams). We want to exploit the sub-optimality and conservatism inherent to μ -synthesis via D/K iterations by exploring the random solution spaces in the vicinity of these controllers to achieve the end goal of this research.

The seed population of controllers was generated by using the two norm-bound uncertainty descriptions from previous, and by varying the magnitude of the scaling coefficient, r_z . Definition of the performance output matrices, along with all other model parameters, were the same. When these controllers were synthesized, we started with synthesizing K_1 first, and then iterating to synthesize K_2 ; this explains why the order of K_2 is greater than the order of K_1 . Some relevant data about the seed populations are provided in table 1. From this seed data, we will feature the performance, in terms of uncertain maximum singular value plots of the open and closed-loop systems, for Controller Pairs 2 and 7. It will be highlighted in chapter 7 that these seeds gave rise to probabilistic robust solutions that did very well with respect to the cost function and associated optimization problem that was posed. Simultaneously, we must recognize that each of these controller pairs resulted

Table 1: Initial Controller Population Resulting from μ -Synthesis

Initial Population Seed Data for Genetic Algorithm						
Controller Pair	E_Δ	r_z	SSV	K_1 order	K_2 order	Worst-Case γ
1	[0.01E, 2E]	10^{-2}	0.9899	100	200	-45.68 dB
2	[0.01E, 2E]	10^{-2}	0.9899	100	248	-45.35 dB
3	[0.01E, 2E]	10^{-3}	0.9900	100	200	-46.02 dB
4	[0.01E, 2E]	10^{-3}	0.1954	100	248	-40.72 dB
5	[0.01E, 2E]	10^{-3}	0.9556	100	228	-40.10 dB
6	[0.05E, 1.5E]	10^{-2}	0.9655	148	248	-45.68 dB
7	[0.05E, 1.5E]	10^{-2}	0.9655	148	296	-45.68 dB
8	[0.05E, 1.5E]	10^{-2}	0.9655	148	296	-44.88 dB

from, and were robust against, different levels of structured norm-bounded uncertainty. The uncertain open and closed loop maximum singular value plots for Controller Pair #2 are shown in figure 37. A similar plot for Controller Pair #7 is shown in figure 38. We see that the combined order of the controller pair #2 is 348. The order of the controller pair #7 is 444. In control theory, these are considered to be high-order systems.

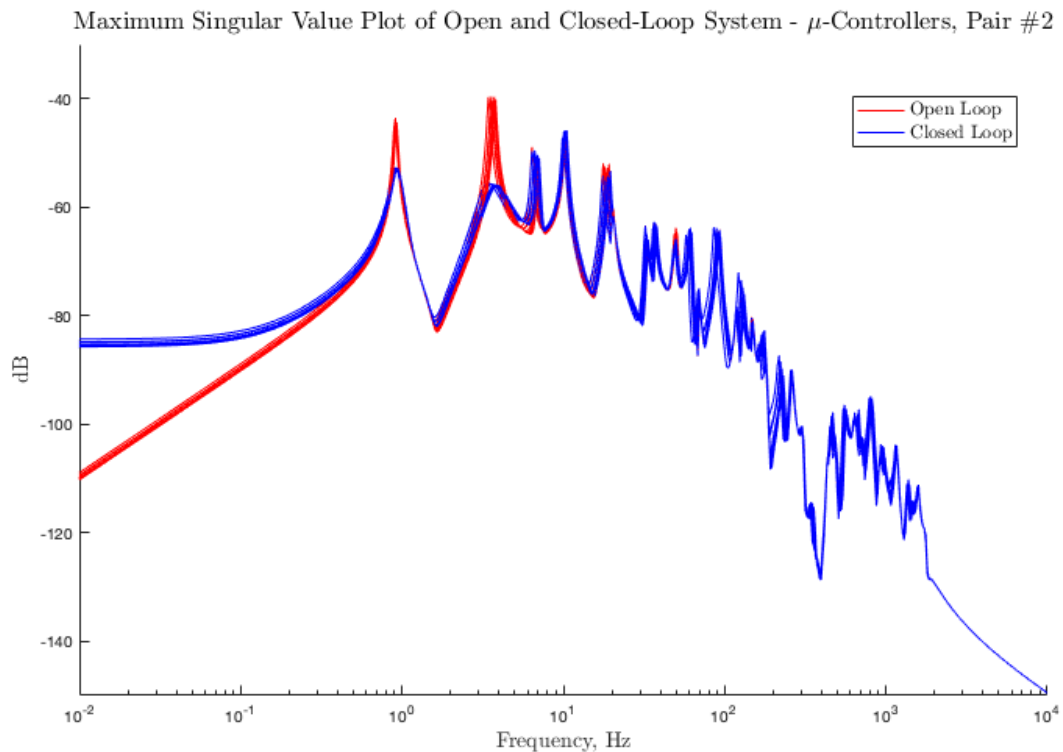


Figure 37: Uncertain maximum singular value plot of open loop system and closed loop system for Controller Pair #2, synthesized with norm-bounded interconnection uncertainty $E_{\Delta,1} \in [0.01E_0, 2E_0]$.

Maximum Singular Value Plot of Open and Closed-Loop System - μ -Controllers, Pair #7

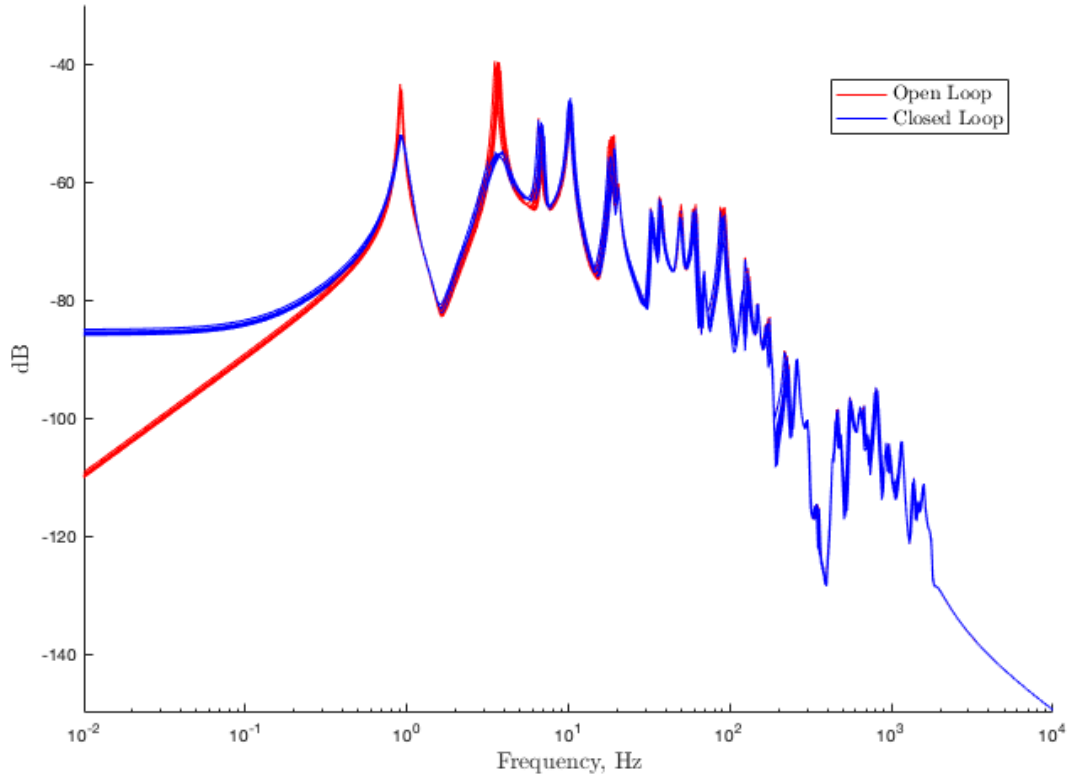


Figure 38: Uncertain maximum singular value plot of open loop system and closed loop system for Controller Pair #7, synthesized with norm-bounded interconnection uncertainty $E_{\Delta,2} \in [0.05E_0, 1.5E_0]$.

7.0 PROBABILISTIC DECENTRALIZED DYNAMIC OUTPUT FEEDBACK \mathcal{H}_∞ SYNTHESIS

Presently, no techniques exist that allow vibration control engineers to design and synthesize decentralized dynamic output feedback controllers for random systems. In this thesis, the uncertainty is concentrated in the portion of a structure that couples two substructures, which we have termed the interconnection between these substructures. For this chapter, we continue to focus on the structural models that were used in chapter 6, with all of the same model parameters that are detailed in appendix B. The interconnection uncertainty is specific to the modulus of the interconnection element between two Euler-Bernoulli beams, with this random uncertainty characterized by a normal distribution.

Controller design and synthesis for this specific problem has faced several challenges:

1. The scenario approach from chapter 5 cannot be used, since the dynamic output feedback \mathcal{H}_∞ synthesis problem is not jointly convex in the plant and controller variables [14, 63]. We are still contending with random interconnection uncertainty.
2. Lightly-damped structures, and their models, are generally high-dimensional. Even after some model reduction is performed, controller design and synthesis for plants that have several hundred states faces design and computational challenges. No model reduction is performed on the systems used in this chapter.
3. It has been shown in the area of decentralized control that imposing a diagonal (or decentralized) structure on the controllers leads to a reduction in performance [9]. This restriction reduces the solution space.

This chapter develops an approach for synthesizing high-dimensional, probabilistic robust, decentralized, dynamic output feedback controllers for lightly-damped structures that are coupled by a random interconnection element. A collection of μ -synthesized controllers, generated using the loop-at-a-time μ -synthesis procedure in chapter 6, are seeds in the optimization problem solved in this chapter. A cost function is constructed that focuses on searching the solution space for decentralized dynamic output feedback controllers that:

1. Stabilize the random system, and
2. Attenuate the infinity norm of the random system mapping disturbance inputs to performance outputs below some level, γ^* .

We note that the a posteriori performance test for this system still requires evaluating the \mathcal{H}_∞ -norm of the entire structure, as detailed in chapter 4.

A common theme in this thesis, in terms of controller performance objectives, is that we seek to attenuate the excitation of low frequency modes. The full-state feedback controller design and synthesis approach in chapter 5 did this via frequency weighting in modal coordinates. The loop-at-a-time μ -synthesis approach in chapter 6 similarly did this via frequency weighting the performance output function in modal coordinates. We retain the our objective to attenuate low-frequency modes in this present chapter, and will show how it is accomplished by cost function construction and by virtue of the fact that we begin our searches in the vicinity of the μ -synthesized solutions from chapter 6. This chapter is structured as follows:

1. A discussion on stochastic optimization using genetic algorithms, which includes theory and details related to:
 - Genetic algorithm-based optimization;
 - How stochastic optimization problems can be posed, and solved, using genetic algorithms;
 - Probability theory that is useful for constructing the cost functions in stochastic optimization problems involving controller synthesis.
 - Genetic algorithm settings used for the optimization problem posed in this thesis.

2. Probabilistic decentralized dynamic output feedback controller synthesis for structures coupled by a random interconnection element, which includes theory and details related to:
 - Cost function construction, including a discussion on computational cost/complexity and how parallel computing makes these high-dimensional problems tractable.
 - Controller synthesis in complex modal coordinates, which leads to a significant reduction in the optimization variables in this problem.
3. Discussion of the results obtained using this new approach to decentralized controller synthesis. Several probabilistically-robust, decentralized, dynamic output feedback controllers were successfully synthesized that attenuated the \mathcal{H}_∞ -norm of the structure below the prescribed level γ^* with probability greater than the $1 - \epsilon_p$ determined in chapter 4. Two of these solutions are highlighted.

7.1 THE TRANSFER FUNCTION MATRIX AND PERFORMANCE OBJECTIVES

We will briefly discuss the transfer function matrix and performance objectives that motivate the techniques developed in this chapter. Recalling the generalized plant structure shown in figure 28, we reformulate this system with:

$$G_1 \sim \left[\begin{array}{c|ccc} A_1 & B_{w,1} & B_{u,1} & B_{p,1} \\ \hline C_{z,1} & 0 & 0 & 0 \\ C_{y,1} & 0 & 0 & 0 \\ C_{q,1} & 0 & 0 & 0 \end{array} \right], \quad G_2 \sim \left[\begin{array}{c|ccc} A_2 & B_{w,2} & B_{u,2} & B_{p,2} \\ \hline C_{z,2} & 0 & 0 & 0 \\ C_{y,2} & 0 & 0 & 0 \\ C_{q,2} & 0 & 0 & 0 \end{array} \right] \quad (7.1)$$

and random interconnection stiffness matrix:

$$K_{\Delta, \text{coup}} \sim \left[\begin{array}{c|c} 0 & 0 \\ \hline 0 & \mathbf{K}_\Delta \end{array} \right] \quad (7.2)$$

where

$$\mathbf{K}_\Delta = \begin{bmatrix} K_{\Delta,11} & K_{\Delta,12} \\ K_{\Delta,21} & K_{\Delta,22} \end{bmatrix} = - \left(\frac{E_\Delta I}{L^3} \right) \left[\begin{array}{cc|cc} 12 & 6L & -12 & 6L \\ * & 4L^2 & -6L & 2L^2 \\ \hline * & * & 12 & -6L \\ * & * & * & 4L^2 \end{array} \right], \quad E_\Delta \sim \mathcal{N}(E_0, 0.16E_0^2) \quad (7.3)$$

with $E_0 = 200$ GPa. The controllers still have the structure:

$$K_1 \sim \left[\begin{array}{c|c} A_{k,1} & B_{k,1} \\ C_{k,1} & D_{k,1} \end{array} \right], \quad K_2 \sim \left[\begin{array}{c|c} A_{k,2} & B_{k,2} \\ C_{k,2} & D_{k,2} \end{array} \right]. \quad (7.4)$$

We form the mapping

$$\begin{bmatrix} w_1 \\ w_2 \end{bmatrix} \rightarrow \begin{bmatrix} z_1 \\ z_2 \end{bmatrix} \quad (7.5)$$

which we call

$$G_{\text{prob}} \sim \left[\begin{array}{c|c} A_{\text{prob}} & B_{\text{prob}} \\ C_{\text{prob}} & D_{\text{prob}} \end{array} \right] \quad (7.6)$$

where the input, output, and state vectors are given by

$$w = \begin{bmatrix} w_1 \\ w_2 \end{bmatrix}, \quad z = \begin{bmatrix} z_1 \\ z_2 \end{bmatrix}, \quad x = \begin{bmatrix} x_1 \\ x_2 \\ \vdots \\ x_{k,1} \\ x_{k,2} \end{bmatrix}. \quad (7.7)$$

Thus, we have

$$A_{\text{prob}} = \begin{bmatrix} A_1 + B_{u,1}D_{k,1}C_{y,1} + B_{p,1}K_{\Delta,11}C_{q,1} & B_{p,1}K_{\Delta,12}C_{q,2} & B_{u,1}C_{k,1} & 0 \\ B_{p,2}K_{\Delta,21}C_{q,1} & A_2 + B_{u,2}D_{k,2}C_{y,2} + B_{p,2}K_{\Delta,22}C_{q,2} & 0 & B_{u,2}C_{k,2} \\ B_{k,1}C_{y,1} & 0 & A_{k,1} & 0 \\ 0 & B_{k,2}C_{y,2} & 0 & A_{k,2} \end{bmatrix}, \quad (7.8)$$

$$B_{\text{prob}} = \begin{bmatrix} B_{w,1} & 0 \\ 0 & B_{w,2} \\ 0 & 0 \\ 0 & 0 \end{bmatrix}, \quad C_{\text{prob}} = \begin{bmatrix} C_{z,1} & 0 & 0 & 0 \\ 0 & C_{z,2} & 0 & 0 \end{bmatrix}, \quad D_{\text{prob}} = \begin{bmatrix} 0 & 0 \\ 0 & 0 \end{bmatrix}.$$

In chapter 4, we declared that the stability and performance tests, with probabilistic metrics, were: The performance test was given by (4.50), which can now be written as:

$$P_{\text{test}} \doteq \hat{\Pr} \left(\|G_{\text{prob}}\|_{\infty} \leq \gamma^* \mid \mathbf{K}_{\Delta} \right) \geq 1 - \epsilon_p \quad (7.9)$$

where we chose $\gamma^* = -45.4$ dB and $\epsilon_p = 0.05$. The stability test is given by:

$$S_{\text{test}} \doteq \hat{\Pr} \left(\operatorname{Re}(\lambda(A_{\text{prob}})) < 0 \mid \mathbf{K}_{\Delta} \right) \geq 1 - \epsilon_s \quad (7.10)$$

where we chose $\epsilon_s = 0.02$.

7.2 STOCHASTIC OPTIMIZATION USING GENETIC ALGORITHMS

Genetic algorithms (GAs) are search methods based on principles of natural selection and genetics [78, 18]. Genetic algorithms repeatedly modify a population of individual solutions to an optimization problem through the processes of: evaluation, selection, recombination, mutation, and replacement.

New populations of individual candidate solutions are formed through these processes, as the populations evolve toward an optimal solution. Much of the terminology used in the genetic algorithm literature is derived from the Darwinian process of natural selection, however, these algorithms actually employ randomized adaptive search methods capable of processing a large number of candidate solutions at each step [18]. The best candidate solutions are carried over, combined with one another, and mutated to form subsequent populations.

The fact that we have a population of candidate solutions, each of which is evaluated against the same cost function, makes this approach amenable to parallelization. This fact allows us to address computational complexity associated with problems that have the following features: 1) have many decision variables, and/or 2) have computationally-expensive cost functions. This chapter is addressing a controller synthesis problem that has both of these qualities. For the techniques developed in this chapter, the number of controller

variables can be between approximately 50,000 and 120,000 variables, however, through a change in controller basis we develop an approach that drops this range to between 1,200 and 1,800 variables. The former case would have been intractable using the computing resources presently available during the writing of this thesis.

7.2.1 Steps in Genetic Algorithm-based Optimization

Previously, we said that genetic algorithms repeatedly modify a population of individual solutions to an optimization problem through the processes of evaluation, selection, recombination, mutation, and replacement. These steps will be explained a bit more:

1. *Initialization* — The initial population of candidate solutions is generated by creating random candidate controller solutions around each given seed controller.
2. *Evaluation* — Once this initial population has been created, each candidate solution is evaluated against the fitness/objective function that is constructed for the problem.
3. *Selection* — Those candidate solutions with higher fitness values are copied more frequently than those with lower values. First, each candidate solution is ranked and arranged from highest to lowest. Then, the raw objective functions are scaled according to their rank. So, an individual with rank r has its objective function values scaled by $1/\sqrt{r}$. This makes poorly ranked solutions more equal in value. Then, a stochastic uniform selection function is invoked, which lays out a line on which each individual corresponds to a section of the line, with length proportional to its scaled value. The algorithm moves along this line in steps of equal size, allocating an individual to retain and use for crossover and mutation. Simultaneously, a subset of these individuals with the highest objective function values are identified as elite individuals, and are guaranteed to survive into the next population.

4. *Recombination* — Combines two or more parts of “parental” solutions to create new solutions, many times referred to as “offspring”. Recombination is also referred to as crossover. An algorithm known as scattered crossover is used at this step [79]. This step works by generating a random binary vector that is used to swap elements of the parent solutions with one another. As an example, given parents p_1 and p_2 , with random binary vector b , we have:

$$\begin{aligned} p_1 &= \begin{bmatrix} a & b & c & d & e & f & g & h \end{bmatrix} \\ p_2 &= \begin{bmatrix} 1 & 2 & 3 & 4 & 5 & 6 & 7 & 8 \end{bmatrix} \\ b &= \begin{bmatrix} 1 & 0 & 0 & 0 & 1 & 0 & 0 & 0 \end{bmatrix}, \end{aligned}$$

resulting in a child c , that becomes a member of the next population:

$$c = \begin{bmatrix} a & 2 & 3 & 4 & e & 6 & 7 & 8 \end{bmatrix}.$$

5. *Mutation* — While recombination is combining two or more parent solutions to create subsequent generations of candidate solutions, mutation randomly modifies parts of solutions during each generation. This process promotes a more thorough investigation into the solution space [18]. A gaussian mutation algorithm is used at this step. For a given candidate solution that is selected for mutation, random elements are chosen similarly to the recombination step, and zero-mean random numbers are added to these elements, whose standard deviation is determined by:

$$\sigma_k = \sigma_{k-1} \left(1 - S \frac{k}{N_g} \right) \quad (7.11)$$

where k represents the generation that we are currently in, and N_g is the total number of generations that we direct the algorithm to run. The initial standard deviation is set to be equal to the range of the initial population — the difference between the largest and smallest elements of all candidate solutions. We have set $S = 1$, meaning that this standard deviation decreases to zero as $k \rightarrow N_g$.

6. *Replacement* — Solutions created by selection, recombination, and mutation replaces the previous candidate solutions, leading to the formation of the subsequent population.

7. Repeat steps 2-6 until a terminating condition is met.

Genetic algorithms have been used in artificial intelligence, machine learning, and control theory for decades. Some control applications can be found in the papers by Fleming, Garrison, and Wang [80, 12, 37, 39]. Attempting to list all of the research that has used these tools would be futile. Moreover, additional details behind these algorithms and their variants can be found in the book by Goldberg [18].

7.2.2 Stochastic Cost Functions and Genetic Algorithms

We will briefly now discuss probabilistic robust controller design and synthesis, as approached originally by Stengel, Garrison, and Wang [30, 12, 31, 37, 32]. These techniques were introduced in chapter 2. The design of a probabilistic robust controller was approached by Garrison in the following way: probabilistic robust control can characterize compensator robustness by defining a probability, $\Pr(p)$, that the closed-loop system will have acceptable performance in the presence of parameter uncertainties. This probability, $\Pr(p)$, is defined to be:

$$\Pr(p) = \int_V \mathbb{I}[G(v), K] \Pr(v) dv \quad (7.12)$$

where G is the plant, K is some candidate controller, V is the space of possible parameter variations, $v \in V$ is a point in V , and $\Pr(v)$ is the probability density function over the parameter variations. $\mathbb{I}[\cdot]$ is the binary indicator function that equals 1 if $G(v)$ and K form an acceptable system and 0 if not. The formation of an acceptable system configuration corresponds to the event p occurring.

A stochastic optimization problem is formulated by defining a cost function, J ,

$$J = f\left(\Pr(p_1), \dots, \Pr(p_n)\right), \quad j = 1 \dots n \quad (7.13)$$

where each element describes the probability that a given plant-controller pair meets some metric of importance to the designer. A search over compensator configurations $K(d)$, where the compensators are parameterized by some vector $d \in D$, with $D \subseteq \mathbb{R}^{n_d}$ is pursued along with an evaluation of the cost function $J(K(d)) = f\left(\Pr_d(p_1), \dots, \Pr_d(p_n)\right)$, $j = 1 \dots n$

allows for us to find the best compensator for our parametrically-uncertain plant. Each $\Pr_d(p_j)$ arises from:

$$\Pr_d(p_j) = \int_V \mathbb{I}_j[G(v), K(d)] \Pr(v) dv \quad (7.14)$$

which can be evaluated using Monte Carlo techniques, turning this integral into the following summation to get an estimate of the integral's value as:

$$\hat{\Pr}_d(p_j) = \frac{1}{N} \sum_{m=1}^N \mathbb{I}_j[G(v_m), K(d)] \quad (7.15)$$

$$\hat{J}(K(d)) = f(\hat{\Pr}_d(p_1), \dots, \hat{\Pr}_d(p_j), \dots, \hat{\Pr}_d(p_n)), \quad j = 1 \dots n \quad (7.16)$$

and from the law of large numbers, the probability estimate \hat{J} approaches its true value, J , as the number of Monte Carlo samples approaches infinity [12, 14]. A very attractive aspect to this general approach is the following: the accuracy of the probability estimate is not dependent upon the order of the plant or candidate controller. A drawback, however, is that we cannot make any a priori guarantees related to meeting stability or performance requirements using these methods. All that we can do, using some results from probability theory that will be provided momentarily, is guarantee accuracy in the probability estimates, along with confidence in these estimates, before executing this optimization. Establishing bounds on estimate accuracy and confidence exploits the fact that probabilistic estimates are generated using summations of indicator functions. The “Yes/No” nature of evaluating whether our system is stable, and meets our defined performance requirements is key for this. Section 7.2.3 addresses Monte Carlo sample bounds for this type of problem.

What all of this means, then is that we pose our problem as an unconstrained, stochastic optimization problem. That is, we want to solve:

$$\begin{aligned} \max_{K(d)} \quad & f(\hat{\Pr}_d(p_1), \dots, \hat{\Pr}_d(p_j), \dots, \hat{\Pr}_d(p_n)), \quad j = 1 \dots n \\ \text{s.t.} \quad & d \in D, D \subseteq \mathbb{R}^{n_d} \end{aligned} \quad (7.17)$$

where the controller variables are parameterized into a vector of length n_d , and are not bounded within the field of real numbers. The actual cost function that is used to solve the probabilistic robust decentralized active vibration controller synthesis problem in this

chapter will be detailed after we discuss our approach to determining how many Monte Carlo samples are required to achieve certain levels of probability estimate accuracy and confidence.

7.2.3 Theoretical Bounds on Probability Estimate Accuracy and Confidence

This section will present some probability inequalities that are essential for establishing bounds on the accuracy and confidence of probability estimates generated using Monte Carlo estimates. First, we define the probability estimate that a system is stable, as

$$\hat{\Pr}(\text{stable}) = \frac{1}{N} \sum_{i=1}^N \mathbb{I}\left(\text{stable} \mid \mathbf{K}_{\Delta,i}\right) \quad (7.18)$$

where $\mathbf{K}_{\Delta,i}$ represents a sample drawn from the random interconnection stiffness matrix defined by (4.3), and stability is with respect to the random system formed by (7.6). This indicator function is constructed as

$$\mathbb{I}\left(\text{stable} \mid \mathbf{K}_{\Delta,i}\right) = \begin{cases} 1, & \text{Re}\left(\lambda(A_{\text{prob}})\right) < 0 \\ 0, & \text{otherwise} \end{cases} \quad (7.19)$$

where A_{prob} is given in (7.6), formed each time a new $\mathbf{K}_{\Delta,i}$ is drawn. The probability inequalities and bounds that are formed from them rely upon the fact that we are using indicator functions to judge the acceptability of certain controller/system pairs. Furthermore, these inequalities are key tools used for determining the minimum number of samples required to compute the reliability of the estimate given by (7.18).

The reliability of an estimate is measured in terms of the closeness of $\hat{\Pr}(\text{stable})$ to $\Pr(\text{stable})$, which is the true probability of stability. Thus, given some $\epsilon \in (0, 1)$, we want to make sure that the event

$$|\hat{\Pr}(\text{stable}) - \Pr(\text{stable})| < \epsilon \quad (7.20)$$

holds with adequately high probability. We refer to this adequately high probability as a confidence. We notice something about the accuracy and confidence in our estimates: if ϵ is chosen to be too large, even with high confidence in our estimate, we introduce noise into

our optimization problem. This was pointed out by Garrison, Wang, and Stengle in their papers [32, 31, 12]. Therefore, it is important that we try to account for this, as we could end up searching for a solution for longer than required, or end up with an inaccurate solution altogether. At the same time, the computational cost that accompanies high accuracy, high confidence estimates must also be balanced. We discuss these considerations in further detail later in this chapter.

We develop the number of Monte Carlo estimates, embedded within the cost function that is evaluated during genetic algorithm optimization, using the Chernoff bound [14]. The Chernoff bound is given by

Theorem 18 (Chernoff bound). *For any $\epsilon \in (0, 1)$ and $\delta \in (0, 1)$, if*

$$N \geq \frac{1}{2\epsilon^2} \log \frac{2}{\delta} \quad (7.21)$$

then, with probability greater than $1 - \delta$, we have $|\hat{\Pr}(\text{stable}) - \Pr(\text{stable})| < \epsilon$.

Proof. The Chernoff bound follows from direct application of the Hoeffding inequality to the random variables x_1, \dots, x_N , defined as

$$x_i = \mathbb{I}\left(\text{stable} \mid \mathbf{K}_{\Delta,i}\right) = \begin{cases} 1, & \text{Re}\left(\lambda(A_{\text{prob}})\right) < 0 \\ 0, & \text{otherwise} \end{cases} \quad (7.22)$$

for $i = 1, \dots, N$. Since $x_i \in [0, 1]$, letting $s_N = \sum_{i=1}^N x_i$ and applying the two-sided Hoeffding inequality [81, 14], we get the Chernoff inequality

$$\Pr\left\{|s_N - E(s_N)| \geq \epsilon\right\} \leq 2e^{-2\epsilon^2/N} \quad (7.23)$$

where $E(s_N)$ is the expectation of the random variable s_N . Through observing that $\hat{\Pr}(\text{stable}) = s_N/N$ and $E(\hat{\Pr}(\text{stable})) = \Pr(\text{stable})$, we have

$$\Pr\left\{|\hat{\Pr}(\text{stable}) - \Pr(\text{stable})| \geq \epsilon\right\} \leq 2e^{-2N\epsilon^2} \quad (7.24)$$

where the bound given previously follows. **Q.E.D.**

A parametric plot that shows the number of Monte Carlo samples, N , required to achieve certain levels of estimate accuracy and confidence, is shown in figure 39. From figure 39,

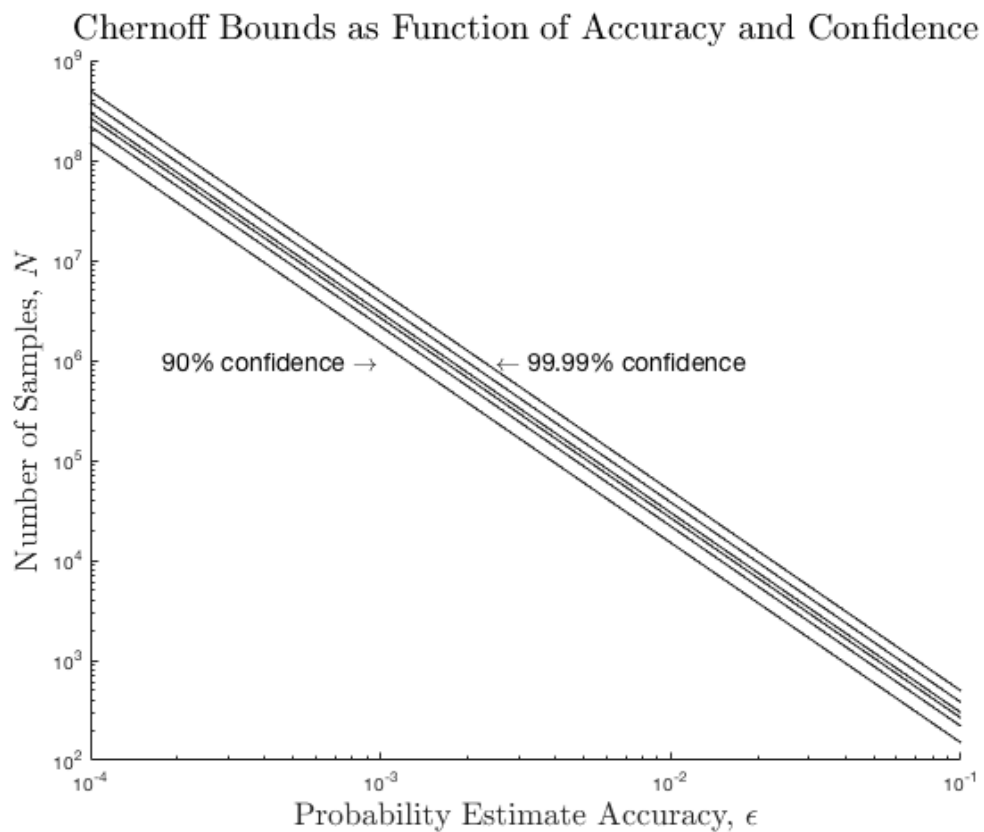


Figure 39: Chernoff bounds as a parametric of accuracy (ϵ) and confidence ($1 - \delta$). This plot illustrates how accuracy is more expensive than confidence. Additionally, this plot aids in a later discussion on probability estimate accuracy and computational complexity.

one thing that we can infer is that confidence is much cheaper than accuracy, using these bounds. This is evidenced by the tight spacing between the 90% and 99.9% confidence lines on this log-log plot.

The Chernoff bound given by theorem 18 is used for both synthesis and analysis of probabilistic robust decentralized controllers in this chapter. These bounds help us establish accuracy and confidence in the probability estimates generated during controller synthesis and analysis. Indicator functions are constructed for calculating a probability estimate of the random controlled system being stable. Similarly, we develop another indicator function for calculating the probability that a certain performance requirement has been met. Development of the performance indicator function is covered in section 7.3. Before getting into the performance function that we construct, we will state the genetic algorithm settings used in this chapter. Choices for many of these settings will be justified by the discussions in section 7.3.

7.2.4 Genetic Algorithm Settings

The settings and functions in table 2 were used for genetic algorithm-based optimization in this research. Genetic algorithm populations of 45 were used for all optimizations. This choice will be detailed in the sections to follow, as the computational complexity of the stochastic cost function used in this thesis was considered along with available computing resources.

Table 2: Genetic Algorithm Settings

Population Data	
Population	45
Elite Children	9
Crossover Children	29
Mutation Children	7
Selection, Crossover, Mutation Functions	
Selection	Stochastic Uniform [79]
Fitness Scaling	Fitness Scaling Rank [79]
Crossover	Crossover Scattered [79]
Mutation	Gaussian Mutation [79]
Stopping Conditions	
Generations	400
Cost Function Limit	100
Cost Function Tolerance	0.001
Stall Generations	40
Time Limit (Actual)	120 hours

7.3 FORMULATING THE PROBABILISTIC DECENTRALIZED DYNAMIC OUTPUT FEEDBACK SYNTHESIS PROBLEM AS A STOCHASTIC OPTIMIZATION PROBLEM SOLVED USING A GENETIC ALGORITHM

The performance test that we want our system to pass was given by (4.50), where the transfer function matrix mapping is between disturbance inputs and performance outputs for the structure. Throughout this research, we have discussed methods that revolve around finding a solution that is below, or minimizes in some way, the \mathcal{H}_∞ -norm of the dynamic system. We are now dealing with a high-dimensional system with random uncertainty, where controller synthesis involves the calculation of probability estimates. Accounting for the computational complexity of any performance functions is a major consideration.

Matlab employs the method by Bruisma for calculating the \mathcal{H}_∞ -norm of a transfer function matrix [82]. This method is based on a relation between the singular values of the transfer function matrix and the eigenvalues of a related Hamiltonian matrix. An alternative method is to solve an \mathcal{H}_∞ -norm feasibility problem by way of the KYP Lemma; unfortunately, the time complexity of types of LMIs grow as $\mathcal{O}(n^6)$ when using parsing software such as YALMIP [66, 83]. The structure of KYP-type problems can be exploited to increase efficiency, as shown by Falkeborn, but this speed increase still makes this computation very expensive for problems containing hundreds of states [84]. The method developed by Bruisma, and as implemented by Matlab, is significantly faster than LMI approaches. This speed increase is especially realized with high-order models.

Before constructing a function that generates the probability estimate

$$\hat{\Pr}\left(\|G_{\text{prob}}\|_\infty \leq \gamma^* \mid \mathbf{K}_\Delta\right) \quad (7.25)$$

we must understand, approximately, how much time this function call requires for state space systems of several hundred states. After all, the closed-loop system that we are studying in this chapter has between 400 and 500 state variables, which depends upon the order of the seed solutions found using the techniques in chapter 6. By running a small experiment, the

computational cost of this function was investigated. The average amount of time required to calculate the \mathcal{H}_∞ -norm of one hundred instances of stable, random 2-input, 4-output stable state space systems was calculated. Five different model orders were considered: 100, 200, 300, 400, and 500 states.

The amount of time required to compute the \mathcal{H}_∞ -norm, using the method developed by Bruisma, sees a polynomial increase with model order. This is shown in figure 40. For state space models possessing 500 states, 2-inputs, and 4-outputs, it took (on average) 8.868 seconds to compute the \mathcal{H}_∞ -norm using Bruisma's approach. These estimates were generated on a computer possessing a 3.0 GHz Intel Core i7 processor. For most analysis problems that we approach in control, this would not be an issue. However, the probabilistic robust synthesis problem that we are developing in this chapter requires (ideally) that we generate a large number of Monte Carlo samples for estimating (7.25). If we refer to figure 39, we see that for an $\epsilon = 0.015$ and confidence $1 - \delta = 0.95$, we would need approximately 8200 Monte Carlo estimates to generate a reasonably-accurate estimate for (7.25). This function call requires approximately 20 CPU hours. If we wanted to evaluate 50 candidate solutions with this function call embedded within a genetic algorithm, this would require approximately 1000 CPU hours.

The term “CPU hour” refers to the amount of computing time required by a computing resource. For processes that are parallelizable, we can reduce the actual hours by dividing these expensive tasks up among all available resources. So, if we have access to a 24-core computer, where each CPU has 3 GHz of processing power, this task would take approximately 40 hours. This implies that it would take almost two days for one generation in a genetic algorithm to be evaluated, for $\epsilon = 0.015$ and $\delta = 0.05$.

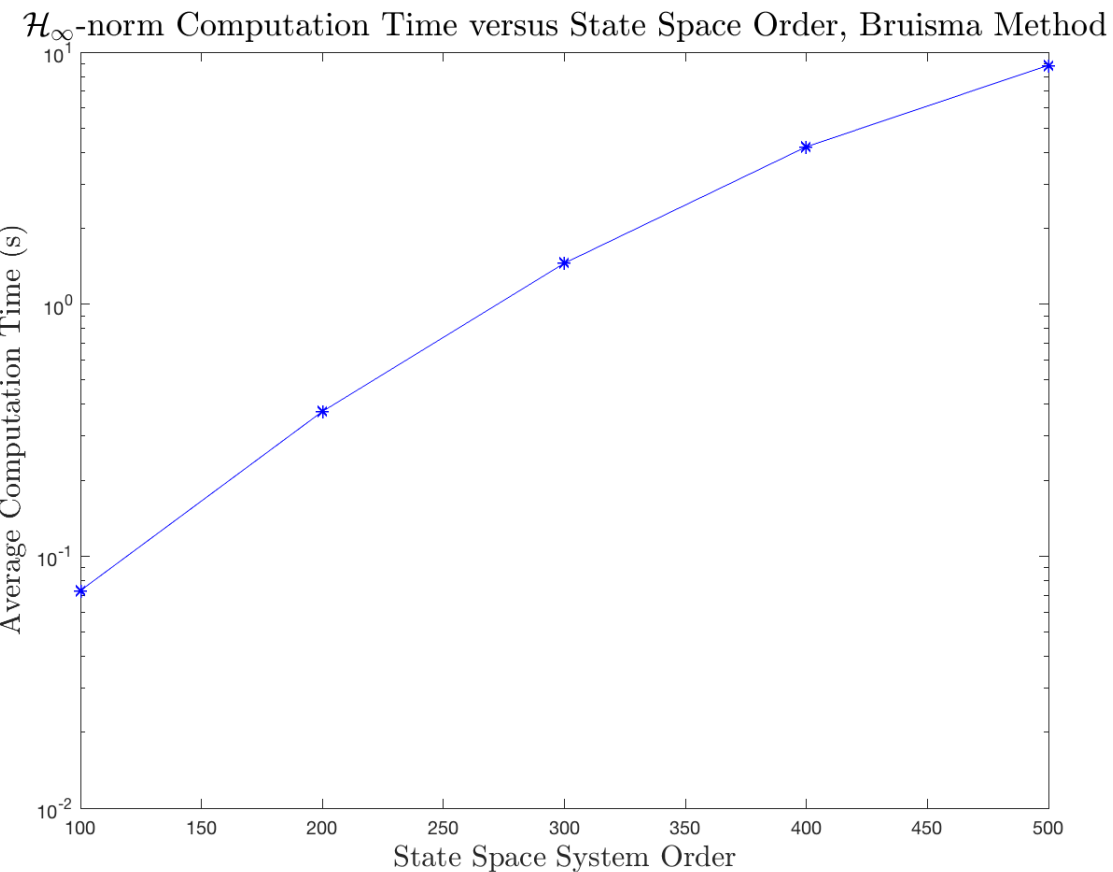


Figure 40: Average \mathcal{H}_∞ -norm computation time versus state space order for a random, 2-input, 4-output, stable state space system.

7.3.1 A Less Expensive \mathcal{H}_∞ -norm Performance Calculation

We can retain the probabilistic performance test defined by equation 4.50 in chapter 4 as an a posteriori measure of success. We also retain our objective related to attenuating the system response at low frequencies. It is clear that calculating the \mathcal{H}_∞ -norm of the structure's disturbance input to performance output mapping is not an efficient way to solve this problem.

For a transfer function matrix $G(s)$, we have that the \mathcal{H}_∞ -norm of the transfer function matrix is less than some positive scalar γ if

$$G(s)^H G(s) - \gamma^2 I < 0, \quad s = j\omega, \omega \in [0, \infty), \cup \{\infty\}. \quad (7.26)$$

This follows from

$$\bar{\sigma}(G^H G) \leq \gamma^2 \quad (7.27)$$

$$\|G\|_\infty \leq \gamma \quad (7.28)$$

meaning that (7.26) is sufficient for checking that a given transfer function matrix G has infinity norm less than γ .

Next, we must discuss how we go about establishing our frequency grid. That is, at what points do we want to check for this negative definiteness? As we will show momentarily, computation demands can be significant should we attempt to compute the infinity norm by constructing a very fine frequency grid. This choice also allows us to focus on a bandwidth that we are most interested in.

7.3.1.1 Selecting a Frequency Grid

In chapter 4 we showed how the disturbance input and performance output matrices of a lightly-damped structure can be scaled in modal coordinates by the magnitude of a filter function, evaluated at the natural frequency corresponding with that structure's mode, to achieve the end of approximate frequency weighting for control design purposes.

Since it is our desire to attenuate the system's response at low frequency modes and by exploiting the fact that the \mathcal{H}_∞ norm of a lightly-damped structure will occur at one of its natural frequencies (see section 5.6 of Gawronski [61]), we can choose to evaluate (7.26) at a the closed-loop system's natural frequencies. Thus, we have:

$$G(j\omega_i)^H G(j\omega_i) - \gamma^2 I < 0, \quad i = [0, \dots, n] \quad (7.29)$$

where each ω_i is a natural frequency of G . This means that this check must be performed up to n times for a given G , where n is equal to the degree of the characteristic polynomial of G .

Something fundamental is worth pointing out at this point. The transfer function matrix, $G \in \mathbb{C}^{m_1 \times r_1}$, where from chapter 3 these dimensions refer to the number of performance outputs and disturbance inputs, respectively. This means that the term $G^H G \in \mathbb{R}^{r_1 \times r_1}$ which in this research is only a 2 by 2 matrix. Computing the eigenvalues of this matrix takes fractions of a millisecond using most numerical approaches. However, the transfer function matrix G_{prob} , given by (7.6), is realized into its equivalent state space formulation during algorithm execution since:

1. Generating random parametric uncertainty while in this physical state space form;
2. This is the basis in which we have elected to perform synthesis and analysis.

Since the closed loop plant order has between 400 and 500 states, this means that in order to form:

$$G_{\text{prob}}(s_i) = C_{\text{prob}}(s_i I - A_{\text{prob}})^{-1} B_{\text{prob}} + D_{\text{prob}} \quad (7.30)$$

we must invert a complex matrix $(s_i I - A_{\text{prob}}) \in \mathbb{C}^{n \times n}$ where n is in the range [400, 500], and the subscript s_i is the complex variable $j\omega_i$, which is each system natural frequency. This is an expensive operation, especially when it must be performed for many frequencies and for many instances of the random system.

We recall that one of our control objectives was disturbance attenuation at low frequencies. We want the system's response to be small at the low frequency modes as the system is excited by broadband disturbance inputs. We can therefore choose to evaluate:

$$G(j\omega_i)^H G(j\omega_i) - \gamma^2 I < 0, \quad i = [0, \dots, n_l] \quad (7.31)$$

where $n_l < n$, with n being equal to the dimension of the state space model specific to (7.6). We choose n_l to include to span half of the controlled model's bandwidth. We note that a stable system also has finite \mathcal{H}_∞ -norm, and so high-frequency modes are not completely ignored.

Calculating the infinity norm across the bandwidth of the structure, at each natural frequency, is still not an inexpensive procedure. Inversion of a 500×500 complex matrix is expensive. To show this, 100 instances of random state space systems with 2 inputs, 4 outputs, and having orders of 100, 200, 300, 400, and 500 were generated and the average amount of time to compute the

1. \mathcal{H}_∞ -norm using Bruisma's approach;
2. Perform the calculation (7.26) across the entire bandwidth of the structure, only performing (7.26) for eigenvalues that have complex parts;
3. Perform the calculation (7.26) up to half of the structure's bandwidth, only performing (7.26) for eigenvalues that have complex parts.

The result of these experiments is shown in figure 41. For a system with 500 states, we see that by only evaluating the modes corresponding with complex-conjugate eigenvalues up to half of the structure's bandwidth, we are able to realize an approximately 8-fold decrease in computation time. Using the extrapolated computation time provided earlier for the case where we perform 8200 Monte Carlo evaluations, we see that one generation will require approximately 113 CPU hours. On a 24-core computing node with 3 GHz processing power per CPU, this suggests that one generation would require approximately 5 “actual hours” for evaluation.

Pseudo \mathcal{H}_∞ -norm Computation Time versus State Space Order, Comparison

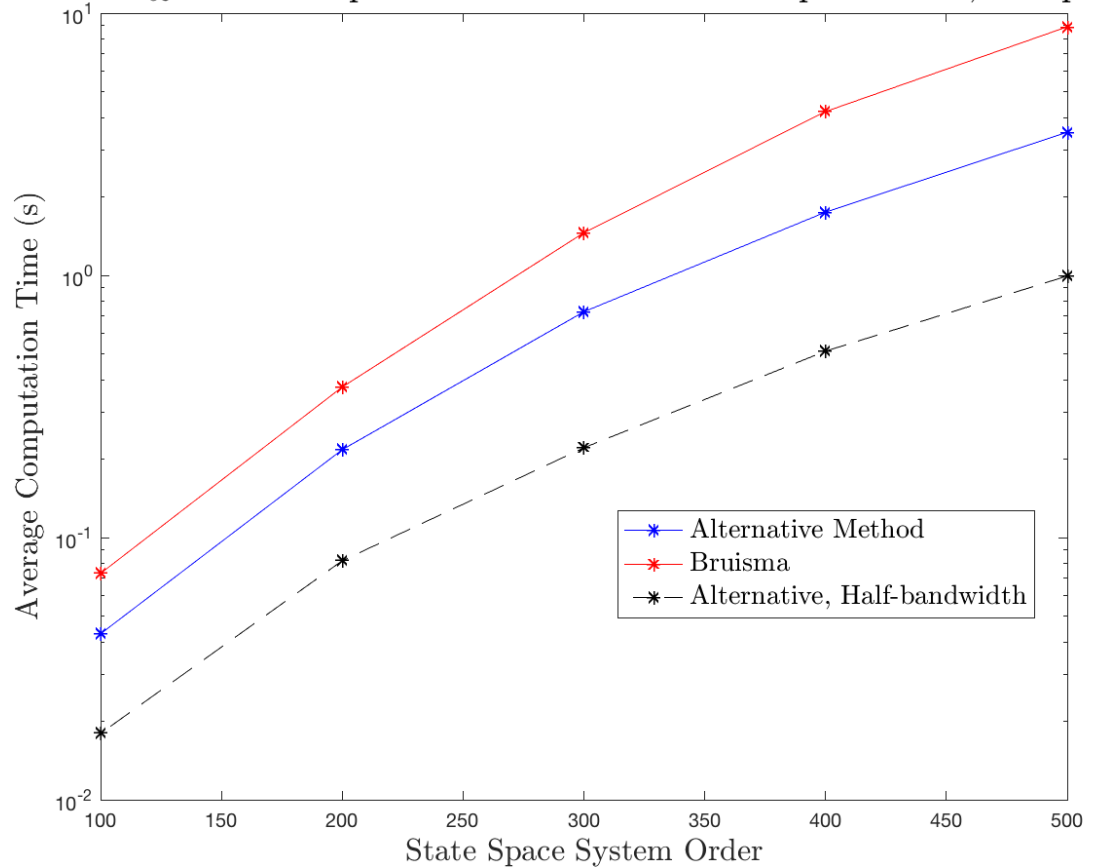


Figure 41: Computation time comparison between Bruisma approach to \mathcal{H}_∞ -norm calculation with evaluation at lightly damped modes across the bandwidth of 2-input 4-output stable state space systems.

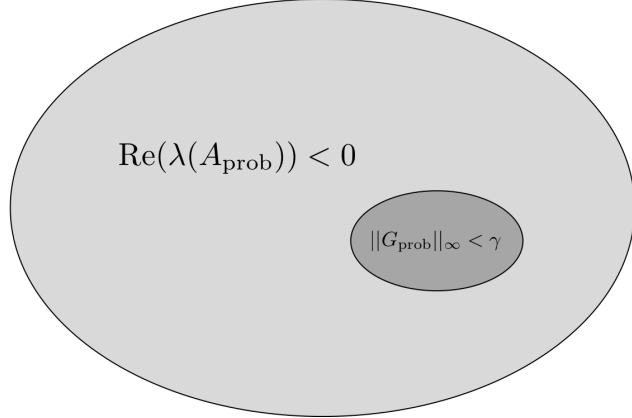


Figure 42: The set of systems with \mathcal{H}_∞ -norm below some scalar value γ is a subset of the stable systems, where both sets are generated by the same uncertainty distributions.

7.3.2 Final Cost Function used for Synthesis

The previous section was used for determining a good way to create a cost function that evaluated the maximum response across all disturbance input/performance output channels at low frequency modes in a manner that is not too computationally expensive. We must strike a balance between probability estimate accuracy, confidence in this estimate, available computing resources, and our ability to thoroughly investigate the solution space. To do this, we recall from chapter 2 that a conditional independence exists between achieving performance and stability. That is, finding a solution that has \mathcal{H}_∞ -norm below some level is guaranteed to exist within the set of stable solutions. This is shown in figure 42. One thing that we can say with certainty is this: the volume of stable solutions is most certainly larger than the volume of solutions that achieve some \mathcal{H}_∞ -norm below some level. We want to exploit this (obvious) property when implementing our final cost function. Thus, the cost function that is used for this optimization problem is given in algorithm 4.

Algorithm 4 Closed Loop Cost Function Formulation and Evaluation

1: **procedure** CLOSED LOOP COST FUNCTION FORMULATION AND EVALUATION

2: Load controllers #1 and #2.

3: Initialize stability and performance counters, $S_c = 0, P_c = 0$.

4: **for** $i = 1$: Number of Monte Carlo Evaluations(N_{mce}) **do**

5: Generate a random interconnection stiffness matrix;

6: Form the closed loop system, G_{prob} , given by (7.6).

7: Perform stability test

8: **if** all real parts of $\lambda(A_{\text{prob}}) < 0$ **then**

9: $S_c = S_c + 1$;

10: Calculate the natural frequencies of A_{prob} : $|\lambda(A_{\text{prob}})|$

11: Remove natural frequencies corresponding to purely-real eigenvalues, and form a frequency grid at of natural frequencies that spans half of the controlled model's bandwidth, called $\Omega_{0.5}$.

12: **for** $ii = 1$: Number of frequency points in $\Omega_{0.5}$ **do**

13: Form

$$G_{\text{prob}}(j\omega_i) = C_{\text{prob}}(j\omega_i I - A_{\text{prob}})^{-1}B_{\text{prob}} + D_{\text{prob}}$$

14: **if** $G_{\text{prob}}(j\omega_i)^H G_{\text{prob}}(j\omega_i) - \gamma^2 I < 0$ **then**

15: $P_c = P_c + 1$;

16: **else**

17: Return to beginning of outermost for-loop.

18: **end if**

19: **end for**

20: **else**

21: Return to beginning of outermost for loop.

22: **end if**

23: **end for**

```

24:    $\hat{\Pr}(\text{stable}) = \frac{1}{N_{mce}} S_c$ 
25:    $\hat{\Pr}(\text{perf}) = \frac{1}{N_{mce}} P_c$ 
26:   Cost =  $\kappa_1 \hat{\Pr}(\text{stable}) + \kappa_2 \hat{\Pr}(\text{perf})$ 
27: end procedure

```

The final cost function is defined to be $\text{Cost} = \kappa_1 \hat{\Pr}(\text{stable}) + \kappa_2 \hat{\Pr}(\text{perf})$ where κ_1 and κ_2 are chosen as positive scalars. We chose $\kappa_1 = 60$ and $\kappa_2 = 40$ so that the maximum cost function value would be 100. This implies that our optimization problem is being cast as:

$$\begin{aligned} & \max_{K_1, K_2} \quad \kappa_1 \hat{\Pr}(\text{stable}) + \kappa_2 \hat{\Pr}(\text{performance}) \\ & \text{s.t.} \quad K_1 \in \mathbb{R}^{v_{k1}}, K_2 \in \mathbb{R}^{v_{k2}}. \end{aligned} \tag{7.32}$$

Furthermore, v_{k1} and v_{k2} correspond to the number of unique controller variables that we must search over. These sizes indicate that the controller variables are vectors. This is a requirement for genetic algorithm-based optimization. Therefore, the controllers are both vectorized and reconstructed as dynamic systems during optimization.

Two aspects to this cost function pseudo code should be recognized:

1. The probability of meeting performance requirements is a subset of the probability of being stable. As a result of this, effort is not wasted looping through our frequency grid given by $\Omega_{0.5}$. This portion of the cost function contains the most expensive computation: repeated calculation of $G_{\text{prob}}(j\omega)$.
2. Another exit criterion exists within the check for positive definiteness. If it is discovered that at any natural frequency, (7.26) is violated, we exit this loop and move on to the next random instance, concluding that the performance test failed.

The cost function given by algorithm 4 was evaluated for random instances of the actual dynamic system under study. Therefore, most of the closed-loop poles of the system were lightly damped. Some, but not all, of the random plant instances met our prescribed performance level given by γ^* , as defined in chapter 4. Therefore, some of the exit criteria were invoked. It was discovered that this cost function, on average, required 0.57 seconds

to execute. Using this information, the parametric plot shown in figure 43 was created for a computer possessing a 3 GHz Intel i7 processor. Recall the considerations that we must balance for this stochastic optimization problem:

1. Available computing resources;
2. Choosing an adequate probability estimate and accuracy, so as to reduce “noise” in our probability estimates;
3. Ability to thoroughly search the solution space.

This optimization problem was solved on shared memory partitions located at the University of Pittsburgh Center for Research Computing, where each node had 24 Xeon Gold 6126 2.6 GHz Processors and 192 GB of (shared) RAM. For this research, we did not enable communication across computing nodes, and so optimization around a certain seed controller was limited to only one node. Because of this, it was decided that genetic algorithm populations would be set to have 45 candidate solutions. On a 24-core node, we can roughly estimate that the approximate actual run time in figure 43 would be doubled, since genetic algorithm parallelization is accomplished by evaluating individual candidates solution cost functions on separate CPUs.

These considerations related to available CPUs, absence of cross-node communication, and cost function complexity led us to select

$$|\hat{\Pr}(\text{stable}) - \Pr(\text{stable})| < 0.04 \quad (7.33)$$

$$|\hat{\Pr}(\text{performance}) - \Pr(\text{performance})| < 0.04 \quad (7.34)$$

with 95 % confidence in these estimates. This means that the number of Monte Carlo samples required, $N_{mce} \geq 1153$. In the equations above, $\epsilon = 0.04$ and $1 - \delta = 0.95$. Using the parametric shown in figure 43 one generation possessing 45 candidate solutions can be evaluated in approximately 21.5 minutes. Note that this estimate is likely to be under-conservative once we find ourselves in good solution spaces, since we will likely exist within the performance subset within figure 42. Conversely, candidate solutions that are unstable will take little time to evaluate. This analysis was performed to understand how to make cost

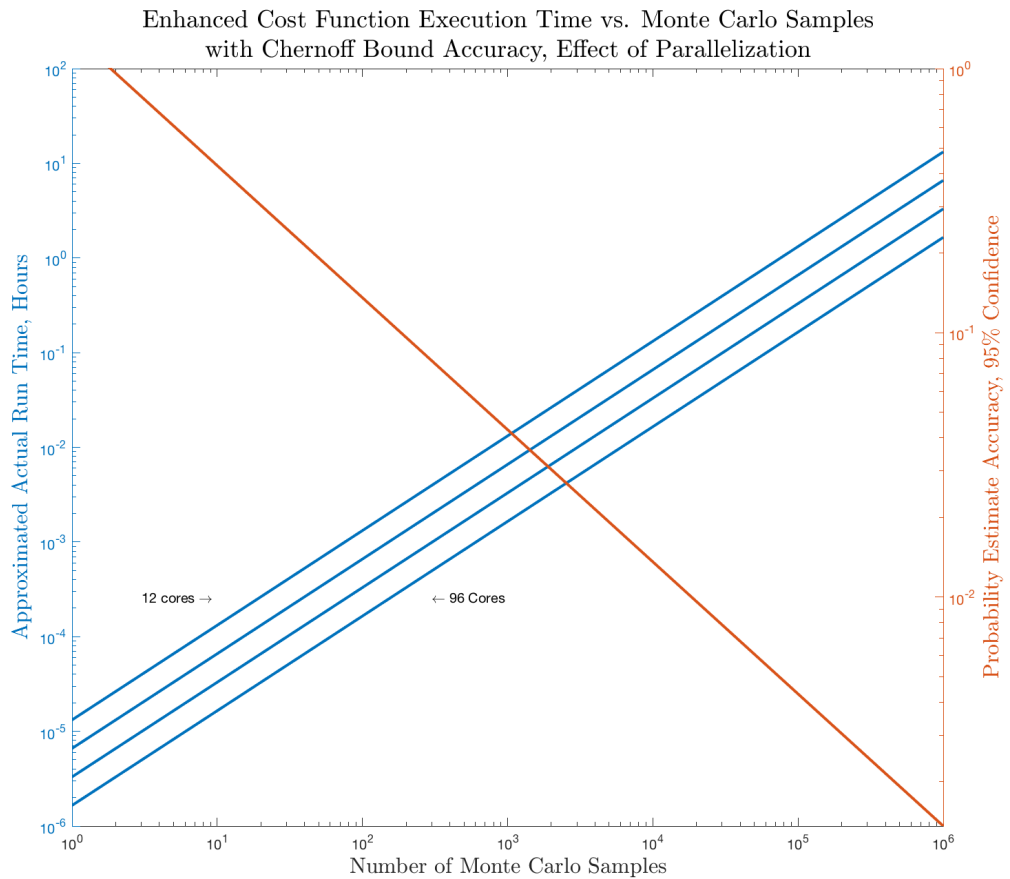


Figure 43: Probability estimate accuracy, 95% confidence, parametric with available computing cores and average computation time required to execute the cost function given by algorithm 4 for one Monte Carlo sample.

function and probability estimate accuracy choices, while balancing these choices against the available computing resources.

7.4 ON REDUCING THE NUMBER OF CONTROLLER VARIABLES

Our seed controllers each have the structure

$$K \sim \left[\begin{array}{c|c} A_k & B_k \\ \hline C_k & D_k \end{array} \right] \quad (7.35)$$

with dimensions $A_k \in \mathbb{R}^{n_k \times n_k}$, $B_k \in \mathbb{R}^{n_k \times m_k}$, $C_k \in \mathbb{R}^{r_k \times n_k}$, $D_k \in \mathbb{R}^{r_k \times m_k}$.

It is well-known that dynamic output feedback \mathcal{H}_∞ synthesis tends to yield controllers that are the same order, or greater than that of the plant [63]. However, we also know that reduced rank controllers can be sought by imposing rank constraints (which are nonconvex) on the controller variables in a semidefinite program. Such constraints are not always necessary, however, they can be incorporated into the μ -synthesis problem when solving the controller synthesis problem as an LMI [63, 85, 86].

Nevertheless, we do not impose these constraints during our μ -synthesis process while generating an initial population of robust dynamic output feedback \mathcal{H}_∞ controllers for this problem. A modest reduction in the size of the nominal controllers would not significantly reduce the computational complexity of the stochastic optimization problem that we need to solve. If we denote our optimization variables as v , we observe that the controller K given above has

$$v = n_k^2 + n_k m_k + r_k n_k + r_k m_k \quad (7.36)$$

variables. Generally, and for the problem that we are solving, m_k , which matches the number of sensors used in feedback, is not all that large. Furthermore, r_k , which matches the number of actuators used with our feedback control laws, is not all that large, either.

The one variable that can be large, especially with structural vibration control problems, is the order of the controller, n_k . We can safely say that

$$n_k > m_k > r_k. \quad (7.37)$$

Clearly, this has ramifications on the complexity of the stochastic controller synthesis problem that we are trying to solve. We can rewrite (7.36) as

$$v = n_k^2 + n_k(m_k + r_k) + r_k m_k \quad (7.38)$$

and can call $v_1 \doteq n_k^2$, $v_2 \doteq n_k(m_k + r_k)$, and $v_3 \doteq r_k m_k$. We can then say that

$$v_1 \gg v_2 > v_3 \quad (7.39)$$

which leads us to ask the question that plagues so many control theorists and has motivated us, over time, to pursue reduced-order controllers: how can we reduce the order of this optimization problem?

Again, we are dealing with a stochastic optimization problem in a high-dimensional solution space. We do not want to perform order reduction on our controller orders given by n_k , since we know that we are starting in a solution space that has robust solutions. We observe, however, that a simple change of basis can be used on the controller basis can help with this problem. That is, we can go into a modal basis to restrict the variables that we must search over within the controller dynamics matrix (generically given by A_k).

7.4.1 A Canonical Similarity Transform for Reducing the Number of Optimization Variables

It is a fundamental fact that any state space system is invariant under any nonsingular similarity transformation [87]. The same argument works for transformations for the controller and the resulting linear fractional transformation between some plant and this controller. That is, we have

$$K \sim \left[\begin{array}{c|c} A & B \\ \hline C & D \end{array} \right] = \tilde{K} \sim \left[\begin{array}{c|c} T^{-1}AT & T^{-1}B \\ \hline CT & D \end{array} \right] \quad (7.40)$$

and since $K = \tilde{K}$, we have for some system G , that $F_l(G, K) = F_l(G, \tilde{K})$. This furthermore implies that $\|F_l(G, K)\|_\infty = \|F_l(G, \tilde{K})\|_\infty$. Since we have equivalence between the linear fractional transformations we can also say that these complex functions share the same characteristic equation. Since their characteristic equations are equivalent, roots to these characteristic equations are equivalent, which implies that the eigenvalues of their state space realizations are equivalent.

Thus, we can calculate the eigenvectors of the controller K and can convert this system into its complex modal form. By the arguments just provided, the closed-loop system's eigenvalues and frequency response functions are invariant under this transformation. Note that leaving the controllers in their complex modal form works specifically for the stability and performance requirements that have been defined in this thesis — if time-domain performance requirements are to be entertained/required, the controllers would have to be converted into a purely-real basis. This can be done using the modal form given in Linear System Theory and Design by Chen [87].

A distinct advantage that we get in our situation is that we have just reduced the number of optimization variables to

$$\tilde{v} = n_k + n_k(m_k + r_k) + m_k r_k. \quad (7.41)$$

That is, we have gone from optimization variables that were $\mathcal{O}(n_k^2)$ to $\mathcal{O}(n_k)$! For high-order controllers, and systems, this reduction is significant.

In fact, we see that for $m_k = 4$ and $r_k = 2$, the number of variables, v , as a function of controller order and accounting for a decentralized structure, will increase as shown in figure 44. Recall that at the end of chapter 6, we said that we would highlight two of the successful seed controller cases. They were controller pairs 2 and 7. which, when in the basis resulting from μ -synthesis, and using (7.36), means that we have 50,904 free variables for controller pair #2 and 110,856 for controller pair #7. This would be a very large solution space to have to search over. By converting the controllers into their modal form, we can realize the significant reduction illustrated in figure 44, and shown exactly in table 3 for the featured controller pairs. Figure 44 helps us see that even higher order controllers can still

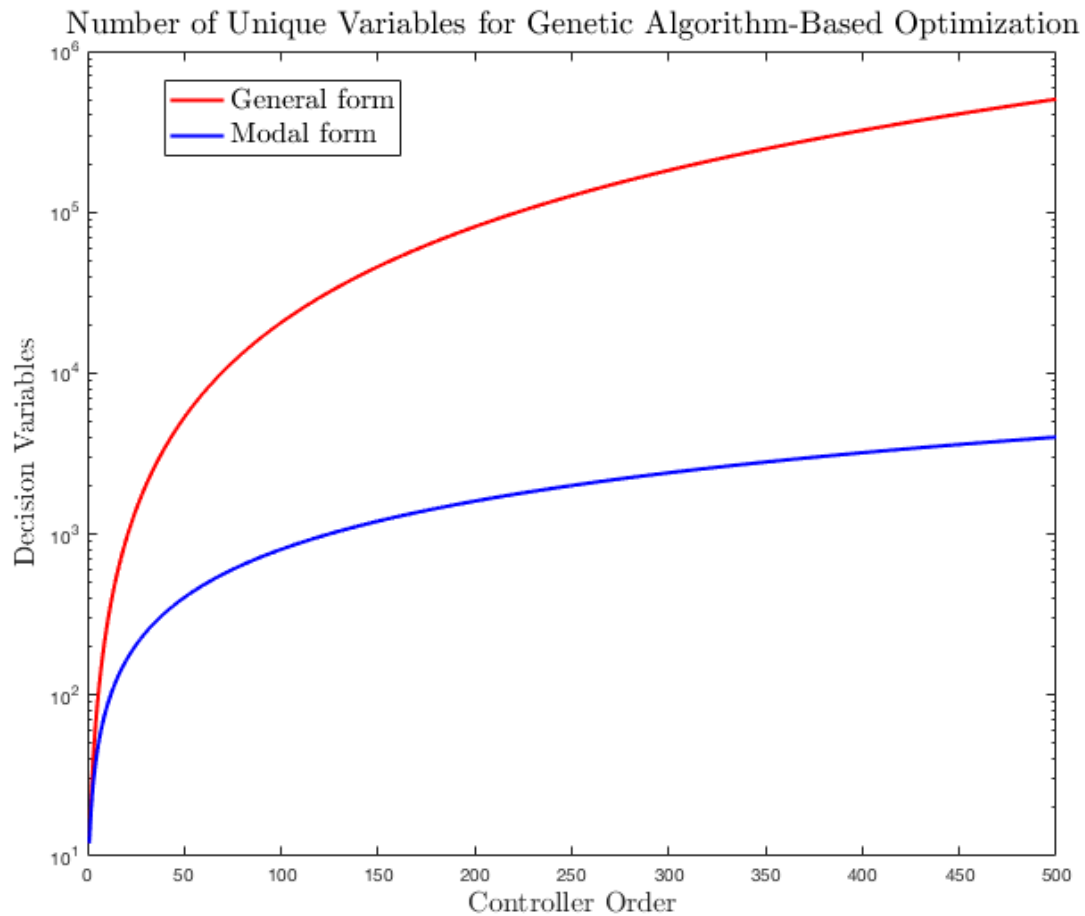


Figure 44: Reducing the seed controllers to a modal basis dramatically reduces the number of controller variables required during optimization.

Table 3: Unique Controller Variables

Pair	$K_1 (n_{k,1}, m_{k,1}, r_{k,1})$	$K_2 (n_{k,2}, m_{k,2}, r_{k,2})$	General From	Modal Form
2	(100, 2, 1)	(200, 2, 1)	50,904	1,204
7	(148, 2, 1)	(296, 2, 1)	110,856	1,708

be solved using the techniques developed in this chapter. As it will be shown momentarily, good solutions were found in a reasonable amount of time using these approaches.

7.4.2 Using Modal μ -Synthesized Seed Controllers for Stochastic Synthesis

By converting each controller into their modal form, we can approach the stochastic synthesis problem by searching over the real and complex parts of the controller system matrices. It is in this reduced, fundamental basis, where we can realize the most compact realization, making our high-dimensional search possible. Solving the problem in this basis is not without challenges, however. Specifically, these challenges are:

1. The eight controller pairs, described in table 1, are generally of different model order. This becomes a concern if we wish to include all controllers as initial population members in one genetic algorithm.
2. All controller pairs are likely to have different numbers (and locations) of purely-real eigenvalues. For real/complex eigenvalues we know that each has an associated real/complex eigenvector, meaning that the corresponding rows/columns in the B and C matrices will have purely-real or real/complex entries.
3. And lastly, which is related to the presence of different numbers of purely-real eigenvalues, how can we include an intelligence into our synthesis process that allows two purely-real eigenvalues to converge and depart from the real-axis, thus becoming a complex conjugate pair?

These obstacles present interesting opportunities, for future research, as we fashion algorithms that are capable of transforming our dynamic controllers into forms that can be used — and searched over — using algorithms specific to artificial intelligence and optimization methods. Theoretically, the initial population matrix could be zero-padded to bring our initial population members up to the maximum dimension of the set of μ -synthesized controllers to address the first challenge. This option was not pursued. To address the second and third challenges, we could have developed an algorithm that allowed complex conjugate pairs of eigenvalues to converge/diverge along the real axis, but developing this approach with sound theory was not pursued at this time. For example, if 5 purely real-valued eigenvalues are all next to one another on the imaginary axis, how do we make a choice about which eigenvalues combine to form complex conjugate pairs? How do we handle the rapid jump/discontinuity that can occur by immediately allowing a pair of real-valued eigenvalues to assume a pair with low damping? Generally, genetic algorithms are well-suited for problems where the objective function is discontinuous and discrete jumps in variable values are normal, however, it was not obvious — at this point in time — that spending the effort to encode this capability would lead to a significant gain.

Thus, the path forward involved the following:

- Initializing random populations around each μ -synthesized controller and executing our searches as completely separate optimization problems. The orders of the decentralized, dynamic compensators were fixed to equal that of each seed of the initial population. This architecture is depicted in figure 45.
- The number of purely-real eigenvalues for each controller was restricted to equal the number of purely-real eigenvalues specific to the μ -synthesized seed controllers.

And so we can see that, already, we have made the following restrictions for our random search:

1. We are not combining all μ -synthesized controllers into one initial population, thus restricting their ability to cross-over with one another;

2. In each separate search space, and generally, we are restricting the order of the controllers to be equal to that of the μ -synthesized seed controllers;
3. We are restricting the number of purely real-valued eigenvalues equal to the number of purely real-valued eigenvalues specific to each μ -synthesized seed controller.

These restrictions bring us to a fundamental assumption that is being made with respect to our approach:

Assumption 2. *With the restrictions 1), 2), and 3) made above, a set of probabilistic robust controllers that maintain the ∞ -norm of our system below some level exists for the random uncertainty set prescribed for the interconnection stiffness element.*

And so we move forward with execution, leveraging access to supercomputing resources in our attempt to test assumption 2 in our search for probabilistically-robust, decentralized controllers that maintain the ∞ -norm of our system below some level.

7.5 RESULTS

In chapter 6, as well as at the beginning of this chapter, we said that we would focus on presenting the results, and analyzing further, those probabilistic decentralized controllers resulting from the second and seventh seeds. In table 4, these final solutions are given by Solutions 1 and 2. We found that each of these solutions achieved the prescribed stability and performance objectives over 99% of the time, with 95% confidence that these estimates are within 0.01 of the true probability. We proceed with analyzing how these controllers performed by comparing their performance around the nominal plant to the seed solutions, showing their random maximum singular value plots against the open-loop plant, and lastly analyze the probabilistic robustness against varying levels of random uncertainty. We can make a few comments about the results shown in table 4:

- All solutions converged due to the cost function tolerance criterion. The algorithm stops if the average relative change is less than the prescribed tolerance (set to ≤ 0.001) for

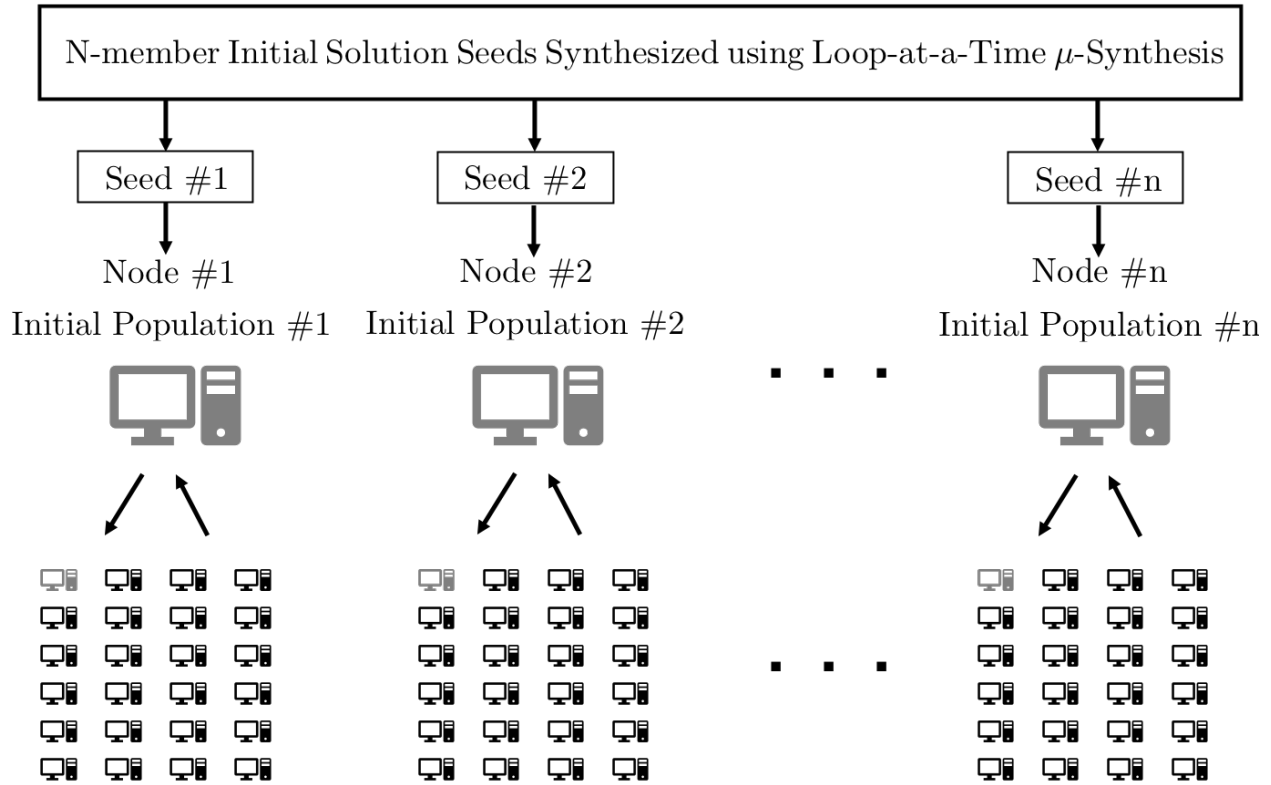


Figure 45: Genetic algorithm based optimization was pursued around individual μ -synthesized seed controllers. Communication between computing nodes was not enabled. Eight seeds were used, meaning eight nodes, each with 24 cores, were involved in searching for probabilistic robust decentralized controllers in this research.

Table 4: Optimization algorithm performance and convergence.

Algorithm Performance Data						
Solutions	μ -Seed Pair	K_1 Order	K_2 Order	Final Cost	Generations	CPU Hours
1	2	100	200	99.653	64	1200
2	7	148	296	99.826	42	1464
3	4	100	248	98.826	84	1464
4	7	148	296	95.299	78	2448

the best cost function value, over the prescribed number of stall generations (set to 40).

These settings are given in table 2.

- The solutions that appear to be the most robust converged in only 64 and 42 generations. This suggests that we either started in, or quickly found our way to a rich solution space.
- With more computing resources, a broader solution space can be investigated while also reducing the algorithm runtime. Furthermore, these new, probabilistic-robust solutions can be placed into a subsequent optimization problem to design against other metrics, if the designer so chooses.

Monte Carlo sampling using Chernoff bounds for probabilistic tests and degradation function construction were set according to: $\epsilon_p = 0.01$, $\delta_p = 0.05$, leading to the requirement that we generate at least 18,445 samples for probability estimates that will be within 0.01 of the true probability, with 95 % confidence in this estimate. Recall that for synthesis, we had $N_{mce} = 1,153$.

7.5.1 Controlled System Performance

We will briefly examine the closed loop performance of the probabilistic robust solutions #1 and #2, with respect to the nominal plant, and also compare performance to the μ -synthesized seed solutions. These results are shown in figures 46 and 47. Note that since the μ -synthesized solutions were used as seeds in this optimization problem, these solutions were evaluated against the same cost function. The resulting solutions, given by solutions #1 and #2, are therefore more probabilistically-robust against the design criteria that was prescribed for this optimization problem.

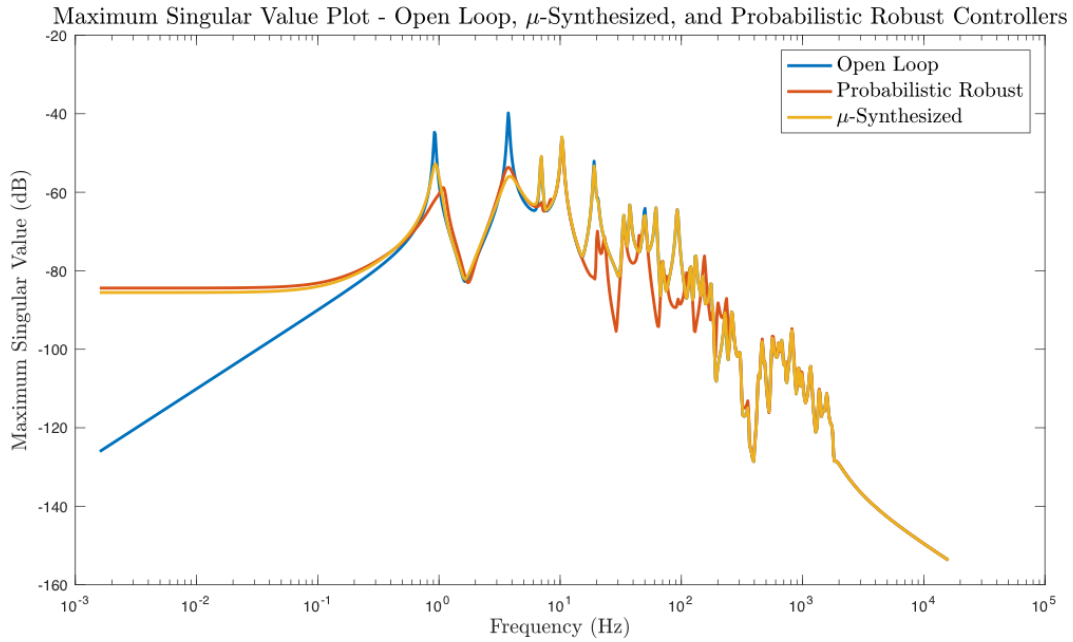


Figure 46: Solution #1, as described in table 4. These maximum singular value plots show the disturbance input/performance output mapping for the open-loop system and both the probabilisitic-robust and associated μ -synthesized seed closed-loop systems. These maximum singular value plots are for the nominal plant, where the interconnection stiffness modulus $E_0 = 200$ GPa. Around the nominal plant, with the exception of the second mode and a few modes in the mid-frequency range, the probabilistic robust solution tends to perform better than the μ -synthesized solution.

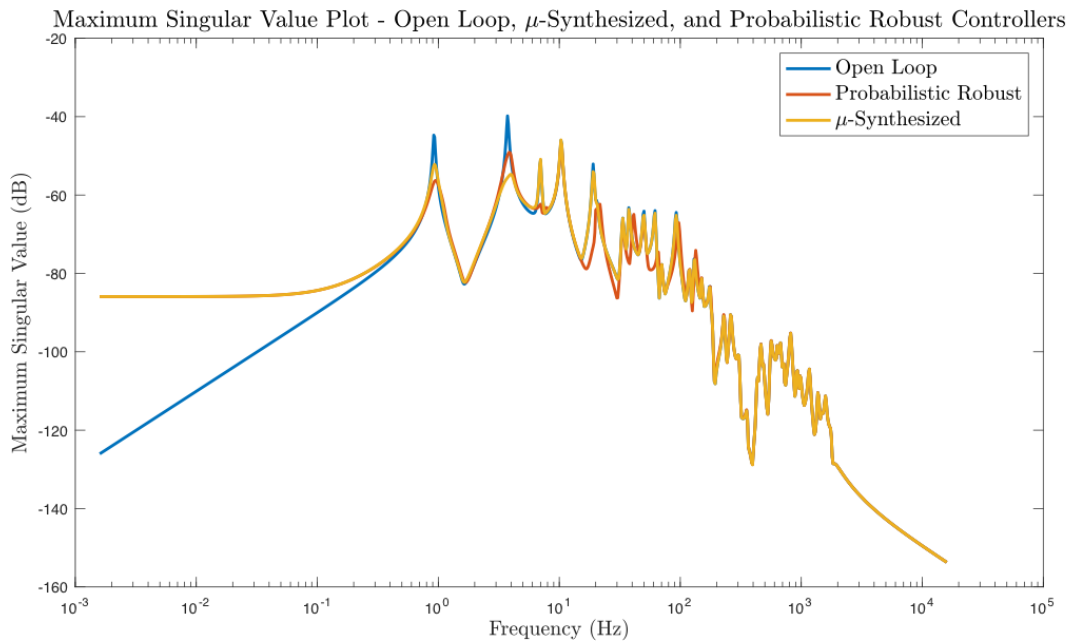


Figure 47: Solution #2, as described in table 4. These maximum singular value plots, mapping the disturbance inputs/performance outputs are around the nominal plant, where the interconnection stiffness modulus $E_0 = 200\text{GPa}$. Similar to solution #1 shown in figure 46, the probabilistic robust solution out-performs the μ -synthesized solution with the exception to the second mode.

Table 5: Solutions #1 and #2 Performance

Stability and Performance of the “Nominal Uncertainty” Case						
Solutions	K_1 Order	K_2 Order	Final Cost	$\hat{\Pr}(\text{stable})$	$\hat{\Pr}(\text{perf})$	$E(G_{\text{prob}} _\infty)$
1	100	200	99.653	0.9934	0.9934	-46.52 dB
2	148	296	99.826	0.9933	0.9933	-46.47 dB

7.5.2 Stability and Performance Tests

The probability of stability (estimate) and performance (estimate) for solutions 1 and 2 are shown in table 5. The probability of being stable, of meeting the performance requirement that $||G_{\text{prob}}||_\infty \leq \gamma^*$, are shown. The \mathcal{H}_∞ -norm was calculated using Bruisma’s approach. In this manner, we are not limiting ourselves to checking within the bandwidth that we defined in executing algorithm 4 for synthesis. One thing that we see is that every stable configuration meets these performance requirements. The equivalence of the estimated probabilities illustrate this. Furthermore, the \mathcal{H}_∞ -norm was calculated using Bruisma’s approach [82], where we clearly see that we have achieved our objective of finding controller solutions such that

$$P_{\text{test}} \doteq \hat{\Pr}\left(||G_{\text{prob}}||_\infty \leq \gamma^* \mid \mathbf{K}_\Delta \right) \geq 1 - \epsilon_p \quad (7.42)$$

where we chose $\gamma^* = -45.4$ dB and $\epsilon_p = 0.05$. The stability test is given by:

$$S_{\text{test}} \doteq \hat{\Pr}\left(\text{Re}(\lambda(A_{\text{prob}})) < 0 \mid \mathbf{K}_\Delta \right) \geq 1 - \epsilon_s \quad (7.43)$$

where we chose $\epsilon_s = 0.02$. We have passed these stability and performance tests with confidence of 95% in our probability estimates.

7.5.3 Comments on Probabilistic Robust Solutions 1 and 2

Tables 4 and 5 summarize the data related to, and performance of, the two solutions that are being featured in this chapter. Some additional comments on these controller solutions are warranted.

Probabilistic Robust Solution #1: The first solution was generated from the μ -synthesized controllers specific to seed #2 (see table 1). μ -synthesis via D/K iterations was executed around the bounded uncertainty $E_{\Delta,1} = [0.01E_0, 2E_0]$.

Probabilistic robust solution #1 has the same number of controller variables as the μ -synthesized seed solution: K_1 has 100 states and K_2 has 200 states.

For the probabilistic robust solution, the worst case \mathcal{H}_∞ -norm within stable set was -46.24 dB. The expected value of the \mathcal{H}_∞ norm was -46.52 dB.

Probabilistic Robust Solution #2: The second solution, which we call solution #2, was generated from the μ -synthesized controllers specific of seed #7 (see table 1). This case is particularly interesting, since μ -synthesis was executed around the bounded uncertainty $E_{\Delta,2} = [0.05E_0, 1.5E_0]$, yet a probabilistic robust solution, for a random uncertainty set that was much larger than the structured norm-bounded set used for μ -synthesis was found around this seed solution.

Probabilistic robust solution #2 has the same number of controller variables as the μ -synthesized seed solution: K_1 has 148 states and K_2 has 296 states.

For the probabilistic robust solution, the worst case \mathcal{H}_∞ -norm within stable set was -46.23 dB. The expected value of the \mathcal{H}_∞ norm was -46.46 dB.

Both the worst-case performance, as well as the limit on the expected value, are due to our diminished ability to affect the fourth mode in this system. This is due to the fact that this mode exists, approximately, in the uncontrollable subspace for the control input locations that we have chosen.

7.5.4 Random Maximum Singular Value Plots of the Open and Closed Loop Systems

The random maximum singular value plots for each of these solutions are given in figures 48 and 49. Only 100 instances of the random open and closed loop plants were generated for the purpose of generating these figures. These random maximum singular value plots show the effect that the random interconnection uncertainty has on the performance of the plant, and may help with extrapolating the utility of these techniques to real systems and the uncertainty that is seen when test data is generated.

7.5.5 Degradation Functions of the Closed-Loop Systems

Just as was done in chapter 5, degradation functions of the closed loop systems were constructed by building, and evaluating, the systems generated from the interconnection stiffness uncertainty sets:

$$\begin{aligned}\mathcal{B}_\Delta(a) &\doteq \left\{ \mathbf{K}_\Delta \in \mathbb{R}^{4 \times 4} : E_\Delta \sim f_\Delta(a) \right\} \\ f_\Delta(a) &\sim \mathcal{N}(E_0, a0.16E_0^2) \\ a &\in [0, 10]\end{aligned}\tag{7.44}$$

where $a = 1$ corresponds to the value used for controller synthesis using algorithm 4. We refer to this value as the variance inflation factor. Notice that we have not placed any kind of hard-bound on these sets. This is something that is also noted for the case where $a = 1$. In doing so, we include some members of the uncertainty set that:

- Have negative interconnection stiffness values. This type of system can be open-loop unstable depending upon how large the interconnection stiffness is with respect to the system's open-loop ability to dissipate energy. This is a situation where energy is actually entering the system through the interconnection stiffness element, or a situation where the slope of the stress/strain curve of the stiffness element is negative.
- Instances where the interconnections stiffness element is approximately equal to zero will be included.

Random Maximum Singular Value Plot of Open and Closed-Loop Systems, Solution #1

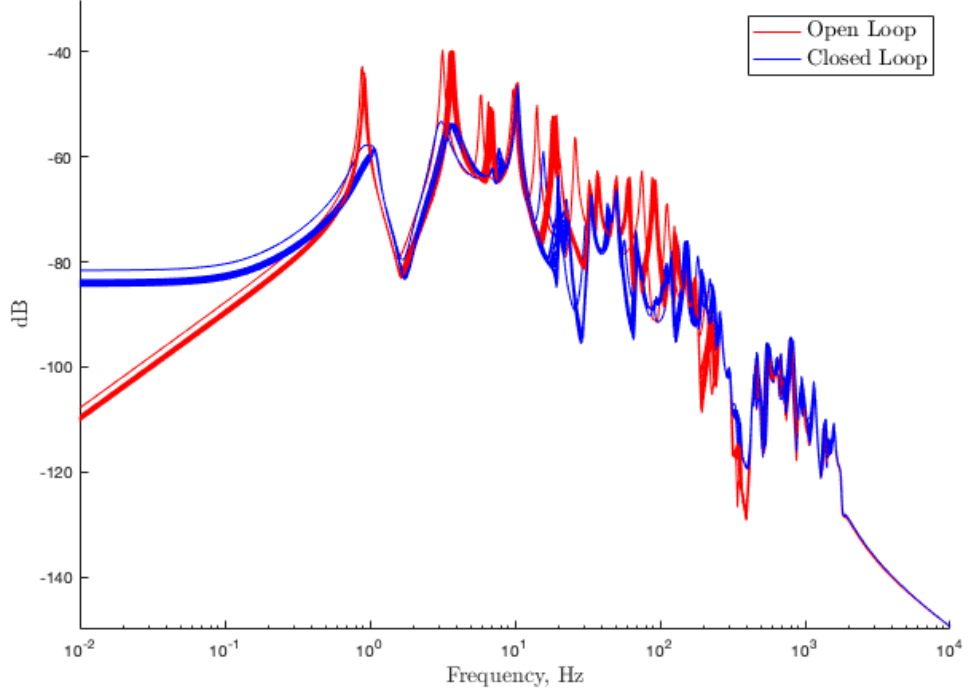


Figure 48: Solution #1, as described in table 4. This random maximum singular value plot was generated for both the open and closed-loop systems, for the first probabilistic robust solution featured in this chapter. Interconnection modulus uncertainty was generated from the distribution $\mathcal{N}(E_0, 0.16E_0^2)$, which was the uncertainty used for synthesis. This probabilistic robust solution was found to maintain stability 99.34% of the time, while maintaining the \mathcal{H}_∞ -norm below our objective of -45.4 dB for 99.34% of the random plants generated by this uncertainty. The equivalence between these probabilistic performance metrics implies that we only failed our performance requirements for those closed-loop plants that were unstable. This solution is probabilistically-robust against the random interconnection uncertainty that was defined for synthesis.

Random Maximum Singular Value Plot of Open and Closed-Loop Systems, Solution #2

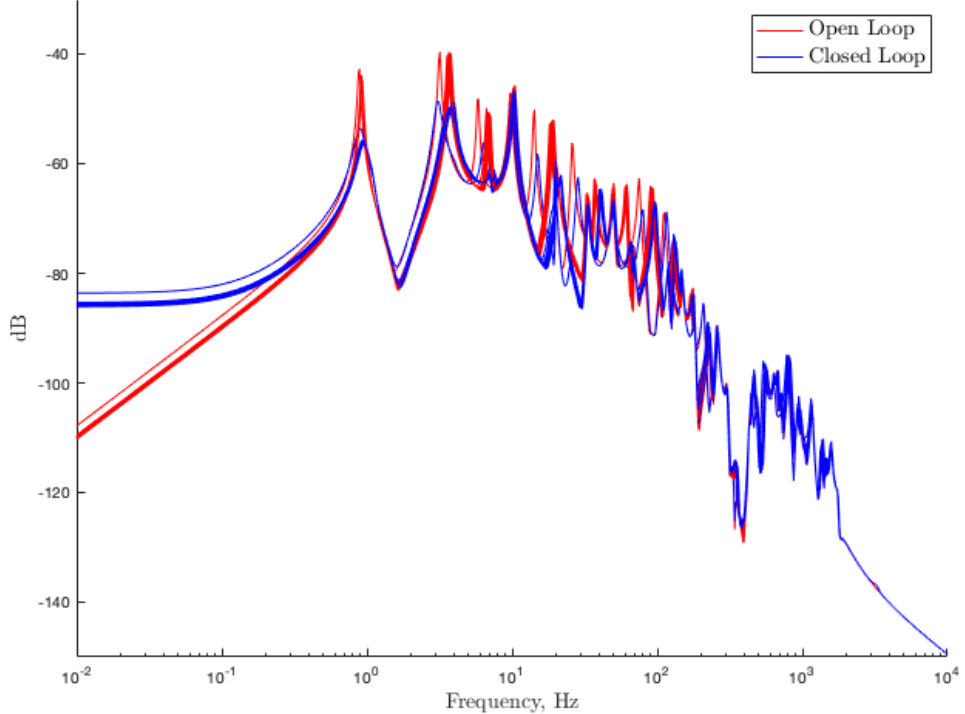


Figure 49: Solution #2, as described in table 4. Interconnection modulus uncertainty was generated from $\mathcal{N}(E_0, 0.16E_0^2)$ for synthesis and analysis. This probabilistic robust solution was found to maintain stability 99.33% of the time, while maintaining the \mathcal{H}_∞ -norm below our objective of -45.4 dB for 99.33% of the random plants generated by this uncertainty. The same insight is realized with respect to the conditional dependence between stability and performance as for solution #1. This solution is probabilistically-robust against the random interconnection uncertainty that was defined for synthesis.

The stability and performance degradation functions were constructed by performing the following calculations as we increased the variance inflation factor, meaning that \mathbf{K}_Δ was generated by the support given by (5.132) as a was increased:

1. Checked for stability by calculating $\hat{\Pr}\left(\operatorname{Re}\left(\lambda(A_{\text{prob}})\right) < 0 \mid \mathbf{K}_\Delta\right)$.
2. Checked for performance by calculating $\hat{\Pr}\left(\|G_{\text{prob}}\|_\infty \leq \gamma^* \mid \mathbf{K}_\Delta\right)$.

These degradation functions for solutions 1 and 2 are shown in figures 50 and 51. The probability estimates that were generated for the construction of these degradation functions is included in appendix G.

7.5.6 On Calculation of Probabilistic Robust Stability and Performance Margins

In a manner congruent with our approach to defining probabilistic stability and performance margins in chapter 5, we can do the same for these solutions. Since this concept was covered earlier, we will not do this, here. Meeting some prescribed margins for probabilistic stability and performance, with respect to variance inflation factors, was not defined/prescribed as a measure of success in this technique. All insights developed for this concept in chapter 5 can be transferred and applied to these results.

7.5.7 A Special Case: No Interconnection Stiffness Element

One special case is examined as we conclude this chapter: the case where no interconnection stiffness element is present. This is a situation where the boundary conditions of our structures are drastically different, leading to two cantilevered beams, as opposed to a clamped-clamped, decentrally-controlled beam configuration. Finding decentralized controllers that can achieve stability good performance both in a coupled and uncoupled configuration was a goal of Lim, Babuska, Craig, Su, Young, Siljak, and many others that work in the area of decentralized structural control, and decentralized control, generally [6, 7, 20, 21, 9]. Using the approaches detailed in this current chapter, as well as chapter 6, both solutions 1 and 2

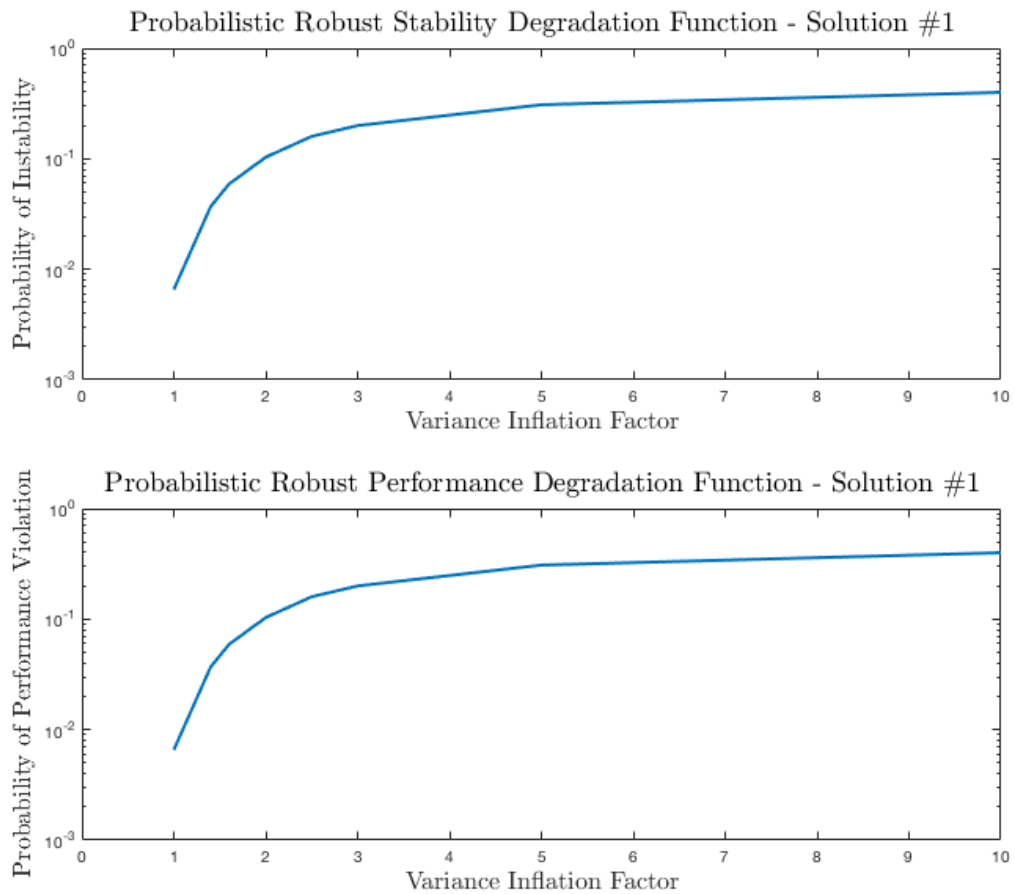


Figure 50: Solution 1 degradation functions. The data that was used to construct this function is included in appendix G. These results show that if the system is stable it almost always meets the performance specification for the systems used in this research.

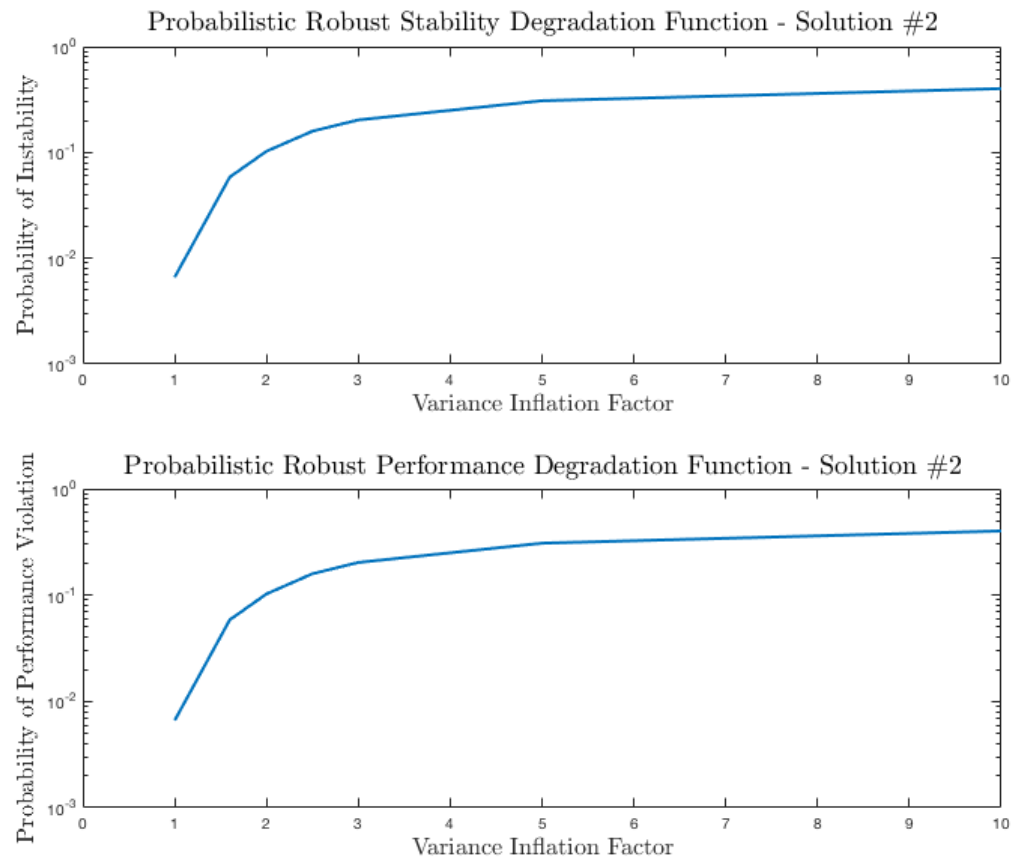


Figure 51: Solution 2 degradation functions. The data that was used to construct this function is included in appendix G.

remain stable when the substructures are completely decoupled. For the case where $\mathbf{K}_\Delta = 0$, we can call the resulting system configuration originally given by (7.6), $G_{\text{uncoupled}}$. We find that

- Solution 1 — $\|G_{\text{uncoupled}}\|_\infty = -45.34 \text{ dB}$
- Solution 2 — $\|G_{\text{uncoupled}}\|_\infty = -32.09 \text{ dB}$

which shows that solution 1 barely misses our originally-prescribed performance objective, with $\gamma^* = -45.4 \text{ dB}$. This result was somewhat expected for this synthesis process. By using $E_\Delta \sim \mathcal{N}(E_0, 0.16E_0^2)$ as the distribution that characterized the interconnection modulus, we are likely to sample random instances of the plant that have close to zero, or slightly negative, interconnection stiffness matrices. Therefore, the (almost) decoupled cases were accounted for during synthesis, leading to this result. In chapter 2, we discussed strongly-coupled systems in decentralized control. Due to the intrinsic strength of the interconnections in structures, we almost always find ourselves dealing with what can be considered a strongly coupled system. Synthesis of decentralized controllers for strongly coupled systems reduces to developing, or applying, decentralized control synthesis strategies that account for the neighboring subsystem's dynamics. In this manner, controller synthesis for strongly coupled systems is really a co-synthesis strategy. Early researchers in decentralized structural control did not initially approach controller synthesis in this manner, leading to decentralized controllers that led to the inability to meet performance requirements, or worse — instability of the superstructure.

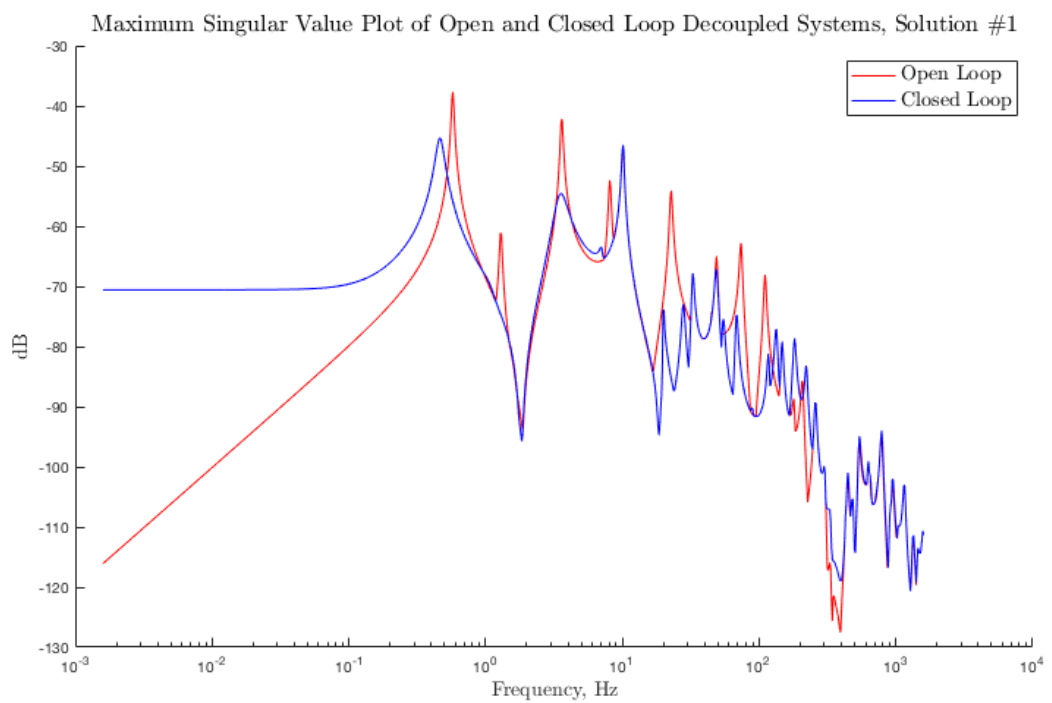


Figure 52: Maximum Singular Value Plot of Uncoupled, Open and Closed-Loop Systems — Solution #1.

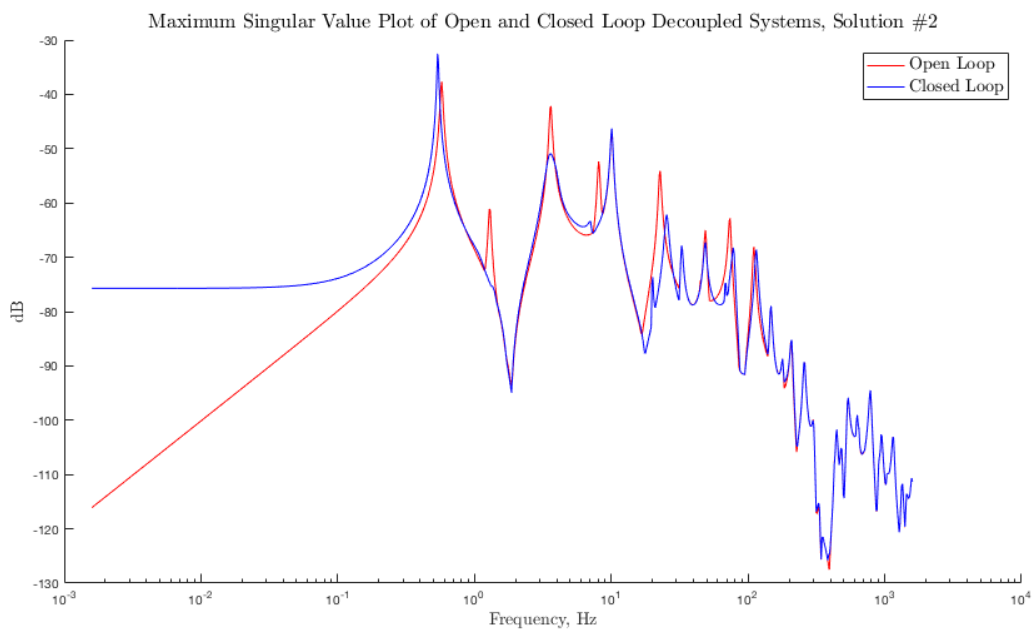


Figure 53: Maximum Singular Value Plot of Uncoupled, Open and Closed-Loop Systems — Solution #2.

7.6 CHAPTER SUMMARY

In this chapter, we have discussed the following:

1. Stochastic optimization using genetic algorithms, including the algorithms and probability theory that is used for solving the controller synthesis problem in this research.
2. Probabilistic decentralized dynamic output feedback controller synthesis for structures coupled by a random interconnection element, which included approaches for:
 - Cost function construction, including a discussion on computational cost/complexity and how parallel computing makes these high-dimensional problems tractable.
 - Controller synthesis in complex modal coordinates, which leads to a significant reduction in the optimization variables in this problem.
3. Discussion of the results obtained using this new approach to decentralized controller synthesis. Several probabilistic robust, decentralized, dynamic output feedback controllers were successfully synthesized that attenuated the \mathcal{H}_∞ -norm of the structure below the prescribed level γ^* with probability greater than the $1 - \epsilon_p$ determined in chapter 4. Two of the solutions that were found were highlighted.

We showed in this chapter by using seed results from loop-at-a-time μ -synthesis via D/K iterations and subsequently by constructing cost functions that balance performance requirements and computational complexity for high-order system, that it is possible to find probabilistic robust, decentralized dynamic output feedback controllers for lightly-damped structures possessing random interconnection uncertainty. The results reported in this research show promise in these techniques, revealing that probabilistic solutions were found in as little as 1200 CPU hours. Since stochastic optimization using genetic algorithms is a parallelizable process, it is certainly feasible for larger problems to be tackled using these approaches. In this research, solution 1 was found after 50 hours on a 24-core machine. In addition to being able to attempt larger controller synthesis problems for higher-order structures/controllers, additional performance requirements can be included during synthesis that may be of importance to the designer. This approach is not limited to only using

the \mathcal{H}_∞ -norm as a performance metric. However, the controller basis must be chosen to be different if time-domain performance requirements are to be included.

8.0 CONCLUSIONS AND FUTURE WORK

The overarching goal of this research was to develop novel, probabilistic-robust decentralized active vibration control strategies for structures possessing random interconnection uncertainty. This research was accomplished by meeting the following objectives:

1. Evaluate stability and performance of a composite controlled structure possessing probabilistic interconnection uncertainty.
2. Achieve structural controller performance requirements when controlled substructures are joined in the presence of interconnection uncertainty.
3. Calculate probabilistic stability and performance margins.

All three of these objectives have been met for controller design, and the associated models, for the full-state and dynamic output feedback control design and synthesis approaches that were developed in this research.

This research developed probabilistic decentralized active vibration control design and synthesis techniques for structures possessing random parametric uncertainty. The uncertainty and complexity of the structures studied in this thesis were concentrated at the point where two portions of a structure adjoin — the structural interconnection. This uncertainty was characterized using random variables. Control design and synthesis approaches that enforce decentralized controller architectures, while accounting for random uncertainty at structural interconnections, were developed for the following canonical control cases:

1. Static full-state feedback control;
2. Dynamic output feedback control.

Control objectives involved achieving some level of stability and performance in probability. The performance objectives in this thesis involved two things, that are not completely exclusive of one another: 1) the attenuation of \mathcal{H}_∞ -norm mapping the disturbance inputs to performance outputs, and 2) attenuation of low-frequency vibration modes. Ancillary to these stability and performance objectives was the development of analysis tools that enable the designer to evaluate the robust stability and robust performance of the synthesized controllers, given that the plant uncertainty is random.

Chapter 5 showed how we can design and synthesize a decentralized, full-state feedback \mathcal{H}_∞ -controller for a lightly damped system with random interconnection uncertainty by solving a high-dimensional, structure-constrained semidefinite program with linear matrix inequality constraints. We also showed that the performance output function for this controller can be designed in complex modal coordinates, and showed that the resulting controller will be real. This approach does not require the designer to make any simplifying assumptions about the damping models used for the system under consideration. Each LMI constraint in this high-dimensional semidefinite program represents a random instance of the uncertain plant under consideration. The resulting controller design approach allows the designer to account for random uncertainty, perform control design in complex modal coordinates, and enforce a decentralized controller structure. If a controller exists, it is guaranteed to meet \mathcal{H}_∞ -norm performance requirements with a priori guarantees that this controller will meet the performance specification with a certain probability and confidence in this probability.

Chapter 6 showed how we can use loop-at-a-time μ -synthesis via D/K iterations to synthesize decentralized robust controllers, where these controllers are robust against some prescribed structured norm-bounded parametric uncertainty in the interconnection stiffness matrix. By virtue of how μ -synthesis via D/K iterations works, and provided the structured singular value is less than 1, we are able to assemble collections of controllers as a result of, and during, the D/K iteration process. These controllers share a common trait — they are robust against the uncertainty that we have modeled. μ -synthesis via D/K iterations is a non-convex controller synthesis strategy that has no guarantee of being globally optimal.

Nevertheless, the D/K iteration process is capable of assembling robust solutions. We then show how we can exploit both the sub-optimality and robustness of the collection of solutions found using μ -synthesis via D/K iterations. These solutions are then used as seed solutions in a high-order stochastic optimization problem in chapter 7 as we develop a technique for synthesizing probabilistic robust decentralized dynamic output feedback controllers.

Chapter 7 developed an approach for synthesizing decentralized controllers that are robust against random interconnection stiffness element uncertainty and attenuate the \mathcal{H}_∞ -norm of the disturbance input to performance output mapping below a level that was at least 6 dB less than the approximate worst-case \mathcal{H}_∞ -norm of the open-loop plant. The approach in chapter 7 exploited properties specific to lightly-damped structures, and accounted for the computational complexity associated with certain approaches to cost function construction. The results indicate that the techniques developed in that chapter can be used with systems and controllers possessing even more variables and that the resulting controllers can be used in a subsequent optimization that incorporates additional constraints. Two of the results from this approach were highlighted, where each decentralized controller pair achieved the following stability and performance objectives over 99% of the time for specified levels of accuracy and confidence:

$$\begin{aligned} \text{Probability of Stability} & \quad \hat{\Pr}\left(\operatorname{Re}\left(\lambda(A_{\text{prob}})\right) < 0 \mid \mathbf{K}_\Delta\right) \geq 0.99 \\ \text{Probability of Performance} & \quad \hat{\Pr}\left(\|G_{\text{prob}}\|_\infty \leq \gamma^* \mid \mathbf{K}_\Delta\right) \geq 0.99. \end{aligned}$$

where $\gamma^* = -45.4$ dB, G_{prob} corresponds to the disturbance input/performance output for the structure, and \mathbf{K}_Δ represents the random interconnection stiffness element that was modeled, with uncertainty in the elastic modulus of this element characterized by $E_\Delta \sim \mathcal{N}(E_0, 0.16E_0^2)$ for synthesis. These probability estimates were generated with 95% confidence that these estimates are within 0.01 of their true probabilities.

8.1 SUMMARY OF CONTRIBUTIONS

This thesis provides the following contributions to the areas of control theory and active vibration control:

1. Treating the interconnection terms randomly and coupling decentrally-controlled substructures in a generalized regulator framework is new.
2. A method for performing robust stability and performance tests and the definition and calculation of margins for controlled structures coupled by a probabilistically-uncertain interface stiffness matrix.
3. A controller design and synthesis approach that permits frequency-weighting of system models via complex-valued performance output functions and synthesis of a structure-constrained high-dimensional semidefinite program for achieving decentralized full-state feedback \mathcal{H}_∞ control in the presence of random interconnections.
4. A controller design and synthesis approach that permits frequency-weighting of system models, synthesis of robust controllers using loop-at-a-time μ -synthesis via D/K iterations for the structured norm-bounded interconnection uncertainty case, and subsequent solution of stochastic optimization problems around the μ -synthesized solutions. This stochastic optimization problem is pursued after imposing an Gaussian distribution over the interconnection uncertainty, and is performed explicitly over the real and complex-parts of the μ -synthesized controllers for computational efficiency.
5. Application of these control approaches to lightly-damped, low and high-dimensional structure models.

8.2 FUTURE DIRECTIONS FOR PROBABILISTIC DECENTRALIZED ACTIVE VIBRATION CONTROL

This research sets the stage for extending these techniques to the more complicated case of including random uncertainty not only in the interconnections, but also in the substructures themselves.

Using the techniques developed in this thesis, the interconnection uncertainty between two substructures can also be represented as a random dynamic system and not just a random interconnection stiffness element. Doing so would require the loop-at-a-time formulations to change slightly, and the system used for probabilistic robust synthesis in chapter 7 would look a bit different since the random interconnection system would introduce additional state variables into the model. Nevertheless, seed controllers can be found using the loop-at-a-time μ -synthesis approach in chapter 6 and the high-dimensional stochastic optimization problem in chapter 7 can be posed in a very similar way. This problem would be a logical next step in this research.

The techniques that were developed in this research are applied to a class of problems that is generally linear. However, the control design and synthesis strategies developed in this research can be applied to many other classes of problems. For example, these probabilistic decentralized control design and synthesis techniques can be applied to uncertain systems that are linear parameter varying and nonlinear. Linear parameter varying and nonlinear control problems have been approached using probabilistic robust control techniques, but only in applications where centralized controllers were synthesized [39, 14]. Extending the techniques to be developed in this research to linear parameter varying and nonlinear systems — that are both large scale and may require decentralized control schemes — will not only be possible but can represent next steps in this research program. Some example applications that have received significant attention in the area decentralized control are:

- Swarms and coordinated unmanned aerial and underwater vehicles
- Power systems and smart grids

- Financial systems and markets

Decentralized control problems in these areas share a common problem: how to handle uncertainty in large scale system interconnections. The techniques developed in this research deliver some tools that enable the incorporation of random interconnection matrices into the analysis and control of large scale systems in many fields.

There are several other aspects to this present research that can be both enhanced and extended. The approaches developed in chapter 7 can be enhanced by enabling cross-node communication on a supercomputer, enabling optimization to be performed more efficiently, across a larger solution space, and also while sharing solution information that is developed within disparate populations. Along these lines, developing an approach that enables the optimization to dynamically change the order of the controllers, along with an analytical approach to enabling complex conjugate solution points to combine to form purely-real solutions, and vice versa, would enhance the adaptability of this algorithm and therefore unlock an even larger solution space.

This research does not provide the “silver bullet” that allows us to control a system that has an infinite amount of uncertainty, or one that experiences significant discontinuities in its dynamics. Developing gain-scheduled or other adaptive schemes that enable transitions across a continuum of probabilistic robust controllers, in a smooth manner, is a goal that can be investigated next. One set of controllers can only be pushed so far — this is evidenced by the definition and analysis of probabilistic margins via degradation functions in chapters 5 and 7. These approaches should next be used in a more adaptive manner so that structures that

- possess even greater amounts of uncertainty;
- have discontinuities or highly-nonlinear behavior in their dynamics;
- require different control objectives in different operating regimes,

can be controlled in the most safe and effective manners possible.

These approaches must be tested in a laboratory setting. There is no substitution for actually putting these controllers to the test on real structures and for using data and models

derived from real structures. Along this same thread, the field of tribomechadynamics, which studies the dynamics of structural interconnections can provide valuable input to the approaches developed in this thesis [8].

APPENDIX A

FULL STATE FEEDBACK MODEL

We consider the general model shown in figure 54, which depicts a four-mass system that is coupled by some spring k_Δ , with the subscript Δ indicating that this spring is an uncertain element. This system has disturbance inputs w_1, w_2 and control inputs u_1, u_2 entering the system in the locations shown.

One thing that will become important when we get into discussing controller objectives and design is the fact that there is no dissipative element included between masses 2 and 3. By modeling the system in this way, we cannot have proportional damping. This model structure leads to a situation where the eigenvectors of the dynamics matrix for this system will be complex.

The open-loop, second-order dynamics equations for the spring-mass-damper model is

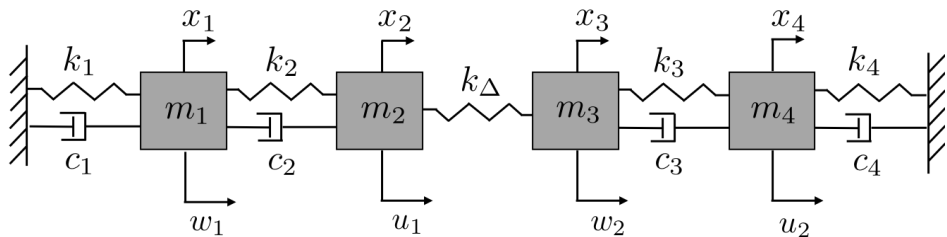


Figure 54: Spring mass damper model with random interconnection stiffness.

given by

$$M\ddot{x} + C\dot{x} + Kx = P_1w + P_2u \quad (\text{A.1})$$

where

- \ddot{x}, \dot{x}, x are the acceleration, velocity, and displacement of each mass;
- M, C, K are the mass, damping, and stiffness matrices;
- P_1, P_2 describe where disturbance and control inputs enter the system, respectively.

A.1 SYSTEM MATRICES AND PARAMETER VALUES

For the system depicted in figure 54, the system parameters are given by:

$$M = \begin{bmatrix} m_1 & 0 & 0 & 0 \\ 0 & m_2 & 0 & 0 \\ 0 & 0 & m_3 & 0 \\ 0 & 0 & 0 & m_4 \end{bmatrix}, \quad C = \begin{bmatrix} c_1 + c_2 & -c_2 & 0 & 0 \\ -c_2 & c_2 & 0 & 0 \\ 0 & 0 & c_3 & -c_3 \\ 0 & 0 & -c_3 & c_3 + c_4 \end{bmatrix} \quad (\text{A.2})$$

$$K = K_0 + K_\Delta \quad (\text{A.3})$$

with

$$K_0 = \begin{bmatrix} k_1 + k_2 & -k_2 & 0 & 0 \\ -k_2 & k_2 & 0 & 0 \\ 0 & 0 & k_3 & -k_3 \\ 0 & 0 & -k_3 & k_3 + k_4 \end{bmatrix}, \quad K_\Delta = \begin{bmatrix} 0 & 0 & 0 & 0 \\ 0 & k_\Delta & -k_\Delta & 0 \\ 0 & -k_\Delta & k_\Delta & 0 \\ 0 & 0 & 0 & 0 \end{bmatrix}. \quad (\text{A.4})$$

The parameters were chosen by defining $m_1 = m_2 = m_3 = m_4 = 1$; $k_1 = k_2 = 100$; $k_3 = k_4 = 150$; and the nominal value for $k_\Delta = 100$. The damping matrix was formed by

$$C = \alpha M + \beta K_0 \quad (\text{A.5})$$

where $\alpha = 10^{-3}$, $\beta = 4 \times 10^{-3}$, which were constants chosen to promote a lightly-damped system; in defining (A.5), this lightly-damped system does not have proportional damping,

which is an intentional choice. Forces enter the system by the matrices P_1 and P_2 :

$$P_1 = \begin{bmatrix} 1 & 0 \\ 0 & 0 \\ 0 & 1 \\ 0 & 0 \end{bmatrix}, \quad P_2 = \begin{bmatrix} 0 & 0 \\ 1 & 0 \\ 0 & 0 \\ 0 & 1 \end{bmatrix} \quad (\text{A.6})$$

which says that disturbances enter masses 1 and 3, with control inputs entering masses 2 and 4.

For k_Δ , we have chosen that the uncertainty be normally-distributed with mean of 100 and standard deviation of 15: $k_\Delta \sim \mathcal{N}(100, 15^2)$.

APPENDIX B

DYNAMIC OUTPUT FEEDBACK MODEL

The structural model in this chapter is derived using elementary finite element analysis/structural dynamic theory, as this is the tool most frequently used to generate complicated structural dynamic models. We are able to treat certain system parameters as being random variables. Specifically, we can account for geometric nonlinearities (length, area moment of inertia in a generalized beam model) and material anisotropies and uncertainty directly and on an elemental basis (elastic modulus, mass density). Only the elastic modulus of an interconnecting element is treated as having random uncertainty. We will only consider transverse (bending) deflection in this model.

A uniform beam of length L_b , mass density ρ , modulus E , cross sectional area A , and area moment of inertia I is depicted in figure 55. This beam will be the subject of control design and analysis in chapters 6 and 7. Also shown in the top of figure 55 are measurements (y_i 's), control inputs, u , and disturbance inputs, w . As discussed in chapter 4, we want to synthesize controllers — in the presence of random interconnection uncertainty — that attenuate, below some prescribed level, the \mathcal{H}_∞ -norm of the mapping between the disturbance inputs w 's and performance outputs, which will be later on denoted by the vector z .

We will now get into discussing how the open loop system was modeled in this portion of the research. We will then discuss what our control objectives are and how the controller synthesis problem is posed.

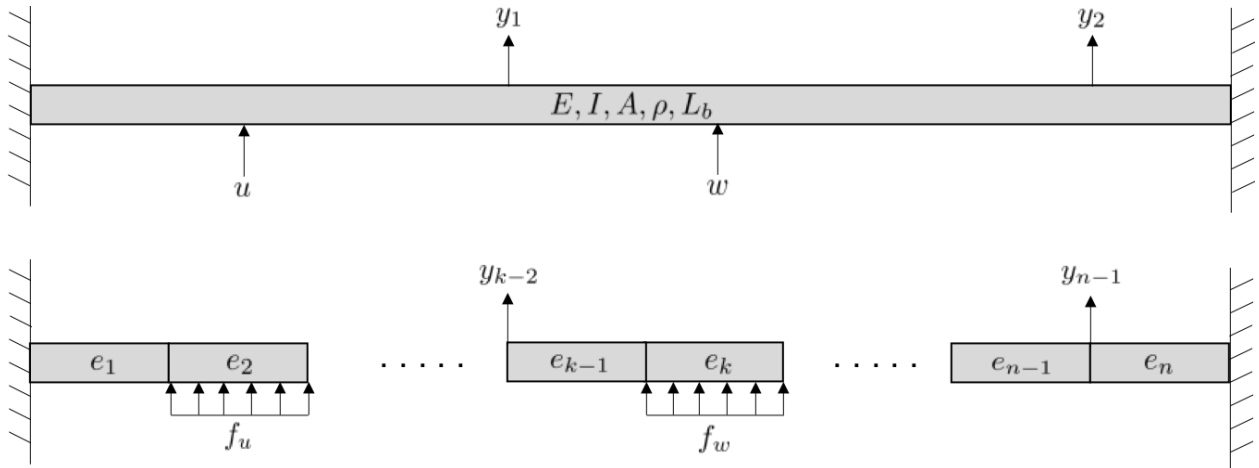


Figure 55: Beam model.

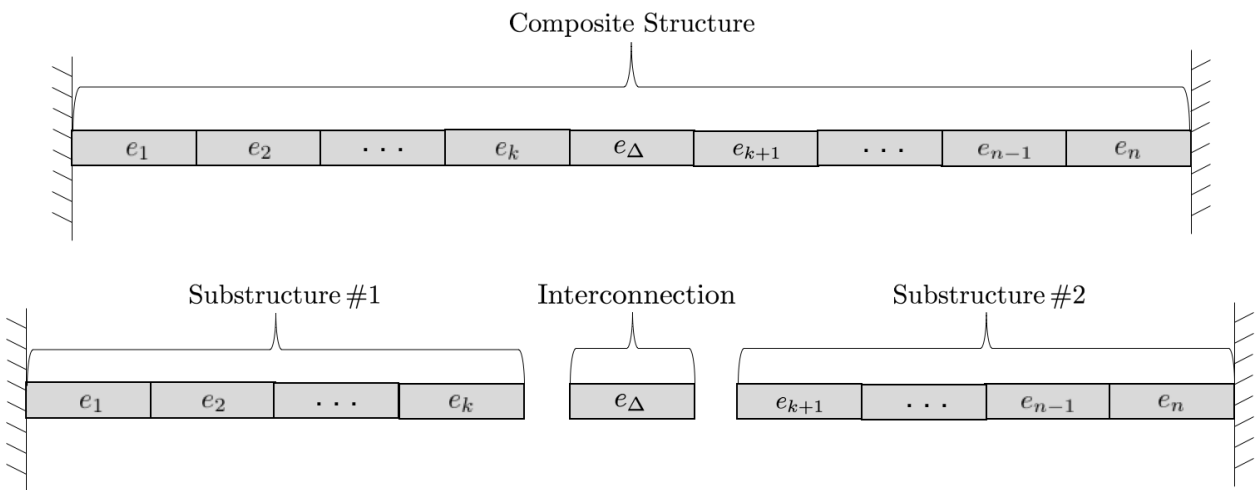


Figure 56: Composite structure decomposed into substructures with uncertain interconnection element.

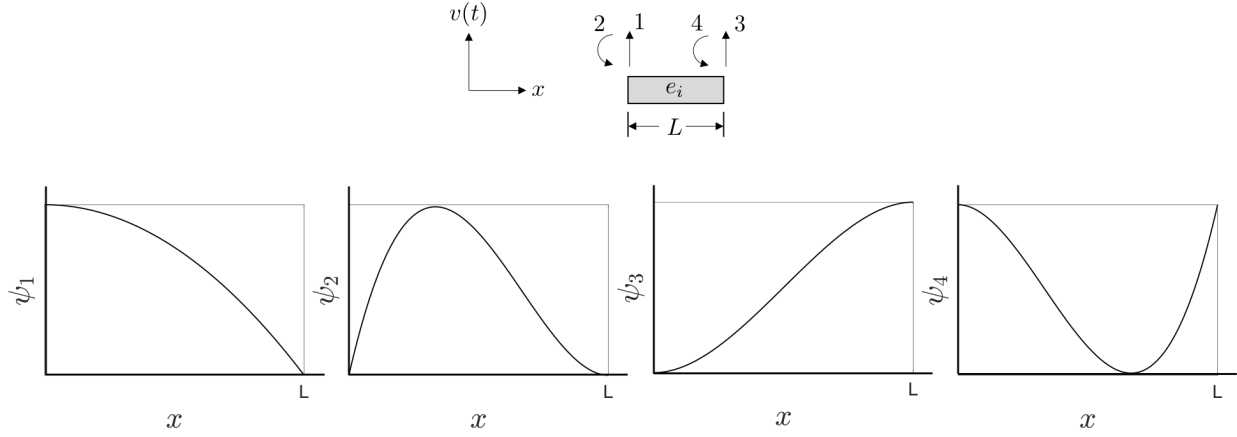


Figure 57: A single finite element statically loaded by forces and moments at ends, with associated elemental shape functions.

We consider a single finite element that is statically loaded at its ends by moments and shears, as shown in figure 57. Each element has some mass density (ρ), elastic modulus (E), cross sectional area (A_{el}), area moment of inertia (I), and length (L) associated with it. The displacement coordinates for transverse motion in a uniform beam can be described by

$$v(x, t) = \sum_{i=1}^4 \psi_i(x) v_i(t) \quad (\text{B.1})$$

with the general solution to (B.1) for a uniform beam being a cubic polynomial, which is given by

$$v(x) = c_1 + c_2 \left(\frac{x}{L} \right) + c_3 \left(\frac{x}{L} \right)^2 + c_4 \left(\frac{x}{L} \right)^3. \quad (\text{B.2})$$

Through considering a uniform beam statically loaded at its ends by moments and shears, we can posit that this element is producing static deflection shapes, ψ_i , such that the shape functions satisfy

$$\psi_1(0) = \psi_3(L) = \frac{d}{dx} \psi_2(0) = \frac{d}{dx} \psi_4(L) = 1 \quad (\text{B.3})$$

$$\text{All other B.C.'s and derivatives} = 0 \quad (\text{B.4})$$

We can obtain the shape functions $\psi_i, i = 1, 2, 3, 4$ using these boundary conditions and (B.2) to find

$$\psi_1 = 1 - 3\left(\frac{x}{L}\right)^2 + 2\left(\frac{x}{L}\right)^3 \quad (\text{B.5})$$

$$\psi_2 = x - 2L\left(\frac{x}{L}\right)^2 + L\left(\frac{x}{L}\right)^3 \quad (\text{B.6})$$

$$\psi_3 = 3\left(\frac{x}{L}\right)^2 - 2\left(\frac{x}{L}\right)^3 \quad (\text{B.7})$$

$$\psi_4 = -L\left(\frac{x}{L}\right)^2 + L\left(\frac{x}{L}\right)^3 \quad (\text{B.8})$$

with these shape functions sketched in figure 57. We then find the mass and stiffness matrices (m_{ij}, k_{ij}) and load vector (p_i) from

$$m_{ij} = \int_0^L \rho A_{el} \psi_i \psi_j dx, \quad k_{ij} = \int_0^L EI \frac{d^2 \psi_i}{dx^2} \frac{d^2 \psi_j}{dx^2} dx, \quad p_i = \int_0^L p(x, t) \psi_i dx \quad (\text{B.9})$$

where we find that the symmetric mass and stiffness matrices are expressed by

$$\mathbf{m}_e = \left(\frac{\rho AL}{420} \right) \begin{bmatrix} 156 & 22L & 54 & -13L \\ * & 4L^2 & -13L & -3L^2 \\ * & * & 156 & -22L \\ * & * & * & 4L^2 \end{bmatrix}, \quad \mathbf{k}_e = \left(\frac{EI}{L^3} \right) \begin{bmatrix} 12 & 6L & -12 & 6L \\ * & 4L^2 & -6L & 2L^2 \\ * & * & 12 & -6L \\ * & * & * & 4L^2 \end{bmatrix} \quad (\text{B.10})$$

and that the disturbance and control input influence vectors are described by

$$\mathbf{p}_{er} = f_r \begin{bmatrix} \frac{L}{2} & \frac{L^2}{12} & \frac{L}{2} & -\frac{L^2}{12} \end{bmatrix}^T \quad r = u, w \quad (\text{B.11})$$

where the subscript, r , indicates that the input influence vectors are specific to either a control input or disturbance input to the system. These mass and stiffness matrices are applicable to uniform beam elements that are statically loaded by shear and moment loads at their ends.

We use the well-known ‘‘Direct Stiffness’’ method for assembling element matrices [88]. This technique involves enforcing compatibility at the element interfaces. By doing so, element local coordinates are mapped into global coordinates through a binary transformation matrix L_e such that

$$\hat{\xi}_e = L_e \Xi \quad (\text{B.12})$$

where $\hat{\xi}_e$ corresponds to elemental coordinates and Ξ are global coordinates. In figure 57, this equates to enforcing that the displacements and rotations are equal to those at the adjoining element.

Each element matrix \mathbf{m}_e or \mathbf{k}_e is then placed into the global structure coordinate system by

$$\mathbf{K}_e = L_e^T \mathbf{k}_e L_e, \quad \mathbf{M}_e = L_e^T \mathbf{m}_e L_e \quad (\text{B.13})$$

where each binary transformation matrix L_e is specific to each element mapping into the global coordinate system. The global mass and stiffness matrices are then given by

$$\mathbf{K}_g = \sum_{e=1}^{N_e} \mathbf{K}_e, \quad \mathbf{M}_g = \sum_{e=1}^{N_e} \mathbf{M}_e. \quad (\text{B.14})$$

By a very similar convention, the global input force vectors are given by

$$\mathbf{P}_{ug} = \sum_{e=1}^{N_e} L_e^T \mathbf{p}_{ue}, \quad \mathbf{P}_{wg} = \sum_{e=1}^{N_e} L_e^T \mathbf{p}_{we} \quad (\text{B.15})$$

where the binary locator matrices are chosen for those elements that are affected by either a control input or disturbance. Constraints are enforced by simply eliminating the degrees of freedom at the extreme ends of the model. See “Structural Dynamics: An Introduction to Computer Methods” by Craig for details [88].

We have now arrived at an undamped structural dynamic model derived from finite element analysis:

$$\mathbf{M}_g \ddot{\xi} + \mathbf{K}_g \xi = \mathbf{P}_{ug} \mathbf{f}_u + \mathbf{P}_{wg} \mathbf{f}_w. \quad (\text{B.16})$$

We have assumed that modal damping exists. Given that there are N_e elements and we consider only transverse vibration, we will have $\frac{N_e}{2}$ modes. Thus, we solve the generalized eigenvalue problem given by

$$(\mathbf{K}_g - \omega_r^2 \mathbf{M}_g) \phi_r = 0, \quad r = 1, 2, \dots, \frac{N_e}{2} \quad (\text{B.17})$$

for each structure mode. We assemble the modal matrix by

$$\Phi = \begin{bmatrix} \phi_1 & \phi_2 & \dots & \phi_{N_e/2} \end{bmatrix}. \quad (\text{B.18})$$

Furthermore, we mass-normalize these eigenvectors such that $\Phi^T \mathbf{M}_g \Phi = I$. We also assume that all modes are orthogonal. In order to add damping to each mode that looks like

$$\mathcal{C} = \Phi^T \mathbf{C}_g \Phi = \text{diag}(2\zeta_r \omega_r M_r), \quad r = 1, \dots, \frac{N_e}{2} \quad (\text{B.19})$$

where ζ_r is some prescribed amount of damping, ω_r is the frequency of each mode, and M_r is the modal mass (which is unity), we must find a way to transform a damping matrix \mathcal{C} back into physical coordinates \mathbf{C}_g . We have chosen to add 2% damping to each mode when creating this model.

To do this, and as is typical in any elementary problem such as this one, we recognize that our eigenvector matrix Φ serves as a new basis

$$\xi(t) = \Phi \eta(t) \quad (\text{B.20})$$

such that

$$\mathcal{M} \ddot{\eta} + \mathcal{C} \dot{\eta} + \mathcal{K} \eta = \mathcal{P}_u \mathbf{f}_u + \mathcal{P}_w \mathbf{f}_w \quad (\text{B.21})$$

where

$$\mathcal{M} = \Phi^T \mathbf{M}_g \Phi, \quad \mathcal{C} = \Phi^T \mathbf{C}_g \Phi, \quad \mathcal{K} = \Phi^T \mathbf{K}_g \Phi, \quad \mathcal{P}_u = \Phi^T \mathbf{P}_{ug}, \quad \mathcal{P}_w = \Phi^T \mathbf{P}_{wg}. \quad (\text{B.22})$$

Recognizing once again that our objective is to add damping to each mode in this model, we follow through with the elementary transformation that will bring (B.19) into physical coordinates. Since

$$\mathcal{C} = \Phi^T \mathbf{C}_g \Phi, \quad (\text{B.23})$$

we have that

$$\mathbf{C}_g = \Phi^{-T} \mathcal{C} \Phi^{-1}. \quad (\text{B.24})$$

An expression for Φ^{-1} can be developed from the orthogonality property of the modes

by

$$\mathcal{M} = \Phi^T \mathbf{M}_g \Phi \quad (\text{B.25})$$

$$I = \mathcal{M}^{-1} \mathcal{M} = (\mathcal{M}^{-1} \Phi^T \mathbf{M}_g) \Phi = \Phi^{-1} \Phi \quad (\text{B.26})$$

$$\Phi^{-1} = (\mathcal{M}^{-1} \Phi^T \mathbf{M}_g) \quad (\text{B.27})$$

which leads to

$$\mathbf{C}_g = (\mathbf{M}_g \Phi \mathcal{M}^{-1}) \mathcal{C} (\mathcal{M}^{-1} \Phi^T \mathbf{M}_g). \quad (\text{B.28})$$

Finally, the damped structural dynamic model, in physical coordinates, is given by

$$\mathbf{M}_g \ddot{\xi} + \mathbf{C}_g \dot{\xi} + \mathbf{K}_g \xi = \mathbf{P}_{ug} \mathbf{f}_u + \mathbf{P}_{wg} \mathbf{f}_w. \quad (\text{B.29})$$

We furthermore suppose that we are able to measure the displacement and velocity of the structure at specific locations along this structure. An output/measurement equation of the form

$$y = \begin{bmatrix} \mathbf{C}_d & 0 \\ 0 & \mathbf{C}_v \end{bmatrix} \begin{bmatrix} \xi \\ \dot{\xi} \end{bmatrix} \quad (\text{B.30})$$

is defined. We assume that we are only able to measure transverse displacements and velocities, and not rotations. This is reflected in the construction of \mathbf{C}_d and \mathbf{C}_v . At this point, we can identify the open loop, damped dynamics model by equations (B.29) and (B.30).

By defining a state vector, $x = [\xi \ \dot{\xi}]^T$, we can transform these equations into their equivalent state space representation

$$\dot{x} = \begin{bmatrix} 0 & I \\ -\mathbf{M}_g^{-1} \mathbf{K}_g & -\mathbf{M}_g^{-1} \mathbf{C}_g \end{bmatrix} x + \begin{bmatrix} 0 \\ \mathbf{M}_g^{-1} \mathbf{P}_{wg} \end{bmatrix} \mathbf{f}_w + \begin{bmatrix} 0 \\ \mathbf{M}_g^{-1} \mathbf{P}_{ug} \end{bmatrix} \mathbf{f}_u \quad (\text{B.31})$$

$$y = \begin{bmatrix} \mathbf{C}_d & 0 \\ 0 & \mathbf{C}_v \end{bmatrix} x. \quad (\text{B.32})$$

The state space system matrices are given by

$$A = \begin{bmatrix} 0 & I \\ -\mathbf{M}_g^{-1}\mathbf{K}_g & -\mathbf{M}_g^{-1}\mathbf{C}_g \end{bmatrix}, \quad B_1 = \begin{bmatrix} 0 \\ \mathbf{M}_g^{-1}\mathbf{P}_{wg} \end{bmatrix}, \quad B_2 = \begin{bmatrix} 0 \\ \mathbf{M}_g^{-1}\mathbf{P}_{ug} \end{bmatrix}, \quad (\text{B.33})$$

$$C_2 = \begin{bmatrix} \mathbf{C}_d & 0 \\ 0 & \mathbf{C}_v \end{bmatrix}. \quad (\text{B.34})$$

The disturbance input force vector, $\mathbf{f}_w \rightarrow w$ and the control input force vector $\mathbf{f}_u \rightarrow u$, arriving at the form:

$$\dot{x} = Ax + B_1w + B_2u \quad (\text{B.35})$$

$$y = C_2x. \quad (\text{B.36})$$

The process for constructing these beam models is performed twice: we formulate two cantilevered beams, independent of one another and with slightly different model parameters, and thereafter couple these cantilevered beams through an interface stiffness element to formulate the composite, fixed-fixed beam structure. The beams, and interface stiffness element, have the model parameters shown in table 6. We note that the bandwidth that is included in the beam models is controlled by the size of the elements used. The number of elements was chosen so that a reasonably high number of modes would be included for modeling and controller synthesis. This choice was made primarily for the purpose of generating models that are considered to be high-order in control theory.

In addition, the code that was written for beam and interconnection stiffness element creation can also accept inputs related to disturbance input, control input, and measurement locations. Of course, arbitrary selection of these locations will inevitably place certain modes into the uncontrollable or unobservable subspaces of the system, making it impossible to sense/control certain system modes. Nevertheless, the chosen input/measurement locations are shown in table 7. Although these parameters may be vector-valued (which is permitted by the code created for this step in the research), we have posed a single-input multi-output controller architecture *for each beam*.

Table 6: Input data for finite element Euler-Bernoulli beam and element creation.

Beam Data			
	Beam #1	Beam #2	Interconnection Element
Mass density (ρ), kg/cm ³	7.8	7.8	7.8
Elastic modulus (E), Pa	200×10^9	200×10^9	200×10^9
# Elements	10	15	1
Total length (L), cm	100	150	10
Element width (b), cm	5	5	5
Element height (h), cm	.5	.5	.5
Boundary conditions	Fixed-free	Fixed-free	Free-free

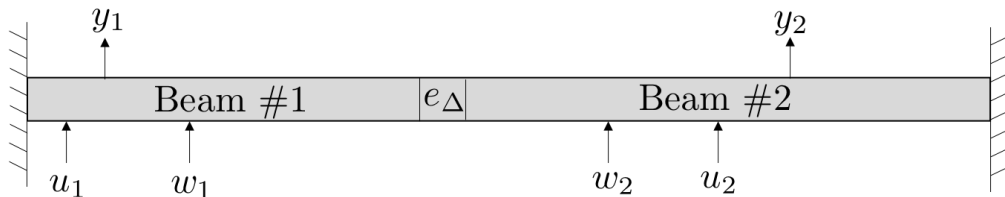


Figure 58: This figure depicts the relative location of control inputs (u_i), disturbance inputs (w_i), and measurements (y_i) along the length of each respective beam, with the approximate location of the uncertain interconnection stiffness element (e_Δ) shown.

Table 7: Input data for beam measurement, disturbance, and control input locations. Distances are with respect to the fixed-end boundary condition.

Input / Output Definitions			
	Beam #1	Beam #2	Interconnection Element (e_Δ)
Location along beam length (cm)			
Control input	10	75	N/A
Disturbance input	40	100	N/A
Measurement	20	50	N/A

The measurements at each location are decomposed into a position and velocity — this means that for our state space system, we end up with (effectively) two measurements for each beam. The control and disturbance inputs are modeled as distributed forces across the closest element to that location, as depicted in figure 55.

APPENDIX C

STABILIZABILITY AND DETECTABILITY OF LIGHTLY-DAMPED STRUCTURES

The system that we study is both stabilizable and detectable. Since we are interested primarily in structural dynamic systems, this assumption is automatically satisfied, as these types of systems do not have any unstable modes.

Theorem 19. *All linear elastic structures with homogeneous equations of motion $\mathcal{M}\ddot{x} + \mathcal{C}\dot{x} + \mathcal{K}x = 0$ with positive definite mass, stiffness, and damping matrices are globally asymptotically stable. Therefore, all linear elastic structural systems are both stabilizable and detectable.*

Proof. We shall sketch a proof via Lyapunov stability theory.

We know that the kinetic energy, T , and the potential energy, V , of the system above are characterized by

$$T = \frac{1}{2}\dot{x}^T \mathcal{M}\dot{x}, \quad \text{and} \quad V = \frac{1}{2}x^T \mathcal{K}x \quad (\text{C.1})$$

Physically, this also makes sense since these quadratic equations must always be positive, further reinforcing the requirement that the system mass and stiffness matrices be strictly positive definite. We can formulate the total energy in this system as

$$H = T + V \quad (\text{C.2})$$

$$H(x, \dot{x}) = \frac{1}{2}\dot{x}^T \mathcal{M}\dot{x} + \frac{1}{2}x^T \mathcal{K}x. \quad (\text{C.3})$$

$H \geq 0$ since both \mathcal{M} and \mathcal{K} are both positive definite, and is equal to zero iff $x = \dot{x} = 0$.

We make the claim that

$$\dot{H} = -\dot{x}^T \mathcal{C} \dot{x} \quad (\text{C.4})$$

A positive definite damping matrix can be defined in several ways:

- Using proportional damping. For some $\alpha, \beta \in \mathbb{R}_+$, $\mathcal{C} = \alpha\mathcal{M} + \beta\mathcal{K}$ is positive definite, since it is usually the sum of two scaled positive definite matrices. Furthermore, if $\mathcal{K} \geq 0$ and $\mathcal{M} > 0$ then $\mathcal{C} > 0$ since $x^T(\mathcal{M} + \mathcal{K})x > 0$. This is true since $x^T\mathcal{M}x > 0$ for any x .
- Using modal damping. When constructing this type of model, as shown in appendix B, we construct a damping model that is diagonal with strictly positive elements. We showed that the damping matrix, in physical coordinates, was constructed from

$$\mathbf{C}_g = \Phi^{-T} \mathcal{C} \Phi^{-1} \quad (\text{C.5})$$

where $\mathcal{C} = \text{diag}(2\zeta_r \omega_r M_r)$ where each element corresponds to a mode. Since the eigenvectors of this system are going to be full rank due to the absence of any rigid body modes and since all modes will be distinct, the matrix \mathbf{C}_g will also be positive definite. This arises from the property that for some positive definite matrix Q and some full rank matrix R ,

$$Q > 0 \Rightarrow R^T Q R > 0. \quad (\text{C.6})$$

Using $\mathcal{M}\ddot{x} + \mathcal{K}x = -\mathcal{C}\dot{x}$, we obtain

$$\dot{H} = \frac{1}{2}\dot{x}^T \mathcal{M}\ddot{x} + \frac{1}{2}\ddot{x}^T \mathcal{M}\dot{x} + \frac{1}{2}\dot{x}^T \mathcal{K}x + \frac{1}{2}x^T \mathcal{K}\dot{x} \quad (\text{C.7})$$

$$= \frac{1}{2}\dot{x}^T(\mathcal{M}\ddot{x} + \mathcal{K}x) + \frac{1}{2}(\ddot{x}^T \mathcal{M} + x^T \mathcal{K})\dot{x} \quad (\text{C.8})$$

$$= -\frac{1}{2}\dot{x}^T \mathcal{C} \dot{x} + \frac{1}{2}(\mathcal{M}\ddot{x} + \mathcal{K}x)^T \dot{x} \quad (\text{C.9})$$

$$= -\dot{x}^T \mathcal{C} \dot{x}. \quad (\text{C.10})$$

Therefore, $\dot{H} = -\dot{x}^T \mathcal{C} \dot{x}$. Since \mathcal{C} is positive definite, $\dot{H} \leq 0$, and energy is dissipating from the system for all $x, \dot{x}, \ddot{x} \in \mathbb{R}^n$. Furthermore, $\dot{H} = 0$ iff $\dot{x} = 0$. Hence, $H(x, \dot{x}) \rightarrow 0$ as $t \rightarrow \infty$. We have shown that any linear elastic system with positive definite mass, stiffness, and damping matrices is stable in the strict sense (global asymptotic stability). Since these

types of systems are stable in the strict sense, they have no unstable modes. Since these systems have no unstable modes, they are always stabilizable and detectable. **Q.E.D.**

APPENDIX D

KYP LEMMA

Lemma 8 (The KYP Lemma, AKA: The Bounded Real Lemma). *Suppose*

$$\hat{G}(s) \sim \left[\begin{array}{c|c} A & B \\ \hline C & D \end{array} \right] \quad (\text{D.1})$$

Then the following are equivalent:

1. $\|G\|_\infty \leq \gamma$

2. There exists a $X > 0$ such that

$$\begin{bmatrix} A^T X + XA & XB \\ B^T X & -\gamma I \end{bmatrix} + \frac{1}{\gamma} \begin{bmatrix} C^T \\ D^T \end{bmatrix} \begin{bmatrix} C & D \end{bmatrix} < 0. \quad (\text{D.2})$$

The KYP (bounded real) lemma can be used to calculate the \mathcal{H}_∞ norm of a system.

Proof. To do this, we will show that 2.) implies 1.). We will first show that if $y = Gu$, then $\|y\|_2 \leq \gamma \|u\|_2$.

From the first block of the LMI given by 2.), we see that $A^T X + XA < 0$. This is seen by a simple Schur Complement argument of this LMI. What this implies is that A is stable, since this is just a Lyapunov Inequality. Because the LMI in 2.) is strict, we can say that

there exists some $\epsilon > 0$ such that

$$\begin{bmatrix} A^T X + XA & XB \\ B^T X & -(\gamma - \epsilon)I \end{bmatrix} + \frac{1}{\gamma} \begin{bmatrix} C^T \\ D^T \end{bmatrix} \begin{bmatrix} C & D \end{bmatrix} \quad (\text{D.3})$$

$$= \begin{bmatrix} A^T X + XA & XB \\ B^T X & -\gamma I \end{bmatrix} + \frac{1}{\gamma} \begin{bmatrix} C^T \\ D^T \end{bmatrix} \begin{bmatrix} C & D \end{bmatrix} + \begin{bmatrix} 0 & 0 \\ 0 & \epsilon I \end{bmatrix} < 0. \quad (\text{D.4})$$

Next, by letting $y = Gu$, we have that the state-space representation is

$$\dot{x} = Ax + Bu \quad x(0) = 0 \quad (\text{D.5})$$

$$y = Cx + Du. \quad (\text{D.6})$$

Now, we can let some energy functional given by $V(x) = x^T X x$. Then, the LMI implies

$$\begin{bmatrix} x \\ u \end{bmatrix}^T \left[\begin{bmatrix} A^T X + XA & XB \\ B^T X & -(\gamma - \epsilon)I \end{bmatrix} + \frac{1}{\gamma} \begin{bmatrix} C^T \\ D^T \end{bmatrix} \begin{bmatrix} C & D \end{bmatrix} \right] \begin{bmatrix} x \\ u \end{bmatrix} \quad (\text{D.7})$$

$$= \begin{bmatrix} x \\ u \end{bmatrix}^T \begin{bmatrix} A^T X + XA & XB \\ B^T X & -(\gamma - \epsilon)I \end{bmatrix} \begin{bmatrix} x \\ u \end{bmatrix} + \frac{1}{\gamma} \begin{bmatrix} x \\ u \end{bmatrix}^T \begin{bmatrix} C^T \\ D^T \end{bmatrix} \begin{bmatrix} C & D \end{bmatrix} \begin{bmatrix} x \\ u \end{bmatrix} \quad (\text{D.8})$$

$$= \begin{bmatrix} x \\ u \end{bmatrix}^T \begin{bmatrix} A^T X + XA & XB \\ B^T X & -(\gamma - \epsilon)I \end{bmatrix} \begin{bmatrix} x \\ u \end{bmatrix} + \frac{1}{\gamma} y^T y \quad (\text{D.9})$$

$$= x^T (A^T X + XA)x + x^T X B u + y^T B^T X x - (\gamma - \epsilon) u^T u + \frac{1}{\gamma} y^T y \quad (\text{D.10})$$

$$= (Ax + Bu)^T X x + x^T X (Ax + Bu) - (\gamma - \epsilon) u^T u + \frac{1}{\gamma} y^T y \quad (\text{D.11})$$

$$= \dot{x}^T X x + x^T X \dot{x} - (\gamma - \epsilon) \|u\|^2 + \frac{1}{\gamma} \|y\|^2 \quad (\text{D.12})$$

$$\dot{V}(x) - (\gamma - \epsilon) \|u\|^2 + \frac{1}{\gamma} \|y\|^2 < 0. \quad (\text{D.13})$$

Now integrating (D.13) in time,

$$\int_0^T \left(\dot{V}(x(t)) - (\gamma - \epsilon) \|u(t)\|^2 + \frac{1}{\gamma} \|y(t)\|^2 \right) dt \quad (\text{D.14})$$

$$= V(x(T)) - V(x(0)) - (\gamma - \epsilon) \int_0^T \|u(t)\|^2 dt + \frac{1}{\gamma} \int_0^T \|y(t)\|^2 dt < 0. \quad (\text{D.15})$$

But, since A is stable, $\lim_{t \rightarrow \infty} x(t) = 0$, which implies that $\lim_{t \rightarrow \infty} V(x(t)) = 0$. Since we said that $x(0) = 0$, we also have $V(x(0)) = 0$. This means that $V(x(0)) = V(x(\infty)) = 0$. Since this is the case,

$$\lim_{T \rightarrow \infty} \left[\dot{V}(x(T)) - \dot{V}(x(0)) - (\gamma - \epsilon) \int_0^T \|u(t)\|^2 dt + \frac{1}{\gamma} \int_0^T \|y(t)\|^2 dt \right] \quad (\text{D.16})$$

$$= 0 - 0 - (\gamma - \epsilon) \int_0^\infty \|u(t)\|^2 dt + \frac{1}{\gamma} \int_0^\infty \|y(t)\|^2 dt \quad (\text{D.17})$$

$$= -(\gamma - \epsilon) \|u\|_2^2 + \frac{1}{\gamma} \|y\|_2^2 < 0. \quad (\text{D.18})$$

Thus, we have that

$$\|y\|_2^2 < (\gamma^2 - \epsilon\gamma) \|u\|_2^2. \quad (\text{D.19})$$

We then have from (D.19) that

$$\|G\|_\infty^2 \leq (\gamma^2 - \epsilon\gamma) < \gamma^2 \quad (\text{D.20})$$

$$\|G\|_\infty < \gamma. \quad (\text{D.21})$$

Q.E.D.

APPENDIX E

KYP DUAL PROOF

Suppose \exists an K s.t. $\left\| F_l(G, \bar{K}) \right\|_\infty \leq \gamma$. By lemma 2, this implies \exists a $q > 0$ s.t.

$$\begin{bmatrix} Q(A + B_2 K)^T + (A + B_2 K)Q & B_1 & Q(C_1 + D_{12} K)^T \\ B_1^T & -\gamma I & D_{11}^T \\ (C_1 + D_{12} K)Q & D_{11} & -\gamma I \end{bmatrix} < 0 \quad (\text{E.1})$$

Let $Y = KQ$. Then,

$$\begin{bmatrix} QA^T + Y^T B_2^T + AQ + B_2 Y & B_1 & QC_1^T + Y^T D_{12}^T \\ B_1^T & -\gamma I & D_{11}^T \\ C_1 Q + D_{12} Y & D_{11} & -\gamma I \end{bmatrix} < 0 \quad (\text{E.2})$$

$$= \begin{bmatrix} QA^T + Y K^T B_2^T + AQ + B_2 K Q & B_1 & QC_1^T + Q K^T D_{12}^T \\ B_1^T & -\gamma I & D_{11}^T \\ C_1 Q + D_{12} K Q & D_{11} & -\gamma I \end{bmatrix} < 0 \quad (\text{E.3})$$

$$= \begin{bmatrix} Q(A + B_2 K)^T + (A + B_2 K)Q & B_1 & Q(C_1 + K D_{12})^T \\ B_1^T & -\gamma I & D_{11}^T \\ (C_1 + D_{12} K)Q & D_{11} & -\gamma I \end{bmatrix} < 0 \quad (\text{E.4})$$

Now, suppose $\exists Q > 0$ and Y s.t.

$$\begin{bmatrix} QA^T + Y^T B_2^T + AQ + B_2 Y & B_1 & QC_1^T + Y^T D_{12}^T \\ B_1^T & -\gamma I & D_{11}^T \\ C_1 Q + D_{12} Y & D_{11} & -\gamma I \end{bmatrix} < 0 \quad (\text{E.5})$$

Let $K = YQ^{-1}$. Then

$$\begin{bmatrix} Q(A + B_2 K)^T + (A + B_2 K)Q & B_1 & Q(C_1 + D_{12} K)^T \\ B_1^T & -\gamma I & D_{11}^T \\ (C_1 + D_{12} K)Q & D_{11} & -\gamma I \end{bmatrix} < 0 \quad (\text{E.6})$$

$$= \begin{bmatrix} QA^T + QK^T B_2^T + AQ + B_2 KQ & B_1 & QC_1^T + QK^T D_{12}^T \\ B_1^T & -\gamma I & D_{11}^T \\ C_1 Q + D_{12} KQ & D_{11} & -\gamma I \end{bmatrix} < 0 \quad (\text{E.7})$$

$$= \begin{bmatrix} QA^T + Y^T B_2^T + AQ + B_2 Y & B_1 & QC_1^T + Y^T D_{12}^T \\ B_1^T & -\gamma I & D_{11}^T \\ C_1 Q + D_{12} Y & D_{11} & -\gamma I \end{bmatrix} < 0. \quad (\text{E.8})$$

Meaning that the following optimization problems are equivalent:

Form 1

$$\min_K \left\| F_l(G, \bar{K}) \right\|_\infty \quad (\text{E.9})$$

Form 2

$$\begin{aligned} & \min_{\gamma, Q, Y} \gamma \\ & \begin{bmatrix} -Q & 0 & 0 & 0 \\ 0 & QA^T + AQ + Y^T B_2^T + B_2 Y & B_1 & QC_1^T + Y^T D_{12}^T \\ 0 & B_1^T & -\gamma I & D_{11}^T \\ 0 & C_1 Q + D_{12} Y & D_{11} & -\gamma I \end{bmatrix} < 0 \end{aligned} \quad (\text{E.10})$$

with the optimal controller given by $K = YQ^{-1}$. **Q.E.D.**

APPENDIX F

PULLING OUT THE DELTA'S IN A PARAMETRICALLY-UNCERTAIN STATE SPACE SYSTEM

The Δ in figure 59 is an uncertainty block. Putting a system into this form allows us to analyze it in different ways, and is sometimes requisite for controller synthesis. The Δ matrix can be real or complex, but it is perhaps easiest to consider the real case.

Before we get into this, the way that this type of system is handled is to create virtual or artificial uncertainty states. These additional inputs and outputs allow us to represent the nominal system, P with unknown parameters, which we can call δ_i , entering as feedback gains around the additive input and output. The model description would look like:

$$\dot{x} = Ax + B_1w + B_2u + B_\Delta u_\Delta \quad (\text{F.1})$$

$$z = C_1x + D_{11}w + D_{12}u + D_{1\Delta}u_\Delta \quad (\text{F.2})$$

$$y = C_2x + D_{21}w + D_{22}u + D_{2\Delta}u_\Delta \quad (\text{F.3})$$

$$y_\Delta = C_\Delta x + D_{1,\Delta}u + D_{2,\Delta}u_\Delta \quad (\text{F.4})$$

$$u_\Delta = \text{diag}(\delta_1 I_1, \delta_2 I_2, \dots, \delta_k I_k) \quad (\text{F.5})$$

where y is our sensor measurement, z is our performance output, and y_Δ and u_Δ are related to the uncertainty terms.

What we see, from things mentioned before, is that we are modeling the system such that we can actually represent the uncertainty as a linear fractional transformation with the

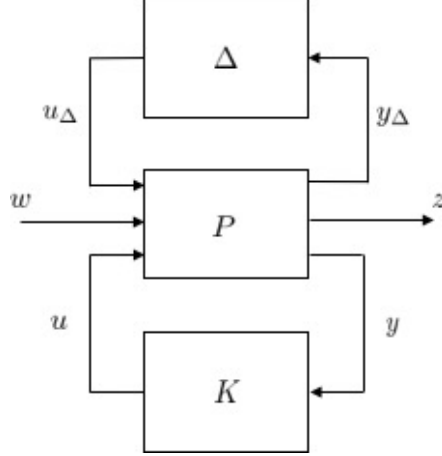


Figure 59: Generalized regulator framework with controller and uncertainty block.

plant P . This helps with modeling and analysis (it is easy to connect LFTs with other LFTs, as the connection is still an LFT).

Our uncertain state space system, with real parametric uncertainty, can assume the form

$$\dot{x} = \left(A + \sum_{i=1}^k \delta_i A_i \right) x + \left(B + \sum_{i=1}^k \delta_i B_i \right) u \quad (\text{F.6})$$

$$y = \left(C + \sum_{i=1}^k \delta_i C_i \right) x + \left(D + \sum_{i=1}^k \delta_i D_i \right) u \quad (\text{F.7})$$

where we clearly see that the uncertainty is entering the system via $\delta_1, \dots, \delta_k$. These can be real or complex, however, we will consider the real case for now and will assert that they must satisfy $\|\delta_i\|_\infty < 1$. This norm constraint can be achieved by some modeling choices.

To get the system into the 5-equation system shown at the beginning of this appendix, an approach that has roots in what is called a Gilbert realization must be used — see paper by Morton and McAfoos [89].

For each $i = 1, \dots, k$

$$\begin{bmatrix} A_i & B_i \\ C_i & D_i \end{bmatrix} \in \mathbb{R}^{(n+n_u) \times (n+n_y)} \quad (\text{F.8})$$

Letting

$$r_i \doteq \text{rank} \begin{bmatrix} A_i & B_i \\ C_i & D_i \end{bmatrix} \quad (\text{F.9})$$

we can factor each matrix, using a singular value decomposition, for example, as

$$\begin{bmatrix} A_i & B_i \\ C_i & D_i \end{bmatrix} = \begin{bmatrix} E_i \\ F_i \end{bmatrix} \begin{bmatrix} G_i & H_i \end{bmatrix} \quad (\text{F.10})$$

where

$$\begin{bmatrix} E_i \\ F_i \end{bmatrix} \in \mathbb{R}^{(n+n_y) \times r_i}, \quad \begin{bmatrix} G_i & H_i \end{bmatrix} \in \mathbb{R}^{r_i \times (n+n_y)} \quad (\text{F.11})$$

leading us to being able to define the “expanded” state space system as

$$\begin{bmatrix} \dot{x} \\ y \\ y_{\delta_1} \\ \vdots \\ y_{\delta_k} \end{bmatrix} = \begin{bmatrix} A & B & E_1 & \dots & E_k \\ C & D & F_1 & \dots & F_k \\ G_1 & H_1 & 0 & \dots & 0 \\ \vdots & \vdots & \vdots & \ddots & \vdots \\ G_k & H_k & 0 & \dots & 0 \end{bmatrix} \begin{bmatrix} x \\ u \\ u_{\delta_1} \\ \vdots \\ u_{\delta_k} \end{bmatrix} \quad (\text{F.12})$$

where we will refer to the dynamics matrix given above as G_{uss} . We now have the formulation for our “open loop uncertain system”. We can represent the uncertain system as an LFT around (F.12), which is

$$y = F_u(G_{uss}, \Delta)u \quad (\text{F.13})$$

where Δ is mapping $y_\delta \rightarrow u_\delta$ and has the structure

$$\Delta = \left\{ \text{diag}(\delta_1 I_{r1}, \dots, \delta_k I_{rk}) : \delta_i \in \mathbb{R} \right\} \quad (\text{F.14})$$

One thing that we see is that uncertainty of this form is norm-bounded and permits the uncertain parameter to exist anywhere within the set Δ with equal probability. Let’s get into an example which can be found in [57].

We can consider a single mode transfer function (which what we get when we decouple our system!), which maps the input force to the displacement output, with uncertainty in

the damping and natural frequency squared terms.

$$G(s) = \frac{1}{s^2 + 2\zeta\omega(1 + \delta_1)s + \omega^2(1 + \delta_2)} \quad (\text{F.15})$$

This transfer function has the state space realization

$$\left[\begin{array}{c|c} \hat{A} & \hat{B} \\ \hline \hat{C} & \hat{D} \end{array} \right] = \left[\begin{array}{cc|c} 0 & 1 & 0 \\ -\omega^2(1 + \delta_2) & -2\zeta(1 + \delta_1) & 1 \\ \hline 1 & 0 & 0 \end{array} \right] \quad (\text{F.16})$$

If we write this system in the form of (F.6) and (F.7) we would have

$$\hat{A} = \begin{bmatrix} 0 & 1 \\ -\omega^2(1 + \delta_2) & -2\zeta\omega(1 + \delta_1) \end{bmatrix} = \begin{bmatrix} 0 & 1 \\ -\omega^2 & -2\zeta\omega \end{bmatrix} + \delta_1 \begin{bmatrix} 0 & 0 \\ 0 & -2\zeta\omega \end{bmatrix} + \delta_2 \begin{bmatrix} 0 & 0 \\ -\omega^2 & 0 \end{bmatrix} \quad (\text{F.17})$$

$$= \begin{bmatrix} 0 & 1 \\ -\omega^2(1 + \delta_2) & -2\zeta\omega(1 + \delta_1) \end{bmatrix} = +\delta_1 \begin{bmatrix} 0 \\ 1 \end{bmatrix} \begin{bmatrix} 0 & -2\zeta\omega \end{bmatrix} + \delta_2 \begin{bmatrix} 0 \\ 1 \end{bmatrix} \begin{bmatrix} -\omega^2 & 0 \end{bmatrix} \quad (\text{F.18})$$

leading us to

$$\left[\begin{array}{c|c} \hat{A} & \hat{B} \\ \hline \hat{C} & \hat{D} \end{array} \right] = \left[\begin{array}{cc|ccc} 0 & 1 & 0 & 0 & 0 \\ -\omega^2 & -2\zeta\omega & 1 & 1 & 1 \\ \hline 0 & -2\zeta\omega & 0 & 0 & 0 \\ -\omega^2 & 0 & 0 & 0 & 0 \\ 1 & 0 & 0 & 0 & 0 \end{array} \right], \quad \Delta = \begin{bmatrix} \delta_1 & 0 \\ 0 & \delta_2 \end{bmatrix} \quad (\text{F.19})$$

where we can now see that we have formed the interconnection diagram shown in figure 59, without any controller included. Nevertheless, this is one way for us to capture uncertainty in this way.

APPENDIX G

DEGRADATION FUNCTION DATA FOR THE PROBABILISTIC ROBUST DYNAMIC OUTPUT FEEDBACK CASE

The tables included in this appendix contain the variance inflation factor and corresponding probability estimates that were generated for stability and performance degradation function construction in chapter 7.

Table 8: Resulting probability estimates for controller 1 as a function of variance inflation factor a . If the controlled system is found to be stable, it highly likely that it will also meet the performance specification for the systems and controllers designed in this research.

Controller 1 Degradation Function Data		
a	$\hat{\Pr}(\text{stable})$	$\hat{\Pr}(G_{\text{prob}} _{\infty} \leq \gamma^*)$
0	1.0000	1.0000
0.5	1.0000	1.0000
1	0.9934	0.9934
1.6	0.9410	0.9410
2	0.8967	0.8967
2.5	0.8405	0.8405
3	0.8004	0.8004
5	0.6917	0.6917
10	0.6012	0.6011

Table 9: Resulting probability estimates for controller 2 as a function of variance inflation factor a . If the controlled system is found to be stable, it highly likely that it will also meet the performance specification for the systems and controllers designed in this research.

Controller 2 Degradation Function Data		
a	$\hat{\Pr}(\text{stable})$	$\hat{\Pr}(G_{\text{prob}} _{\infty} \leq \gamma^*)$
0	1.0000	1.0000
0.5	1.0000	1.0000
1	0.9933	0.9933
1.6	0.9414	0.9414
2	0.8973	0.8973
2.5	0.8411	0.8410
3	0.7970	0.7970
5	0.6917	0.6917
10	0.5985	0.5985

BIBLIOGRAPHY

- [1] Laura Ryan Ray and Robert F. Stengel. Application of stochastic robustness to aircraft control systems. *Journal of Guidance, Control, and Dynamics*, 14(6):1251–1259, 1991.
- [2] Robert F. Stengel and Laura Ryan Ray. Stochastic robustness of linear time-invariant control systems. *IEEE Transactions on Automatic Control*, 36(1):82–87, 1991.
- [3] Roy R. Craig and C. J. Chang. Substructure Coupling for Dynamic Analysis and Testing. Technical report, University of Texas at Austin, Austin, TX, 1977.
- [4] Roy R. Craig and C. J. Chang. A review of substructure coupling methods for dynamic analysis. *International Journal of Analytical and Experimental Modal Analysis*, 2:59–72, 1987.
- [5] Dragoslav D. Siljak. *Large-Scale Dynamic Systems: Stability and Structure*. Dover Publications, 1st edition, 1978.
- [6] Kyong B. Lim. A robust control design framework for substructure models. *Journal of Guidance, Control, and Dynamics*, 19(1):181–190, 1996.
- [7] Vit Babuska. *Substructure-based Control of Flexible Structures*. PhD thesis, University of Texas at Austin, 1993.
- [8] Matthew R. W. Brake. *The Mechanics of Jointed Structures*. Springer Nature, 2018.
- [9] Dragoslav D. Siljak. *Decentralized Control of Complex Systems*. Courier Corporation, 2011.
- [10] D.D. Siljak. Parameter space methods for robust control design: A guided tour. *IEEE Transactions on Automatic Control*, 34(7):674–688, 1989.
- [11] Laura Ryan Ray and Robert F. Stengel. A Monte Carlo approach to the analysis of control system robustness. *Automatica*, 29(1):229–236, 1993.
- [12] C.I. Morrison and R.F. Stengel. Design of robust control systems for a hypersonic aircraft. *Journal of Guidance, Control, and Dynamics*, 21(1):58–63, 1998.

- [13] M. Vidyasagar. Randomized algorithms for robust controller synthesis using statistical learning theory. *Automatica*, 37(10):1515–1528, 2001.
- [14] Roberto Tempo, Giuseppe Calafiore, and Fabrizio Dabbene. *Randomized Algorithms for Analysis and Control of Uncertain Systems with Applications*. Springer-Verlag, London, 2nd edition, 2013.
- [15] S Boyd, L El Ghaoui, E Feron, and V Balakrishnan. *Linear Matrix Inequalities in System and Control Theory*, volume 15. SIAM, 1994.
- [16] G.C. Calafiore and M.C. Campi. The scenario approach to robust control design. *IEEE Transactions on Automatic Control*, 51(5):742–753, 2006.
- [17] Kemin Zhou and John C. Doyle. *Essentials of Robust Control*. Prentice Hall, 1st edition, 1999.
- [18] David E Goldberg. *Genetic Algorithms*. Pearson Education India, 2006.
- [19] Peiman G. Maghami and Kyong B. Lim. Synthesis and control of flexible systems with component-level uncertainties. *Journal of Dynamic Systems, Measurement, and Control*, 131(5):051005, 2009.
- [20] Tzu-Jeng Su, Vit Babuska, and Roy R. Jr. Craig. Substructure-based controller design method for flexible structures. *Journal of Guidance, Control, and Dynamics*, 18(5):1053–1061, 1995.
- [21] Tzu-Jeng Su and Roy R. Jr. Craig. A Decentralized Linear Quadratic Control Design Method for Flexible Structures. Technical report, University of Texas at Austin, Austin, TX, 1990.
- [22] Peter M Young, Matthew P Newlin, and John C Doyle. μ -analysis with real parametric uncertainty. In *Decision and Control, 1991., Proceedings of the 30th IEEE Conference on*, pages 1251–1256. IEEE, 1991.
- [23] Vincent D. Blondel and John N. Tsitsiklis. A survey of computational complexity results in systems and control. *Automatica*, 36(9):1249–1274, 2000.
- [24] Richard P. Braatz, Peter M. Young, John C. Doyle, and Manfred Morari. Computational complexity of μ calculation. *IEEE Transactions on Automatic Control*, 39(5):1000–1002, 1994.
- [25] K D Young. A distributed finite-element modeling and control approach for large flexible structures. In *Third Annual NASA/DOD CSI Conference*, pages 151–161, San Diego, CA, 1989.
- [26] Lubomir Bakule. Decentralized control: An overview. *Annual Reviews in Control*, 32(1):87–98, 2008.

- [27] Yang Wang, Jerome P. Lynch, and H. Law Kincho. Decentralized \mathcal{H}_∞ controller design for large-scale civil structures. *Earthquake Engineering and Structural Dynamics*, 38(3):377–401, 2009.
- [28] F Palacios-Quinonero, J M Rossell, and H R Karimi. Semi-decentralized strategies in structural vibration control. *Modeling Identification and Control*, 32(2):57–77, 2011.
- [29] Hamid Reza Karimi, Josep M. Rossell, Josep Rubió-Massegú, and Francisco Palacios-Quiñonero. Vibration control strategy for large-scale structures with incomplete multi-actuator system and neighbouring state information. *IET Control Theory & Applications*, 10(4):407–416, 2016.
- [30] Christopher I Morrison and Robert Stengel. Stochastic robustness synthesis applied to a benchmark control problem. *International Journal of Robust and Nonlinear Control*, 5(1):13–31, 1995.
- [31] Christopher I Morrison and Robert F Stengel. Robust control system design using random search and genetic algorithms. *IEEE Transactions on Automatic Control*, 42(6):835–839, 1997.
- [32] Qian Wang and Robert F Stengel. Probabilistic control of nonlinear uncertain systems. In *Probabilistic and randomized methods for design under uncertainty*, pages 381–414. Springer, 2006.
- [33] Mathukumalli Vidyasagar. Statistical learning theory and randomized algorithms for control. *IEEE Control Systems Magazine*, 18(6):69–85, 1998.
- [34] M Vidyasagar. Randomized algorithms for robust controller synthesis using statistical learning theory. *Learning, Control and Hybrid Systems*, 37:3–24, 1998.
- [35] V. Koltchinskii, C.T. Abdallah, M. Ariola, P. Dorato, and D Panchenko. Improved sample complexity estimates for statistical learning control of uncertain systems. *IEEE Transactions on Automatic Control*, 45(12):2383–2388, 2000.
- [36] V. Koltchinskii, C.T. Abdallah, M. Ariola, and P. Dorato. Statistical learning control of uncertain systems: theory and algorithms. *Applied Mathematics and Computation*, 120(1):31–43, 2001.
- [37] Qian Wang and Robert F. Stengel. Searching for robust minimal-order compensators. *Journal of Dynamic Systems, Measurement, and Control*, 123(2):233, 2001.
- [38] Qian Wang and Robert F Stengel. Robust nonlinear control of a hypersonic aircraft. *Journal of Guidance, Control, and Dynamics*, 23(4):577–585, 2000.
- [39] Qian Wang and Robert F. Stengel. Robust control of nonlinear systems with parametric uncertainty. *Automatica*, 38(9):1591–1599, 2002.

- [40] G Calafiore and B T Polyak. Randomized algorithms for probabilistic robustness with weak and complex structured uncertainty. *IEEE Transactions on Automatic Control*, 45(12)(12):2218–2235, 2001.
- [41] Pramod Khargonekar and Ashok Tikku. Randomized algorithms for robust control analysis and synthesis have polynomial complexity. In *Decision and Control, 1996., Proceedings of the 35th IEEE Conference on*, volume 3, pages 3470–3475. IEEE, 1996.
- [42] John Rust. Using randomization to break the curse of dimensionality. *Econometrica*, 65(3):487–516, 1997.
- [43] J.C. Doyle, A Packard, and K Zhou. Review of LFTs, LMIs, and μ . *Proceedings of the 30th IEEE Conference on Decision and Control, 1991*, pages 1227—1232 vol.2, 1991.
- [44] B. Scott May. *Probabilistic robust control: theory and applications*. PhD thesis, Caltech, 1997.
- [45] B.Scott May and James L. Beck. Probabilistic control for the active mass driver benchmark structural model. *Earthquake Engineering and Structural Dynamics*, 27(11):1331–1346, 1998.
- [46] Teodoro Alamo, Roberto Tempo, and Eduardo F. Camacho. Randomized strategies for probabilistic solutions of uncertain feasibility and optimization problems. *IEEE Transactions on Automatic Control*, 54(11):2545–2559, 2009.
- [47] Vladimir Koltchinskii, C.T. Abdallah, M. Ariola, P. Dorato, and D. Panchenko. Statistical learning control of uncertain systems: It is better than it seems.
- [48] Teodoro Alamo, Roberto Tempo, Amalia Luque, and Daniel R. Ramirez. Randomized methods for design of uncertain systems: Sample complexity and sequential algorithms. *Automatica*, 52:160–172, 2015.
- [49] M. Vidyasagar. *A Theory of Learning and Generalization with Applications to Neural Networks and Control Systems*. Springer, 1st edition, 1997.
- [50] Shu-Xiang Guo. Non-probabilistic robust reliability method and reliability-based performance optimization for active vibration control of structures and dynamic systems with bounded uncertain parameters. *Journal of Vibration and Control*, 22(6):1472–1491, 2016.
- [51] Luis G. Crespo and Sean P. Kenny. Robust Control Design for Systems With Probabilistic Uncertainty. Technical Report March, NASA, 2005.
- [52] Luis G Crespo and Sean P Kenny. Reliability-based control design for uncertain systems. *Journal of Guidance, Control, and Dynamics*, 28(4):1–30, 2005.
- [53] John C. Doyle, Bruce A. Francis, and Allen R. Tannenbaum. *Feedback Control Theory*. Courier Corporation, 2013.

- [54] C Soize. A comprehensive overview of a non-parametric probabilistic approach of model uncertainties for predictive models in structural dynamics. *Sound and Vibration*, 288(3):623–652, 2005.
- [55] George Stefanou. The stochastic finite element method: Past, present and future. *Computer Methods in Applied Mechanics and Engineering*, 198(9-12):1031–1051, 2009.
- [56] G. I. Schuëller. Computational stochastic mechanics - Recent advances. *Computers and Structures*, 79(22-25):2225–2234, 2001.
- [57] Gary Balas. *Robust Control of Flexible Structures: Theory and Experiments*. PhD thesis, California Institute of Technology, 1990.
- [58] Peter M Young and John C Doyle. Computation of μ with real and complex uncertainties. In *Decision and Control, 1990., Proceedings of the 29th IEEE Conference on*, pages 1230–1235. IEEE, 1990.
- [59] Carsten Scherer. Theory of robust control (lecture notes), 2001.
- [60] Guang-Ren Duan and Hai-Hua Yu. *LMIs in Control Systems: Analysis, Design, and Applications*. CRC Press, 2013.
- [61] Wodek Gawronski. *Advanced Structural Dynamics and Active Control of Structures*. Springer-Verlag New York, 1 edition, 2004.
- [62] R.L. Dailey. Lecture Notes for the Workshop on H_{infinity} and mu Methods for Robust Control. In *American Control Conference*, page 116, San Diego, CA, 1990. American Control Conference.
- [63] Pascal Gahinet and Pierre Apkarian. A linear matrix inequality approach to Hinfinity control. *International Journal of Robust and Nonlinear Control*, 4(4):421–448, 1994.
- [64] Giuseppe Carlo Calafiore. Random convex programs. *SIAM Journal of Optimization*, 20(6):3427–3464, 2010.
- [65] Stephen Boyd and Lieven Vandenberghe. *Convex Optimization*. Cambridge University Press, 2004.
- [66] Johan Lofberg. Yalmip: A toolbox for modeling and optimization in matlab. In *Computer Aided Control Systems Design, 2004 IEEE International Symposium on*, pages 284–289. IEEE, 2004.
- [67] Matthew Peet. MAE 598: LMI Methods in Optimal and Robust Control, 2016.
- [68] Fuzhen Zhang. *The Schur complement and its applications*, volume 4. Springer Science & Business Media, 2006.

- [69] Olof Troeng, Bo Bernhardsson, and Claudio Rivetta. Complex-coefficient systems in control. *Proceedings of the American Control Conference*, pages 1721–1727, 2017.
- [70] M.X. Goemans and D.P. Williamson. Approximation algorithms for MAX-3-CUT and other problems via complex semidefinite programming. *Proceedings of the 33rd Annual ACM Symposium on Theory of Computing (STOC)*, 2001.
- [71] Sondipon Adhikari. An unified parametric-nonparametric uncertainty quantification approach for linear dynamical systems. In *48th AIAA/ASME/ASCE/AHS/ASC Structures, Structural Dynamics, and Materials Conference*, page 2396, 2007.
- [72] W. Gawronski and K. B. Lim. Frequency weighting for the H-infinity and H2 control design of flexible structures. *Journal of Guidance, Control, and Dynamics*, 21(4):664–666, 1998.
- [73] Gary J Balas, John C Doyle, Keith Glover, Andy Packard, and Roy Smith. μ -analysis and synthesis toolbox: For use with matlab. 2001.
- [74] Gary Balas. *Robust Control Toolbox User's Guide*. The MathWorks, Inc., March 2018.
- [75] Matthew P Newlin and Peter M Young. Mixed problems and branch and bound techniques. *International Journal of Robust and Nonlinear Control*, 7(7):145–164, 1997.
- [76] Peter M. Young. Structured singular value approach for systems with parametric uncertainty. *International Journal of Robust and Nonlinear Control*, 11(7):653–680, 2001.
- [77] Gary Balas, Richard Chiang, Andy Packard, and Michael G. Safonov. *Robust Control Toolbox For Use with MATLAB*. 2006.
- [78] Kumara Sastry, David Goldberg, and Graham Kendall. Genetic Algorithms. In E.K. Burke and G. Kendall, editors, *Search Methodologies*, chapter 4, pages 97–125. Springer, Boston, MA, 2005.
- [79] The Mathworks. *Global Optimization Toolbox User's Guide*. The Mathworks, Natick, r2018a edition, 2012.
- [80] P.J Fleming and R.C Purshouse. Evolutionary algorithms in control systems engineering: a survey. *Control Engineering Practice*, 10(11):1223–1241, 2002.
- [81] Wassily Hoeffding. Probability inequalities for sums of bounded random variables. *Journal of the American Statistical Association*, 58(301):13–30, 1963.
- [82] N.A. Bruisma and M. Steinbuch. A fast algorithm to compute the \mathcal{H}_∞ norm of a transfer function matrix. *System Control Letters*, 14(4):287–293, 1990.
- [83] Ragnar Wallin and Anders Hansson. KYPD: A solver for semidefinite programs derived from the Kalman-Yakubovich-Popov lemma. In *Computer Aided Control Systems Design*, pages 697–704, New Orleans, LA, 2004.

- [84] Rikard Falkeborn, Johan Löfberg, and Anders Hansson. Low-rank exploitation in semidefinite programming for control. *International Journal of Control*, 84(12):1975–1982, 2011.
- [85] Robert Orsi, Uwe Helmke, and John B. Moore. A Newton-like method for solving rank constrained linear matrix inequalities. *Automatica*, 42(11):1875–1882, 2006.
- [86] Seog Joo Kim, Young Hyun Moon, and Soonman Kwon. Solving rank-constrained LMI problems with application to reduced-order output feedback stabilization. *IEEE Transactions on Automatic Control*, 52(9):1737–1741, 2007.
- [87] C T Chen. Linear System Theory and Design, 1999.
- [88] Roy R. Jr. Craig. *Structural Dynamics: An Introduction to Computer Methods*. John Wiley & Sons, 1981.
- [89] B Morton and R. McAfros. A μ -test for robustness analysis of a real-parameter variation problem. In *American Control Conference*, pages 135–138, Boston, MA, 1985. IEEE.